BRITISH THESIS SERVICE

DX180309 **Page Count** x306

Awarding Body: Salford University

Thesis By : RADOJCIC R

We have assigned this thesis the number given at the top of this sheet.
In your notification to ASLIB, please quote this number so that it can be included in their *Index to Theses with Abstracts*.

THE BRITISH LIBRARY
DOCUMENT SUPPLY CENTRE

THE PREPARATION OF THIN FILM GRADED BAND GAP SOLAR CELLS

A THESIS PRESENTED FOR THE DEGREE OF DOCTOR OF PHILOSOPHY IN THE UNIVERSITY OF SALFORD

BY

R. RADOJCIC

DEPARTMENT OF ELECTRICAL ENGINEERING
UNIVERSITY OF SALFORD
SALFORD M5 4WT

AUGUST 1978

ACKNOWLEDGEMENTS

The author wishes to thank Dr. A.E. Hill and Professor M.J. Hampshire for their continuous encouragement and guidance throughout this project. Thanks are also due to Mr. Wilson Reddish for helping to provide the funds for the project. Valuable technical advice and assistance of Mr. I.E. Harrison is also acknowledged.

ABSTRACT

The Preparation of Thin Film Graded Band Gap Solar Cells

Thin film solar cells with a band gap graded in the thickness direction were prepared by vacuum evaporation of various alloys of Cadmium Sulphide (CdS) and Cadmium Telluride (CdTe) onto glass substrates. Theoretical computer analyses were carried out and show that a solar cell with a graded band gap surface layer ought to be a more efficient photovoltaic converter than a conventional homojunction device. A vacuum evaporator capable of multiple simultaneous co-evaporations was built and used initially to deposit only the CdS and CdTe films and subsequently mixed and graded films of Cadmium Sulphide Telluride (CdS_xTe_{1-x}). The composition of the mixed and graded films was controlled by a set of shutters built above the sources, rather than by the control of the temperature of the sources. The electronic properties of the films were adjusted by co-evaporation of dopant materials such as Cadmium (Cd), Indium (In) and Copper (Cu), and measured by Hall Effect measurements. The physical properties of the films such as the band gap, crystal phase and grain size were investigated by optical transmission measurements, X-ray analysis and scanning electron microscopy respectively. Finally, p-n junctions

with n-type graded band gap surface layers on top of either pure p-type CdTe films or mixed p-type $CdS_{0.5}Te_{0.5}$ films were prepared. However, the photoresponse of these structures was low, probably due to very short minority carrier life-times, lack of low resistance contacts and cross diffusion of dopant materials. Nevertheless, the characteristics of individual materials and the spectral response of the devices indicated that if these problems could be solved, a successful solar cell could be made.

CONTENTS

		PAGE
CHAPTER I	INTRODUCTION	
	1.1 INTRODUCTION	1
	1.2 NATURE OF SOLAR ENERGY	3
	1.3 SOLAR ENERGY COLLECTION DEVICES	4
	1.3.1 THERMAL COLLECTORS	5
	1.3.2 PHOTOCHEMICAL COLLECTORS	6
	1.3.3 BIOLOGICAL COLLECTORS	8
	1.3.4 PHOTOVOLTAIC COLLECTORS	9
	1.4 CONCLUSION	10
CHAPTER 2	PHOTOVOLTAIC CONVERTERS	
	2.1 HISTORY OF DEVELOPMENT OF PHOTOVOLTAIC CONVERTERS	11
	2.2 PRINCIPLE OF OPERATION	13
	2.2.1 ELECTRICAL PROPERTIES	13
	2.2.1 MATERIAL PROPERTIES	16
	2.2.2.1 THE BAND GAP	16
	2.2.2.2 THE ABSORPTION COEFFICIENT	18
	2.2.2.3 DIFFUSION LENGTH	19
	2.2.2.4 SURFACE RECOMBINATION	21
	2.2.2.5 HETEROJUNCTIONS	23
	2.2.2.6 CONTACTS	24
	2.2.3 CONFIGURATION OF SOLAR CELLS	25
	2.3 PHOTOVOLTAIC DEVICES	27
	2.3.1 SILICON SOLAR CELLS	28
	2.3.1.1 SINGLE CRYSTAL CELLS	29
	2.3.1.2 LOW COST CELLS	30

2.3.2 GALLIUM ARSENIDE SOLAR CELLS 33

2.3.2.1 HETEROSTRUCTURES 34

2.3.3 CADMIUM SULPHIDE SOLAR CELLS 36

2.3.3.1 COPPER SULPHIDE CELLS 37

2.3.3.2 INDIUM PHOSPHIDE CELLS 40

2.3.4 TERNARY SEMICONDUCTOR SOLAR CELLS 42

2.3.5 CADMIUM TELLURIDE SOLAR CELLS 43

2.3.5.1 COPPER TELLURIDE CELLLS 44

2.3.5.2 CADMIUM SULPHIDE CELLS 45

2.3.6 OTHER SOLAR CELLS 46

2.4 CONCLUSION 48

CHAPTER 3 MATERIAL ASPECTS OF CADMIUM SULPHIDE TELLURIDE

3.1 INTRODUCTION 50

3.1.1 GRADED BAND GAP MATERIALS 50

3.1.2 EXISTING GRADED BAND GAP DEVICES 51

3.1.2.1 GALLIUM ALLUMINIUM ARSENIDE 51

3.1.2.2 ZINC MERCURY TELLURIDE 52

3.1.2.3 CADMIUM MERCURY TELLURIDE 53

3.2 CADMIUM SULPHIDE TELLURIDE 54

3.2.1 INTRODUCTION 54

3.2.2 THE BAND GAP 55

3.2.3 ABSORPTION COEFFICIENT 57

3.2.4 DIFFUSION LENGTH 57

3.2.5 CRYSTAL STRUCTURE 58

3.2.6 FORMATION OF A JUNCTION 59

3.2.7 COMPATABILITY WITH LOW COST TECHNOLOGY 61

CHAPTER 4 THEORETICAL ASSESSMENT OF GRADED BAND GAP SOLAR CELLS

4.1 INTRODUCTION 63

4.2 THE BAND DIAGRAM OF CdS_xTe_{1-x} SOLAR CELL 65

4.3 THEORETICAL ANALYSES 67

4.3.1 SOLAR SPECTRUM 70

4.3.2 ABSORPTION OF PHOTONS 72

4.3.3 CURRENT CONTRIBUTION FROM THE GRADED LAYER 75

4.3.4 CURRENT CONTRIBUTION FROM THE DEPLETION LAYER 89

4.3.5 CURRENT CONTRIBUTION FROM THE BASE LAYER 91

4.3.6 RECOMBINATION CURRENT AND SERIES RESISTANCE 95

4.3.7 DEPLETION LAYER 97

4.4 RESULTS OF CALCULATIONS 99

4.4.1 METHOD 99

4.4.2 DISTRIBUTION OF MINORITY CARRIERS 100

4.4.2.1 THE EFFECT OF SURFACE BAND GAP 101

4.4.2.2 THE EFFECT OF THICKNESS 102

4.4.2.3 THE EFFECT OF SURFACE RECOMBINATION 103

4.4.2.4 THE EFFECT OF DIFFUSION LENGTH 104

4.4.2.5 CONCLUSION 104

4.4.3 PHOTOCURRENT IN GRADED BAND GAP DEVICE 106

4.4.3.1 THE EFFECT OF SURFACE BAND GAP 107

4.4.3.2 THE EFFECT OF SURFACE RECOMBINATION 109

4.4.3.3 THE EFFECT OF WIDTH OF SURFACE LAYER 110

4.4.3.4 THE EFFECT OF DUFFUSION LENGTH 111

4.4.3.5 THE EFFECT OF BASE LAYER BAND GAP 112

4.4.3.6 THE EFFECT OF OTHER PARAMETERS 114

4.4.4 OPTIMISATION OF A GRADED BAND GAP DEVICE 115

4.4.5 COMPARISON WITH OTHER TYPES OF SOLAR CELLS 118

CHAPTER 5 EXPERIMENTAL APPARATUS AND METHODS

5.1 VACUUM EVAPORATOR 121

5.1.1 INTRODUCTION 121

5.1.2 THE SOURCES 122

5.1.3 THE SUBSTRATE 124

5.1.4 THE MASKS 125

5.1.5 THE CRYSTAL MONITORS 126

5.1.6 THE SHUTTERS 128

5.2 MONITORING THE DEPOSITION CONDITIONS 131

5.2.1 VACUUM PRESSURE 131

5.2.2 SUBSTRATE TEMPERATURE 132

5.2.3 SOURCE TEMPERATURE 132

5.2.4 DEPOSITION RATES 133

5.3 DEPOSITION PROCEDURES 135

5.3.1 DEPOSITION OF CdS FILMS 135

5.3.2 DEPOSITION OF CdTe FILMS 137

5.3.3 DEPOSITION OF MIXED FILMS 138

5.3.4 DEPOSITION OF DIODES 139

5.4 MEASUREMENT OF FILM PROPERTIES 141

5.4.1 THE HALL EFFECT APPARATUS 141

5.4.2 THE BAND GAP MEASUREMENTS 143

5.4.3 THE CRYSTALLOGRAPHIC MEASUREMENTS 144

5.4.4 THE SURFACE ANALYSES 145

5.4.5 THE MEASUREMENT OF SOLAR CELL PARAMETERS 146

CHAPTER 6 MATERIAL PROPERTIES OF CdS,CdTe AND CdS_xTe_{1-x} FILMS

6.1 INTRODUCTION 148

6.2 CADMIUM SULPHIDE THIN FILMS 149

6.2.1 INTRODUCTION 149

6.2.2 DEPOSITION PARAMETERS 152

6.2.2.1 SUBSTRATE TEMPERATURE 153

6.2.2.2 RATE OF DEPOSITION 154

6.2.2.3 STOICHIOMETRY CONTROL 155

6.2.3 RESULTS 156

6.2.3.1 ELECTRONIC PROPERTIES 156

6.2.3.2 PHYSICAL PROPERTIES 159

6.2.4 DISCUSSION 160

6.3 CADMIUM TELLURIDE THIN FILMS 163

6.3.1 INTRODUCTION 163

6.3.2 DEPOSITION PARAMETERS 165

6.3.3 RESULTS 165

6.3.3.1 ELECTRONIC PROPERTIES 165

6.3.3.2 PHYSICAL PROPERTIES 169

6.3.4 DISCUSSION 171

6.4 MIXED CdS_xTe_{1-x} THIN FILMS 173

6.4.1 INTRODUCTION 173

6.4.2 RESULTS 174

6.4.2.1 P-TYPE FILMS 175

6.4.2.2 N-TYPE FILMS 176

6.4.3 DISCUSSION 181

6.5 CONCLUSION 189

CHAPTER 7 SOLAR CELL - RESULTS AND CONCLUSIONS

7.1 DEVICE WITH CdTe BASE LAYER 186

7.1.1 LAEGE AREA DEVICES 186

7.1.2 SMALL AREA DEVICES 188

7.1.2.1 SAMPLES WITH COPPER ELECTRODE 188

7.1.2.2 SAMPLES WITHOUT COPPER ELECTRODE 192

7.1.3 DISCUSSION 193

7.2 DEVICES WITH $CdS_{0.45}Te_{0.55}$ BASE LAYER 195

7.2.1 DEVICES ON METAL SUBSTRATES 196

7.2.2 DEVICES ON CONDUCTING GLASS 197

7.2.2.1 PHYSICAL PROPERTIES 197

7.2.2.2 SERIES RESISTANCE 199

7.2.2.3 PHOTORESPONSE 200

7.2.2.4 THE JUNCTION 201

7.2.2.5 STABILITY AND REPRODUCABILITY 202

7.2.3 DISCUSSION 202

7.3 CONCLUSION 204

APPENDIX I DEFINITION OF AIR MASS TECHNOLOGY A1

APPENDIX II TRANSFORMATION OF SOLAR CURVES A2

APPENDIX III COMPUTER PROGRAMS A5

APPENDIX IV SUBSTRATE CLEANING A11

APPENDIX V PRODUCTION OF MASKS A12

APPENDIX VI QUARTZ CRYSTAL MONITORS A16

APPENDIX VII DESIGN OF PNEUMATIC SHUTTERS A18

APPENDIX VIII DESIGN OF SHUTTER CONTROL UNIT A22

REFERENCES

1.1 INTRODUCTION

Energy is a commodity which forms the base of modern civilisation. In the past, the growth and the development of society was invariably associated with a greater energy demand that was adequately met by more extensive and more efficient exploitation of fossil fuels. Indeed, the growing industrialisation of the world is mirrored in the growing energy needs (figs. 1.1 and 1.2). The industrialisation was made possible by ready availability of a cheap and convenient energy supply. However, barring a drastic change of pattern of development, the fossil fuels will in the relatively near future become inadequate to satisfy the demand for energy. There are various projected estimates as to how long these fuels will last, but it is obvious that, at the present rate of growth and development, it is a matter of tens or maybe hundreds of years (table 1.1). Furthermore, as the fossil fuels become scarcer, real price will become increasingly prohibitive (table 1.2). Therefore it is vital for alternative energy sources to be found and developed. There is a number of known energy sources which could be developed to replace the fossil fuels. These fall in two broad classes: renewable and non-renewable energy sources. Fission and fusion fuels,

although available in large quantities are non-renewable energy sources and would be eventually exhausted. Furthermore, development of fission and fusion reactors still poses great technological and environmental problems. Direct solar energy, wind and wave power, which are manifestations of solar energy, are renewable, almost infinite energy sources. Tapping this energy source has some great advantages, which cannot be equalled by any other energy source. These are:

a. The supply of energy is virtually infinite. Each year the worlds solar energy income at ground level is about 3.10^{24} Joules. In comparison, the present proven world fossil fuel reserve equals about one week's supply of solar energy at the earths surface,

b. The energy source is renewable, unlike fossil fuels which can be used just once, and

c. Exploitation of this energy is not detremental to the environment i.e. it is clean and non-polluting, unlike fossil and nuclear fuels. However, solar energy suffers from some great disadvantages. Firstly, solar energy is diffuse, i.e. energy falling per unit area is very low compared with energy flux density found in fossil fuels. Secondly, the energy supply is variable with geographical position, with time of year and day, and with metheorological conditions. Thus, solar energy can be used only in conjunction with effective energy storage devices.

2. NATURE OF SOLAR ENERGY

Solar irradiance, i.e. the amount of energy arriving per unit area per unit time, just outside the earth's atmosphere, is on the average 1.35 KW/m^2 (1). Variation of this with seasons is negligable at only 3.4% (2). Solar spectral irradiance, i.e. the energy per unit area per unit time within a particular spectral waveband, outside earth's atmosphere is very similar to the radiation of a black body at 5900 K (figure 1.3). However, the solar spectrum is modified substantially by the atmosphere. Even with clear, cloud free skies, 30% of incident energy is lost through scattering and absorption by the atmosphere. Scattering by various air molecules, water vapour, dust and other atmospheric components results in diffusion of solar energy arriving at the earth's surface. Absorption, principally by ozone, water vapour and carbon dioxide, results in depletion of energy in the ultra-violet, near infra-red and middle infra-red ranges of the spectral curve (figure 1.3). The effect of clouds is mainly in scattering the light, rather than absorbing it, and the thickness of the cloud cover determines how much of this scattered light can reach the surface of earth. As a result of this, for example in UK, 60% of the annual global radiation is received in diffuse radiation (table 1.3).

The annual mean global irradiance on a horizontal plane is shown on figure 1.4. In northern latitudes the mean irradiance is low mainly due to seasonal variations, i.e. the long nights and the low angle of the sun during the winters but on the clear summer days the irradiance can be as high as 800-900 W/m^2 even in these locations (figure 1.5).

It is obvious that, since the energy distribution is so variable, any energy collecting and converting device needs to be suited to the particular location where it is going to be used. Continuous improvement of collecting and processing of the irradiance data will make optimum design of such devices increasingly possible [4].

3. SOLAR ENERGY COLLECTION DEVICES

Various devices for collecting solar energy have been designed. They can be sub-divided into several classes, according to the principle of their operation, i.e. into thermal collectors, photovoltaic collectors, photochemical collectors and biological collectors.

3.1 THERMAL COLLECTORS

Thermal collectors, as their name indicates, transform solar energy into heat. There are two types of these devices: low temperature and high temperature systems.

Low temperature thermal collectors, the most common of which is the flat plate collector, are the most developed of all the solar energy devices (for example 3,4). Flat plate collectors are responsive to a wide band of solar energies and are therefore fairly efficient (figure 1.6). The principle of their operation is very simple so that they lend themselves to mass production at relatively low cost. The UK pay back time i.e. the time required to amortise the value of the installation costs by a 4 m^2 flat plate collector, providing about 900 $KWh/m^2/year$ (i.e. efficiency 45%) is around 16 years. However taking into account inflation and rise of cost of alternative energy this figure can come down to 5 years.(4) Judicious use of technology could further increase the collection efficiency of flat plat collectors, and reduce the heat losses of associated hot fluid storage tanks (5), thus making the system an economically viable source of energy for such domestic applications as space heating and hot water supply.(6)

For applications other than space heating, such as powering of heat engines in order to produce electricity or mechanical power, low temperature converters are not adequate because the efficiency of a heat engine increases with increasing difference of temperature between.its hot and cold reservoirs. To obtain these larger temperature differences it is necessary to concentrate sunlight by use of reflectors (parabolic mirrors) or refractors (lenses), and collect the energy from the focal point. Such systems have been made, but are economical only on a relatively large scale , such as an electrical generating plant on a scale of tens or hundreds of MWs, where the temperature difference of up to 1000^{o}C can be obtained [7].These systems have the basic disadvantages of being viable only in direct sunlight, this limiting their use to a limited number of geographical locations, and of needing an accurate sun-tracking mechanism in order to mantain the position of the collector at the focas.

3.2 PHOTOCHEMICAL COLLECTORS

Photochemical systems convert solar energy into chemical energy. Basically the conversion exploits a kind of a cyclic system where a reaction takes place absorbing solar energy and producing a given set of

products,ts, which can be recombined giving off energy and releasing the original reactants. (8). The principal advantage of such a system is that the products of the reaction can store this chemical energy conveniently for an indefinite period of time without any loss, unlike for example the hot water storage tanks used in conjunction with thermal collectors. The simplest of the photochemical reactors is water which can be decomposed into hydrogen and oxygen by an electrochemical process or by simple redox reaction stimulated by solar energy , (9) and the two gases can subsequently be recombined releasing energy in form of heat and reforming water. Photochemical systems could be made inexpensively, and the energy could be released from the system in form of heat (photothermochemical systems) (4) or electricity (photoelectrochemical in photogalvanic systems) (10). In spite of the great potential that this system shows, relatively little work has been done in the field. A number of chemical systems that will perform the cycle have been found but none have been developed. Most of them suffer from disadvantage of being responsive to a relatively narrow bandwidth of solar spectrum, this showing low overall efficiency (figure 1.6).

3.3 Biological Collectors

There is a number of different natural processes which can be used to collect and store solar energy. The most obvious of these is the process of photosyntheses where carbon dioxide and water are combined into oxygen and an organic material. These organic materials are rich in energy and have been used as the source of energy via the fossil fuels. The overall world efficiency of photosynthetic conversion of solar energy is about 0.1% but investigations show that for particular plants under optimal conditions, this figure can be as high as 5% [11]. It has been demonstrated that "energy plantations" even using poor soil but growing specialised crop can be competative with solid fossil fuels.[12] The advantage of such a system would be that the energy can be conveniently and indefinitly stored, and can be easily converted into solid, liquid or gaseous fuels by conventional processes such as pyrolysis or fermentation. Additional source of energy could be cellulose contained in large quantities in the waste from many present-day processes, which can be fermented into alcohol[13]. Alternatively certain bacteria and algae can, in presence of sunlight, produce gaseous hydrogen . Biological systems offer great potential as a source of energy

because they are inexpensive, convenient, flexible and use existing technology. They are also ecologically very attractive. However, their efficiency is relatively low.

3.4 Photovoltaic Converters

Photovoltaic converters have the advantage of converting solar energy directly into electrical energy, with no intermediate steps, and electrical energy is considered the highest grade energy because it is clean, it can be converted into mechanical energy with greatest efficiency, and it is used for most modern technological processes and appliances. Because of this, solar cells have been mainly developed and used for space projects. Photovoltaic converters can reach efficiencies of up to 20% , but so far have been shown to be economically unattractive for terrestrial applications. In addition, various batteries, which are natural storage systems associated with solar cells, tend to be expensive. As a result, the payback time for this system is tens of years. However, intensive investigations and use of various available technologies, are making photovoltaic converters increasingly competitive.

4. CONCLUSION

It appears that conversion of solar energy, by any of the above mentioned methods, is at present technologically feasible, but economically still not competitive enough with fossil fuels. However, with improving technology, and rising prices of conventional fuels solar energy converters are becoming an increasingly attractive source of energy.

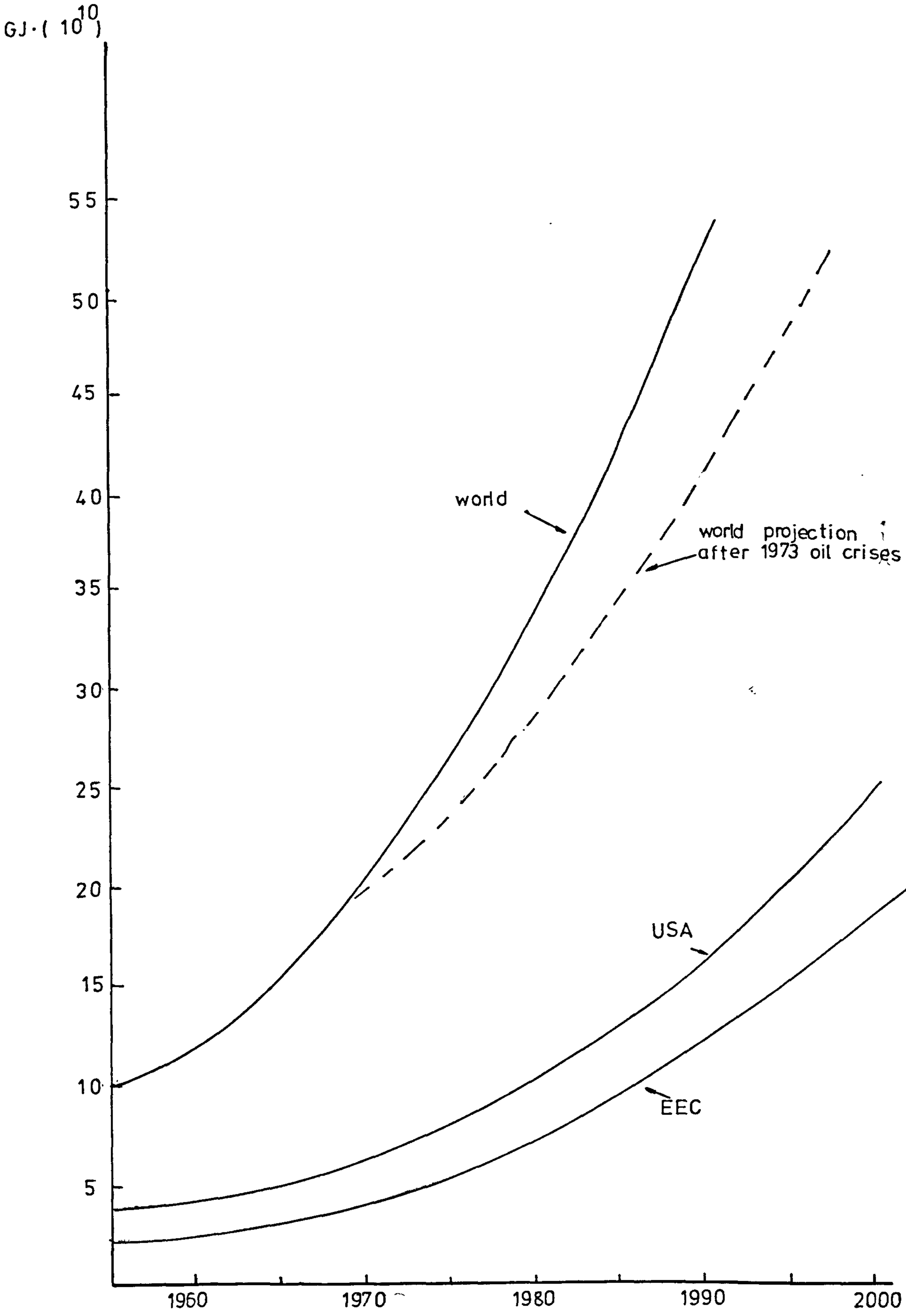

FIGURE 1.1 energy consumption extrapolated to year 2000 based on period 1955 – 1973 (ref 4)

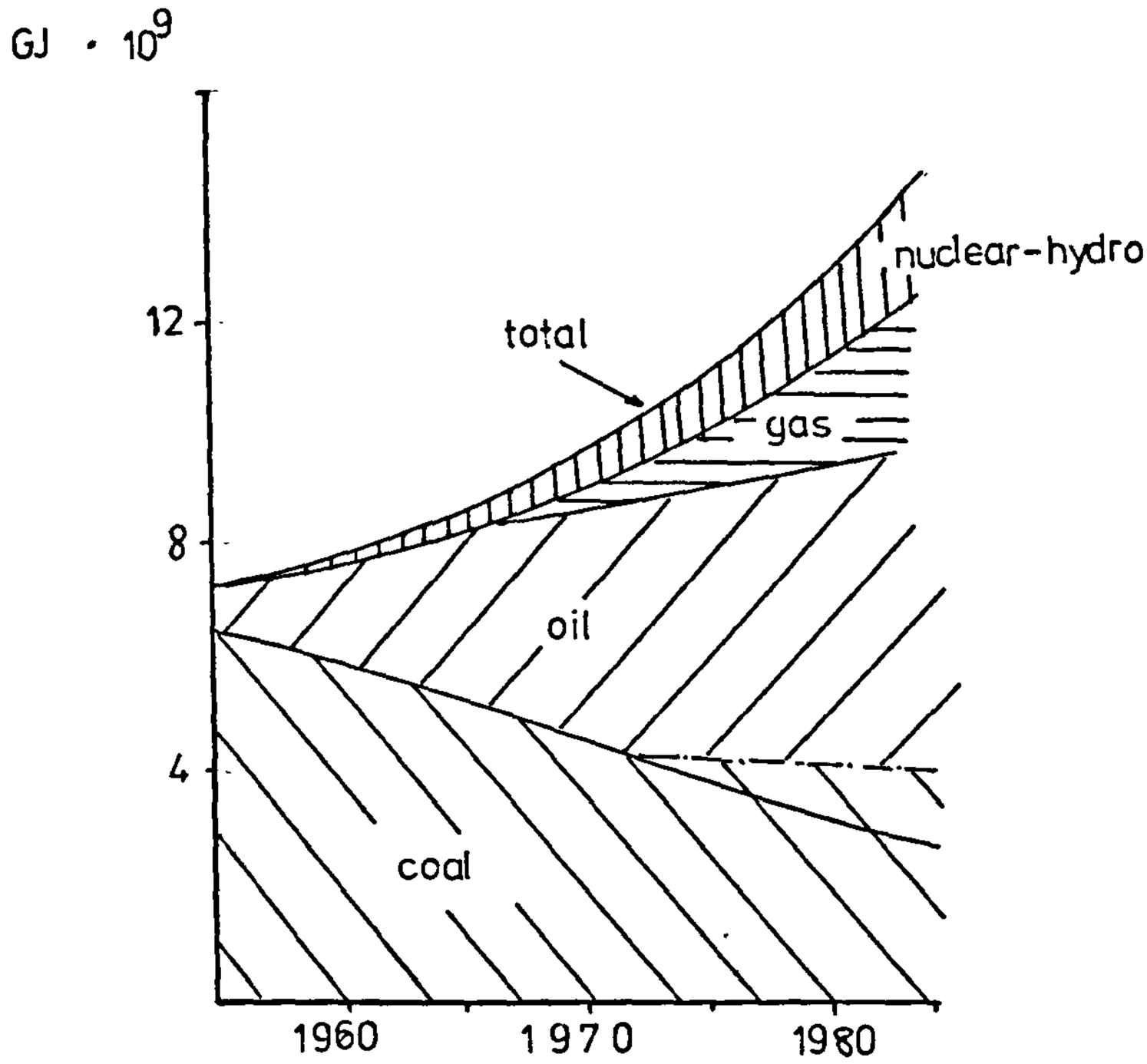

FIGURE 1.2 contribution of conventional fuels to the energy demand of UK (ref 4)

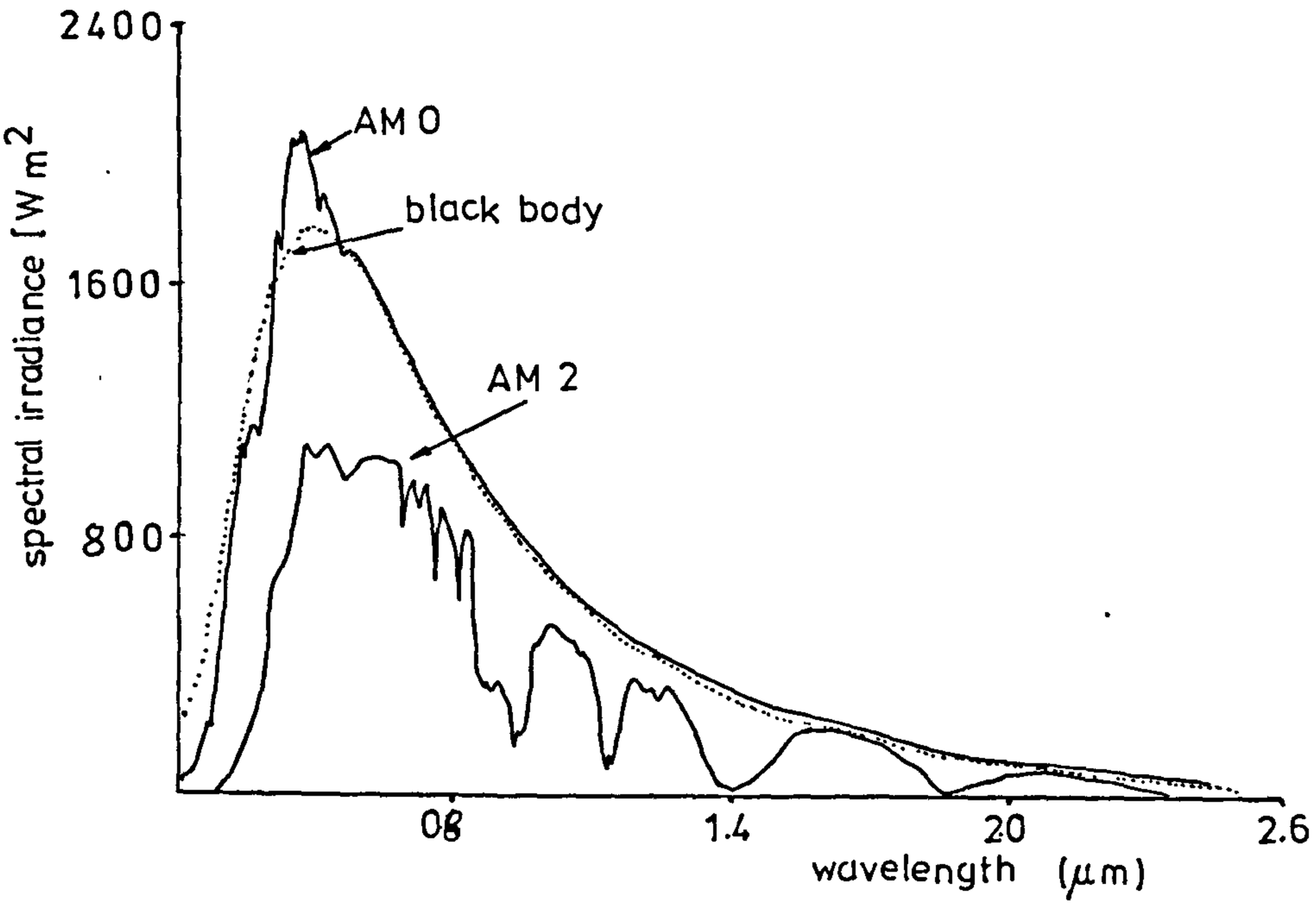

FIGURE 1.3 spectral irradiance curves for AM0 and AM 2 conditions and for a black body at 5762 K

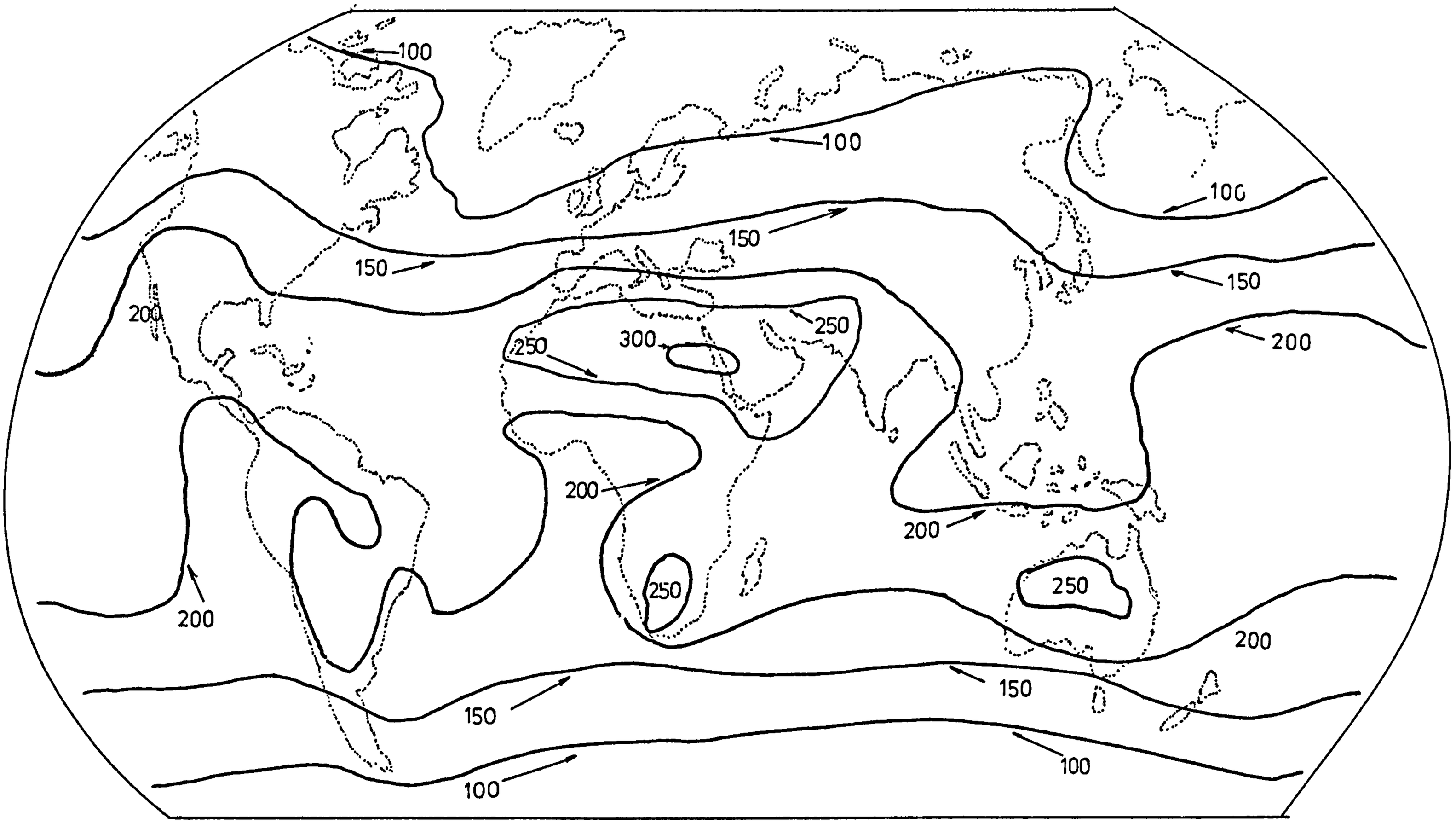

FIGURE 1.4 anuual mean global irradiance at the surface of the earth in Wm^{-2} averaged over 24 hours

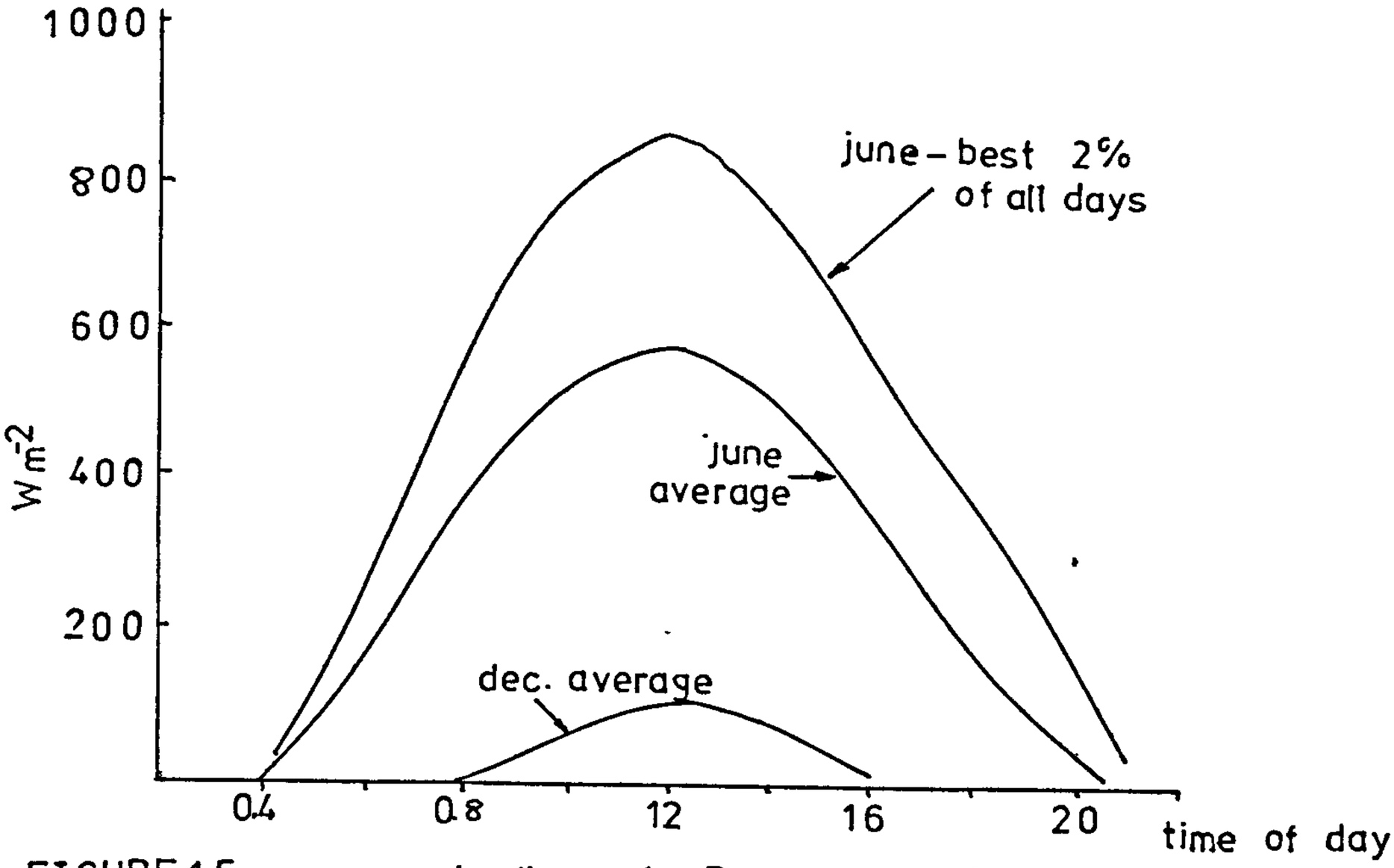

FIGURE 1.5 mean irradiance for December and June in Kew in the scuth of UK

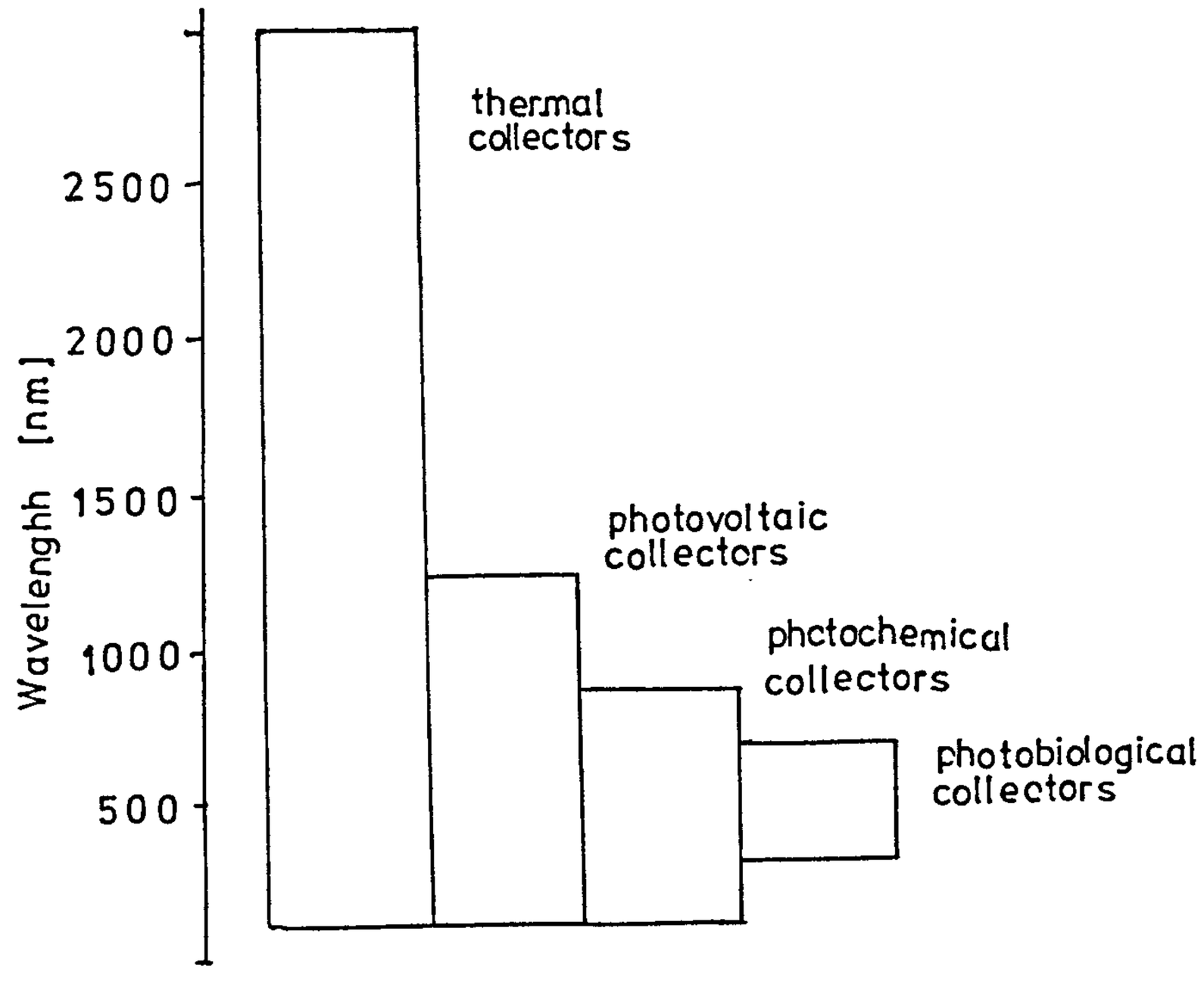

FIGURE 1.6 wavelengths potentially utilised by different solar energy collectors

ENERGY SOURCE	PRESENT KNOWN RANGE	RESERVES tonnes	LIFE AT 1971 RATE OF CONSUMPTION (YEARS)	LIFE AT FUTURE RATE OF CONSUMPT (YEARS)	POTENTIAL FUTURE RESERVES	LIFE AT 1971 RATES	LIFE AT FUTURE RATES
OIL	LOWEST	81.10^9	32	16	250.10^9	100	30
	HIGHEST	91.10^9	36	18	370.10^9	140	40
COAL	LOW	132.10^9	60	30	1100.10^9	500	150
	HIGH	2240.10^9	1000	190	4900.10^9	2200	250
URANIUM	LOW	$0.9.10^9$		16-75	$1.3.10^6$		20-75
	HIGH				$3.3.10^6$		37.75
SHALE TAR SAND	LOW	99.10^9	39	25	280.10^4	110	40
	HIGH	122.10^9	18	29	510.10^9	200	57
NATURAL GAS	LOW	$34.10^{12}m^3$	33	15	$90.10^{12}m^3$	90	25
	HIGH	$48.10^{12}m^3$	45	19	$340.10^{12}m^3$	330	40

TABLE 1.1 WORLDS FUEL RESERVES

TYPE OF FUEL	FUEL PRICE p/GJ in 1973 TERMS		RATIO OF PRICES AT 1973 AND 1990 IN TERMS OF 1973 PRICES
	1973	PROJECTED TO 1990	
COAL	20	52-58	26 - 2.9
CRUDE OIL	22	70-95	3.2 - 4.2
GAS	33	110-120	3.3 - 3.6

TABLE 1.2 UK FUEL PRICES TO MAJOR INDUSTRIAL USERS

(REF 4)

MEAN SOLAR IRRADIATION (SOUTH OF BRITAIN)	JAN	FEB	MAR	APR	MAY	JUN	JUL	AUG	SEP	OCT	NOV	DEC
AVAIL. SOLAR IRRA	204	3.92	7.62	11.54	15.56	17.37	15.82	18.62	10.02	5.69	2.80	1.69
DIFFUSE RADIATION	1.45	2.55	4.41	6.67	8.61	9.28	9.17	7.61	5.54	3.30	1.80	1.17
PERCENT-AGE D IFFUSE	71.1	65.1	57.9	57.8	55.3	53.4	57.9	55.8	55.3	57.9	64.2	69.2

TABLE 1.3 AMOUNT OF DIFFUSE SOLAR RADIATION IN SOUTH OF BRITAIN BASED ON PERIOD 1950-1974
IRRADIANCE IN $MJ/m^2/DAY$

2.1 HISTORY OF DEVELOPMENT OF PHOTOVOLTAIC CONVERTERS

The photovoltaic effect, i.e.the generation of current and voltage from light incident on a suitable structure, was first observed by Becquerel in 1839 when he detected a photovoltage in illuminated electrolytic cells. Later, in 1876 Adams and Day observed a true photovoltaic effect in a solid state Selenium structure, and in 1904 Hallwacks detected it in copper- cuprous oxide structures. Development of rectifiers and theories explaining the photovoltaic effect led to further improvement of these cells, so that the efficiency of Selenium photodetectors reached 1%. They were not intended or used as energy conversion devices but rather as light-meters and photodetectors. With the advent of silicon technology there were several attempts in fabricating silicon photodiode, but it wasn't until 1954 that an efficient (6%) device was produced[14]. In the same year a photovoltaic device in Cadmium Sulphide (CdS) was made [15], and two years later Gallium Arsenide (GaAs) cells were reported[16]. These discoveries led to the possibility of using the photovoltaic cells as solar energy conversion devices and several production lines were established[17]. But, in spite of the fact that by late fifties the efficiency in terrestriallight of silicon solar cell

reached 12%, they were unable to compete with fossil fuels. However, the great potential of solar cells as power generators for space projects was clearly demonstrated by the now famous Vanguard I satellite in 1958[17]. Since then, most effort has been concentrated on producing high efficiency devices for satellites, i.e. projects where cost was unimportant. Silicon solar cells were, by far, most well developed and arrays providing Kilowatts of power were not uncommon. In the sixties, work on Cu_2S-CdS thin film solar cells was intensified and it was only in 1967[18], thirteen years after the original discovery, that the mechanism of the photovoltaic effect in this cell was understood. These thin film cells were then of interest primarily because their power output to total weight ratio was favourable; a parameter of importance for space projects.

It was only in the recent years, in the seventies, that the development of solar cells for terrestrial applications became a real proposition. With this shift of interest the cost became a primary consideration , and more research was done on the development of low cost thin film solar cells. Interest was centered both on large area thin film cells and the devices working in conjunction with concentrators. New materials were developed for solar cell applications and a continuous effort was put into increasing the

efficiency of the existing ones. At present , a number of governments and companies have extensive programmes for research and development of solar cells for terrestrial applications[19,4], and photovoltaic power is becoming an increasingly possible solution to the energy problem.

2.2 PHOTOVOLTAIC CONVERTERS - PRINCIPLE OF OPERATION

The principle of operation of photovoltaic converters is in essence very simple. Considering only the solid state devices, the photovoltaic effect can be defined as the generation of charge carriers when incident radiation ionises the region in or near the built-in barrier of a semiconductor. The generated charge carriers are then swept over the potential barrier i.e. a current flows through the device and power can be delivered to a suitable load. The built-in potential barrier can be caused in a semiconductor by a semiconductor to metal junction, a simple p-n homojunction or a heterojunction. In each case the device behaves as a diode.

2.2.1 ELECTRICAL PROPERTIES

A detailed equivalent circuit for a solar cell under illumination has been described by Handy[20], Wolf[21] and others, but the most common simplified configuration is a current generator in parallel with

a diode, as shown in figure 2.1. The I-V characteristic of such a circuit is described by:

$$I = I_o \left[e^{q(V-IR_s)/kT} - 1 \right] + \frac{V-IR_s}{R_{SH}} - I_L$$

1.

$$\Rightarrow \ln\left[\frac{I+I_L}{I_o} - \frac{V-IR_s}{I_o R_{SH}} + 1 \right] = \frac{q}{kt} (V-IR_s)$$

where I_o is the leakage current of the diode whose value depends on the type of the junction and the material properties of the semiconductor,

I_L is the photogenerated current,

q is the electronic charge

T is the operating temperatures

k is Boltzman constant

R_s is the series resistance

R_{SH} is the paralell resistance

A plot of the above equation is shown in figure 2.2, together with the effect of series and shunt resistances. By a choice of an appropriate load (R_L) the device can be biased to operate under the maximum power conditions (V_{mp} and I_{mp}). Figure 2.2 also defines some of the basic figures of merit of a solar cell: open circuit voltage (V_{oc}), short circuit current (I_{sc}) and the fill-factor (FF). The fill factor describes

the squareness of the I-V characteristic and is defined as

$$FF = V_{mp}I_{mp} / V_{oc}I_{sc} \qquad 2$$

From equation 1 the expression for the power output of the cell is:

$$P = -IV = -I\left[\frac{kT}{q}\,\ell n\,(\frac{I+I_L}{I_o} - \frac{V-IR_s}{I_oR_{SH}} + 1) + IR_s\right] \qquad 3$$

Thus, from equation 3, for maximum power output, i.e. for optimum conversion efficiency a solar cell should satisfy the following requirements:

a. series resistance R_s should be low
b. parallel resistance R_{SH} should be high
c. leakage current I_o should be low
d. photogenerated current I_L should be high
e. operating voltage V should be high

All of the above conditions are reflected in the three basic parameters; open circuit voltage and short current which should be as high as possible, and the fill factor which should be close to unity, and all depend upon the basic material properties of a semiconductor.

2.2.2 MATERIAL PROPERTIES

Figure 2.3 shows a simple band diagram of a p-n homojunction under illumination. If the incoming photon energy ($h\nu$) is larger than the value of the forbidden band-gap (Eg), the photon is absorbed, i.e. an electron-hole pair is created. If the carrier life-time is sufficiently long, the photogenerated minority carrier diffuses to the junction where the built-in field sweeps it to the other side. Hence, the current (I_L) flows through the device. This simple diagram illustrates the photovoltaic effect and also defines most of the material requirements for a solar cell, such as the band gap (Eg), absorption coefficient (α), diffusion length (L), surface recombination velocity and cell geometry.

2.2.2.1 THE BAND GAP

Since solar radiation covers a spectrum of energies ranging roughly between 0.3 eV and 3 eV, a primary consideration for a photovoltaic converter is the choice of the semiconductor, i.e. the choice of the width of the band-gap. It is clear that only the photons with energies greater than the band-gap are going to be absorbed by the semiconductor. Consequently,

given the value of various electronic parameters such as the carrière life-time and surface recombination velocity, and given the geometry of a solar cell, short circuit current can be calculated from:

$$I_{sc} = q \int_{Eg}^{\infty} Q(h\nu)\, N_{PH}(h\nu)\, d\,(h\nu) \qquad 4$$

where $Q(h\nu)$ is the internal quantum efficiency and $N_{PH}(h\nu)d(h\nu)$ is the number of incident photons with energy $h\nu$ on the bandwidth $d(h\nu)$. It can be seen that a decreasing energy gap would render an increasing short circuit current. However, from figure 2.3 it can be seen that the built in voltage is:

$$V_{Bi} = q\, Eg - q(E_{fn} + E_{fp}) \qquad 5$$

where E_{fn} and E_{fp} are the depths of the fermi level from the conduction and valence band in the n and p type semiconductor respectively. This built-in barrier provides the e.m.f. for the circuit and is related to the open circuit voltage . Hence from equation 5 it is obvious that a decreasing energy gap would render a decreasing open circuit voltage. Thus, since the short-circuit current is directly proportional , and the open circuit voltage is inversely proportional to the band-gap width, an optimum value exists. For solar radiation, at AMO conditions (see App. I), this optimal value of the band gap can be easily calculated to be around 1.5 eV [22], as is shown

in figure 2.5. Thus, once the band gap is fixed the conversion efficiency is limited to about 45%[23,24] as is shown in figure 2.4. The optimal value of the band-gap shifts upwards with an increasing operating temperature [25] and with differing atmospheric conditions[26]. However these variations are only a few tenths of an eV.

2.2.2.2 THE ABSORPTION COEFFICIENT

By Lambert's law of absorption, for photons with energy ($h\nu$) greater than the band gap of the semiconductor :

$$\phi_x(h\nu) = \phi_o(h\nu)e^{-\alpha(h\nu)x} \qquad 6$$

where $\phi_x(h\nu)$ is the photon flux of energy $h\nu$ at a distance x from the surface of the semiconductor at which $\phi_o(h\nu)$ photons are normally incident. Consequently the rate of photogeneration of carriers at a point x in a semiconductor is given by

$$g(x) = \alpha(h\nu)\phi_o(h\nu)\, e^{-\alpha x} \qquad 7$$

The parameter "$\alpha(h\nu)$" is the absorption coefficient and is defined as the thickness of material necessary to reduce the incident photon flux by a factor of 2.718 (exponential e). It is a strong function of

energy of photons relative to the band-gap of the semiconductor and is shown for a few common semiconductors in figure 2.6. By definition and from equations 6 and 7, it is evident that if the absorption coefficient is high, the photons will be absorbed in a relatively small thickness of material. For direct semiconductors the slope of the plot of absorption coefficient versus the photon energy is very steep, as shown, and thus the absorption coefficient and therefore the absorption and generation rate is very high. Consequently in thin film solar cells, where the material thickness is typically microns or tens of microns, direct semiconductors are used. However this also means that the bulk of the absorption takes place close to the surface of the semiconductor and thus, for efficient collection of photogenerated carriers, the junction must be no further than a few diffusion lengths away from the surface. Therefore, the surface layer in a homojunction solar cell must necessarily be thin.

2.2.2.3 DIFFUSION LENGTH

The electronic parameter that bears most effect on the collection efficiency of the photogenerated carriers is the minority carrier diffusion length.

Carriers generated more than a diffusion length away from the potential barrier will recombine before they reach the junction. This is especially important in the indirect semiconductors where the generation of carriers takes place in a relatively wide region of the semiconductor. The minority carrier diffusion length can be controlled to an extent by the impurity concentration in the bulk of the semiconductor. In the direct semiconductors where the principle mechanism of recombination is direct band-to-band transition, the minority carrier life-time is inversely proportional to the majority carrier concentration and thus to the impurity density. In the indirect semiconductors recombination is essentially via the inter-band levels which are introduced by faults in the crystal lattice, including the doping impurities. Furthermore, scattering of the carriers, and thus the mobility is also adversely influenced by a high carrier concentration. Thus, a decreasing doping concentration leads to an increasing mobility and life-time of minority carriers, and therefore to an increasing diffusion length [27]. However, as can be seen from figure 2.3 and equation 5, a decreasing doping concentration leads to an increasing depth of fermi levels E_{fn} and E_{fp}, and thus reduces the value of the open circuit voltage. In addition, decreasing impurity concentration leads to an increasing bulk resistivity of the semiconductor which

reflects itself very strongly in the value of the series resistance of the cell. Therefore, the impurity concentration is a crucial parameter since it influences all three figures of merits of a solar cell; short circuit current via the diffuseion length, open circuit voltage via the size of the built-in barrier, and the fill factor via the series resistance. A typical compromise value of carrier concentration for most solar cells is of the order of $10^{23} m^{-3}$ ($10^{17} cm^{-3}$) resulting in about 0.1 Ωcm bulk resistivity.

Crystal imperfections also have an adverse effect on the minority carrier diffusion length and thus a good quality crystal is required for an efficient solar cell. In polycrystalline, thin films solar cells, it is the high density of crystal defects, such as grain boundaries, that limit the diffusion length and the overall conversion efficiency . In single crystal solar cells with good diffusion lengths higher doping concentrations can be tolerated, and the bulk resistivity can be made as low as 10^{-3} Ω m.

2.2.2.4 SURFACE RECOMBINATION

Carriers generated dose to the surface of the semiconductor may diffuse to the surface where they can recombine. For indirect semiconductors with low absorption coefficient, such as silicon, this

does not pose a very serious problem because the bulk of absorption takes place further away from the surface . However, for direct semiconductors, like GaAs, these surface recombination losses are significant. Consequently, GaAs homojunction solar cell is less efficient than Silicon, in spite of the fact that its predicted theoretical efficiency is better. This problem of significant surface recombination velocity can be avoided by the "window effect". If a heterojunction is made between two semiconductors, the top one having a sufficiently wide band-gap, most of the solar radiation will be transmitted through the surface layer, and the bulk of the absorption will take place in the narrow band-gap semiconductor, very close to the junction and away from the surface. Thus, the surface layer is transparent to the major portion of solar radiation and hence it is known as the window effect. Theoretical calculations [28] indicate that an idealised heterojunction has the potential of having higher conversion efficiencies than a homojunction. However, matching two semiconductors to form a good heterojunction poses additional problems.

2.2.2.5 SEMICONDUCTORS FOR HETEROJUNCTION SOLAR CELL

Since the value of the open circuit voltage of a heterojunction is largely determined by the narrower of the two band-gaps [29], the small band-gap should not be less than about 1.1 eV[30]. The larger band-gap value should exceed 1.5 eV to maintain the window effect. In order to avoid a discontinuity in the barrier itself, the impurity concentration and the electron affinity of the two semiconductors must be well matched. Furthermore, a large density of recombination centers in the junction resulting in a large leakage current can be caused by a mismatch of the lattice parameters. The leakage current has a strong effect on the open circuit voltage as can be seen from equation 1. in its idealised form with $R_S = 0$ and $R_{SH} = \infty$:

$$V_{oc} = \frac{kT}{q} \ln\left[\frac{I_L}{I_o} + 1\right] \qquad 8$$

Consequently, for photovoltaic applications, the two semiconductors forming a heterojunction must have lattice constants differing by no more than a few percent. These conditions, thus limit the number of possible compatible semiconductor pairs applicable to photovoltaic heterjunctions[31,32].

An alternative way of minimising the surface recombination velocity via the window effect is by using a graded-band-gap layer, i.e. instead of a single homogenios large band gap surface layer, a semiconductor whose band-gap decreases in the thickness direction can be used[29]. Such a structure would provide the window effect as well as an additional built-in field whose effect would be to increase the drift velocity and therefore the diffusion length of photogenerated carriers, thus increasing the collection efficiency. If the grading of the band-gap is controlled, the junction is effectively a homojunction and the density of the recombination centers is less than in a conventional heterojunction. The theoretical efficiency of such a structure is higher than that of any other configuration [30,33].

2.2.2.6 CONTACTS

The effect of contacts on the performance of a solar cell is also very marked because the resistance of the contacts can drastically reduce the fill factor. Making an ohmic, low resistance contact to the back of the solar cell doesn't pose much of a problem. However the top contact has to transmit light as well as to satisfy the electrical conditions. Initially, metal films thin enough to transmit most

of the light have been used, but the resistance of such films tended to be too high. The most common solution is to use a metal grid. For a good collection efficiency the spacing between the bars of the grid should be small, and the bars should be wide in order to maintain low resistance. However, the grid contact covers some of the active area of the solar cell and thus its area should be kept to a minimum. Therefore there is an optimum configuration of a grid, and it can be calculated [30]. It is also possible to use conducting transparent coatings, such as SnO_2 and In_2O_3 as a top electrode, but they have to be matched to the surface semiconductor in order to avoid a non-ohmic contact.

2.2.3 CONFIGURATION OF SOLAR CELLS

The configuration of a good solar cell can be deduced from all the above mentioned restrictions. For a simple p-n homojunction an indirect semiconductor with a band-gap close to 1.5 eV is required . The surface layer ought to be thin, in order to place the junction within a diffusion length from the region where the majority of absorption takes place. The base layer ought to be relatively thick and both back and front should be ohmic contacts in order to keep the series resistance low. The bulk

material should be low resistivity, good crystalline material doped to about $10^{23}cm^{-3}$. Typical of this type of cell is the Silicon homojunction cell.

For a heterojunction solar cell, the two semiconductors ought to have band gaps of about 1.1 eV and 2 eV. There lattice constants and electron affinities should be well matched. The impurity concentration should be around 10^{23} m^{-3} and, again, the choice of the contact material is vital. A good example of a heterojunction photovoltaic device is the CdS-InP solar cell or the $Ga_xAl_{1-x}As$-GaAs cell.

2.3 PHOTOVOLTAIC CONVERTERS - TYPES AND TECHNOLOGY

A number of different solar cells are in existence at present and each device has its own advantages and disadvantages. However, basically there are two types of cells; single crystal and thin film. Single crystal solar cells, such as Silicon (Si) or Gallium Arsenide (GaAs) devices have small areas and are expensive, but also have high conversion efficiency and are therefore attractive for space applications. The cost of single crystal cells is so high that, at present, they could be economically viable for wide terrestrial applications only when used in conjunction with solar concentrators. Thin film solar cells have limited conversion efficiencies due to poor material properties. But the techniques used in producing thin film devices can be readily adapted to mass production so that large area devices could be fabricated at more acceptable costs. Throughout the years, the development of photovoltaic devices for terrestrial applications has been aimed at reducing the cost of solar cells; firstly by improving the conversion efficiency, and secondly by improving the technology of production of cells.

2.3.1 SILICON SOLAR CELLS

Ever since the first silicon solar cell was made[14] there has been a continuous effort in improving its efficiency. The twenty years of research and development resulted in the increase of conversion efficiency from an initial 6% to around 15% (as demonstrated by the Comsatt non-reflection cell (CNR) in AMO illumination)[34]. The Silicon homojunction cell is understood better than any other cell and its efficiency has been brought closest to its predicted theoretical maximum of about 22% [35].

Due to the fact that modern semiconductor industry is dominated by Silicon, the technology for production of Silicon cells is well developed. The basic single crystal material used for Silicon cells has been grown by a number of methods and the barrier has been formed by diffusion, ion implantation and epitaxy. The choice of the crystal growth method and barrier formation technique is made by various considerations such as the desired output, environmental properties, radiation resistance and cost factors. Antireflection coatings, encapsulating techniques and methods of interconnecting the cells into arrays have all been perfected for Silicon devices. A summary of cell fabrication parameters is given in table 2.1.

2.3.1.1 SILICON SINGLE CRYSTAL HOMOJUNCTION CELLS

Various methods have been developed for improving the performance of Silicon homojunction cells. The incorporation of an electric field in the bulk Silicon resulting from an impurity gradient was shown to increase radiation resistance [36,37]. The provision of a 'back surface field' (BSF) i.e. a retarding field near the back contact increased the collection efficiency by reducing the back surface recombination[38,39]. Finer control of doping led to an increase of carrier lifetimes and to an improvement of open circuit voltage [40]. New dopants such as Lithium[41] and Alluminium [42] have been found to improve the radiation resistance of the cells. Placing the junction closer to the surface (less than 0.3 μm) [43], elimination of a 'dead layer' at the surface caused by high concentration of diffused dopants, and refinement of the grid contact, all improved the short wavelength response (violet cell) which has previously been limited to about 0.3 μm wavelength[44]. Suitable texturing of the surface was found to promote multiple interactions between the light and the surface, thus reducing the reflection losses [34]. The antireflection coatings [45] and various encapsulating methods further improved the performance of the Silicon solar cell.

Silicon homojunction solar cells with new geometries have also been researched. A vertical multijunction cell (VMJ) has been developed [46,47] where a series of interconnected p-n homojunctions, grown perpendicularly to the surface of the wafer, is illuminated from the side, contrary to the conventional front wall illumination. This configuration of a solar cell gives high voltage and low current output, has good performance with highly concentrated light and is resistant to particle irradiation [48]. A "grating" solar cell where the surface layer is not continuous but consists of a grid of appropriately doped silicon, showed improved collection efficiency, especially with carriers excited by the blue wavelengths, and requires less thermal treatment than a conventional cell [49,50].

Thus , the work on the Silicon homojunction solar cell has been very intense, resulting in the fact that this type of the cell has been developed almost to the maximum and is the most used cell for the space projects.

2.3.1.2 LOW COST SILICON SOLAR CELLS

In spite of the fact that silicon is one of the most abundant materials on earth, the cost of Silicon devices at tens of pounds per Watt output is two orders of magnitude too high to make conventional

Silicon single crystal photoconverters competitive with other energy sources for terrestrial applications. This is mainly due to the fact that the production of single crystal wafers of Silicon is a multi-step costly process. Consequently, alternative approaches in fabricating solar cells based on Silicon have been developed. Since processing of Silicon resulting in dislocation - free wafers costing about £1000/m^2, which is acceptable for complex semiconductor devices, is far too costly for any large area devices, efforts to by-pass or improve this processing have been made. Calculation show that an adaptation of conventional Czozralski pulling technique to grow larger diameter ingots at higher speeds can appreciably reduce the cost of the finished solar cells [51]. Development of metal - semiconductor (Schottky barrier)[52] or metal-insulator-semiconductor (MIS)[53] types of devices could reduce the cost of Silicon based cells by avoiding the diffusion doping process, while still maintaining relatively high efficiencies[54]. Heterojunction cells using monocrystalline or polycrystalline Silicon as the base material have also been made and the Tin Oxide-Silicon (SnO_2-Si) single crystal solar cell, while cheaper to fabricate than the homojunction cell, has an efficiency of about 10% [55]. Attempts to produce large area Silicon films by sputtering [56], vacuum deposition [54] and chemical vapour deposition [58] on substrates such

as graphite, sapphire or metallurgical Silicon have resulted in working polycrystalline Silicon cells. However, these devices showed efficiencies of only a few percent. Solar cells fabricated from zone-melted Silicon rods [58], from amorphous Silicon [60] and from upgraded metallurgical Silicon have also been investigated and seem promising. Polycrystalline Silicon cells produced by 'casting' methods are commercially available at quite acceptable costs. Another promising method of reducing the cost, while maintaining the efficiency, of Silicon cells is the growth of Silicon ribbons, directly from the melt, which by'passes the costly processes of cutting, lapping and polishing of wafers, associated with Czozralski pulled ingots. There are several methods of growing Silicon wafers, namely the 'dendritic web technique' [61], the 'Stepanov technique' [62] and the "edge-defined film-fed technique (EFG)" [63], the latter being the most promising. Growth of Silicon ribbons from the melt is still in the development stage but relatively large slices (1.3 m by 0.012 m) of useful thickness (500μ) and with electrical characteristics suitable for solar cells (life time of about 100 μs, resistivity less than 10Ω cm) have been grown , resulting in solar cells with efficiencies of approximately 8% AMO[64].

2.3.2 GALLIUM ARSENIDE SOLAR CELLS

Ever since the original demonstration of the photovoltaic effect in Gallium Arsenide (GaAs)[16], the solar cells made out of this material were seen as possible improvements over Silicon cells, In spite of the fact that GaAs is not nearly as abundant a material as Silicon, and that the development of its technology is inferior to Silicons, GaAs is an attractive semiconductor for solar energy conversion because the value of its band gap is close to the theoretically predicted optimum (figure 2.5) and because as a direct material it has high absorption coefficient (figure 2.6). However, initial practical results with a p-n GaAs homojunction were disappointing with conversion efficiency of less than 10%. The interest in GaAs solar cells returned after calculations showed that its poor performance was mainly due to large surface recombination losses[65]. Treatment of the surface could not sufficiently reduce these losses which are high because GaAs is a direct semiconductor. However, the use of the window effect in GaAs based heterojunction cells did reduce these losses by so much that GaAs based cells are more efficient energy converters than silicon cells.

2.3.2.1 GALLIUM ARSENIDE HETEROSTRUCTURES

Several heterojunction structures with GaAs as the base material have been made, but the most notable of these is the p-Gallium Alluminium Arsenide ($Ga_xAl_{1-x}As$) - n GaAs device, where the surface layer consists of a solid solution of about 20% GaAs and 80% AlAs (x=0.2). Such a solid solution is a semiconductor with an indirect band gap of 21 eV and a direct band gap of 2.6 eV, and is thus suitable as a window material. In addition, the lattice constant of $Ga_{0.2}Al_{0.8}As$ is very well matched to the GaAs lattice so that the density of interface states is low. The cell performance is promising, since it demonstrates high short circuit current and open circuit voltage, due to the widths of the band-gaps and reduced surface losses, and low series resistance due to the fact that thicker surface layer (1μ) does not decrease the minority carrier collection. Consequently, using practical values for various parameters, calculations predict that the $Ga_xAl_{1-x}As$-GaAs cell can be 27% efficient in AMO illuminations, and already, only a few years of development have resulted in a 14% efficient device [66]. Due to its great potential this cell has recently commanded a lot of attention [67,68,69] and new techniques are being developed[70,73] for growth of large area devices.

Pure Alluminium Arsenide (AlAs) is a semiconductor with an indirect and direct band gap of 2.15 eV and 2.9 eV respectively, and is thus also suitable for a window material. Epitaxial AlAs surface layers grown on GaAs base layers have resulted in structures with conversion efficiency of 13.5% AMO [72]. Thin films AlAs on GaAs cells made by vapour phase deposition on graphite substrates, have shown good transport properties, but poor overall conversion efficiency due to the high resistance of the AlAs layer caused by grain boundaries[73]. Attempts at using even wider window materials, such as Tin oxide (SnO_2) have also been made [74].

An alternative way of using the window effect is via a graded band gap surface layer where $Al_xGa_{1-x}As$ solid solution with the value of the composition parameter 'x' varying in the thickness direction forms the surface layer for a GaAs base. (figure 2.7). Theoretically, this structure should achieve the best conversion efficiency and is currently being investigated[75,76].

For terrestrial applications, GaAs based solar cells seem even less feasible than Silicon devices. However GaAs cells have reached efficiences of 23% with concentrated AM1 light [77] and with suitable design of cells, concentrators and tracking mechanisms, they may become economically competitive in some geographical locations.

2.3.3 CADMIUM SULPHIDE SOLAR CELLS

Cadmium Sulphide (CdS) is a wide band gap (2.4 eV) direct semiconductor. Since it is a compound semiconductor consisting of elements from groups II and VI in the periodic table of elements, CdS has a degree of ionicity sufficiently large for most of the properties of the single crystal material to be maintained in thin films. Consequently, due to the fact that the technology of preparation of thin films readily lends itself to the fabrication of large area devices, it is this ability of maintaining good electronic properties in thin films that makes CdS an attractive material for photovoltaic conversion. In addition, its wide band gap makes CdS a good window material for heterojunctions and Schottky barrier devices. The photovoltaic effect in CdS was first detected in single crystal Schottky barriers [15] but most of the subsequent work was done with thin film CdS. Initially a variety of Schottky barrier CdS solar cells were investigated primarily because they had the potential of having good power output to module weight ratio and because CdS was more resistant to nuclear radiation than Si. However, the conversion efficiency of this cell was small. Subsequently, a variety of heterojunctions with better conversion efficiencies were developed.

2.3.3.1 COPPER SULPHIDE - CADMIUM SULPHIDE SOLAR CELL

Copper Sulphide (Cu_2S) - CdS solar cell was the first, and up to date the best developed thin film solar cell. The Cu_2S layer can be formed on single crystal wafers or polycrystalline vacuum deposited films by dipping CdS for short period of time (5s) into a hot (90°C) Copper Chloride (CuCl) solution. Ion exchange takes place and a layer few hundred monolayers thick of degenerate p-type Cu_2S is formed on top of the CdS. This layer is thin enough so that there is no loss of efficiency when the cell is operated in the "front wall mode" i.e. when the narrow band gap (about 1.4 eV) Cu_2S is the surface layer on the illuminated side. Thus, in this case, due to the fact that the junction is so near to the surface, the window effect does not offer any advantages. This type of a cell was initially developed to average efficiences of around 5% mainly by empirical methods, and a review of this early development was given by Shirland in 1966 [78]. Unlike in Si solar cell, the mechanism of the photovoltaic effect in the Cu_2S-CdS cell was not clearly understood. Unexplained phenomena like the cross-over of the light and dark current - voltage characteristics, the generation of photocurrent by photons of energies less than the band gap of CdS, instabilities in the

performance etc. were observed. Several models developed [79,80] to explain some of this behaviour were found incomplete. In 1968, however, Shiozawa et al. [18] demonstrated that the bulk of photogeneration takes place in the Cu_2S layer, which was previously seen more as a metal layer than a semiconductor. The cross-over of the I-V characteristics, the photocapacitance and the optical degradation phenomena were explained by a presence of a set of interface states that stimulated tunnelling [81,82]. Thus a model of the Cu_2S-CdS cell evolved (figure 2.8) but new modifications are still made [83]. Subsequent development did not result in a substantial increase of conversion efficiency, which has been brought up to about 7% to 8% [84], but rather on a much improved stability of the cell and lower fabrication cost.

The performance of the Cu_2S-CdS solar cell was found to deteriorate when the device was operated in atmospheric conditions. This was due to the oxidation of the Cu_2S layer [85,86] resulting in copper deficiency and/or precipitation of metallic copper rendering $Cu_{1.8}S$, $Cu_{1.9}S$ and $Cu_{1.96}S$ rather than the stoichiometric Cu_2S [87]. Better control of the formation of Cu_2S layers was found to solve this problem and to improve the cell stability. Improvement of the CdS layers by finer control of the vacuum deposition process used to evaporate the semiconductor

films, resulted in further improvement of the performance and stability of this cell [88,89]. Optimisation of geometry and method of formation of the grid electrode and development of the incapsulation process [90] also improved the cell. At present, a life-time of 15 to 20 years of operation under terrestrial conditions can be expected for the Cu_2S-CdS thin film solar cells [84]. With this improved stability the Cu_2S-CdS solar cell appears more attractive for terrestrial applications, because the processes used to fabricate it are suited for mass production; especially the dip method of formation of Cu_2S layer. Attempts to avoid the relatively costly vacuum deposition of CdS were made by depositing semiconductor films by screen printing[91], chemical bath deposition [92] or gas transport reactions[93]. The most notable method of further reducing the cost of the Cu_2S-CdS solar cell is by spraying some, or all of the layers of the cell [94,95,96]. Spraying of a suitable mixture of liquid chemicals (thiourea and CdCl) onto a hot substrate (400°C to 600°C) results in a chemical reaction which deposits polycrystalline CdS films of good quality. A comprehensive review of the development and potentials of the Cu_2S-CdS cell has been published by Stanley in 1975.[97]. Thus, the Cu_2S-CdS solar cell, in spite of its relatively low efficiency, at the moment seems the solar cell most likely

to be mass produced for terrestrial applications, and a number of experimental solar houses using this type of cells already do exist[98].

2.3.3.2 CADMIUM SULPHIDE-INDIUM PHOSPHIDE SOLAR CELL

Unlike the Cu_2S-CdS solar cell, the CdS-Indium Phosphide (InP) device has not been developed by empirical means. A survey of various semiconductors indicated that InP, a III-V semiconductor with a direct band gap, was well suited for photovoltaic conversion [31]. Its band gap at 1.35 eV is close to the theoretical optimum, and being a direct semiconductor the absorption lengths are short and hence the requirements for the minority carrier diffusion length are not particularly critical. Moreover, in spite of the fact that it has a zincblende type of crystal structure, its lattice parameter (5.869 Å) can be matched to that of cubic CdS (5.850 Å) to within 0.3%, implying that the interface ought to be dislocation free. Furthermore, the electron affinities of CdS and InP are such that there is no interface discontinuity in the junction. Thus, a p-type InP with an n-type CdS window can be an almost ideal heterojunction pair for solar energy conversion. Devices, prepared by a two source vacuum evaporation of CdS onto Czozralski pulled single crystal p-type InP wafer, had conversion efficiency of 12.5% AM2[99].

This high conversion efficiency is due to both, the fact that the internal quantum efficiency, i.e. the number of carriers generated by each absorbed photon for InP-CdS cell with an anti reflection coating (SiO) is around 90% , and that the spectral response of the cell is quite wide due to the widths of the two band-gaps. The optimisation of the thickness of the CdS layer and the use of the "close space" technique, rather than vacuum evaporation, to grow CdS, rendered 14.4% AM2 efficient cells [100]. Furthermore , this structure is stable so that its life-expectancy of operation under normal atmospheric conditions is quite high [108]. Attempts have been made to reduce the cost of this cell by producing a wholly thin film device by chemical vapour deposition of InP into Molybdenum substrates [102], but the performance of the resultant cells was poor.

The InP/CdS solar cell is relatively new and not fully developed yet. Maximum conversion efficiences of 17% AM2 are expected [99] and of those cells can be made at less cost than Si or GaAs devices, this type of cell could perhaps even be used for terrestrial applications.

2.3.4 TERNARY SEMICONDUCTOR CELLS

Several ternary I-III-VI_2 semiconductors, i.e. materials constituted from elements from groups I,III and VI in the periodic table of elements have properties suitable for photovoltaic conversion. The most notable of these are the copper indium di-selenide ($CuInSe_2$) , copper indium di-telluride ($CuInTe_2$) and copper indium di-sulphide ($CuInS_2$), all of which have lattice constants and electron affinities which are compatable with those of CdS so that they could form good base materials for CdS heterojunctions.

$CuInSe_2$ with a direct band gap of around 1 eV[103] and a lattice mismatch with CdS of 1.2% in the most developed of the ternary semiconductors. Initial investigations of CdS-$CuInSe_2$ heterojunctions were encouraging. Junctions were made by vacuum evaporation of CdS onto $CuInSe_2$ (doped p-type by annealing in Selenium vapour) crystals prepared by melt growth from stoichiometric mixture of the constituents. Samples yielded AM2 efficiency in excess of 10% [106]. However, it appears that $CuInSe_2$ crystals tend to form microcracks and are unstable. Nevertheless thin films of $CuInSe_2$ have been prepared[104] implying that thin film structure is possible.

$CuInTe_2$ is more stable than $CuInSe_2$ and this is more attractive for photovoltaic conversion. Thin films of $CuInTe_2$ have been investigated and the results indicate that fairly good thin films (mobility $\mu \sim 12\ cm^2V^{-1}s^{-1}$) can be obtained in p-type doping by fast evaporation of the material onto a suitably heated substrate[105].

$CuInS_2$ has a larger band gap than either CuInSe, or $CuInTe_2$ at approximately 1.5 eV. This ternary semiconductor can also be prepared in both p- and n-types so that a homojunction cell in this material may be made. Theoretical efficiency of a $CuInS_2$ homojunction cell is as high as that for GaAs cell at 28%. However the thin film samples prepared from $CuInS_2$ had initial conversion efficiences of only 3% [106].

2.3.5 CADMIUM TELLURIDE SOLAR CELL

Cadmium Telluride (CdTe), like CdS, is a II-VI semiconductor and is thus a material suitable for thin film solar cells. Like CdS, it is a direct material and therefore has high adsorption coefficient. Its band gap at about 1.5 eV is almost ideal for solar energy conversion. However, like on GaAs, which is also a direct, narrow band gap semiconductor, the surface recombination losses in CdTe are prohibitably high for efficient solar energy conversion. Consequently,the p-n homojunction solar cells, made by diffusion of p-type dopant into an n-type single crystal of CdTe, resulted in initial 4% [107] and subsequent 6% [108] conversion efficiency in direct

terrestrial sunlight. In spite of the fact that the spectral response of these cells was good, the efficiency could not be increased due to the surface losses. Thus, as is the case with GaAs, CdTe can be used only in heterojunction type of solar cells.

2.3.5.1 COPPER TELLURIDE-CADMIUM TELLURIDE SOLAR CELLS

The Copper Telluride ($Cu_{2-x}Te$)-CdTe solar cell is similar to the Cu_2S-CdS device in the sense that like in the Cu_2S-CdS cell, the $Cu_{2-x}Te$ layer is a degenerate p-type semiconductor formed by dipping CdTe into a hot cuprous solution. The substrate CdTe could be an n-type single crystal wafer or thin film prepared by vapour reaction on top of a highly conducting layer of CdS which served as a back contact [109]. However, unlike in the CdS cell, the bulk of the photogeneration of carries takes place in CdTe layer. Thus , the main role of the $Cu_{2-x}Te$ layers is to decrease the surface losses and form the junction. Conversion efficiencies of 6% for thin film samples and 7½% for single crystal samples were accorded for this type of cell in terrestrial light. Cells prepared in an analagous way except that the $Cu_{s-x}Te$ layer was formed by flash evaporation, resulted in a similar performance [110]. However, both types of cells were unstable due to oxygen-induced traps in the interface between the $Cu_{2-x}Te$ and the CdTe layers [111]. Ionic bombardment cleaning of the surface of CdTe, prior to flash evaporation, followed by thermal assisted diffusion

of Copper, from Cu_2Te into ClTe, resulted in stable cells with average efficiencies of around 6% [112]. A similar cell was made by spraying a Cu_2S layer on top of CdTe [113], and the performance was quite similar to that of the Cu_2Te-CdTe cells.

2.3.5.2 CdS - CdTe SOLAR CELL

An n-type CdS window on top of p-type CdTe base, heterojunction device is an attractive structure for photovoltaic conversion because both materials lend themselves to the thin film technology, and their band-gaps at 2.4 eV and 1.5 eV respectively are well suited for solar energy conversion. In spite of the fact that the CdS-CdTe pair has a crystal mismatch of 9.7% , it appears to be the best available combination of the II-VI semiconductors for photovoltaic conversion [114]. Initial experimental samples were quite encouraging with conversion efficiency of around 4% [115] with simulated 50 mW/cm^2 solar light. Subsequent systematic development of this type of cell resulted in 8% efficient devices. A number of different deposition techniques have been tried for preparation of the CdS-CdTe devices, namely the "close-space" vapour deposition (CSVT) in H_2 gas, vacuum deposition from two sources and spray pyrolises [16] . All thin film cells on crystalline or amorphous substrates and cells grown by deposition

of one component onto the single crystal wafer of the other component, have been investigated. The spray pyrolises technique where CdS is deposited onto single crystals of CdTe resulted in, on average, 6% efficient devices. A modification of this structure, where a wider band gap solid solution such as $Zn_xCd_{1-x}S$ replaces CdS as the window material should result in an improvement of the maximum theoretical efficiency from 17% for pure CdS to 23% for a suitable mixed $Zn_xCd_{1-x}S$ [114]. It was also determined that mixed films of $Zn_xCd_{1-x}S$ may be deposited by the spraying technique[137].

The CdS-CdTe heterojunction solar cell could possibly be improved by replacing the CdS layer with a graded band gap CdS_xTe_{1-x} semiconductor, in a similar fashion as the Ga_xAl_{1-x} As-GaAs heterojunction cell could be improved by use of a graded band gap $Ga_xAl_{1-x}As$ layer. However, initial experimental results did not indicate this. Further discussion of this structure follows in the following chapters.

2.3.6 OTHER SOLAR CELLS

In recent times a number of new materials have been considered for use in photovoltaic converters, mainly in order to reduce the cost of solar cells sufficiently so that they may become commercially competitive source of energy. The most notable of

the new approaches are the copper-copper oxide devices and the devices using organic semiconductors.

The copper-copper oxide (Cu-Cu_2O) combination forms a Schottky barrier. Cu_2O is a semiconductor with a direct band gap of 1.95 eV and it has been widely used in the 1930's and 1940's. Since, the semiconductor layer and the barrier can be formed in a single step by oxidation of copper sheets, it could be possible to produce these cells at a realtively low cost. At present the conversion efficiencies of these devices are low, but with improved technology and understanding, the efficiency may be substantially increased[118].

The use of some organic compounds, which behave as semiconductors when they polymerise, offers an exciting possibility for creation of a new type of a very cheap solar cell. Substantial research has been carried out in this field since, even at conversion efficiency as low as 2% AM1 their organic cells could be much less costly than any other photovoltaic device [119]. At present, a metal to organic semiconductor Schottky barrier is the most common structure and usual conversion efficiences are less than 1% [120]. However, it may be possible to develop more efficient p-n homo-or heterojunctions.

2.4 CONCLUSION

It has been stated above that the research and development in the field of photovoltaic energy conversion has two goals; firstly to produce solar cells with better conversion efficiences and, secondly to produce solar cells at lower cost.

At present, with improved existing technology and the development of new types of cells conversion efficiency of around 20% AMO seems possible. However, totally new approaches may improve this figure. For example, the use of an appropriate photoluminescent material as a filter in front of a photovoltaic converter would improve the overall conversion efficiency of the system.by converting very energetic photons i.e. photons with energies much larger than the band gap of the semiconductor, into a greater number of less energetic photons, which would result in larger short circuit currents.

Reduction of the cost of the solar cells for terrestial applications could also be achieved by further development. Adaption of new technology, such as for example the spraying of the semiconductors, would result in a decrease of the cost of solar cells. The storage systems used in conjunction with solar cells also add greatly to the cost of terrestial solar power. This may be by-passed by coupling solar arrays with existing electric grid networks [121].

In any case, the need for further development is accepted and research programmes are carried out by many companies and governments.

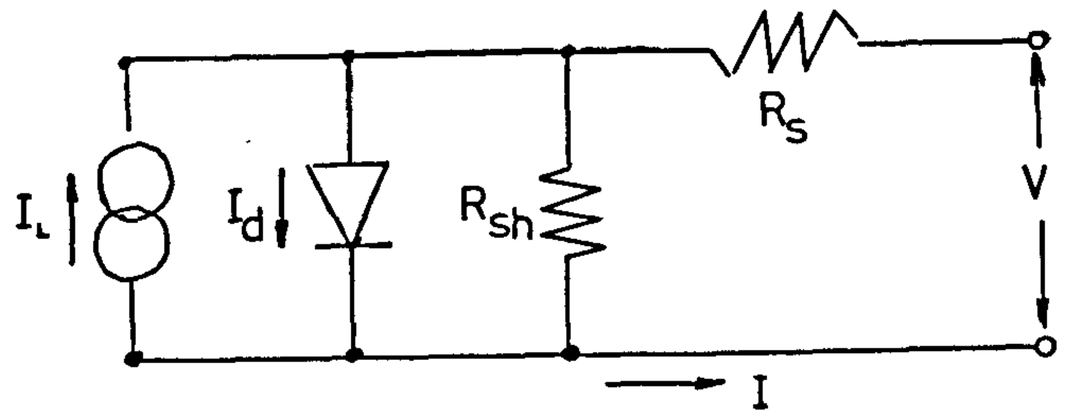

FIGURE 2.1. Equivalent circuit of a solar cell

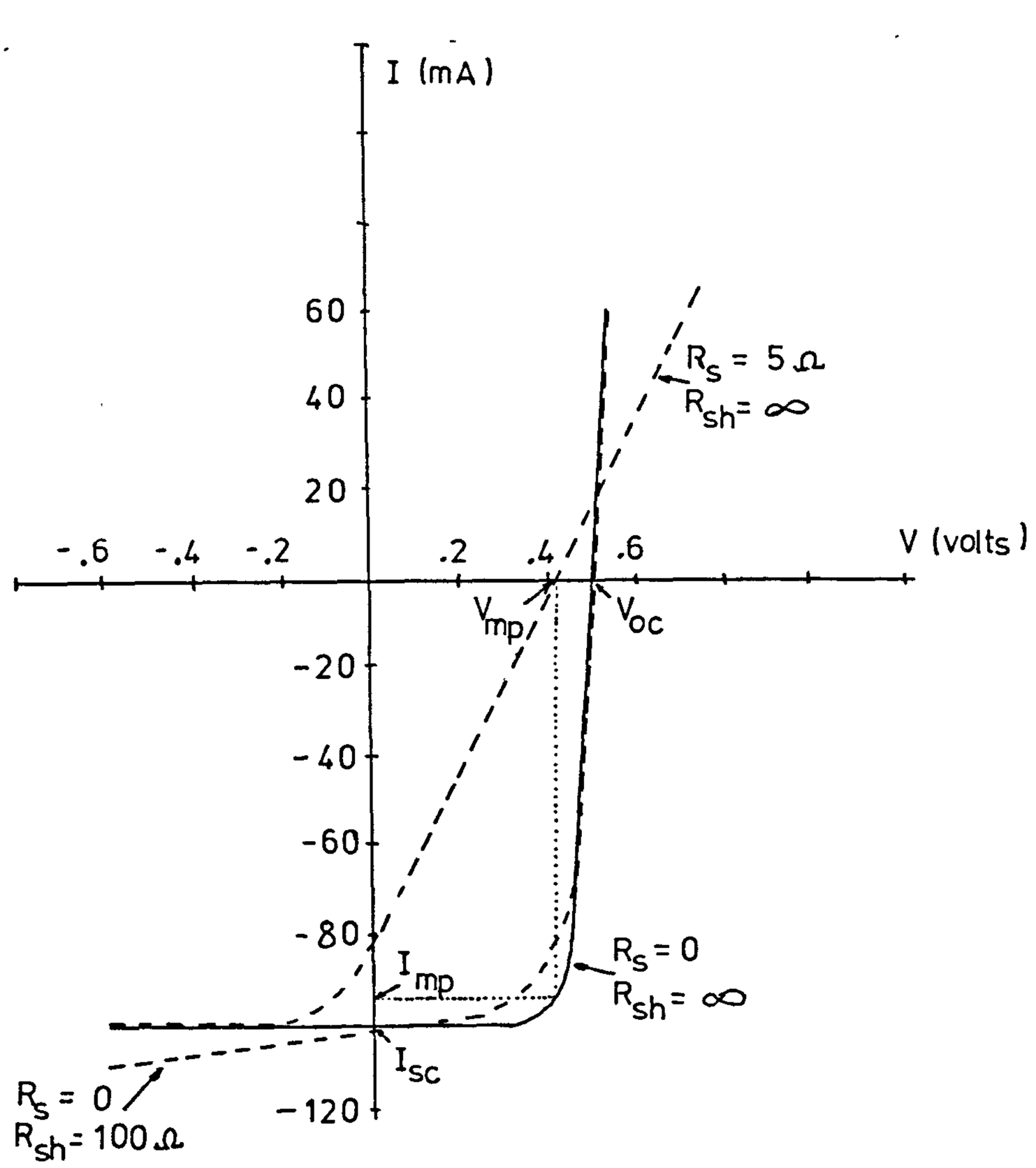

FIGURE 2.2 . I-V characteristic of a solar cell

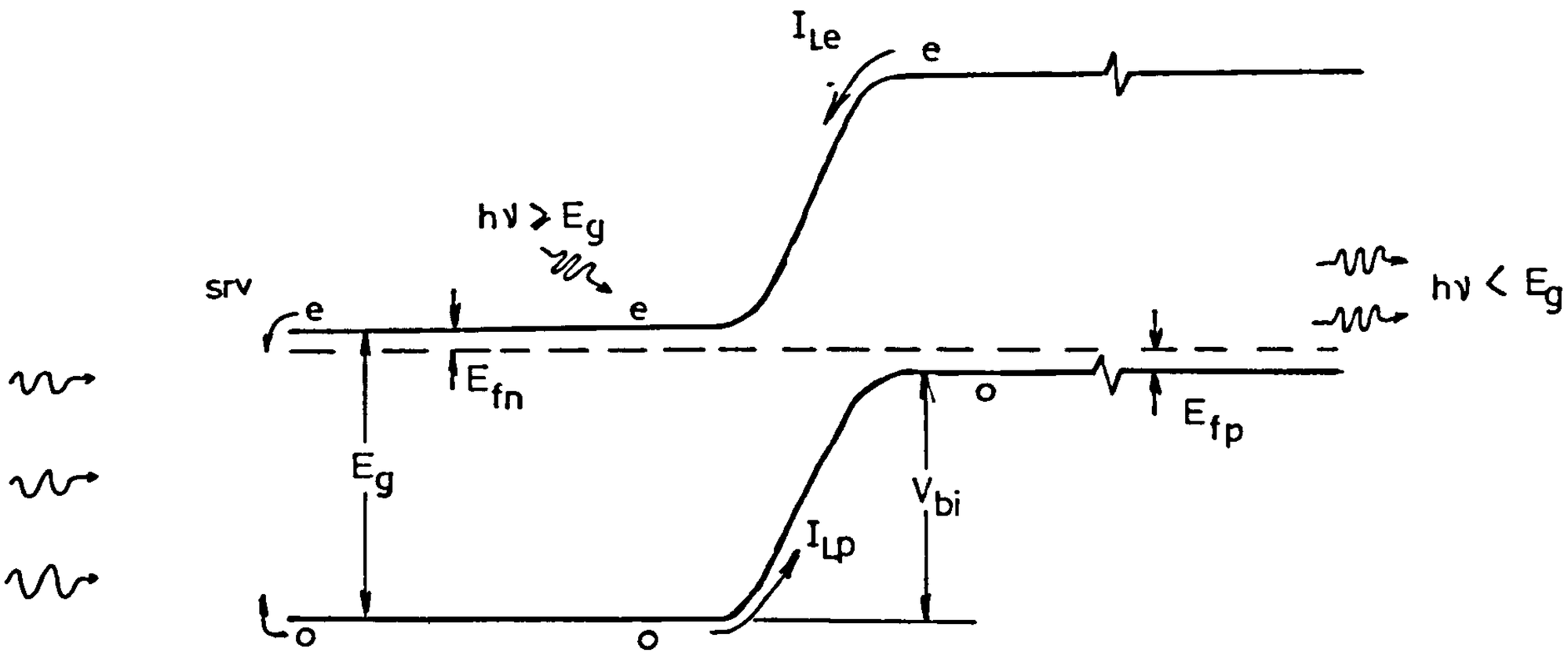

FIGURE23 . A p-n junction under illumination

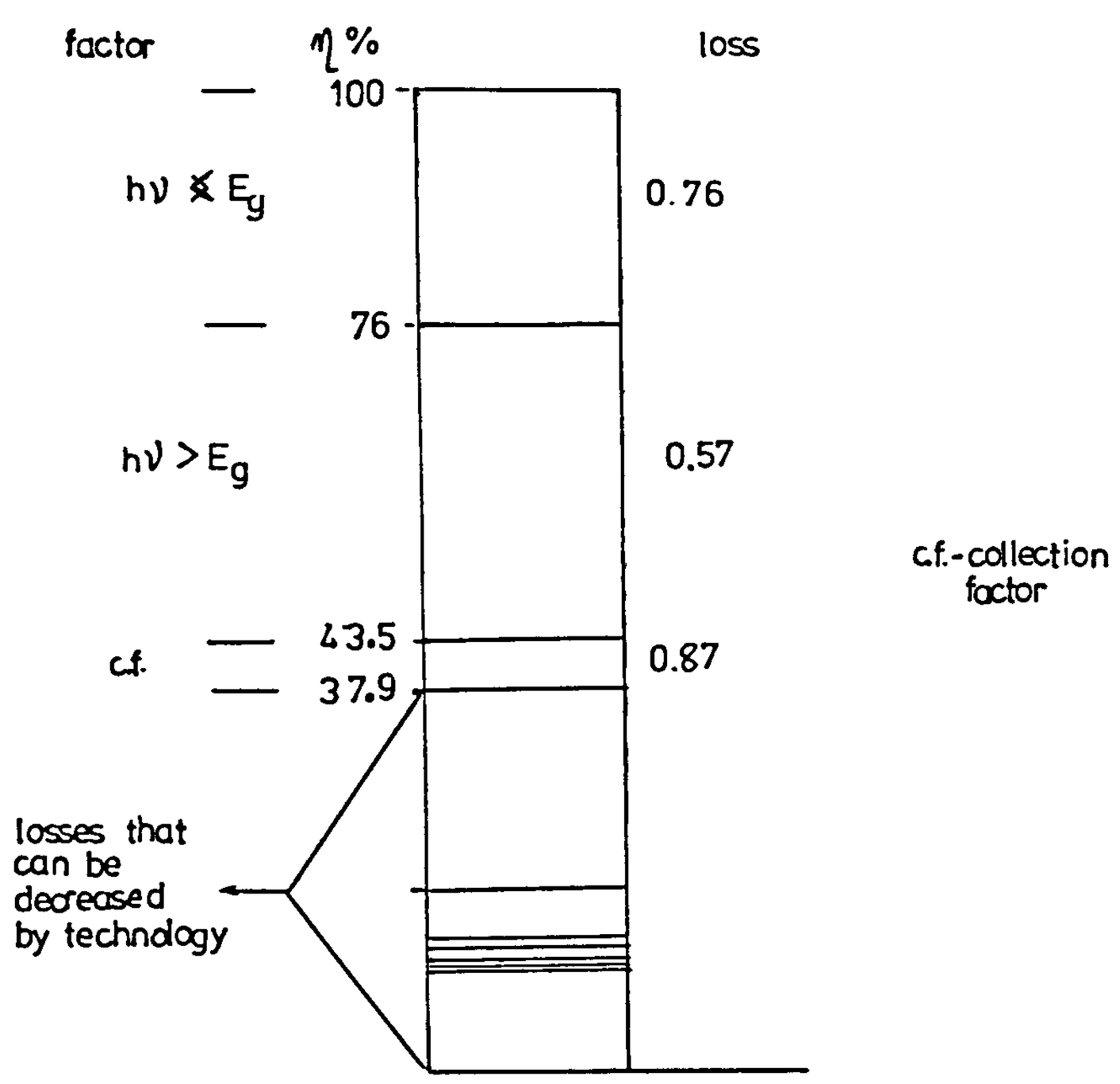

FIGURE 24 . A bar diagram representing the losses of a Si solar cell (ref 17)

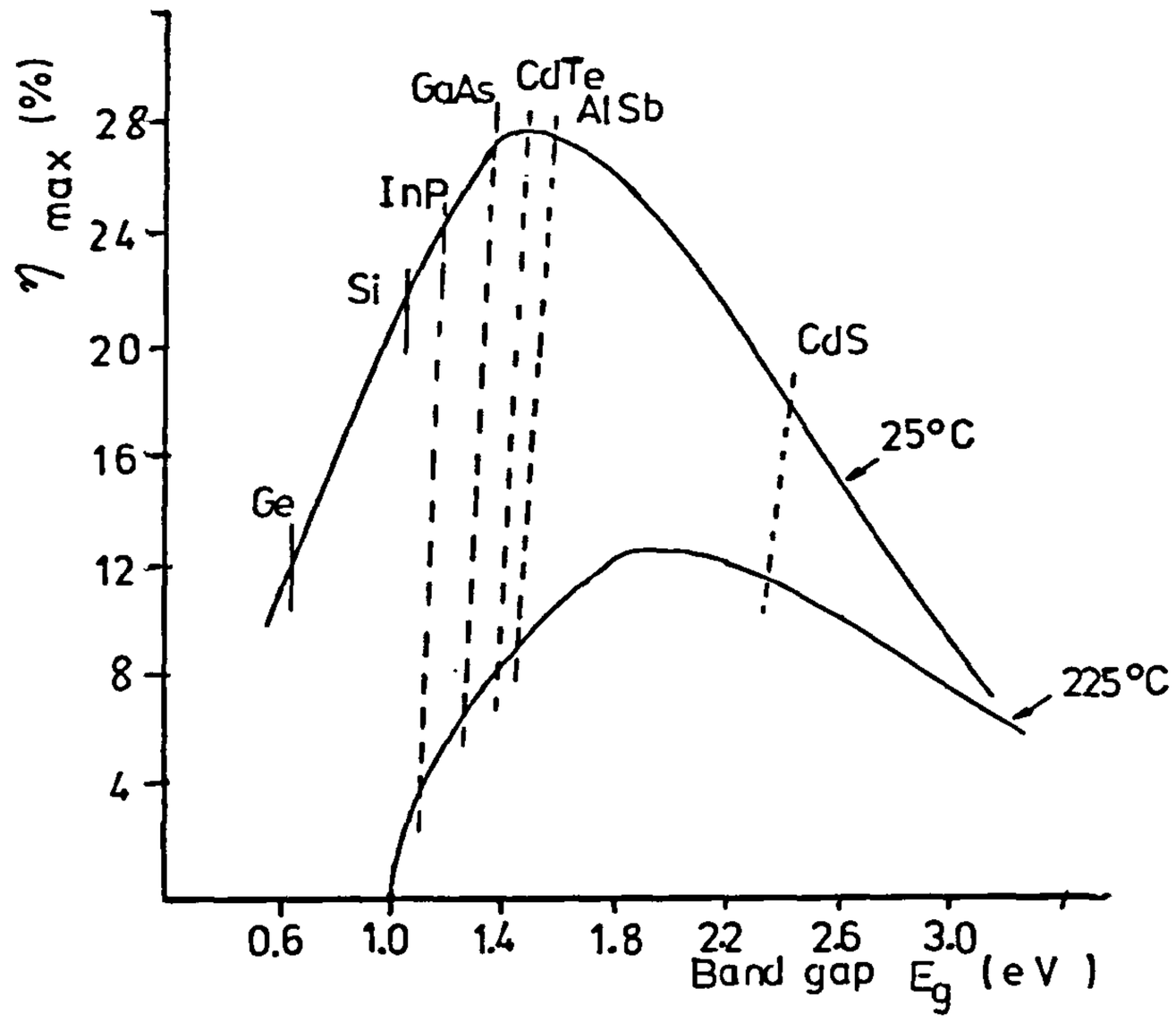

FIGURE 2.5 . Maximum efficiency η_{max} as a function of energy gap E_g at 25 and 225 °C

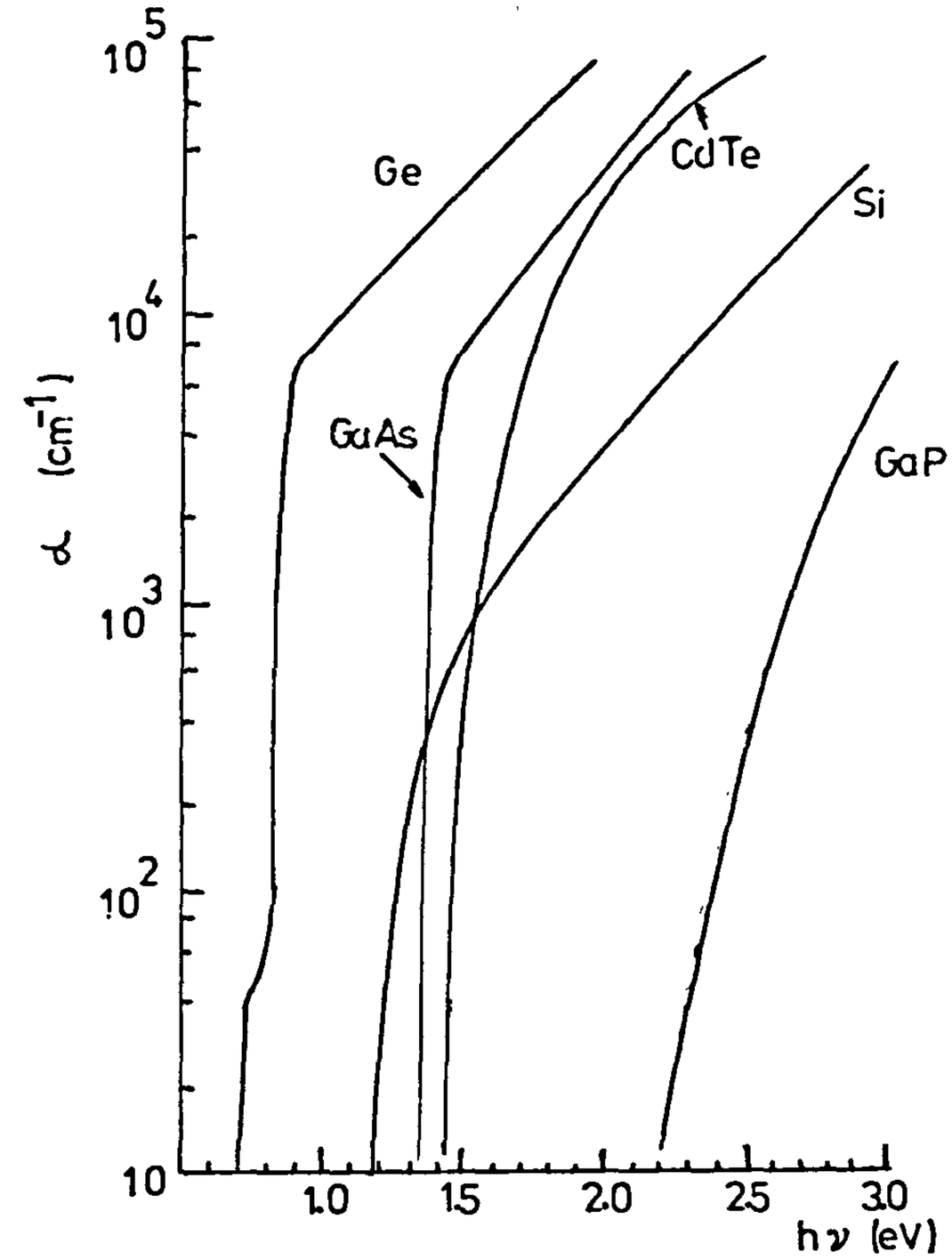

FIGURE 2.6 . Absorption coefficient α vs. photon energy $h\nu$ for some semiconductors

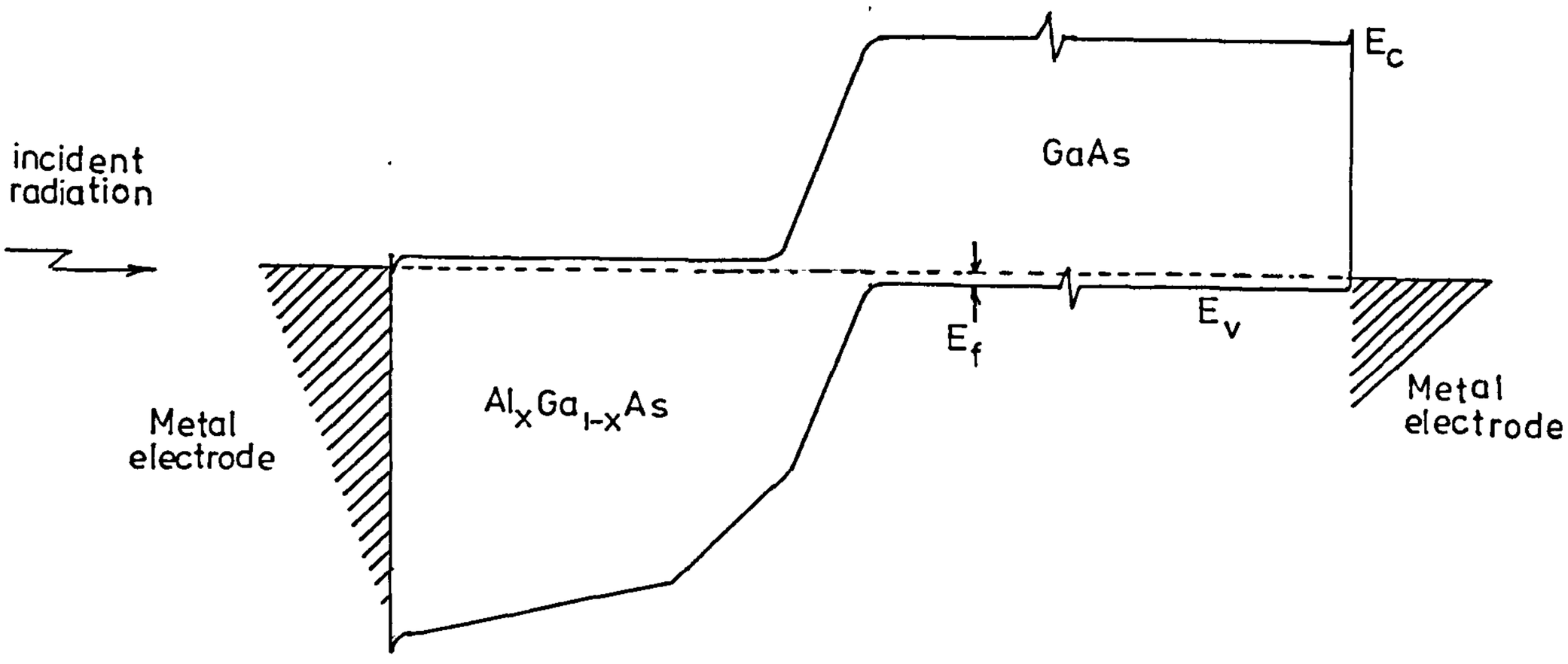

FIGURE 2.7 Energy-band diagram for n/p graded band-gap $Al_xGa_{1-x}As-GaAs$ solar cell [ref 75]

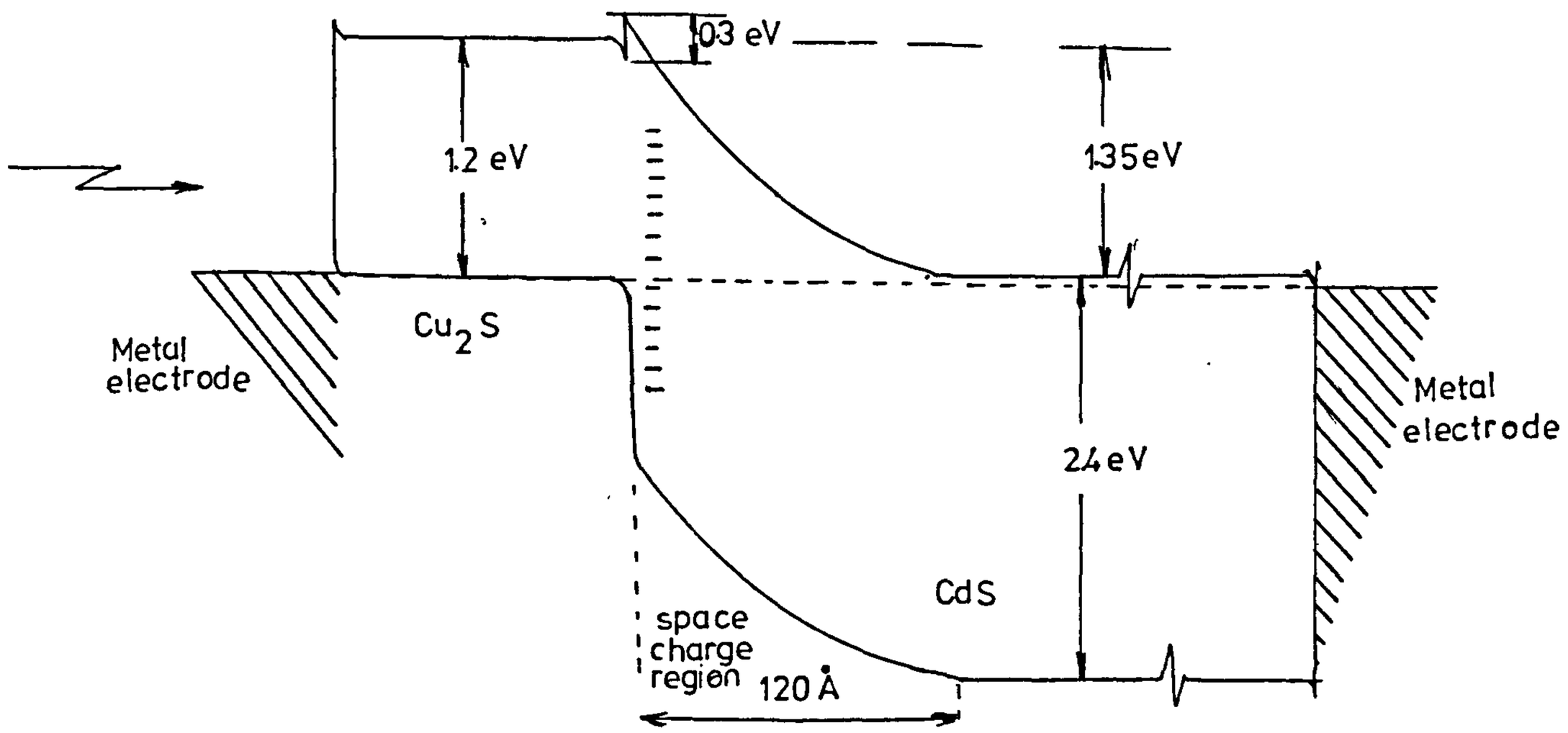

FIGURE 2.8 Band diagram of the Cu_2S-CdS solar cell [ref 1.8]

SILICON PROPERTIES	USUALL SINGLE CRYSTAL RESISTIVITY 0.01 TO 100 cm DOPANTS: DONORS P,As,Li ACCEPTORS B, A_L DISLOCATION DENSITY 0 To $10^5 cm^{-2}$ CARRIER LIFETIME o.L to 100μs ORIENTATION 100,LLL or RANDOM
GROWTH TECHNIQUES	CZOZRALSKI PULLED FLOAT ZONED DENDRITIC POLYCRYSTAL THIN FILMS-EPITAXIAL OR EVAPORATED
JUNCTION FORMATION	DIFFUSION ION IMPLANTATION EPITAXY
SURFACE FINISH	LAPPED CHEMICAL POLISH MECHANICAL POLISH
CONTACTS	PLATED (Ni,Ni-Cu-Au,A_L) EVAPORATED(TiA_GTiPd A_G,A_G,Au)
ANTIREFLECTION COATINGS	DIFFUSION FORMED ORGANIC LAYERS EVAPORATED (SiO,TiO_2,C_EO_2)
COVERS	GLASS CERIUM DOPED GLASS QUARTZ SAPPHIRE F.E.P. TEFLON $A_{L_2}O_3$

TABLE 2.1 SUMMARY OF VARIOUS TECHNOLOGIES APPLIED FOR Si SOLAR CELLS (AFTER REF 37)

CHAPTER 3

3.1 INTRODUCTION

3.1.1 Graded Band Gap Materials for Solar Cells

Grading of the width of the energy band gap of a semiconductor may be achieved by forming a solid solution of two materials with different band-gaps, in such a way that a concentration of the constituents varies along the thickness of the sample, i.e. if a solid solution is formed from semiconductors A and B, with band gaps Eg_A and Eg_B respectively, a graded band gap can be formed when the concentration of component B varies from 0% to 100% so that the band gap of the mixture would vary from Eg_A to Eg_B. The usual notation for such a structure is $A_x B_{1-x}$ where 'x' is the composition factor and varies between 1 and zero. If the values of the band-gaps of the constituent semiconductors are suitable, the use of a graded band gap layer for the surface layer of a solar cell could be very advantageous for several reasons. Firstly, if the wider of the two band gaps is great enough, the surface recombination losses are minimised via the window effect, which provides the principal advantage of heterojunction solar cells. Secondly, the grading of the band gap results in a built-in electric field the effect of which would be to aid the collection of

the photogenerated carriers. Thirdly, it is possible to form a junction with an oppositly doped semiconductor in such a way that the junction is a homojunction. Consequently the principal disadvantage of heterojunction solar cells, such as the interface spike and the high density of interface states induced by the crystal mismatch, can be avoided. Thus, for photovoltaic conversion applications a structure with a suitable graded band gap surface layer could be more advantageous than either a simple homojunction or heterojunction structure. Theroetical calculations show that maximum attainable efficiencies of simple homojunction or heterojunction cells is around 25% to 30% while those for graded band gap cells could be as high as 35% [33,122].

3.1.2 Existing Graded Band Gap Solar Cells

3.1.2.1 GaAs-AlAs System

Several graded band gap structures have been investigated but the most prominent is the Gallium Alluminium Arsenide (GaAlAs) graded band gap solid solution. The solid solution is formed by an epitaxial technique where Al is diffused into GaAs single crystal in such a way that a concentration gradient of Al is established. Solid solution $Ga_xAl_{1-x}As$ can be doped both p- and n-type, and it is possible to make a homojunction with oppositly doped GaAs. Calculations

indicate [75,76] that for this structure it is most advantageous to vary the composition factor between 0.8 and 0 in a thickness of approximately 1_{μ}, resulting in a grading of a band gap from 2.6 eV direct band gap and 2.7 eV indirect band gap of $Ga_{0.2}Al_{0.8}As$ layer to 1.4 eV direct band gap of pure GaAs. The $Ga_xAl_{1-x}As$ graded band gap cell is still in the development stage but it has the potential of becoming the most efficient single crystal solar cell, especially if used in conjunction with solar concentrators. The experimental samples that have been made clearly show a response to the blue wavelength light superior to that of the conventional GaAlAs heterostructure.

3.1.2.2 ZnTe - HgTe System

A solid solution of Zinc Telluride (ZnTe) and Mercury Telluride (HgTe) can be prepared in any proportion i.e. the composition factor 'x' in the Zinc Mercury Telluride ($Zn_xHg_{1-x}Te$) solid solution may be varied between zero and one, resulting in a band gap variation between 2.2 eV and 0 eV. Since both p- and n-type $Zn_xHg_{1-x}Te$ may be made a p-n homojunction can be formed. A solar cell with p-type surface layer $Zn_x\ Hg_{1-x}Te$ with a band gap graded from 2.2 eV to approximately 1 eV can be expected to have a very good spectral response and therefore high conversion efficiency. An attempt to produce such a

cell by liquid phase epitaxy has resulted in a disapointingly low conversion efficiency of around 1% [123], mainly due to the poor transport properties of the semiconductor.

3.1.2.3 CdTe-HgTe System

Cadmium Mercury Telluride ($Cd_xHg_{1-x}Te$) solid solutions can also be prepared for all composition factors, but the band gap can be varied only between about 1.5 eV and 0.3 eV. However, the lattice mismatch between CdTe and HgTe, as for GaAs-AlAs system, is almost non-existant. Solar cells have been made by liquid phase epitaxy with the surface layer band gap graded between 1.5 eV and about 1 eV on top of the base layer which had a uniform band gap of about 1 eV . The surface band gap value, in this cell, is too small to show the window effect but measurements and calculations indicated that the built in field caused by the grading of the band-gap resulted in a four-fold increase of the minority carrier diffusion length [29,124]. However, the efficiency of these cells was at best 4% [123]. It may be possible to improve this figure by placing the junction in a region of larger band gap and thus increasing the open circuit voltage. The poor performance of the $Cd_xHg_{1-x}Te$ cell, like that of $Zn_xHg_{1-x}Te$ cell, is mainly due to the technological factors i.e. poor control over the epitaxial process resulted in poor semiconductor properties.

3.2 Material Aspects of Cadmium Sulphide Telluride Solar Cell

3.2.1 Introduction

The structures investigated in this work use graded band gap solid solutions of CdS and CdTe. There has been a previous attempt [125,126,127] at producing graded band gaps in Cadmium Sulphide Telluride (CdS_xTe_{1-x}), by vacuum co-evaporation of the constituent semiconductors onto a heated substrate. A solar cell was made by an initial co-evaporation of pure CdTe with Cu, which resulted in a p-type CdTe film, followed by a concurrent steady increase of the deposition rate of CdS so that eventually the deposition rates of CdS and CdTe were equal, resulting in a layer of $CdS_{0.5}Te_{0.5}$. A subsequent steady decrease of evaporation rate of CdTe and Cu resulted in an n-type surface layer with a band gap graded up to 2.4 eV. Thus, in this cell the junction formed was not an abrupt one, but a diffuse junction which was concurrent with the grading of the band-gap. These cells had good spectral sensitivity but the total conversion efficiency was only a few percent, mainly due to poor transport properties of the semiconductor caused probably by inadequate control of the growth parametars. The development of this type of solar cell was discontinued

but subsequent additional information on solid solutions of CdS_xTe_{1-x} indicated that with improved technology this cell may be improved.

CdS_xTe_{1-x} solid solution can be prepared in all proportions; there is no miscibility gap as was initially suspected [127]. Thus, a graded solid solution can be made throughout the total available range. The material parameters of the solid solution of CdS_xTe_{1-x} also seem to be compatable with many requirements necessary for preparation of an efficient solar cell.

3.2.2 The Band Gap of CdS_xTe_{1-x}

Both CdS and CdTe are direct semiconductors with respective band gap of 2.4 eV and 1.5 eV. However, according to most accounts [128,129,130] in a solid solution CdS_xTe_{1-x}, "bowing" of the band-gap occurs so that for solutions containing less than approximately 40% of CdS and more than about 10% CdTe ($0.1 < x < 0.4$) the band gap values are less than that of pure CdTe by few tenths of eV. Thus the band gap of the solid solution can be in the range between 2.4 eV to approximately 1.3 eV as is shown in figure 3.1. This lowering of the band-gap has been observed in several other II-VI solid solutions, such as $Zn_xSe_{1-x}Te$,

$Zn_xS_{x-1}Te$ etc. It is conventional to express the variation of the band gap (Eg) with the composition parameter (x) in a general solid solution $A_{1-x}B_x$ in the form of a quadratic equation:

$$Eg(x) = Eg_A + (Eg_B - Eg_A - c)x + cx^2 \qquad (1)$$

where 'c' is the "bowing parameter" and Eg_A and Eg_B are the band gaps that correspond to pure constituent semiconductors, and in the case of CdS_xTe_{1-x} are. 2.4 eV and 1.5 eV respectively. There are several estimates of the value of the parameter for the wurzite crystal structure of the solid solution; namely 2.0 $\pm$ 0.1 according to Hill and Richardson [128], 1.68 $\pm$ 10% according to H. Tai et al [130] and 1.74 $\pm$ 5% according to Tanaka et al [129]. Thus, as is seen in equation 1 and figure 3.1, the relation between the band gap and the composition factor is non-linear. Nevertheless the band gap of CdS_xTe_{1-x} may be varied with no discontinuities in the range between 2.4 eV and 1.4 eV, which is a range almost ideal for solar energy conversion. A pure CdS band-gap of 2.4 eV is sufficiently wide to maintain low surface recombination losses via the window effect, since it would transmit approximately 76% of the total energy, and 90% of the total number of photons, present in the solar spectrum. A pure CdTe band gap at 1.5 eV is almost ideal for the base layer of the solar cells, as has been discussed in

Chapter 2. Thus, if the surface layer of a solar cell has a band gap graded from 2.4 eV to 1.5 eV , and if the base layer is a semiconductor with 1.5 eV band gap a good spectral response could be expected from such a device.

3.2.3. Absorption Coefficient of CdS_xTe_{1-x}

Both CdS and CdTe are direct semiconductors, and thus the solid solution CdS_xTe_{1-x} is also expected to be a direct material with an absorption coefficient as high as that of CdS and CdTe (approximately 10^6 m^{-1} to 10^7 m^{-1}). In a solar cell, when the window effect minimises the surface losses, a large value for the absorption coefficient is advantageous because then a realtively small value of the diffusion coefficient can be tolerated, and the cell need not be very thick.

3.2.4 Diffusion Lengths in CdS_xTe_{1-x}

Diffusion lengths of minority carriers in CdS and CdTe, as is the case with all II-VI semiconductors, are short when compared to those of indirect semiconductors such as Si or Ge. The maximum diffusion lengths in single crystals of direct II-VI semiconductors

are of the order of tens of microns, while in Si lengths as large as milimeters are possible. So, even in an ideal case, a relatively short diffusion length can be expected for solid solution CdS_xTe_{1-x}, especially because there is a large lattice mismatch between CdS and CdTe which could introduce many imperfections in the lattice structure of the solid solution. Furthermore, in polycrystalline thin films there is also a large density of grain boundaries, which could further reduce the diffusion length of the carriers. However, the grading of the band gap results in an electric field the effect of which could be quite appreciable. Thus, if the band gap of the CdS_xTe_{1-x} layer is graded from 2.4 eV to 1.5 eV in a thickness of 1 μm, the resulting field is 9.10^5 V/m. This field superimposes a drift velocity on top of the usual carrier diffusion velocity and should have a marked effect on the diffusion length. Thus if the built-in field caused by the grading of the band gap, is in the correct direction, this field will sweep the carriers towards the junction, and thus improve the carrier collection efficiency.

3.2.5 Crystal Structure of CdS_xTe_{1-x}

Both CdS and CdTe can be formed in either hexagonal wurzite or cubic zinc-blende structures, depending upon the conditions of the formation of the material. However, CdS is predominantly hexagonal and

CdTe is cubic, and the lattice mismatch between these two structures is 9.8% . Solid solutions of CdS_xTe_{1-x} appear in both crystalline phases depending upon the composition of the mixture, i.e. for CdS rich solutions (x > approx. 0.7) CdS_xTe_{1-x} is mainly hexagonal, while for CdTe rich solutions (x < approx 0.4) it is mainly cubic. Between these two limits CdS_xTe_{1-x} forms in a mixture of the two phases. Thus, the lattice constant of the CdS_xTe_{1-x} crystals depends on the composition parameter. The large crystal mismatch in CdS-CdTe alloys can have adverse effect on the transport properties of the solid solution. However, since the band gap shows "bowing" properties and $CdS_{0.5}Te_{0.5}$ has approximately the same band gap as pure CdTe, it may be sufficient to grade the surface layer only to a mixture with a composition factor of 0.5. This would have no effect on the built-in field and the photon absorption efficiency, but could reduce the overall crystall mismatch present in the graded layer, and could thus reduce the density of crystal faults.

3.2.6 Formation of a Junction

CdS appears only as an n-type semiconductor which is a property not uncommon among the wide band-gap materials. However CdTe can be doped so as to form both

conductivity types. Thus, it can be expected that for CdS rich solutions CdS_xTe_{1-x} will be only n-type while the CdTe rich solutions may be doped either way. Previous research of CdS_xTe_{1-x} did not investigate the doping properties of the solid solution as a function of the composition factor, and thus it was not known how high a value of the composition factor excludes the possibility of p-type doping. In the structures prepared by Bonnett [125,126,127] the p-n junction was a diffuse junction and it was not investigated exactly how the transition from p to n-type took place. Since CdS rich solutions are n-type the graded band gap CdS_xTe_{1-x} layer must be all n-type material, and the base therefore must be p-type. The p-type base may be either pure CdTe or $CdS_{0.5}Te_{0.5}$, if it is possible to prepare a p-type solution with a composition factor of 0.5. The use of p-$CdS_{0.5}Te_{0.5}$ layer rather than pure p-CdTe would be more advantageous because then there would be no crystal mismatch between the surface and base layers, i.e. the junction would be tthruly a homojunction. In the case when CdTe is used as the base layer, even if the narrow band gap of the graded layer was identical to that of CdTe, the junction would not be a true homojunction because the two sides would have different crystal phases and probably different electron affinities etc. Thus, in principle, it should be possible to fabricate a homojunction solar cell with a graded band gap surface layer.

3.2.7 Compatability with Low Cost Technology

Solid solutions of CdS_xTe_{1-x} are direct semiconductors with large absorption coefficients so that a solar cell made in this material need not be thick, i.e. a thin film cell is possible. Furthermore, being constituted from II-VI semiconductors with a relatively large degree of ionicity the transport properties of thin film polycrystalline CdS_xTe_{1-x} could be good enough for an efficient solar cell. So far, CdS_xTe_{1-x} has been prepared only in thin film form, either by flash evaporation of the mixture of the constituents, or by controlled co-evaporation. Thus, it seems possible that graded band gap CdS_xTe_{1-x} films may be deposited by vacuum evaporation, which is a process that could readily be adapted to fabrication of large area devices, at a relatively low cost. Furthermore, since spraying of CdS is a process that is fairly well developed, and since it has been shown that even solid solutions of $Cd_xZn_{1-x}S$ can be sprayed, it may be possible to spray CdS_xTe_{1-x} as well. Thus, CdS_xTe_{1-x} is a solid solution which is compatable with existing technology developed for production of large area devices at a relatively low cost. In this work , the method used to deposit CdS_xTe_{1-x} films is vacuum evaporation by resistive heating, which is a technique that is well understood and developed and widely applied.

Therefore, it appears that a solar cell with a graded band gap surface layer fabricated from CdS_xTe_{1-x} solid solution could offer some advantages over the existing thin film cells, while retaining their principal attractions, such as the low cost of production.

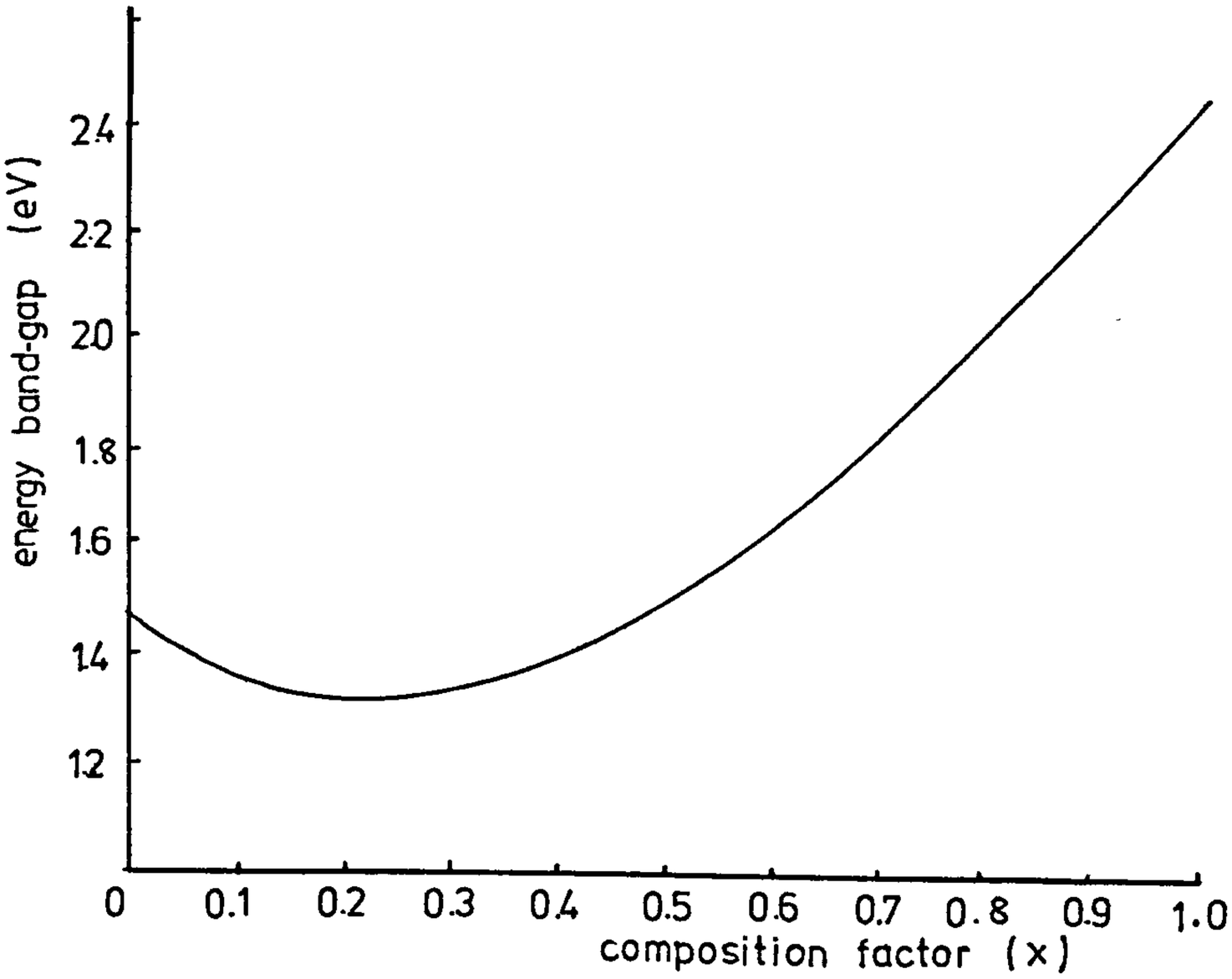

FIGURE 3.1 energy band gap of CdS_xTe_{1-x} solid solution vs. the composition of the solution (ref 128)

CHAPTER 4

Theoretical Assesment of Graded Band Gap Solar Cells

4.1 Introduction

The advantages that a structure with a position dependant band gap may have for photovoltaic applications have been realised long ago. Theoretical investigations of the behaviour of the photovoltaic effect in such structures have been carried out by several researchers. In 1957 Tauc [131] showed that an emf can be generated by an illuminated semiconductor with a graded band gap and that this emf is proportional to the product of the total change of the band gap along the illuminated section, and the photoinduced change of the minority carrier conductivity. Later Emtage [122] came to a similar conclusion.
In 1971 Marfaing and Chavalier [132] carried out a complete analyses of the photovoltaic effect in graded band gap structures taking in account the emf caused by the variation of the effective mass of carriers, the variation of doping concentration and the variation of the band-gap, the last term being dominant and essentially equal to the value calculated by Tauc. Konstantinov and Tsarenkov [133] made similar calculations in order to show that if the built-in-field caused by the grading of the band gap is large enough the surface recombination losses can be eliminated.

However, all the above treatises considered the effects in the graded band gap alone, i.e. the emf of the considered structures was to be provided by the grading of the band gap rather than by a p-n junction . However, in 1960, in his review of the possible improvements of performance of solar cells, Wolf [30] suggested that a graded band gap surface layer followed by a p-n junction could be advantageous for solar cells. Emtage [122] also considered this configuration and after extensive calculations predicted a maximum efficiency of 35%. However, he ignored the losses caused by carrier recombination, reflection and series resistance, and the gains that could result from the improved collection of photogenerated carriers. Marfaing [29] also considered a cell with a graded band-gap followed by a p-n junction and also predicted maximum efficiency of 35%. However, in both models it was assumed that the graded band gap layer provides an emf additional to that generated by the p-n junction and in order to achieve this Marfaing showed that the impurity concentration must be very low. More recently Hutchby and Fudrich [75] and Kongai and Takahashi [76] considered a graded band gap $Ga_xAl_{1-x}As$-GaAs solar cell. In these cases most of the loss mechanisms have been taken in account and the main role of the graded band gap surface layers is to

reduce the surface losses and to provide a drift field which would assist the collection of the photogenerated carriers, rather than to provide an additional emf. In this section, a theoretical analyses of a thin film graded band gap CdS_xTe_{1-x} solar cell is given.

4.2 The Band Diagram of CdS_xTe_{1-x} Solar Cell

CdS is a direct n-type material with a band gap of 2.4 eV and electron affinity (Ψ) of 4.79 eV. CdTe has a direct band gap of 1.5 eV and electron affinity of 4.28 eV. It is assumed that in the solid solution CdS_xTe_{1-x} both the band-gap and the electron affinity vary smoothly between the composition factors x_1 and x_2 which correspond to the compositions of the solid solution at the two extremes of the structure. Since there is no miscibility gap in the CdS-CdTe alloys the assumption is reasonable. It is assumed that uniform n-type doping of the graded band gap layer can be achieved. This assumption is also reasonable since n-type CdS_xTe_{1-x} mixed films ought to exist throughout the range of the compositions. If uniform doping is achieved, the conduction band of the graded band-gap layer is pinned by the Fermi level. Thus, there is a slope in the vacuum level of

the graded structure ($\psi x_1 - \psi x_2$, where ψx_1 and ψx_2 correspond to the electron affinities of the solid solution with compositions x_1 and x_2 respectively). There is also a slope in the valence band of the structure ($Egx_1 - Egx_2$) which accounts for the difference of the band-gaps of the solid solutions with compositions x_1 and x_2. This slope in the valence band represents the built in field. It is further assumed that an abrupt homojunction can be formed between the n-type graded layer and p-type base layer whose electron affinity and band gap are identical to those which exist in the graded layer in the immediate vacinity of the junction i.e. it is assumed that an ordinary abrupt homojunction can be formed with the narrow band gap end of the graded layer. It is also assumed that ohmic contacts can be made to both p- and n-type semiconductors. The band diagram that results from above considerations is shown in fig 4.1. Figure 4.1 also defines some of the parameters necessary for the following calculations such as the thickness of each region of the device and the corresponding band-gap values.

4.3 Theoretical Analyses

In order to analyse theoretically the behaviour in an illuminated graded band gap structure, an expression for the current flowing through the device is obtained. The total photocurrent flowing through the junction can be considered as the sum of current components generated in the various layers of the cell, i.e. :

$$J_T = J_P + J_n + J_{DL} - J_R \qquad (2)$$

where J_T - total photocurrent flowing through the device

J_P - The photocurrent generated in the n-type graded band gap layer

J_n - electron photocurrent generated in the p-type base layer

J_{DL} - photocurrent generated in the depletion layer itself

J_R - recombination current.

An expression for each current component is derived from the two basic semiconductor transport equations in one dimension;

from the current density equation :

$$J = q\mu p\varepsilon - qD_p \frac{dp}{dy} \qquad (3)$$

where q - electronic charge

μ - mobility of minority carriers

p - density of minority carriers

ε - electric drift field acting on the carriers

D_p - diffusion coefficient of the minority carriers

and the continuity equation

$$\frac{\partial p}{\partial t} = G - U - \frac{1}{q}\frac{dJ}{dy} \tag{4}$$

where $\frac{\partial p}{\partial t}$ - carrier concentration at a given time instant

G - generation rate of carrier pairs

U - recombination rate of carrier pairs

Similar equations can be written for the p-type semiconductor. In the case of a steady state situation when carrier concentration does not vary with time and a dynamic equilibrium is established.

$$\frac{\partial p}{\partial t} = 0 \tag{5}$$

Under normal solar illumination, the injection rate is relatively low, i.e. the minority carrier density is small with respect to majority carrier density so that the recombination rate can be written as

$$U = \frac{p - p_o}{\tau_p} = \frac{\Delta_p}{\tau_p} \tag{6}$$

where p_o - thermal equilibrium density of minority carriers

p - total density of minority carriers

τ_p - minority carrier life-time

The rate of generation of carrier pairs caused by the illumination of a semiconductor is given by Lambert's Law:

$$G(y) = \alpha N e^{-\alpha y} \tag{7}$$

where

$G(y)$ is the generator rate at a point y away from the surface of the semiconductor

N - density of photons incident in the semiconductor

α - absorption coefficient.

Since the absorption coefficient is a function of photon energy and the band gap, equation 7 is strictly true for the case of monochromatic illumination. Furthermore, in the case of graded band gap semiconductor, the position of the effective 'surface' of the semiconductor, i.e. the point where the absorption of photons starts is also a function of photon energy. Thus, the incoming solar radiation is considered as a series of monoenergetic photon beams, and equation 7 will be applied to each beam separately. Furthermore, since there is no convenient analytical expression that describes the solar spectrum, the problem is solved by numerical means.

From the considerations above equation 4 reduces to:

$$O = \Sigma G(g) - \frac{\Delta p}{\tau_p} - \frac{1}{q}\frac{dJ_p}{dy} \qquad (8)$$

4.3.1 Solar Spectrum

Solar spectrum is conventionally described by a relation between the spectral irradiance (P) averaged over a small bandwidth centered at a wavelength λ) in W m^{-2} μm^{-1} and the wavelength (λ)in μm, as is shown in figure 4.2 and table 4.1 for the particular case of AMO radiation (1). However, for calculations on semiconductor solar cells, a more convenient way of describing the spectrum is to relate the energy of photons (E) (rather than the wavelength) with the photon flux (N) (rather than the spectral power irradiance). Thus the standard solar curve has to be transformed to yield a relationship between the energy (E in eV) and photon flux (N in $m^{-2}sec^{-1}eV^{-1}$) The conversion of photon wavelength to photon energy is carried out by use of:

$$E = \frac{hf}{q} = \frac{hc}{q\lambda} \qquad (9)$$

where E - energy of photons in eV

h - Plank constant

c - speed of light

λ - the wavelength of photons in m

The transform of spectral irradiance (P) to photon flux (N) is more complex and is fully described in appendix II. The conversion is performed by:

$$N = P \frac{hc}{qE^2} \frac{1}{E} \qquad (10)$$

where N - photon flux i.e. number of photons with energy E, averaged over a small bandwidth ΔE, arriving at a unit area in a unit time i.e. $m^{-2}s^{-1}eV^{-1}$

P - spectral irradiance in W $m^{-2}\mu m^{-1}$

E - energy of photons corresponding to the central wavelength λ

Using equations 9 and 10 the data from table I is transformed into data given in table II which is described by the solar flux vs energy curve in figure 4.3. The data represented by the curve in figure 4.3 is then separated into 100 distinct "energy channels". Each 'channel' is considered as a monoenergetic beam of photons containing N_n photons of energy E_n where the energy E_n is the central energy of that particular beam. The number of photons in each beam, and the energy of each beam is given in table III. Simplified in this fashion, the information describing the solar spectrum can now be stored in a computer file in form of 100 numbers.

Because the spectral curve continues quite far into infra red, a limited photon energy range used was between 4.00 eV and 0.4 eV. This energy range contains 96.83% of all the energy in the solar spectrum. After the conversion was carried out the total available energy stored in the 100 channels was 96.16%.which was considered as an acceptable loss of accuracy.

4.3.2 Absorption of Photons in a Graded Band Gap Semiconductor

As previously mentioned, the absorption coefficient of a semiconductor is a function of the energy of the incoming radiation and the band gap and the conventional approximation for the absorption coefficient of a direct semiconductor is given by:

$$\alpha \propto \left[h\nu - Eg \right]^{\frac{1}{2}} \qquad (11)$$

This approximation matches quite well the sharp slope of the α versus $h\nu$ curve of a direct semiconductor, but for higher photon energies (relative to the band gap Eg) the approximation is not applicable. Furthermore, in the case of polycrystalline films, the absorption edge is not as well defined as it is for single crystal materials. Consequently the approximation for the absorption coefficient that will

be used is that the absorption coefficient is a constant , i.e. that it can have only two values: zero in the case when photon energy is less than the band gap and, same constant value in the case when photon energy is larger than the band gap. This approximation greatly simplifies the mathematics and gives a reasonable interpretation of the situation, especially when the true $\alpha = f(h\nu)$ function is not clearly defined in a polycrystalline film.

Since the solar spectrum is expressed in terms of 100 monoenergetic photon beams, the absorption of a given beam 'n' in the graded band gap semiconductor will start at some point y_n such that the band gap at that point ($Eg(y_n)$) is equal to the energy of that beam ($h\nu_n$), i.e. the absorption will occur when

$$Eg(y_n) \leqslant h\nu_n \tag{12}$$

Consequently, the position of the point y_n, where the absorption starts, is:

$$y_n = \frac{Eg_o - h\nu_n}{Eg_o - Eg_D} \quad :D \tag{13}$$

Thus, for a particular photon beam 'n' energy of which is less than the surface band gap (Eg_o) and more than the band gap at the edge of the graded layer (Eg_D) ($Eg_o > h\nu_n > Eg_D$) the generation rate of carrier pairs is given by:

$$G(y_n) = \alpha N_n \, e^{-\alpha(y-y_n)} \quad \text{in region where } y_n < y < D \qquad (14a)$$

$$\text{and } G(y) = 0 \quad \text{in region where } 0 < y < y_n \qquad (14b)$$

For photon beams where the energy is larger than the surface band gap, the absorption starts at the surface ($y_n = 0$) and the generation rate is:

$$G(y) = \alpha N_n e^{-\alpha y} \quad \text{for all } y \text{ such that } 0 < y < D \qquad (14c)$$

And for beams with energy less than the narrow band gap:

$$G(y) = 0 \quad \text{for all } y \qquad (14d)$$

i.e. these photon beams are transmitted.

Thus, since the solar spectrum is expressed in terms of 100 numbers, the generation rate due to each of the 100 photon beams can be calculated numerically.

4.3.3 Current Contribution from the Graded Layer

The current density and the continuity equations (3 and 8) can be combined in the usual way resulting in:

$$O=\Sigma G(y) - \frac{\Delta p}{\tau_p} - \frac{d}{\xi}(p_o+\Delta p)p\frac{d\mu}{dy} - \mu\varepsilon \frac{d}{dy}(p_o+\Delta p) - \mu(p_o+\Delta p)\frac{d\varepsilon}{dy} + D_p \frac{d^2(p_o+\Delta p)}{dy^2} \quad (15)$$

In order to solve equation 15 a number of assumptions are now made:

a) The effective masses of carriers (m_n^*, m_p^*) are assumed to be constant throughout the structure. In solid solution CdS_xTe_{1-x} the effective masses ought to vary with the composition factor x and thus, in fact, are position dependant in a graded band gap structure. However, if the effective masses vary between the values that they have in pure CdS and pure CdTe, the maximum change of the effective masses would be around 50% (45% for electron and 23% and 58% for light and heavy holes respectively) of the values they hold in pure CdS. The variation of the effective mass along a structure gives rise to an electric built-in field. However the magnitude of this field is assumed to be negligable with respect to that caused by the change of the band-gap so that the effect of variation of

effective masses is neglected , and the approximation is assumed valid.

b) The density of majority carriers (electrons) and the impurity concentration is assumed constant and position independent. It has already been assumed in section 4.2 that the depth of Fermi level below the conduction band is constant through the graded region which requires that the impurity concentration and the integrated density of states is constant. In principle, this assumption is valid because the achievement of uniform doping is a technological factor and the integrated density of states will vary only slightly as the effective mass varies.

c) The minority carrier (hole) lifetime (τ_p) and the hole diffusion length (L_p) is assumed to be constant throughout the graded layer. In principle, this assumption is not true because the life-time should vary with the composition factor x firstly because the composition is changing and secondly because the strain in crystallites is increasing with the decreasing composition factor. However, in practice in polycrystalline films the life-time is limited by crystal faults such as grain boundaries and measurements indicated that the grain sizes is independent of composition factor. Thus the assumption may be made.

d) The minority carrier mobility (μ_p) is assumed to be position independent. Hole mobility, like the diffusion length, does in principle change with the composition factor, but in practice is limited by

the polycrystallinity of the films and is thus constant.

e). The minority carrier diffusion coefficient (D_p) is assumed to be position independent. This assumption must be made as a consequence of assumptions c and d.

Resulting from some of these assumptions, it follows that the electric field acting on thercarriers is due to the grading of the band gap alone, as a result of the electric field arising from the slope of the valence band (see fig 4.1). Furthermore, the slope of the valence band is assumed to be linear within the graded region so that

$$\varepsilon = \frac{Eg_O - Eg_D}{O - D} = \frac{\Delta Eg}{D} \qquad (16)$$

where Eg_O - band gap at the surface of graded region

$y = O$

Eg_D - band gap at the end of graded eqn.

$y = D$

ε - built in electric field

Therefore, following from equation 16

$$\frac{d\varepsilon}{dy} = O \qquad (17)$$

Thus, equation 15 may now be simplified into:

$$\frac{d^2}{dy^2}(\Delta p+p_o) - \frac{kT}{q}\varepsilon\frac{d}{dy}(\Delta p+p_o) - \frac{1}{L^2_p}\Delta p = -\frac{1}{D_p}\Sigma G(y) \quad (18)$$

Since the graded region is an n-type semiconductor the equilibrium concentration of minority carriers (p_o) may be assumed to be small with respect to the concentration of photoexcited minority carriers (Δp) so that equation 18 reduces to:

$$\frac{d^2\Delta p}{dy^2} - \frac{kT}{q}\varepsilon\frac{d\Delta p}{dy} - \frac{1}{L^2}\Delta p = -\frac{1}{D_p}\Sigma G(y) \quad (19)$$

Equation 19 is a differential equation of second order describing the photogeneration of carriers, so that the solution of equation 19 represents the distribution of the excess minority carriers (Δp) as a function of position in the graded layer (g). Equation 19 is now solved separately for each of the 100 monoenergetic photon beams, the sum of which represents the solar spectrum. It is assumed that each photon beam produces a certain distribution of photogenerated carriers (Δp) and that the sum of the distributions from all 100 beams corresponds to the distribution of the carriers that would be caused by illumination by the complete solar radiation. Thus for any given photon beam 'n' with energy $h\nu_n$ such that

$h\nu_n > Eg_D$ and $y_n > D$ equation 19 reduces to:

$$\frac{d^2\Delta p_{n_2}}{dy^2} - \frac{kT}{q}\,\epsilon\,\frac{d\Delta p_{n_2}}{dy} - \frac{1}{L^2}\,\Delta p_{n_2} = -\frac{1}{D_p}\,N_n e^{-\alpha(y-y_n)} \qquad (20a)$$

for $y_n < y < D$

and

$$\frac{d^2\Delta p_{n_1}}{dy^2} - \frac{kT}{q}\,\epsilon\,\frac{d\Delta p_{n_1}}{dy} = \frac{1}{L^2}\,\Delta p_{n_1} = 0 \qquad \text{for } y < y_n \qquad (20b)$$

In the case when photon energy is larger than the surface band gap the absorption starts at the surface and

$$y_n = 0$$

may be substituted into equation 20a.

The solution of equation 20b represents the distribution of the holes (Δp_{n_1}) between the surface of the graded layer (y=0) and the position where the absorption starts (y_n). This is the region where this particular photon beam 'n' does not generate any electron-hole pairs. Solution of 20a represents the distribution of holes (Δp_{n_2}) between y_n and the edge of the depletion layer (y=D). It is to be noted

that in order to obtain an expression for the distribution of photogenerated carriers valid throughout the graded band gap region, it is essential to use both equations 20a and 20b, because each one describes an essentially different physical situation. Other treatises of similar type (75, 76, 124) have attempted to solve the problem by use of a single equation, analagous to equation 20a, and 2 boundary conditions. However, a single equation is inadequate to express the distribution of photogenerated carriers anywhere in the graded region. Furthermore, of the 2 boundary conditions used, one pertains to the surface recombination velocity and is thus valid in the region where the single equation is invalid.

Equations 20a and 20b can now be solved by usual analytical means applicable to second order differential equations, both homogeneous and non-homogeneous.

The complimentary function of the equation yields:

$$x_1 = \frac{q}{2kT}\varepsilon + \sqrt{\left[\frac{q}{2kT}\varepsilon\right]^2 + \frac{1}{L^2}} \qquad (21a)$$

$$x_2 = \frac{q}{2kT}\varepsilon - \sqrt{\left[\frac{q}{2kT}\varepsilon\right]^2 + \frac{1}{L^2}} \qquad (21b)$$

Quantities χ_1 and χ_2 represent the inverse of the effective diffusion lengths of carriers in the same and the opposite directions to the field caused by the grading of the band gap.

The solution to equation 20a and 20b may now be written as

$$\Delta p_{n_1} = A\, e^{\chi_1 y} + B\, e^{\chi_2 y} \qquad (22a)$$

$$\Delta p_{n_2} = Ce^{\chi_1 y} + Ee^{\chi_2 y} + Fe^{-\alpha y} \qquad (22b)$$

where

$$F = - \frac{\alpha N_n e^{\alpha y_n}}{Dp(\alpha^2 + \frac{q}{kt}\,\alpha\varepsilon - \frac{1}{L^2})} \qquad (23)$$

which is obtained from the particular integral part of the solution of 20b. Quantities A,B,C and E are arbitrary constants values of which can be determined from boundary conditions for equations 22a and 22b. the boundary conditions are:

$$\frac{d\Delta p_{n_1}}{dy} \Big/ \Delta p_{n_1} = S \quad \text{at } y = 0 \qquad (24a)$$

$$\frac{d\Delta p_{n_1}}{dy} = \frac{d\Delta p_{n_2}}{dy} \quad \text{at } y = y_n \qquad (24b)$$

$$\Delta p_{n_1} = \Delta p_{n_2} \qquad \text{at } y = y_n \qquad (24c)$$

$$\Delta p_{n_2} = 0 \qquad \text{at } y = D \qquad (24d)$$

Condition 24a states that the surface recombination factor S is a constant of the surface, rather than being related to the carrier concentration at the surface. By definition of the surface recombination velocity :

$$-q\mu\varepsilon\Delta p \Big|_{y=0} + q D \frac{d\Delta p}{dy}\Big|_{y=0} = J_s = q \Delta p \Big|_{y=0} R \qquad (25)$$

where J_s is the surface recombination current

R is the surface recombination velocity.

The reversed signs of the left hand side of equation 25 are consistant with the problem since the surface current flows in the negative direction. Rearranging equation 25 yields the boundary condition:

$$\frac{d\Delta p}{dy} \Big/_{\Delta p\ y=0} = \frac{R}{Dp} + \frac{q}{kT}\varepsilon = S = \text{constant} \qquad (26)$$

Conditions 24b and 24c state that there is continuity at the point $y=y_n$ where both 22a and 22b are valid. The final boundary condition states that

the depletion layer acts as a perfect sink for the carriers so that the carrier concentration at the edge of the depletion layer must be very small or zero; or otherwise the current flowing through the device would tend to infinity.

The four boundary conditions yield the solution for the four arbitrary constants as follows:

$$A = B \cdot \frac{K_1}{K_2} \tag{27a}$$

$$B = E(K_{11} - K_9) - F(K_{12}-K_{10}) \tag{27b}$$

$$C = - E\cdot K_3.K_5 - F\cdot K_4K_5 \tag{27c}$$

$$E = F \frac{K_{13}K_{15} - K_{14}(K_{10}-K_{12}) + \alpha K_8)}{K_{13}K_{16} - K_{14}(K_9+K_{11}) - K_{14}} \tag{27d}$$

where $K_1 = S - \chi_2$ (28)

$K_2 = \chi_1 - S$

$K_3 = \exp(\chi_2 D)$

$K_4 = \exp(-\alpha D)$

$K_5 = \exp(-\chi_1 D)$

$K_6 = \exp(\chi_1 y_n)$

$$K_7 = \exp\ (\alpha_2 y_n)$$

$$K_8 = \exp\ (-\alpha y_n)$$

$$K_9 = \frac{K_2K_3K_5K_6}{K_1K_6+K_2K_7}$$

$$K_{10} = \frac{K_2K_4K_5K_6}{K_1K_6+K_2K_7}$$

$$K_{11} = \frac{K_2K_7}{K_1K_6+K_2K_7}$$

$$K_{12} = \frac{K_2K_8}{K_1K_6+K_2K_7}$$

$$K_{13} = \alpha_1 K_6$$

$$K_{14} = \alpha_2 K_7$$

$$K_{15} = K_{12}\frac{K_1}{K_2} - K_{10}\frac{K_1}{K_2} + K_4K_5$$

$$K_{16} = K_9\frac{K_1}{K_2} - K_{11}\frac{K_1}{K_2} - K_3K_5$$

Thus for any given photon beam 'n' with N_n photons of energy $h\nu_n$ it is possible to calculate the density of the photogenerated carriers (Δp) at any point in the graded band gap region using equations 22a and 22b. The current flowing through the device caused by the absorption of the photon beam 'n' can then

be expressed as:

$$J_{p_n} = q\,\mu\,\Delta p_n \Big|_{y=D}\,\varepsilon \;-\; q\,D_p \left.\frac{d\Delta p_n}{dy}\right|_{y=D} \qquad (29)$$

Since, as is stated by equation 24d, the concentration of the minority carriers at the edge of the depletion layer (y=D) is effectively zero, the drift field component of the current is negligable so that equation 29 approximates to:

$$J_{p_n} = -\,q\,D_p \left.\frac{d\Delta p_n}{dy}\right|_{y=D} \qquad (30)$$

Thus, by differentiating equation 22b, an expression for the current due to absorption of a photon beam 'n' is found to be:

$$J_{p_n} = -q\,D_p(\chi_1 C e^{\chi_1 D} + \chi_2 E e^{\chi_2 D} - \alpha F e^{-\alpha D}) \qquad (31)$$

And the total current due to the absorption of all photon beams whose energy is less than the surface band gap (Eg_o) and more than the narrowest band gap (Eg_D) is given by the sum of current components expressed by equation 31

$$J_p(\text{bulk}) = \Sigma\, J_{p_n} \qquad (32)$$

In the case of photon beams with energy greater

than the surface band gap the absorption starts at the surface (y_n=O) , and all photon beams may be summed up and considered as a single beam since the absorption coefficient is a constant. Let

$$N_T = \Sigma N_n \quad \text{when} \quad h\nu_n \geq Eg_o \tag{33}$$

The distribution of carriers excited by these photons may then be obtained from a modification of equation 20a; namely

$$\frac{d^2\Delta p_s}{dy^2} - \frac{kT}{q}\,\varepsilon\,\frac{d\Delta p_s}{dy} - \frac{1}{L^2}\,\Delta p_s = -\frac{1}{D_p}\,\alpha\, N_T\, e^{-y\alpha} \tag{34}$$

where Δp_s is the carrier concentration caused by the photon beams absorbed at the surface (y_n=O). Equation 34 is valid throughout the graded band gap region, from the surface (y=O) to the edge of the depletion layer (y=D). The solution is obtained in the usual way:

$$\Delta p_s = A^1 e^{\chi_1 y} + B^1 e^{\chi_2 y} + C^1 e^{-\alpha y} \tag{35}$$

where χ_1 and χ_2 are obtained from the complimentary function and are identical as in equation 21a and 21b, and

$$C^1 = \frac{-\alpha N_T}{D_p(\alpha^2+\frac{kT}{q}\alpha\varepsilon - \frac{1}{L^2})} \tag{36}$$

Artbitrary constants A^1 and B^1 may again be deduced from the boundary conditions which are in this case:

$$\frac{d\Delta p_s}{dy} /_{\Delta p_s} = S \qquad \text{at } y = O \tag{37a}$$

$$\Delta p_s = O \qquad \text{at } y = D \tag{37b}$$

The boundary conditions are the same as those described previously in 24a and 24d. Following from this:

$$B^1 = C^1 \frac{K_4+K_{18}\frac{K_{17}}{K_2}}{K_3+K_{18}\frac{K_1}{K_2}} \tag{38a}$$

$$A^1 = B^1 \frac{K_1}{K_2} + C^1 \frac{K_{17}}{K_{12}} \tag{38b}$$

where

$$K_{17} = S + \alpha$$

and

$$K_{18} = \exp(\chi_1 D)$$

It is to be noted that since equation 34 is valid throughout the layer unlike either 24a or 24b, a single equation and two boundary conditions are sufficient to describe the distribution of carriers.

The current contribution due to photon beams absorbed at the surface can then be expressed as:

$$J_p(\text{surface}) = -qD_p(\chi_1 A^1 e^{\chi_1 D} + x_2 B^1 e^{\chi_2 D} - \alpha C^1 e^{-\alpha D}) \tag{39}$$

And the total hole current generated in the graded region is:

$$J_p = J_p(\text{bulk}) + J_p(\text{surface}) \tag{40}$$

4.3.4 Current Contribution from the Depletion Layer

In the depletion layer the built in electric field is assumed to be so large that any electron-hole pairs photoexcited are collected before any recombination takes place, i.e. 100% collection efficiency is assumed. Thus, it is necessary to find the number of photons absorbed in the depletion layer which lies between g=D and $y=D_2$.

The total number of generated carriers caused by absorption of a photon beam 'n' is calculated from the integral of equation 14a, thus the number of electron hole pairs photogenerated in the depletion layer is given by this antegral between the limits of y=D and $y=D_2$ i.e.:

$$(np) = \int_{y=D}^{y=D_2} \alpha N_n e^{-\alpha(y-y_x)} dy = N_n e^{\alpha y_n} \left[e^{-\alpha D} - e^{-\alpha D_2} \right] \quad (37)$$

Thus, the current produced in the depletion layer by a photon beam 'ν' with an energy greater than the band gap at the edge of the depletion layer ($h\nu_n > Eg_D$) is

$$J_{DL_{n1}} = q\, N_n e^{\alpha y_n} \left(e^{-\alpha D} - e^{-\alpha D_2} \right) \quad (38)$$

Because the grading of the band gap continues to a point inside the depletion layer ($y=D_2$), the absorption of some photon beams starts inside the depletion layer itself. For those photon beams with energy less than

Eg_D and more than Eg_{D1} ($D<y_n<D_1$), the current contribution is:

$$J_{DLn_2} = q\, N_n\, e^{\alpha y_n}\, (e^{-\alpha y_n} - e^{-\alpha D_2}) \qquad (39)$$

and the total current contribution from the depletion layer is then:

$$J_{DL} = \Sigma J_{DLn_1} + \Sigma J_{DLn_2} \qquad (40)$$

The width of the depletion layer was calculated by the use of standard equations relating the width of the depletion layer to the built-in voltage, doping concentrations, density of states and permittivity of the material.

4.3.5 Current Contribution from p-type Base Layer

The base layer is a uniform band gap semiconductor with the same band gap as the narrow band gap of the graded layer. The band gap for $y > D_1$ is uniform and all the photon beams with energy less than Eg_{D_1} are transmitted. Because , the absorption coefficient is a constant, all the photons with energy larger than this band gap (Eg_{D_1}) and which are transmitted to the base layer may be considered as monoenergetic photons. Thus it is necessary to find the number of photons with energy hν larger than the band gap (Eg_{D_1}) incident in the base layer ($y = D_2$).

The number of photons in a photon beam 'n' with energy larger than Eg_{D_1} , which are absorbed by the semiconductor, is given by an integral of equation 14a

$$N_{ABS} = \int_{y=g_n}^{y=D_2} N_n \alpha e^{-\alpha(y-y_n)} dy = N_n e^{\alpha y_n} (e^{-\alpha y_n} - e^{-\alpha D_2}) \qquad (41)$$

Because a given photon beam 'ν' contains N_n photons, the number of photons incident on the base layer is:

$$N_{B_n} = N_n - N_{ABS} = N_n \, e^{-\alpha(D_2-y_n)} \qquad (42)$$

and the total number of photons incident in the base layer is:

$$N_{BT} = \Sigma N_{B_n} \tag{43}$$

Because the base layer is a uniform band gap semiconductor, and the depletion layer is a perfect sink for carriers, the problem may be considered as if N_{B_n} monoenergetic photons were incident on a semiconductor with infinite surface recombination velocity. The base layer is a p-type semiconductor so that the basic equation 15 is modified to:

$$O=G(y) - \frac{\Delta n}{\tau n} - \frac{d\mu_n}{dy}\left[(n_o+\Delta n)E\right] - \frac{d}{dy}(n_o+\Delta n)\mu_n E - \frac{dE}{dy}\mu m$$

$$(n_o+\Delta n) - D_n \frac{d^2}{dy^2}(n_o+\Delta n) \tag{44}$$

In a uniform band gap semiconductor mobility is constant and there is no drift field so that equation 44 reduces to

$$\frac{d^2\Delta n}{dy^2} - \frac{1}{L^2}\Delta n = \frac{1}{D_n} G(y) \tag{45}$$

where $G(y) = N_{BT}\ \alpha\ e^{-\alpha y}$

It is to be noted in order to simplify the mathematics and because the number of photons incident on the base layer is known point $y=D_2$ is considered as the origin i.e. $y^1 = O$.

A general solution to equation 45 is obtained in the usual way:

$$\Delta n = A\, e^{\frac{1}{L} y^1} + K\, e^{-\alpha y^1} \tag{46}$$

where

$$K = \frac{-\alpha N_{BT}}{D_n(\alpha^2 - \frac{1}{L_n^2})}$$

The boundary conditions are

$$\Delta n = O \quad \text{at } y^1 = O \tag{47a}$$

$$\Delta n = O \quad \text{at } y^1 = T \tag{47b}$$

Condition 47a states that the depletion layer is a perfect sink effectively producing an internal surface with infinite recombination velocity. Condition 47b assumes that the thickness of the base layer is appreciably larger than the inverse of the absorption coefficient so that the number of excess carriers at $y^1 = T$ may be neglected.

From the boundary conditions it is deduced that:

$$A = -B - K \qquad -B - K \tag{48a}$$

$$B = \frac{K(e^{-\alpha T} - e^{T/L})}{\left[e^{T/L} - e^{-T/L}\right]} \tag{48b}$$

The current contribution from the base layer is then given by:

$$J_n = q\,D_n \left.\frac{d\Delta n}{dy}\right|_{y=0} = qD_n\left(\frac{A}{L} - \frac{B}{L} - \alpha K\right) \qquad (49)$$

4.3.6 Recombination Current and Series Resistance

When a junction is formed between two oppositely doped semicondcutors or two different semiconductors, a number of electron states may be formed within the band-gap in the vicinity of the depletion layer. These states act as recombination centres so that the carriers moving across the junction may be lost due to recombination via the centres. This recombination results in a recombination current which is analogous to the ideal diode diffusion leakage current. Sometimes, especially in the heterojunctions when the mismatch of crystal lattices may induce a large density of recombination centers, the recombination current dominates the forward characteristic of the diode. Thus the recombination current may be an important factor in any theoretical assessment of the performance of a solar cell.

However, it is not the aim of this work to predict the absolute conversion efficiency of a graded band-gap CdS_xTe_{1-x} solar cell but rather to demonstrate the advantages of graded band gap cells over the conventional homojunction and heterojunction cells, and to find optimal parameters for graded band gap cells. Thus it is the relative conversion efficiencies that are to be calculated, not the absolute conversion efficiencies. It is assumed that the recombination current in the graded CdS_xTe_{1-x} cell is of about the same magnitude as the recombination current in a conventional

homojunction cell with the same band gap in the depletion layer so that in a calculation representing relative conversion efficencies the effects of recombination current is irrelevant. Thus recombination current is not going to be taken into account in the calculations. This assumption may be made because the junction in the CdS_xTe_{1-x} cell is assumed to be a homojunction rather than a heterojunction, as has been previously discussed.

In the case of series resistance, similar assumptions are made. Ideal contacts are assumed so that the series resistance is dominated by the bulk resistivity of the semiconductors. Again, since it is the relative output that is of interest if structures with similar bulk resistances are compared , then the series resistance effect may be ignored.

4.3.7 The Depletion Layer

The magnitude of the built-in voltage barrier in a p-n junction is given by:

$$V_{bi} = Eg - (Ef_n + Ef_p) \tag{50}$$

where Eg is the band gap in the depletion layer and Ef_n, Ef_p are the depths of Fermi leads into the band gap and providing Boltzman statistics apply, these are given by:

$$Ef_n = kT \ \ell n \frac{N_C}{N_D} \tag{51a}$$

$$Ef_p = kT \ell n \frac{N_U}{N_A} \tag{51b}$$

where N_C, N_U are the densities of states on the conduction and valence band respectively.

N_D, N_A are the concentration of donor and acceptor impurities on the n-type and p-type sides of the junction respectively.

The magnitude of the voltage barrier in an illuminated solar cell is less, than V_{bi} . The magnitude of the voltage barrier effects the photocurrent via the width of the depletion layer as:

$$W = D_2 - D = \sqrt{\frac{N_a + N_D}{N_A N_D} \frac{2 \varepsilon_s V_{bi}}{q}} - V \qquad (52)$$

where ε_s is the relative permittivity of the semiconductor and V is the reduction in the potential barrier produced as a result of the photocurrent. V is chosen and used in the calculation of the width of the depletion layer. The magnitude of the built-in voltage and the effective forward bias voltage V together with the recombination in the barrier, all effect the power output of the solar cell. However, because the output of the graded band gap device is compared with that of a homojunction device the actual magnitude of the barrier is irrelevant as long as a constant and consistant value is used for both devices.

4.4 Results of the Calculations

4.4.1 Method of Calculation

It has been mentioned in section 4.3 that the solar spectrum is represented by 100 photon beams. This data, along with semiconductor constants formed a data file for the main programs. Two programs are written; one calculated the distribution of photogenerated carriers in a graded band gap semiconductor while the other calculated the photocurrent flowing through a device with a graded band gap surface layer. In both programs equations derived in section 3.3 were applied separately to each photon beam using the appropriate photon energies ($h\nu$) corresponding to that particular channel. The procedure was repeated for each channel and the effects were summed to simulate illumination of the whole of the solar spectrum. The effects of various material and physical properties on the performance of the device were deduced by variation of the imput data. The flow diagrams of the two programs are shown in figures 4.4 and 4.5 respectively while the programmes themselves, written in Fortran are given in Appendix III.

4.4.2 Distribution of the Photogenerated Minority Carriers

Using equations 22 to 28 a program was written to calculate the density of the photogenerated holes at 50 points in a graded band gap semiconductor. Only a graded band gap layer was considered , rather than the whole solar cell. The effect that each particular parameter, such as the surface band gap (Eg_o), thickness of the layer (W), surface recombination velocity (S) and minority carrier diffusion length (L_p), had on the distribution of the carriers was found by variation of the values of those parameters alone. and is illustrated on figures 4.6 to 4.9. Where it is not otherwise stated the values of the parameters representing material and physical properties of the semiconductor layer were:

Surface Band gap	(Eg_o)	2.42 eV
Narrow Band gap	(Eg_w)	1.5 eV
Thickness of the layer	(W)	1μ
Minority of carrier diffusion length	(L_p)	0.5μm
Hole diffusion coefficient	(D_p)	2.6 $10^{-5} m^2 s^{-1}$
Surface recombination velocity	(S)	10 cm/s
Absorption coefficient	(α)	5.10^6 m^{-1}

4.4.2,1 The Effect of the Surface Band Gap on the Distribution of the Carriers

Figures 4.6a and 4.6b show the distribution of the photogenerated carriers in a graded band gap semiconductor with the surface band gap of 2.4 eV and 1.9 eV respectively. The distribution of the carriers generated by the photon beams absorbed close to the surface (y_n=0.05μ), in the center of the layer (y_n=0.5μ) and close to the narrow band gap end of the semiconductor (y=0.9μm) are shown, as well as the sum of all the individual carrier distributions. It can be seen that the peak of the individual carrier distributions does not necesaarily coincide with the point where the rate of generation of the carriers is the highest ($y=y_n$). This is due to the field caused by the grading of the band gap, which pushes the carriers towards the narrow band gap end of the semiconductor. Thus, the peaks of the carrier distributions are shifted by larger amounts in the semiconductor with the greater surface band gap . Furthermore, fewer photons are absorbed close to the surface of the semiconductor when the surface band gap is large (Eg_o=2.4 eV) so that the total concentration of the carriers in this region is less than in the case of a semiconductor with a smaller surface band gap (Eg_o=1.9 eV). However, the concentration of the carriers in the narrow band gap region of the semiconductor is

greater when the surface band gap is large, due to both, a greater shift of the carrier distributions and the greater number of photons being absorbed closer to this region. Thus, it can be expected that the current generated in the semiconductor is larger in the case when the surface band gap is 2.4 eV rather than 1.9 eV.

4.4.2.2 The Effect of the Thickness of the Layer on the Distribution of the Carriers

Figure 4,7 a,b and c show the distributions of the photo carriers generated by the same photon beam ($h\nu_n$ = 1.95 eV) in semiconductor layers of different thickness (W=5μ, 1μ, 0.5μ respectively). In the case of the thickest layer (fig a) the peak of the distribution coincides with the point where the rate of generation of carriers is the greatest i.e. $y = y_n$, unlike in the case of thinner layers where the distributions are shifted toward the narrow band-gap end of the semiconductor. This is due to the fact that the field, caused by the grading of the band gap, increases with a decreasing thickness and thus has an increasing effect on the distribution of the carriers . As can be expected, the effect is the same, as that caused by a decrease of the magnitude of the surface band gap.

4.4.2.3 The Effect of the Surface Recombination on the Distribution of the Carriers

Figure 4.8 shows the effect of different surface recombination velocities on the distribution of the carriers generated by a photon beam absorbed close to the surface (y_n = 0.05) of a graded band gap semiconductor. The greater the surface recombination velocity, the greater is the surface current and consequently the smaller is the concentration of the carriers at the surface, as is expressed by equation 25. Thus, a large recombination velocity results in a decreased concentration of the carriers at the surface so that some of the carriers generated in the bulk of the semiconductor diffuse towards the surfaces against the field caused by the grading of the band gap.

This results in a slight shift of the distribution of carriers away from the surface as well as a decrease of the density of carriers as is shown in fig 4.8. If the semiconductor layer is thin enough, the effect of this migration of carriers can be propagated even to the opposite end of the semiconductor layer. The effect of the surface recombination is seen only by the carriers generated by the photon beams which are absorbed at or near the surface of the semiconductor.

4.4.2.4 The Effect of the Diffusion Length on the Distribution of the Carriers

Figure 4.9 illustrates the effect of the minority carrier diffusion length on the distribution of carriers generated by a photon beam absorbed close to the middle ($y_n \sim 0.4\mu$) of a graded band gap semiconductor layer. A decrease of the life-time and hence diffusion length results in a decrease of the concentration of carriers throughout the layer. Furthermore, a decreasing minority carrier life-time results in a shift of the carrier distributions toward the point where the absorption of the photon beam starts (y_n). Thus, as the life-time of the carriers decreases, the shape of the carrier distribution ceases to be altered by the diffusion and drift processes and, in an extreme case, it would be dominated by the exponential decay described by the absorption process.

4.4.2.5 Conclusion

The curves described by figure 4.6 to 4.9 demonstrate some of the advantages for photovoltaic conversion of a graded band gap semiconductor over a conventional uniform semiconductor, such as the window effect and the effect of the built in field . However a greater

significance of these curves is that they satisfy the conditions deduced from basic physical principles, thereby proving that that the model used is a correct one, in that two equations and four boundary conditions are necessary to describe the whole physical process.

4.4.3 Photocurrent in a Graded Band Gap Solar Cell

Using equations derived in section 4.3, the photocurrent generated in an illuminated graded band gap solar cell is calculated by use of a computer program. The method used to calculate the photocurrent is illustrated by the flow diagram in figure 4.5. The calculated magnitude of the photocurrent may not be a realistic one because a few loss mechanisms have been neglected. However, the model used to calculate the photocurrent enables the graded band gap solar cell to be optimised and compared with a homojunction device. Where it is not otherwise stated, the parameters representing the material and physical properties of the solar cell, are as follows:

Surface Band Gap	(Eg_o)	2.4eV
Base layer band gap	(Eg_w)	1.5eV
relative permitivity	(ε)	7.1
density of states in the conduction band	(N_c)	$1.429.10^{24}m^{-3}$
density of states in the valence band	(N_u)	$1.51.10^{26}m^{-3}$
density of donors in the n-type layer	(N_D)	$5.10^{23}m^{-3}$
density of acceptors in the p-type layer	(N_A)	$15.10^{23}m^{-3}$
diffusion coefficient of carriers	(D_n,D_p)	$2.58 \cdot 10^{-5}m^2/s$
electron diffusion length in the p-type layer	(L_n)	1μm
hole diffusion length in the n-type layer	(L_p)	0.3μm
absorption coefficient	(α)	$5.10^{6}m^{-1}$
surface recombination velocity	(S)	$1.10^{2}cm/s$

thickness of the base layer (T)	1.5 μm
thickness of the surface layer (D)	0.5 μm

The values of the band gaps chosen correspond to those of pure CdS and either pure CdTe or mixed $CdS_{0.5}Te_{0.5}$ respectively. The value chosen for the relative permitivity of the semiconductor is that of pure CdTe, although it would make virtually no difference if the value of CdS was used (9.9). The densities of states have been calculated using average effective masses of CdS and CdTe. The doping concentrations correspond to typical values of carrier densities measured in CdS and CdTe films of approximately 10Ω cm resistivities. The diffusion coefficients have been calculated from the Einstein relationship using typical mobility values and measured in thin films of CdS and CdTe (see CH 6). The diffusion lengths have been estimated within an order of magnitude from the lowest lifetimes published for CdS and CdTe.

In order to optimise the cell each of the above parameters was individually varied and the resultant effect in the photocurrent was noted.

4.4.3.1 The Effect of the Surface Band Gap in the Photocurrent

The value of the band gap at the surface of the graded band gap layer effects the current components from every layer of the cell. Decreasing the value of the surface band gap decreases the window effect so that an increasing proportion of absorption takes place

in the surface layer and therefore the current generated in this region also increases. However, the loss of the window effect also implies that a larger proportion of carriers is generated near the surface of the semiconductor so that an increasing number of carriers is lost by surface recombination. Thus, the larger the surface recombination velocity, the larger is the optimum value of the surface band gap required for maximum current output from the surface layer as is shown in figure 4.10.

The optimum value of the surface band-gap is also effected by the thickness of the surface layer. The thicker that this layer is, the larger the surface band gap ought to be in order to increase the proportion of photons absorbed close to the depletion layer. In thin layers, with small surface recombination velocity, a large proportion of photons penetrates the graded band gap layer so that the optimum surface band gap required for maximum hole current is less than 2.4 eV as is shown in fig 4.11.

However, a decreasing value of the surface band gap results in a decreasing proportion of photons reaching the depletion and base layer so that the current components from the regions also depend strongly on the value of the surface band gap. Thus, in most cases, the optimum value of the surface band gap required for maximum total current output from the cell, is 2.4 eV as is shown in figure 4.12. The only exception to this

is when the surface recombination is very low and the surface layer is very thin in which case the total current is slightly larger with smaller surface band gaps because the bulk of generation takes place close to the depletion layer, regardless of the value of the surface band gap.

4.4.3.2 The Effect of the Surface Recombination on the Photocurrent

Surface recombination, a property of the surface of the semiconductor where the carriers may be able to recombine with relative ease, is a factor that is hard to control and yet this factor has significant effect in the performance of a solar cell. Surface recombination effects the carriers excited close to the surface of the semiconductor. The window effect of the graded band gap cell, maintains this number at relatively low levels so that the overall effect of the surface recombination on the total photocurrent flowing through a graded band gap device is small, as is shown in figure 4.13 . Figure 4.13 also shows the effect of increasing surface recombination velocity on the photocurrent flowing through a homojunction type of a device. Since in a homojunction the absorption of photons of all energies greater than the band gap starts at the surface, the very large number of carriers excited at or close to the surface is susceptible to the

surface recombination. Thus an increasing surface recombination velocity effects the total photocurrent in a homojunction cell far more than it does the current in a graded band gap cell. Figure 4.13 illustrates this and clearly demonstrates the advantage of the use of the window effect.

4.4.3.3 The Effect of the Width of the Surface Layer on the Photocurrent

The width of the graded band gap surface layers is a parameter which, like the surface band gap, influences the magnitude of all of the current components. For a given set of conditions, such as the hole diffusion length and the surface recombination velocity, there is an optimum value of the width of the surface layer. In both, a graded band gap cell and an homojunction cell, the optimum width of the surface layer required for maximum hole current is lowered by an increasing surface recombination velocity. The number of carriers lost by surface recombination decreases with a thin surface layer, and a layer thickness must be chosen to minimise this decrease without undue loss of absorption within the layer. As is shown in figure 4.14 , for a similar set of conditions , the optimum width of the surface layer required for maximum hole current is smaller and better defined for a homojunction cell than for a graded cell because in a homojunction cell all the absorption starts at the surface itself. However, as is the case with a

small value of the surface band gap, a thick surface layer results in a decrease of current components from the depletion and base layers due to a decrease of the number of photons reaching these layers. Thus, the optimum width of the surface layer required for maximum total photocurrent is less and better defined than that required just for maximum hole current, as is shown in figure 4.15.

The optimum width of the surface layer is also, of course, directly related to the minority carrier diffusion length as is illustrated by figure 4.16. Furthermore, the optimum width is also related to the magnitude of the absorption coefficient, so that large absorption coefficients favour thin surface layers, as is illustrated by figure 4.17.

Thus the optimum width of the surface layer has to be tailored to the surface recombination velocity, hole diffusion length and the absorption coefficient.

4.4.3.4 The Effect of the Diffusion Lengths in the Photocurrent

The magnitude of the hole photocurrent is, as expected, a strong function of the hole diffusion length, as is shown in figure 4.18. The fact that in a graded band gap cell the absorption is gradual and that the built-in field assists the transport of carriers makes the current in the graded cell less sensitive to a

decrease in the value of the hole diffusion length than that in the homojunction cell. Furthermore, the fact that a major part of the total current generated in a homojunction device is generated in the surface layer makes the performance of this type of cell more dependent on the hole diffusion length than that of the graded band gap cell, where, due to the window effect, the current components from the base and depletion layers form a significant portion of the total current.

The effect of the electron diffusion length on the performance of a cell is similar to that of the hole diffusion length. However, the base current being a more significant component of the total current, the performance of a graded cell is more sensitive to the decrease of electron diffusion length than that of a homojunction type of a cell.

4.4.3.5 The Effect of the Base Layer Band Gap on the Photocurrent

The choice of the band gap in the base layer, i.e. in the depletion layer, is very important for two reasons, firstly this choice determines the minimum energy of photons that can be absorbed in the structure, and secondly it determines the magnitude of the voltage output of the cell and the leakage current (I_o). According to the calculations

carried out by Loferski (see Chapter 2) the compromise between these two considerations for a homojunction cell results in an optimum band gap value of about 1.5 eV . A similar type of investigation was carried out for both a homojunction cell and a graded band gap cell using the product of the current efficiency (total photocurrent divided by the total number of photons incident on the structure) and the band gap in the depletion layer (considering the voltage output of the cell as directly proportional to this band gap) as a factor proportional to the power output of the cell. It is found, in agreement with Loferski , that the optimum band gap for a homojunction device is 1.5 eV . However, the optimum base layer band gap in a graded cell with a surface band gap of 2.4 eV is found to be about 1.3 eV, as is shown in figure 4.19. The reason for the shift of the optimum band gap in a graded cell is that in a graded cell the low energy photons, which are much more numerous than the high energy ones (see fig 4.3) are absorbed more efficiently than they are in a homojunction cell. This makes the current gain caused by an increased number of absorbed photons greater than the voltage loss caused by a decrease of the band gap, thus making 1.3 eV rather than 1.5 eV the optimum base band gap.

4.4.3.6 The Effect of Other Parameters in the Photocurrent

The rest of the parameters representing physical and material properties of the cell listed in section 4.4.3. have no, or very little effect on the photocurrent, but ought to have an effect on the overall performance of the cell. The densities of states in the two bands ($N_C N_V$), the permittivity of the semiconductor (ε) and the donor and acceptor densities (N_D,N_A) effect the magnitude of the photocurrent only slightly via the width of the depletion layer as is shown by equation 52. However, the concentration of impurities, i.e. donors and acceptors, is very important in determining the series resistance of the cell. Similarly with the thickness of the base layer which, if larger than the electron diffusion length, has no effect on the photocurrent, but has an effect on the series resistance of the cell.

4.4.4 Optimisation of the Graded Band Gap Solar Cell

It is now possible to deduce the optimal configuration of a graded band gap solar cell. Since the absorption coefficient is a property of the material itself, and cannot be varied, the width of the surface layer has to be chosen to fit the absorption coefficient. The value of the absorption coefficient, assumed to be independent of energy, is typically $10^6 m^{-1}$ to $10^7 m^{-1}$ for both CdS and CdTe; thus, a mean typical value of $5.10^6 m^{-1}$ is assumed. The optimum width of the surface layer for this absorption coefficient is about 0.5μm, as is shown in figure 4.17. The optimum width of the surface layer is modified by the magnitude of the hole diffusion length and surface recombination velocity. The magnitude of the surface recombination velocity, which is also a property of the material, is assumed to be 10^3 m/s (10^5 cm/s) which is a compromise between the surface recombination large enough to totally deplete the layer from the carriers generated near the surface (10^6 m/s) and zero surface recomination, as is shown in figure 4.13. From figure 4.15 it is deduced that the optimum width of the surface layer for this surface recombination is about .4μm. The diffusion length of the holes in the graded band gap layer, is assumed to be 0.1μm, which corresponds to the typical grain size observed

in the mixed and graded films of CdS_xTe_{1-x} (see chapter 5). This low value of the hole diffusion length has the tendency to reduce the optimum width of the surface layer to about 0.2μm. Finally, in order to obtain low series resistance the surface layer ought to be as wide as possible. However, obtaining the exact value of the optimum width of the surface layer is not crucial because, the deviation of about 0.1 μm in the width of the surface layer from the optimum results in, at most, 5% decrease of the total photocurrent. Thus, the value chosen as the optimum width of the surface layer is about .3μm $\pm$ .1μ. The value of the surface band gap that results in the largest photocurrent in a graded band gap cell is the maximum value allowed, i.e. 2.4 eV of pure CdS. The optimum value of the band gap in the base and depletion layers is 1.3 eV to 1.4 eV, as is shown in figure 4.19. The thickness of the base layer ought to be as large as possible in order to keep the series resistance low. Since the value has no effect on the photocurrent, as long as it is larger than the electron diffusion length, (assumed to be 0.1 μm) a value of about 1μ for the width of the base layer is chosen.

As has been indicated in previous sections, the values chosen for the other constants (D_n,D_p,N_c,N_p,N_A,ε) have been deduced from published data and measurements made on mixed films of CdS_xTe_{1-x} and from considerations about series resistance of the cell. The doping concentrations of about $10^{23}m^{-3}$

resulted in 10 Ωcm resistivity of the films which is about right for II-VI semiconductor solar cells.

Thus, a solar cell with a 0.3 μm thick n-type surface layer with a band gap graded between 2.4 eV and 1.3 to 1.4 eV on top of a p-type base layer with a band gap of 1.3 to 1.4 eV and 1μ thick ought to be an optimum graded band gap CdS_xTe_{1-x} solar cell. The total photocurrent of this thin film cell is calculated to be 302 A/m^2 . Assuming a typical photovoltage of about 0.5 V, the photocurrent implies that the power efficiency of the cell could be about 11.5%.

4.4.5 Comparison of a Graded Band Gap cell and Other Types of Cells

In figures 4.10 to 4.19 it is the normalised current, i.e. the percentage of the maximum recorded current, that is plotted against the variable parameter. This method of presentation was chosen in order to demonstrate the effect and the magnitude of the effect of the variable parameter on the photocurrent generated in both the graded band gap cell and the homojunction cell. This method of presentation also demonstrates clearly the advantages of a graded band gap solar cell over a homojunction cell. Figure 4.13 clearly shows the advantage of the window effect. Figures 4.14 to 4.16 show that due to the gradual absorption, thicker surface layers may be used in the graded cells than in the homojunction cells and thus lower series resistances can be obtained. The fact that smaller diffusion lengths can be tolerated in the graded cell than in the homojunction cell implies that the efficiency of collector of photogenerated carriers is higher in the graded cell than in the homojunction cell. Furthermore, the radiation resistance of the graded band gap cell can be expected to be better than that of the homojunction cell,due to , again, the fact that the performance of the graded cell is less sensitive to the variations of the diffusion lengths. However, the advantages of the graded band gap solar cell over a conventional homojunction solar cell is

most clearly mirrored in the magnitudes of currents generated in each structure. When an optimal graded band gap solar cell is compared with the optimal homojunction solar cell (thickness of the surface layer is 0.2μm and the rest of parameters are same as in the optimal graded cell), the current generated in the graded cell is 1.75 times larger than the one generated in a homojunction cell. Assuming that similar voltage outputs can be obtained from both types of devices , this implies that the conversion efficiency of a thin film graded band gap cell could be 1.75 times larger than that of a thin film homojunction cell.

Comparison between the graded band gap cell and a heterojunction cell was not made because the method of calculation ofr photocurrent in the graded and homojunction cells could not easily be adopted to calculate the photocurrent in a heterojunction type of a cell. However, in spite of the fact that the graded and heterojunction structures share the same advantages such as the window effect, the performance of a graded band gap cell can be expected to be better than that of a heterojunction cell for two main reasons. Firstly, due to the built-in field, the effective diffusion length, and hence the efficiency of collection of the photogenerated carriers, can be expected to be higher in the surface layer of the graded cell than in either of the two layers in a heterojunction cell, provided that cells made from similar materials are compared (similar carrier life-times etc.). Secondly,

due to the fact that the junction in the graded band gap cell is essentially a homojunction, the recombination current, and hence the overall leakage current, in the heterojunction cell can be expected to be much higher than the one in the graded band gap cell, especially of the crystal lattice mismatch between the two layers of a heterojunction is as large as the one between CdS and CdTe.

Thus, this theoretical analyses clearly points out the advantages of a graded band gap solar cell over the conventional solar cells, and efficiencies almost twice as large as those encountered in homojunction cells can be expected.

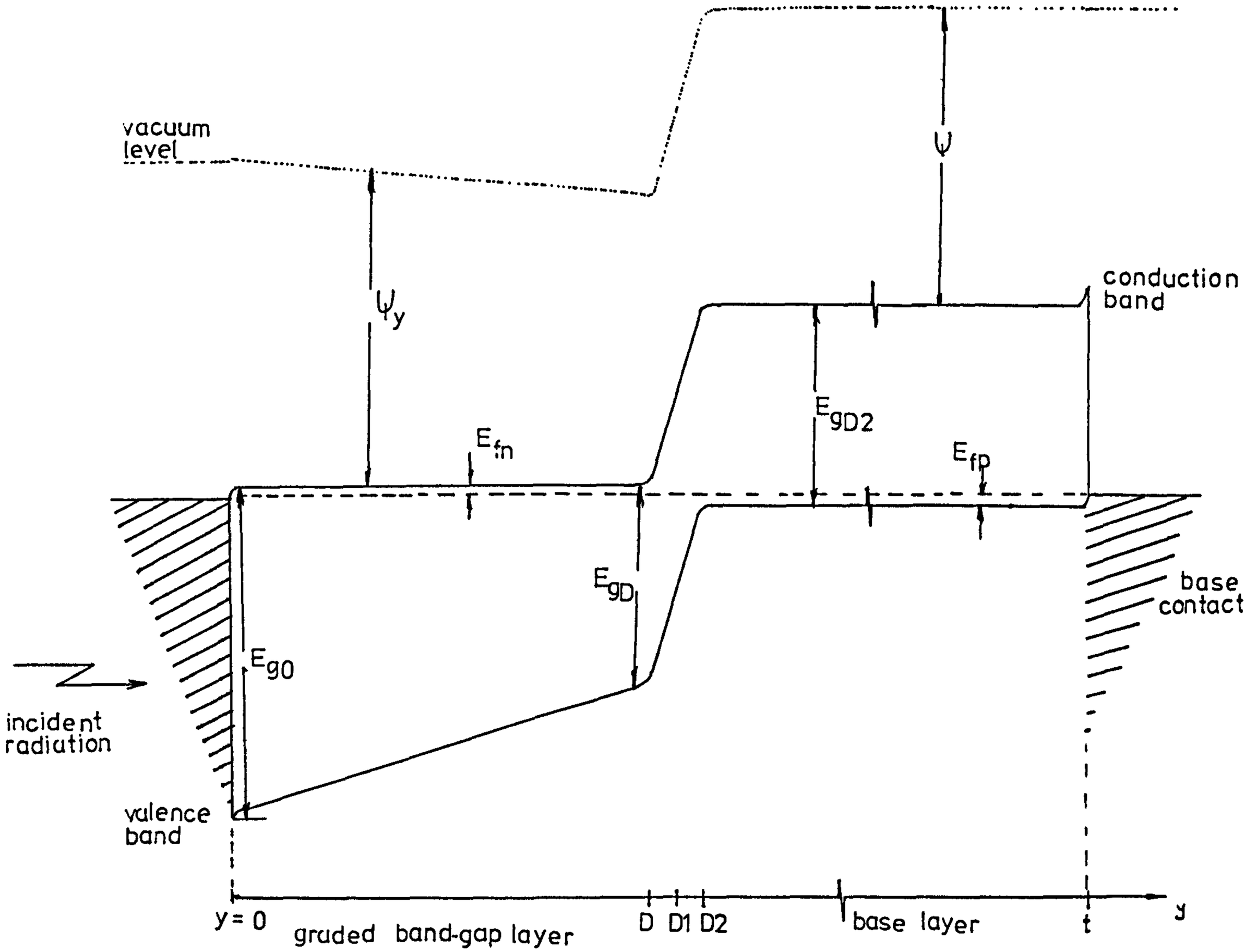

FIGURE 4.1 band diagram of a graded band gap CdS_xTe_{1-x} solar cell

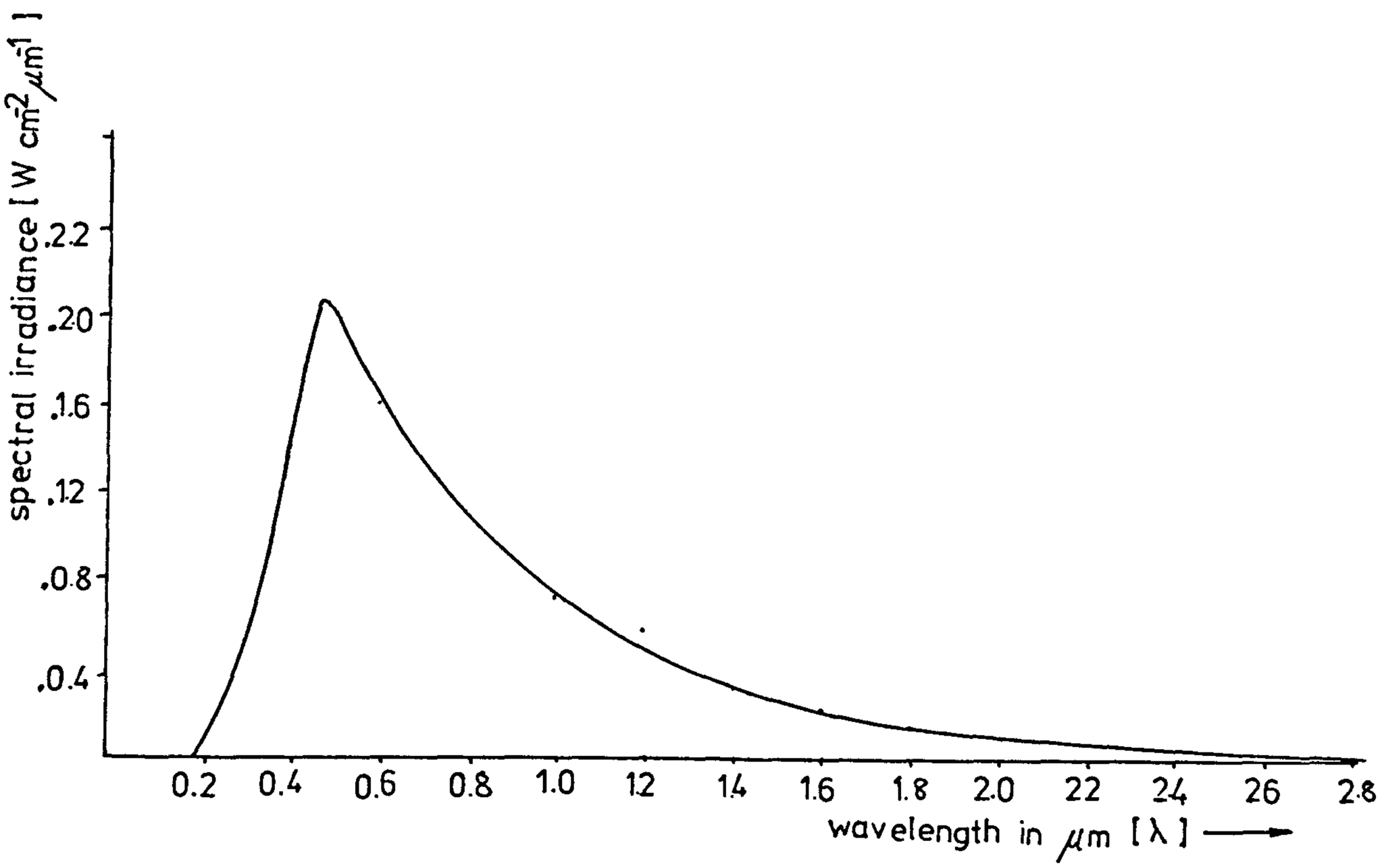

FIGURE 4.2 power spectral irradiance (P) vs the wavelength (λ) of the solar spectrum at AM-0 conditions

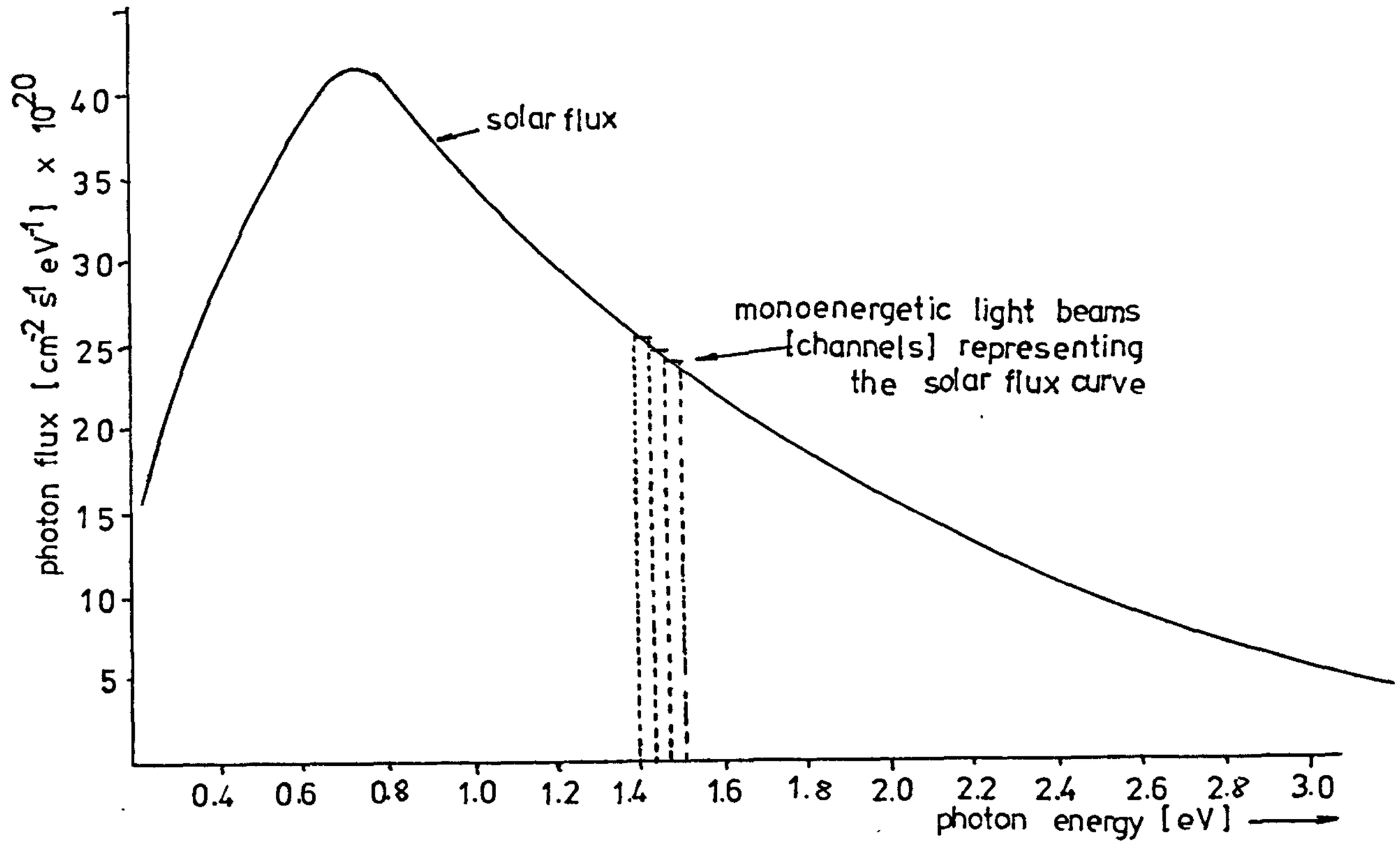

FIGURE 4.3 photon flux density vs photon energy for the AM-0 radiation

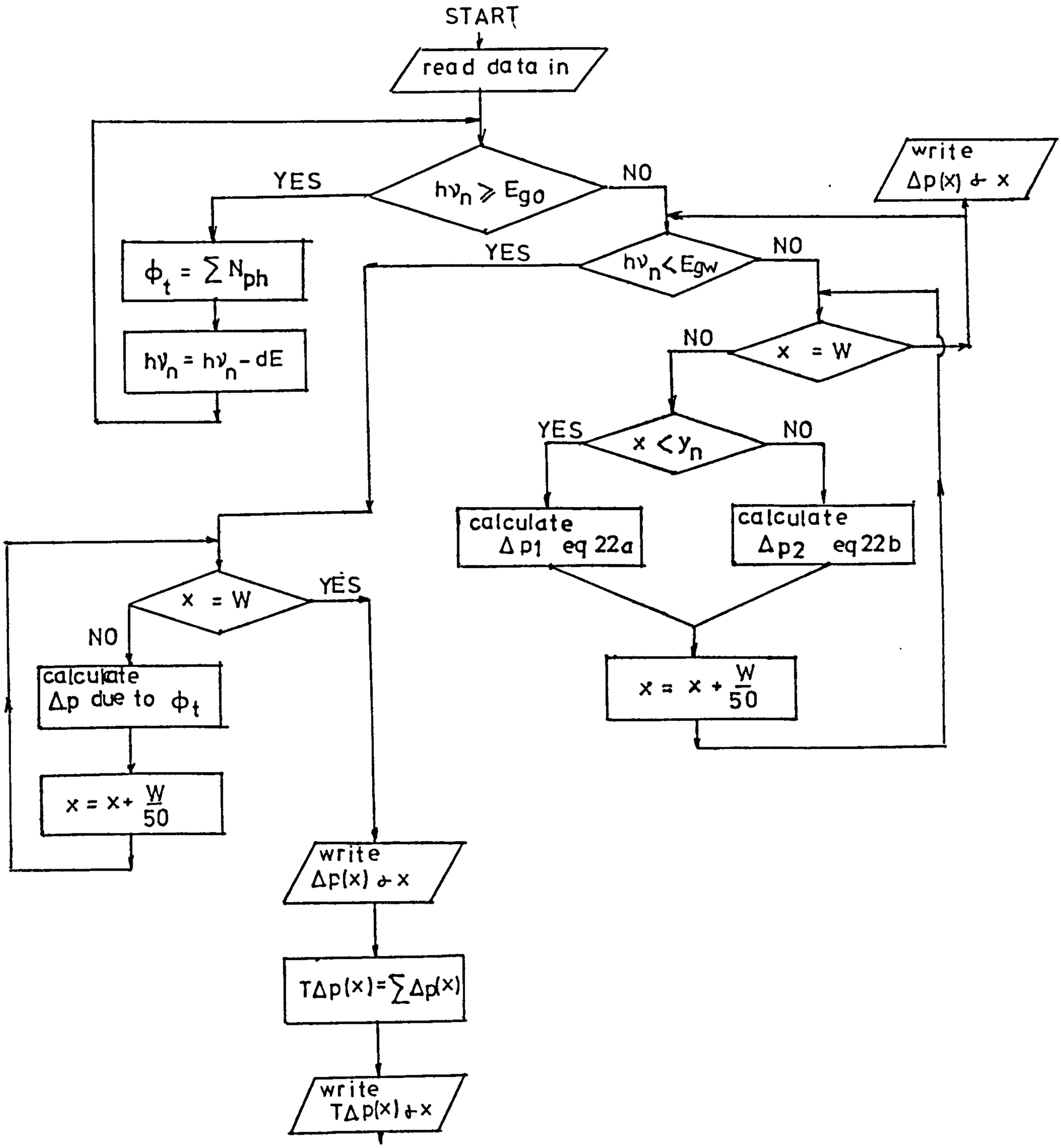

FIGURE 4.4 flow diagram of a program used to calculate the distribution of carriers in a graded band gap semiconductor

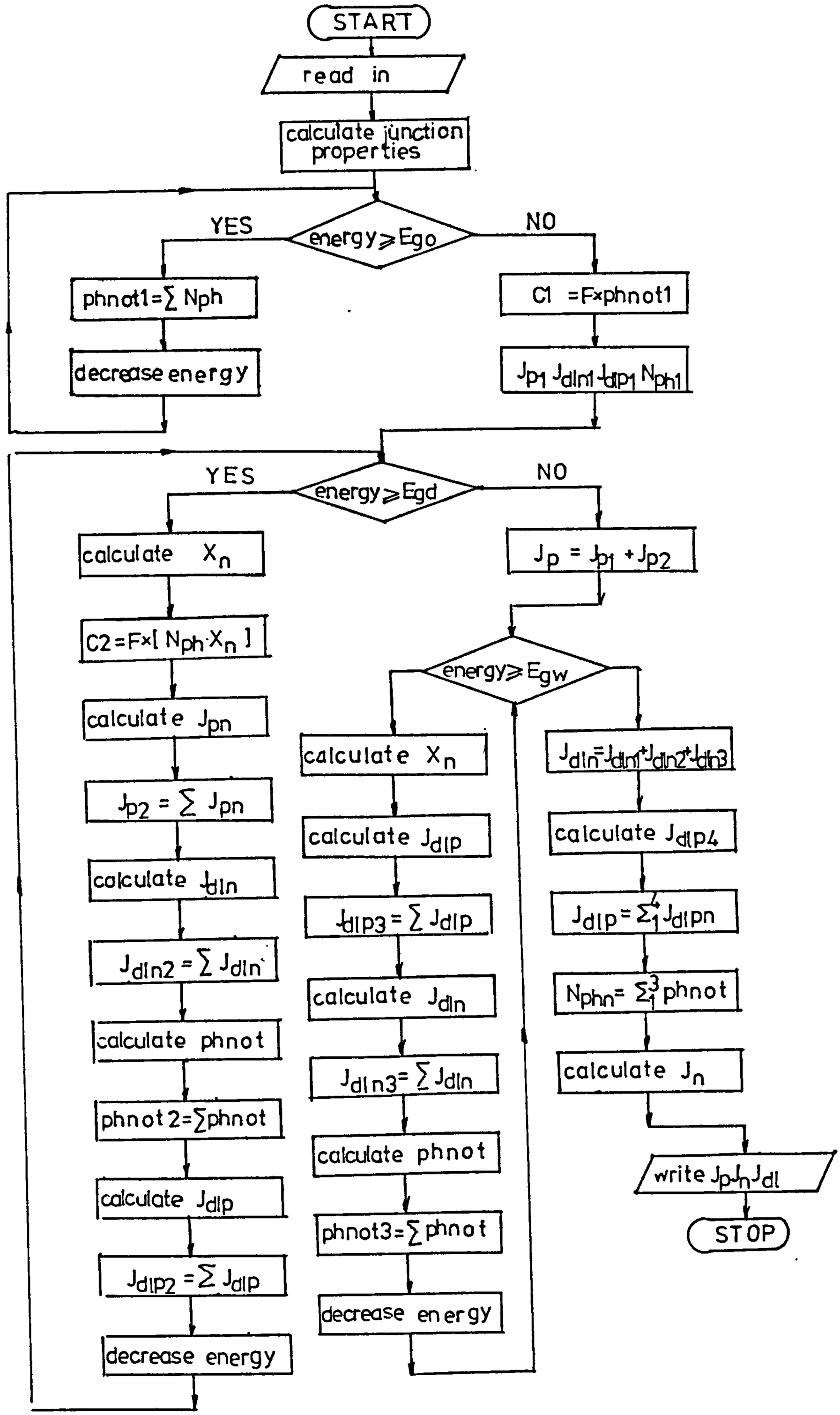

FIGURE 4.5 flow diagram of a program used to calculate the photccurrent in a solar cell

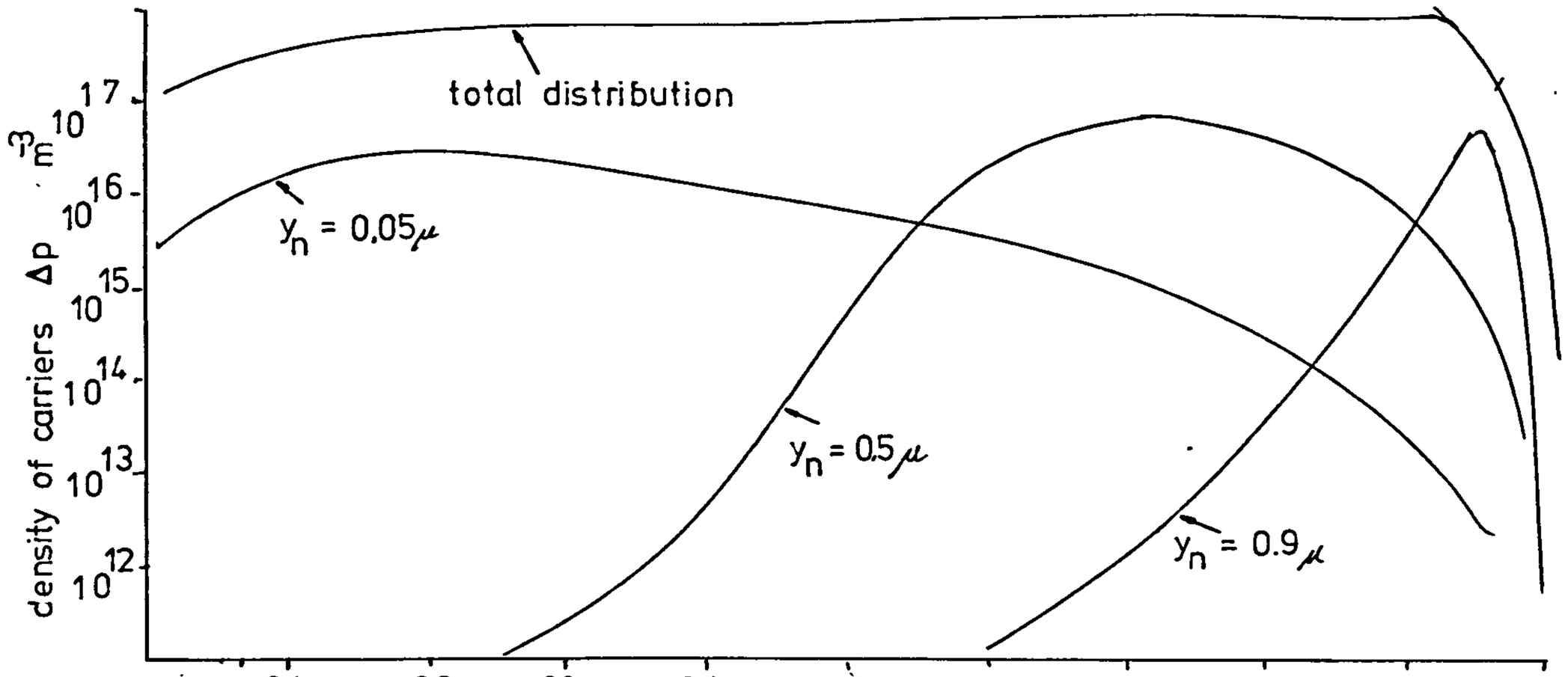

FIGURE 4.6a distribution of carriers due to different photon beams in a semiconductor with a surface band gap of 2.4 eV
[y_n - point where the absorption of a given photon beam begins]

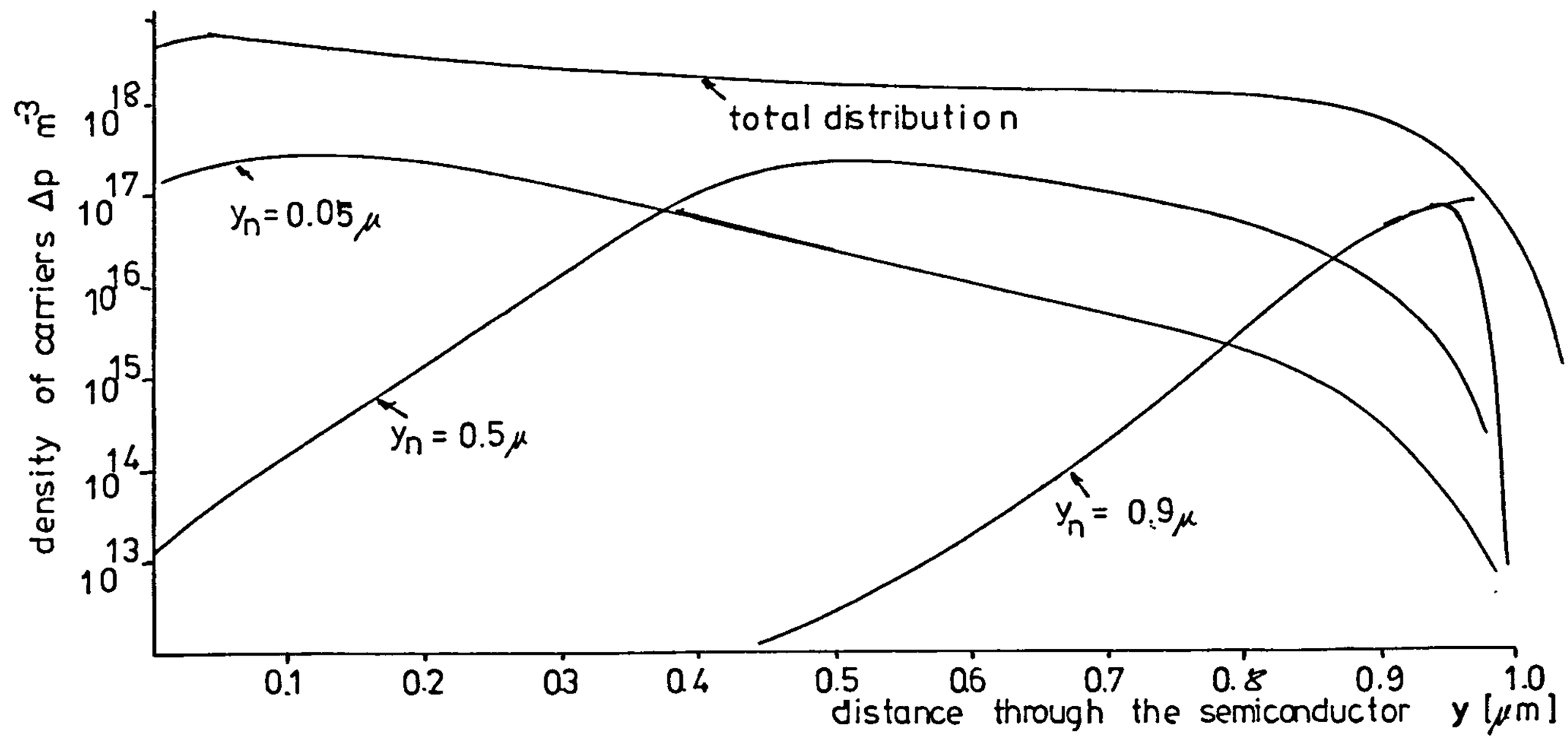

FIGURE 4.6b distribution of carriers due to different photon beams in a semiconductor with a surface band gap of 1.9 eV

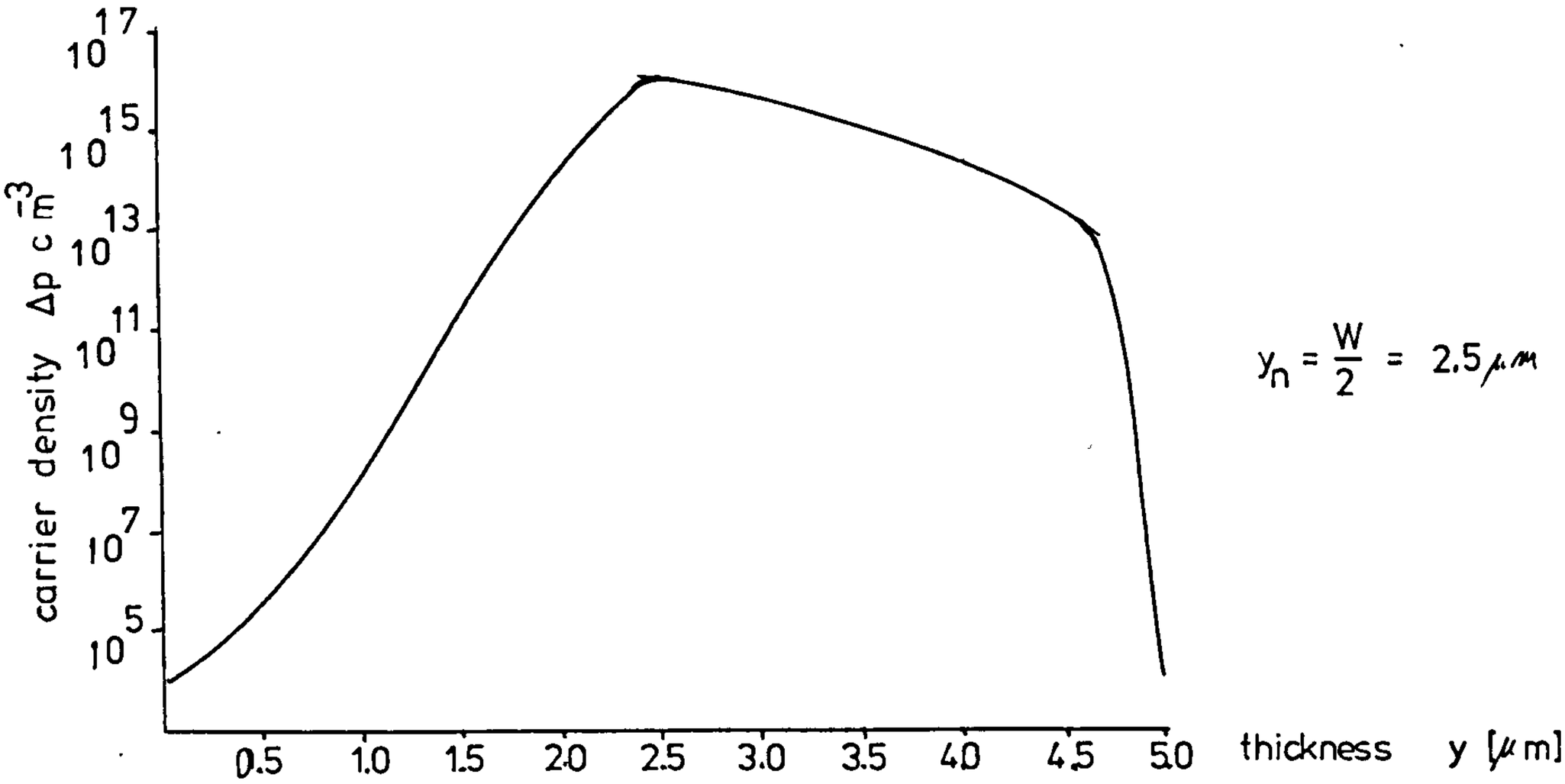

fig a

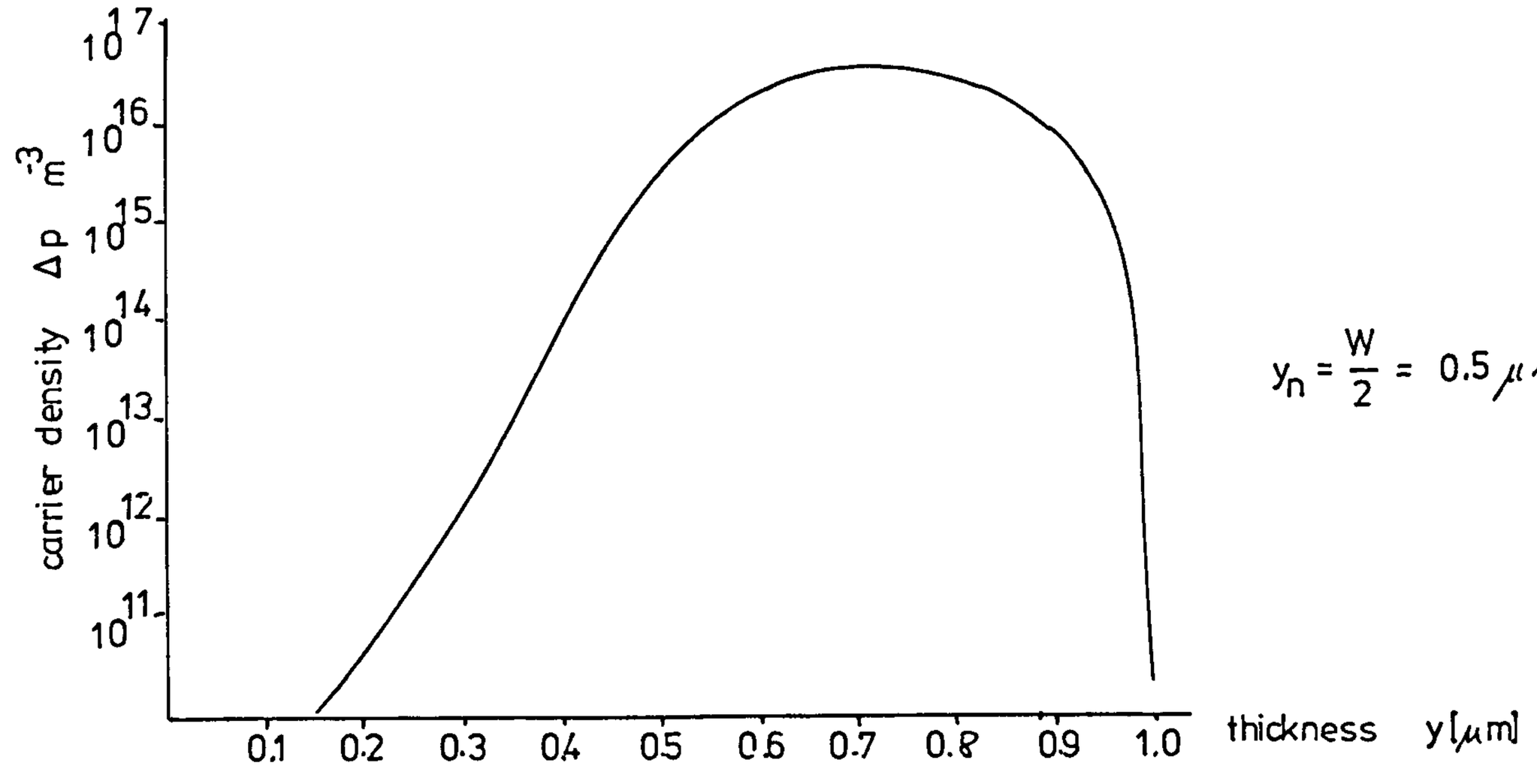

fig b

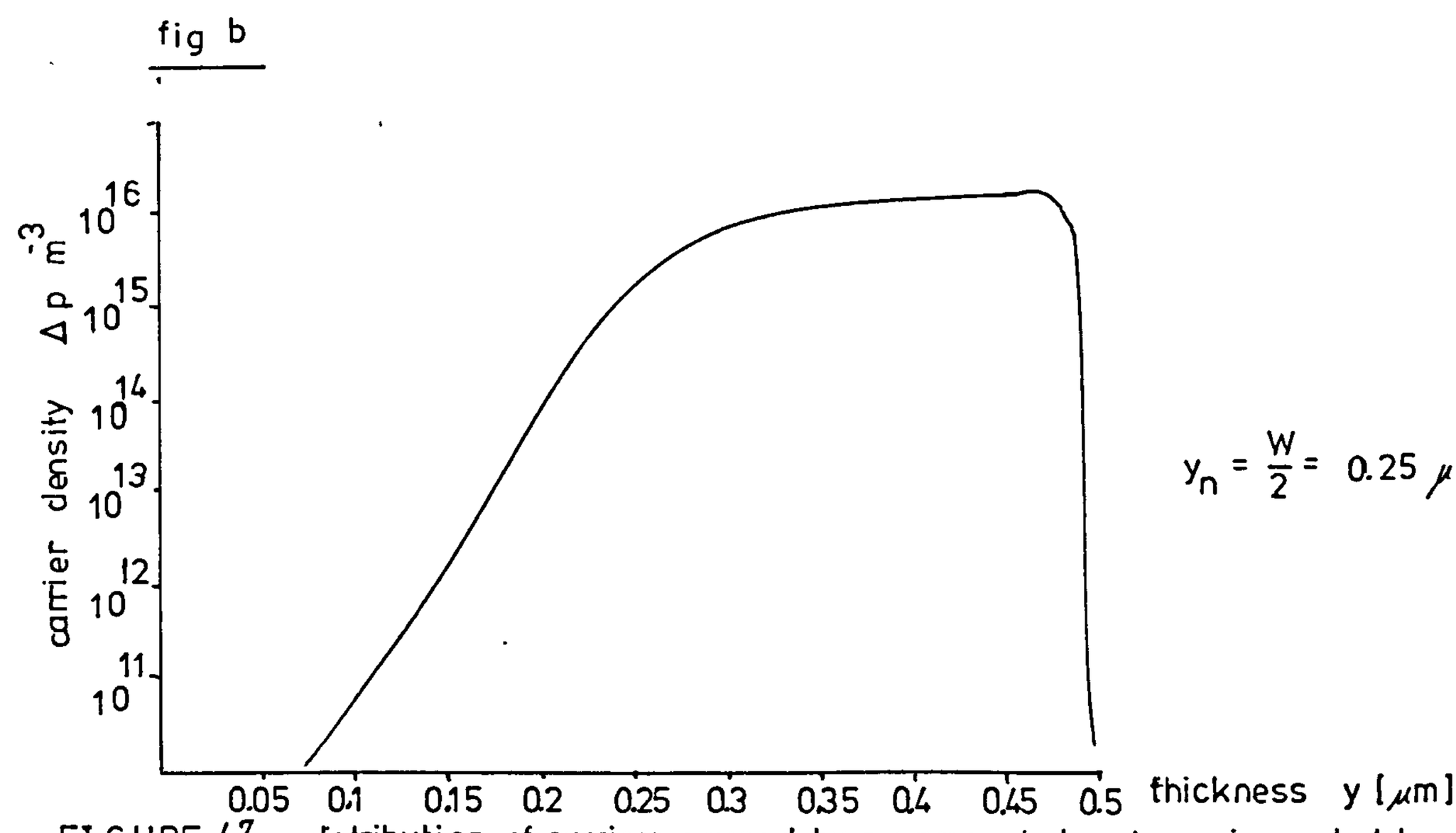

FIGURE 47 distribution of carriers caused by a same photon beam in graded band gap layers [E_{g0} = 24eV] of different thicknesses W
[photon beam energy = 1.95 eV]

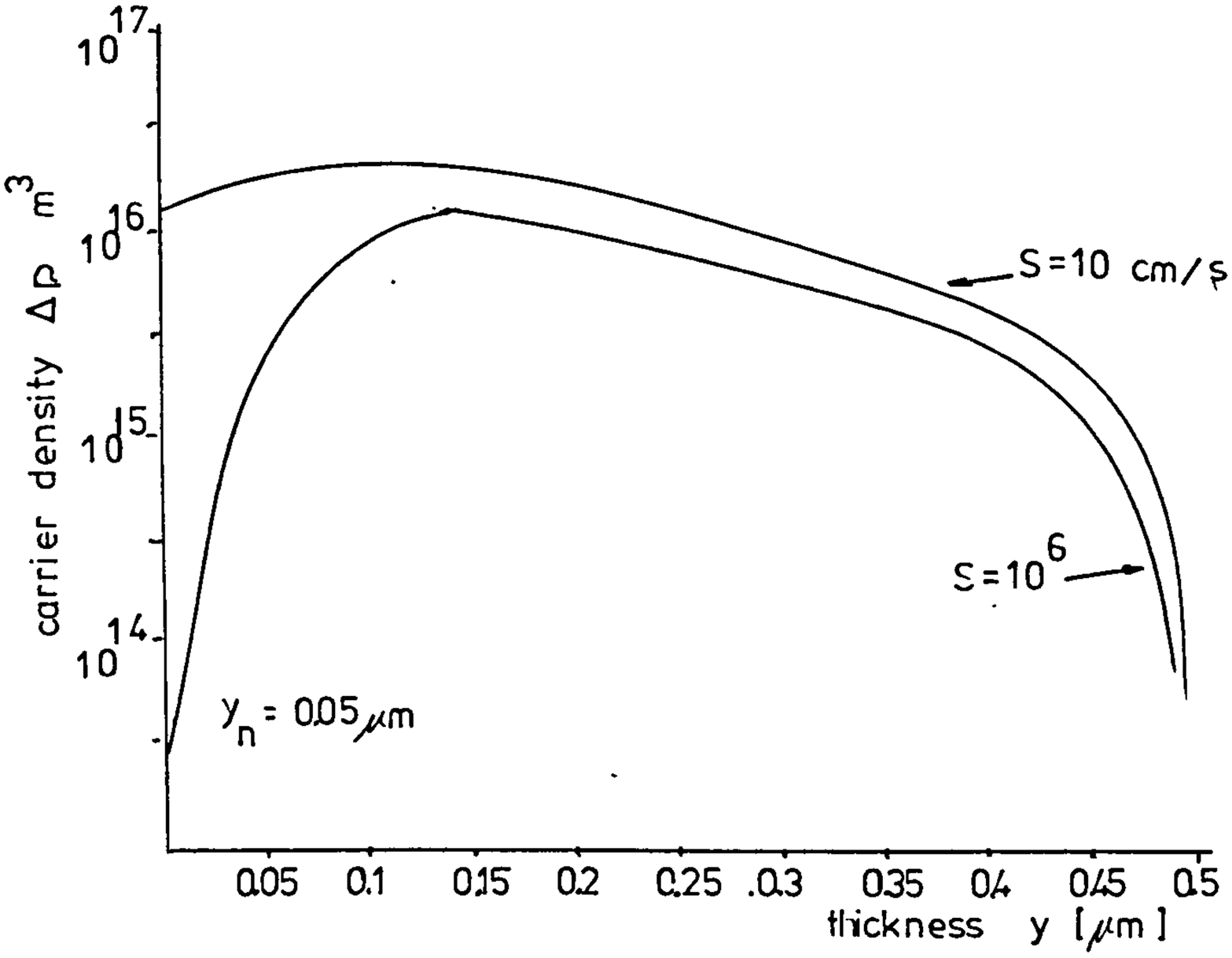

FIGURE 4.8 distribution of carriers for different surface recombination velocities [S]

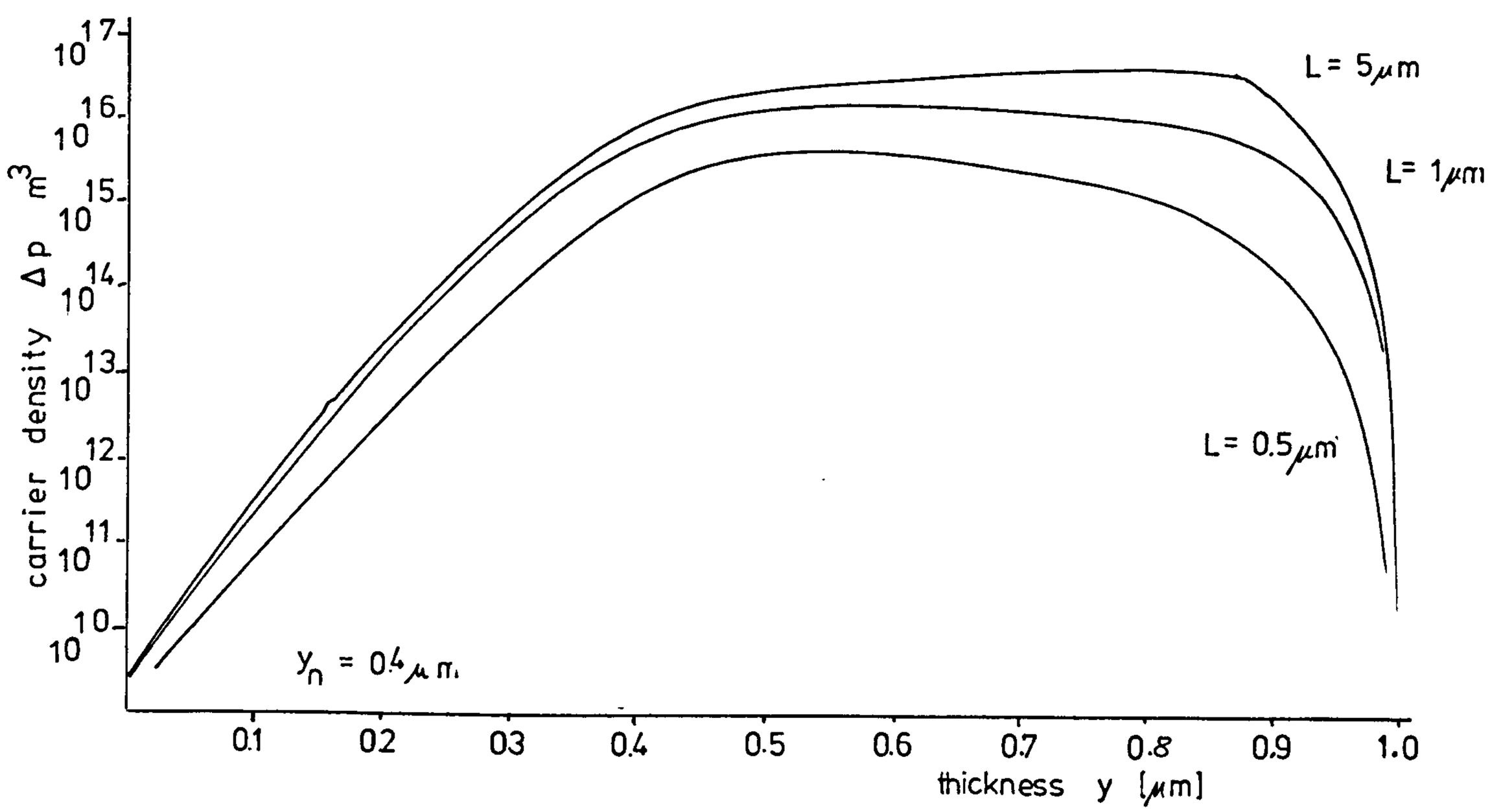

FIGURE 4.9 distribution of carriers for different minority carrier diffusion lengths [L]

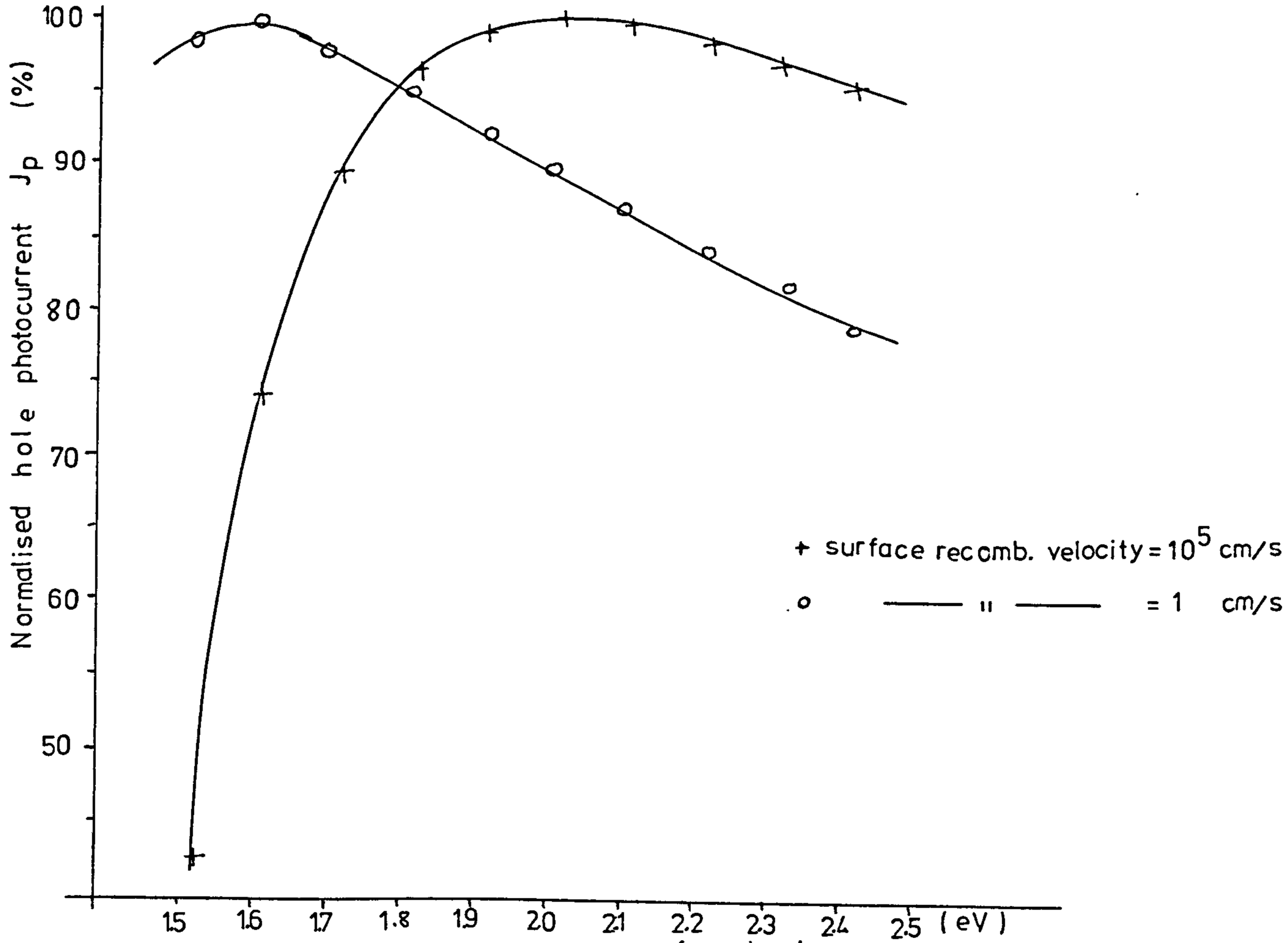

FIGURE 4.10 J_p vs E_{g0} for different surface recombination velocities

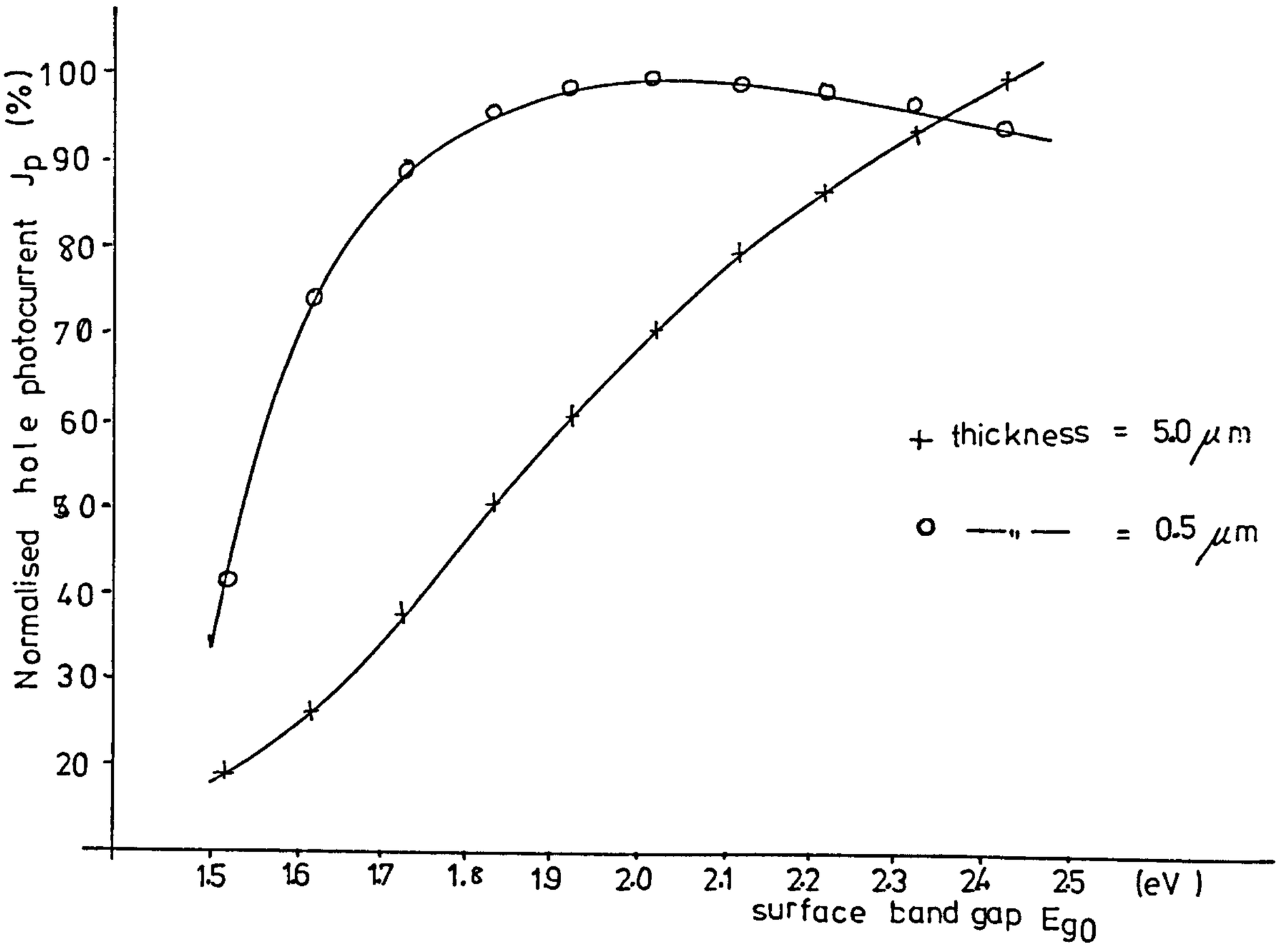

FIGURE 4.11 J_p vs E_{g0} for different thicknesses of the surface layer

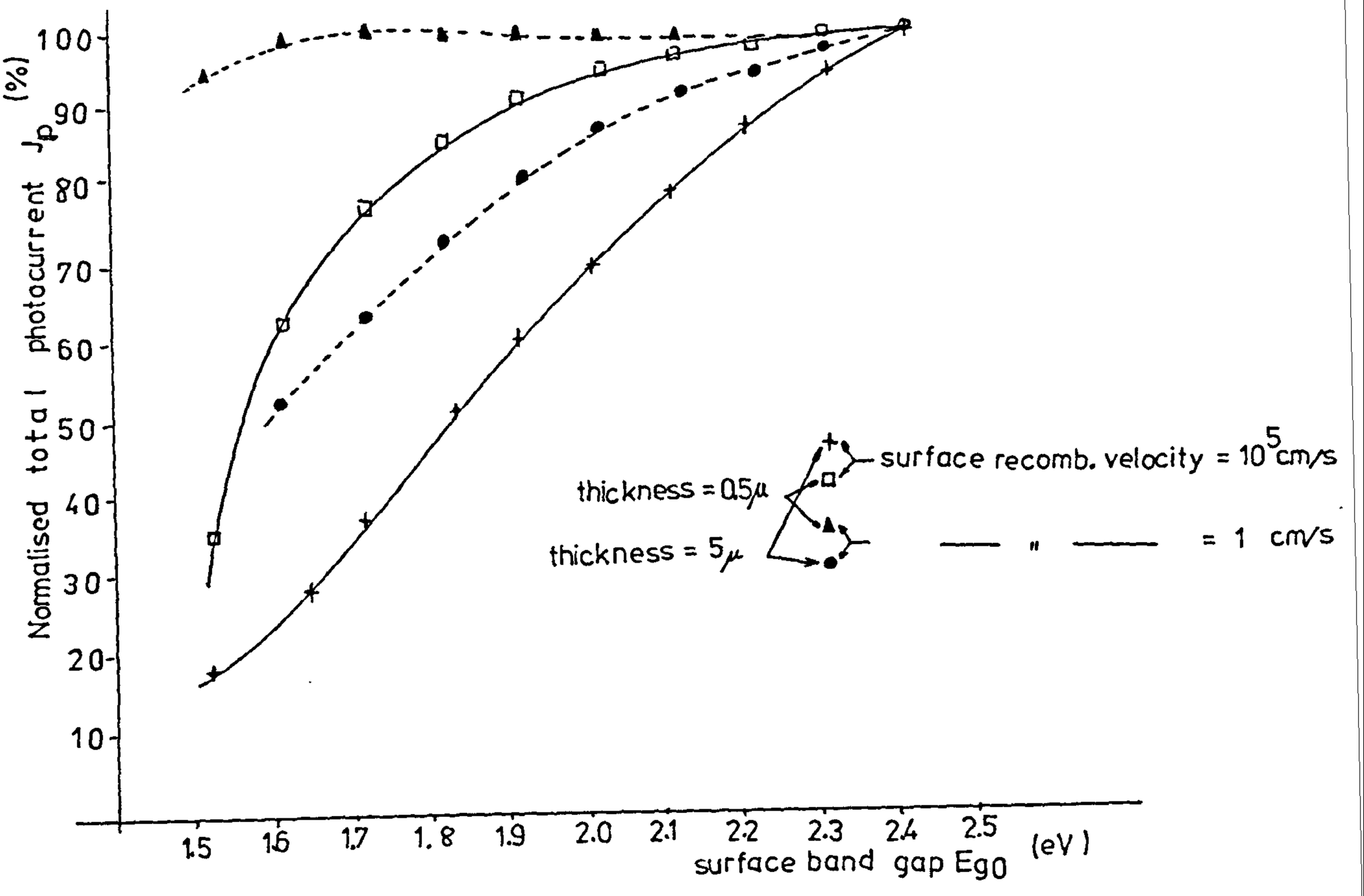

FIGURE 4.12 Total photocurrent vs the surface band gap

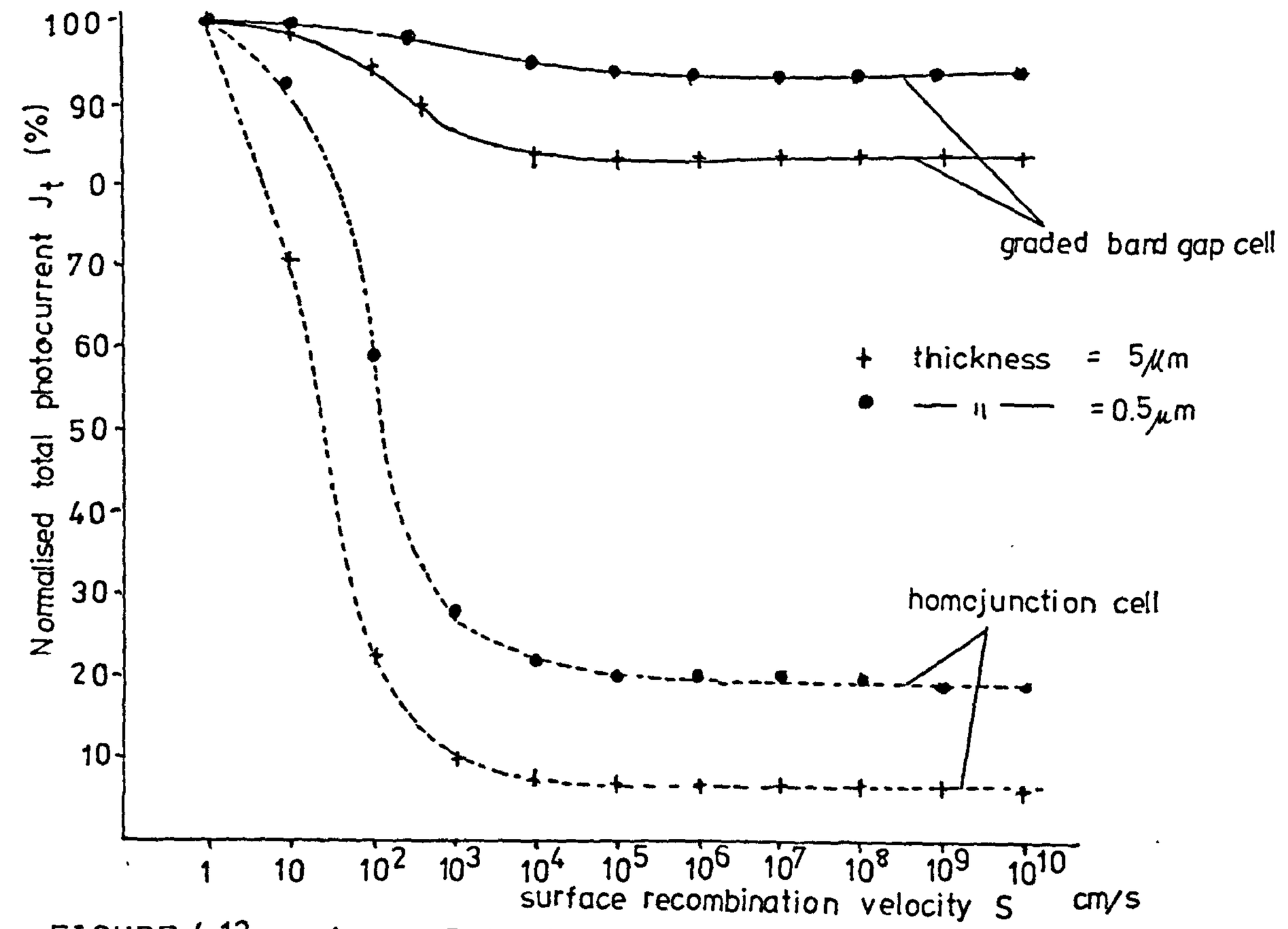

FIGURE 4.13 J vs S for different thicknesses of the surface layer

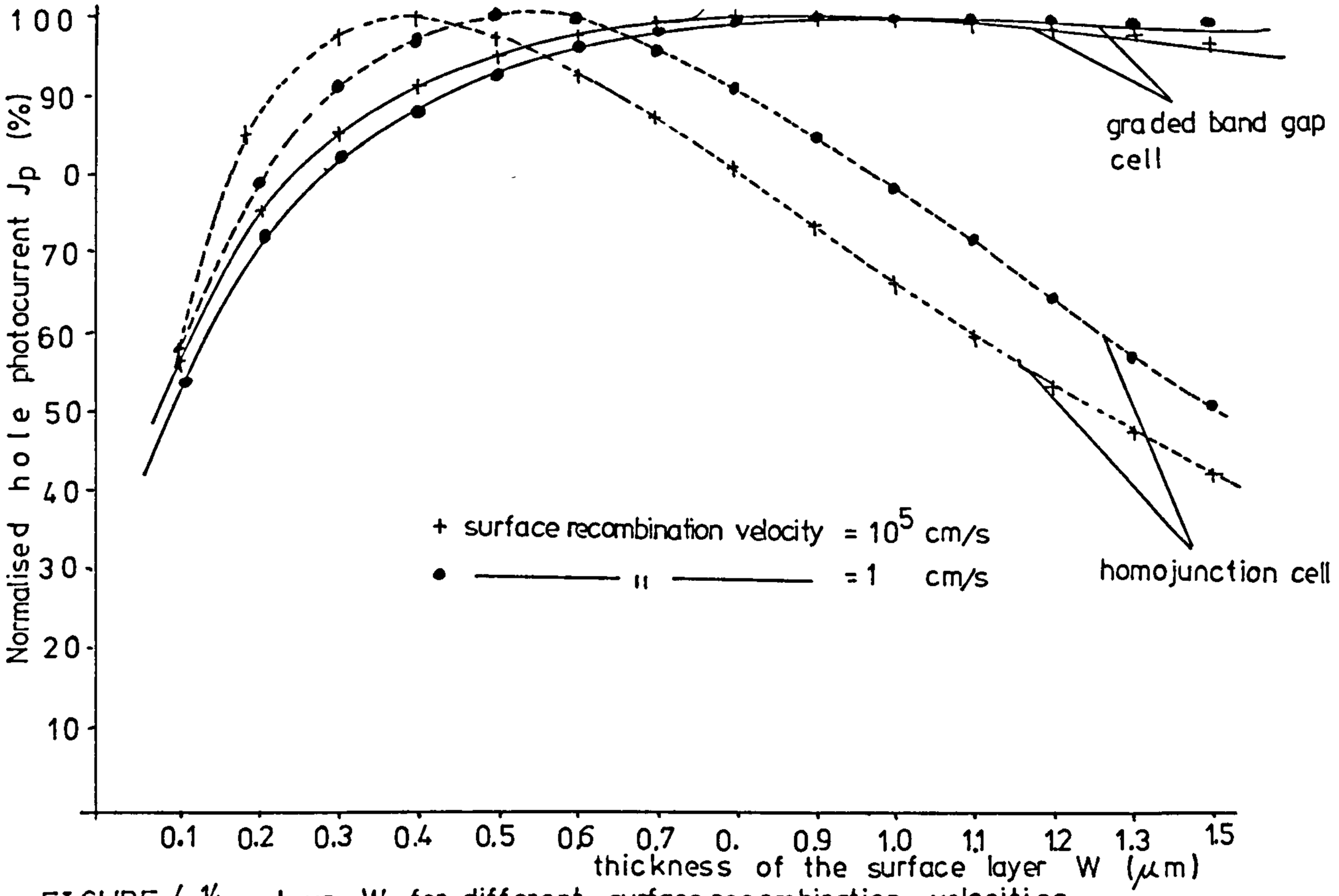

FIGURE 4.14 J_p vs W for different surface recombination velocities

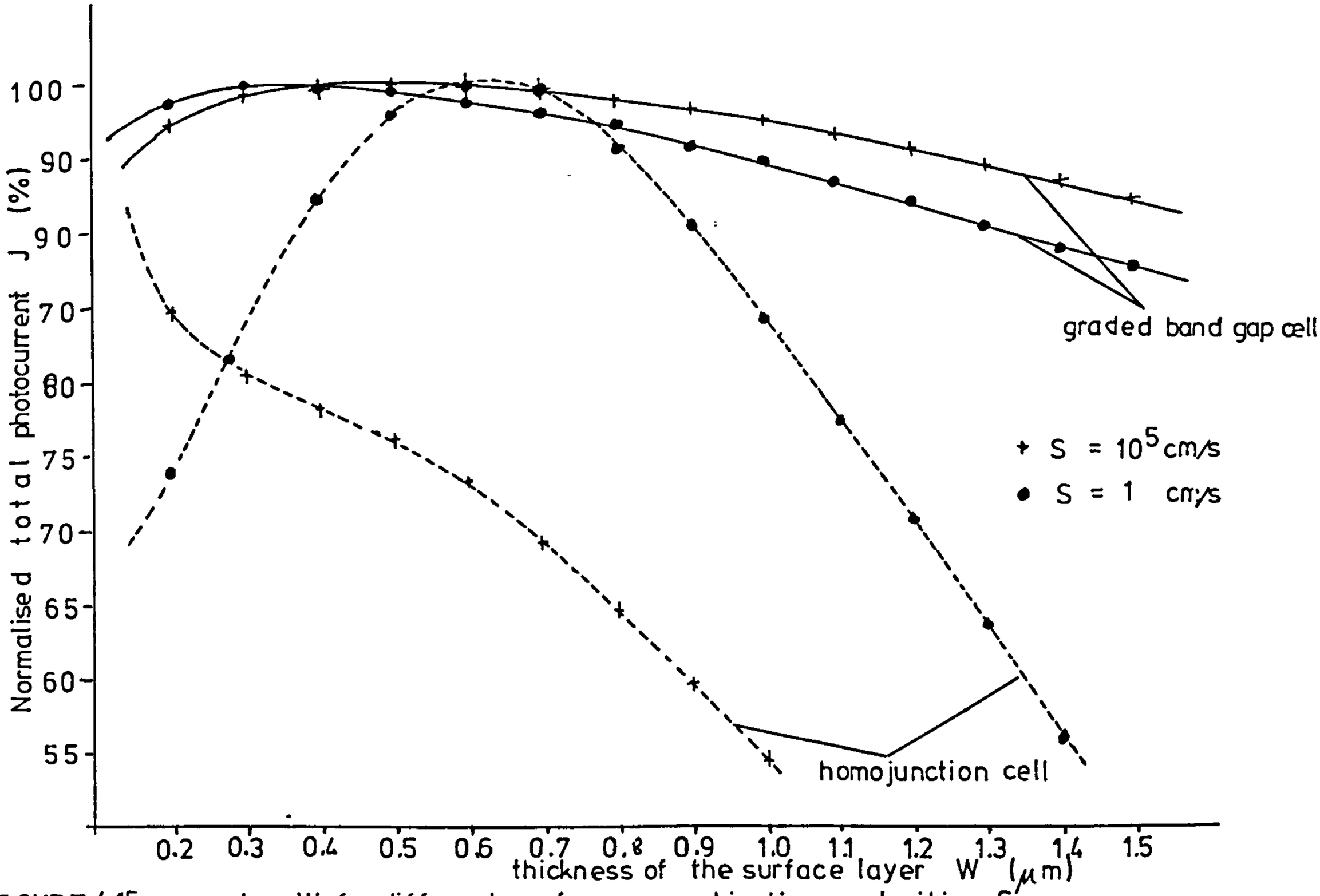

FIGURE 4.15 J_t vs W for different surface recombination velocities S

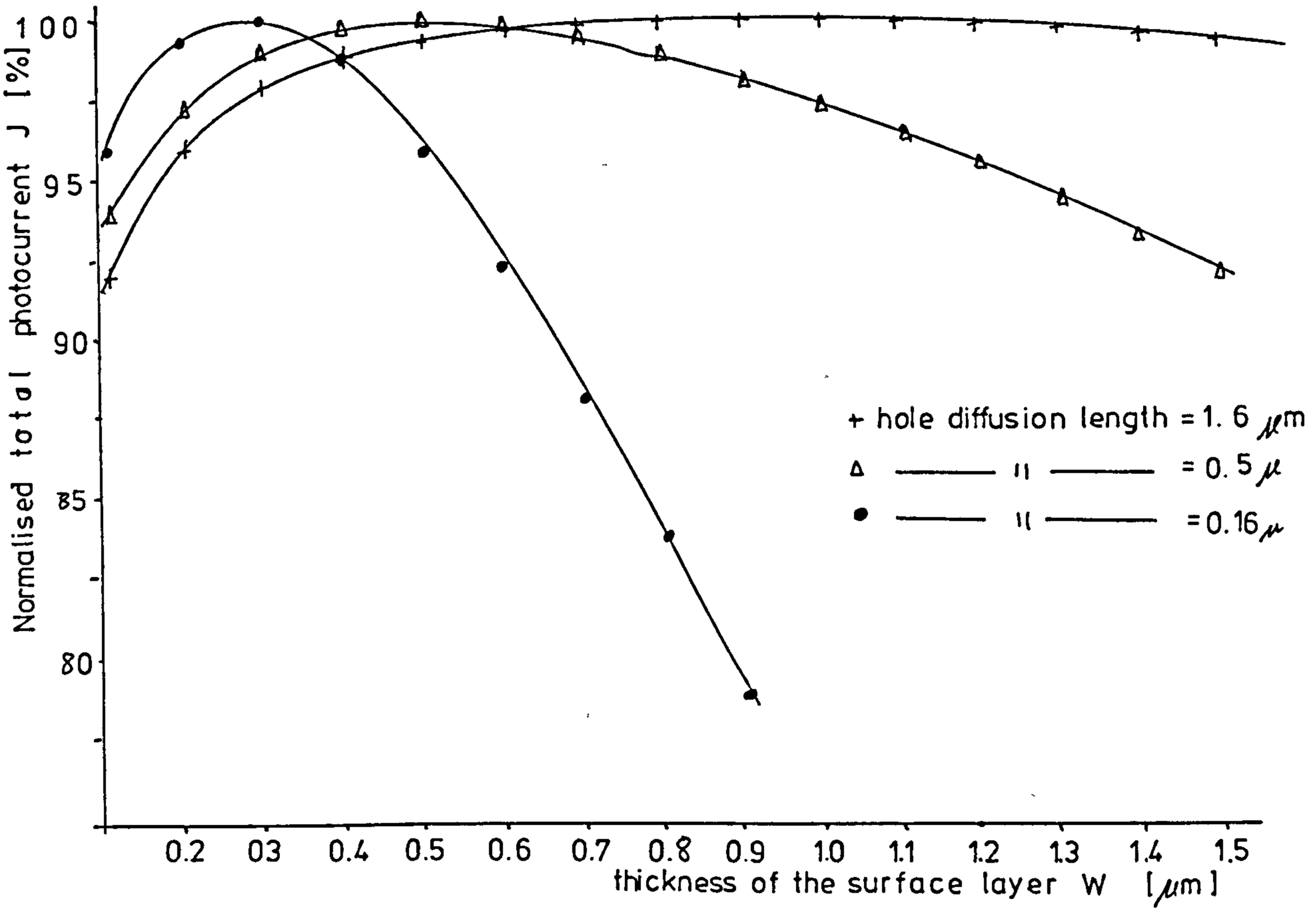

FIGURE 4 16 J vs. W for different hole diffusion lengths

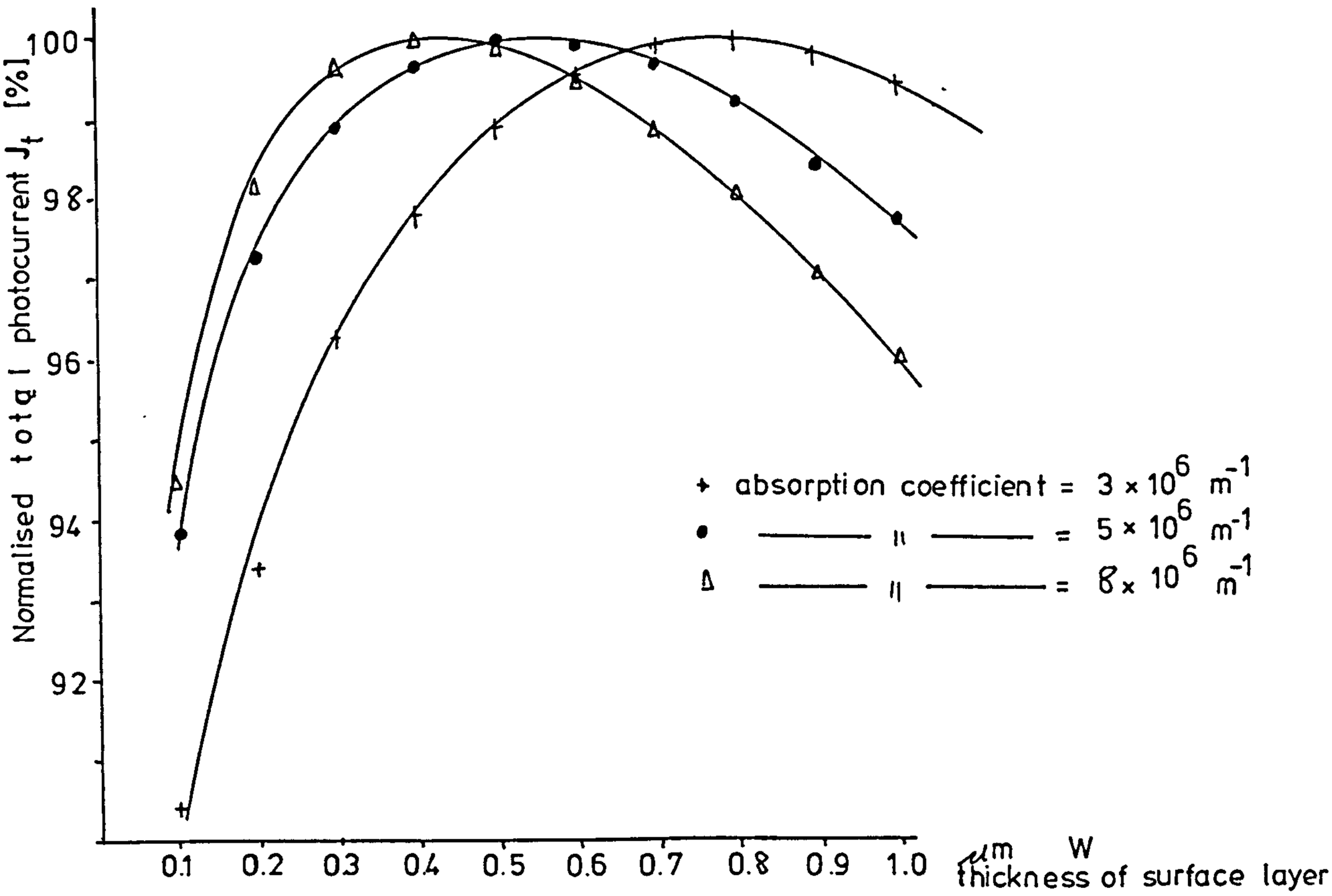

FIGURE 4 17 J vs W for different absorption coefficients

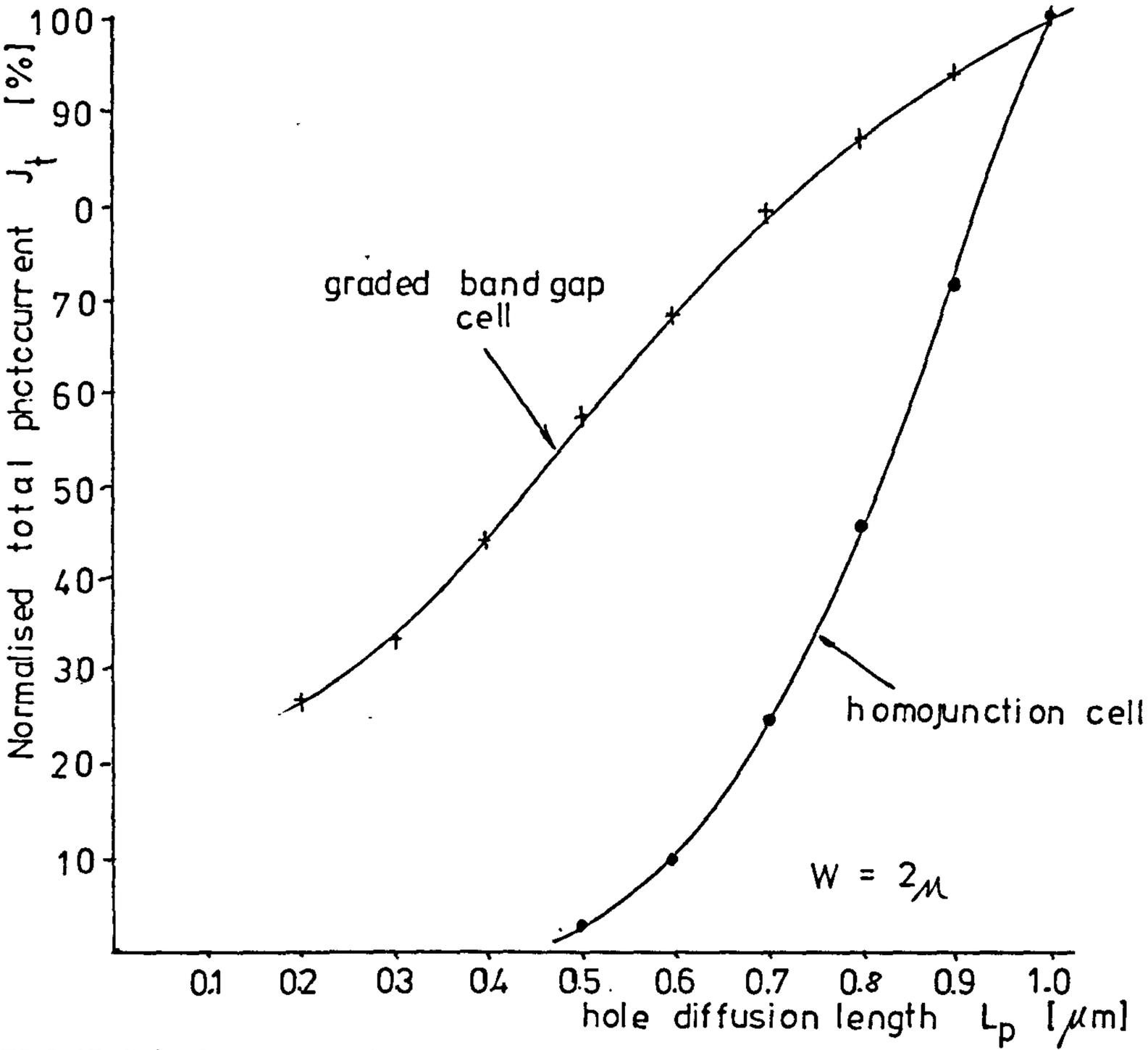

FIGURE 4 18 J_t vs L_p for a graded and a homojunction cell

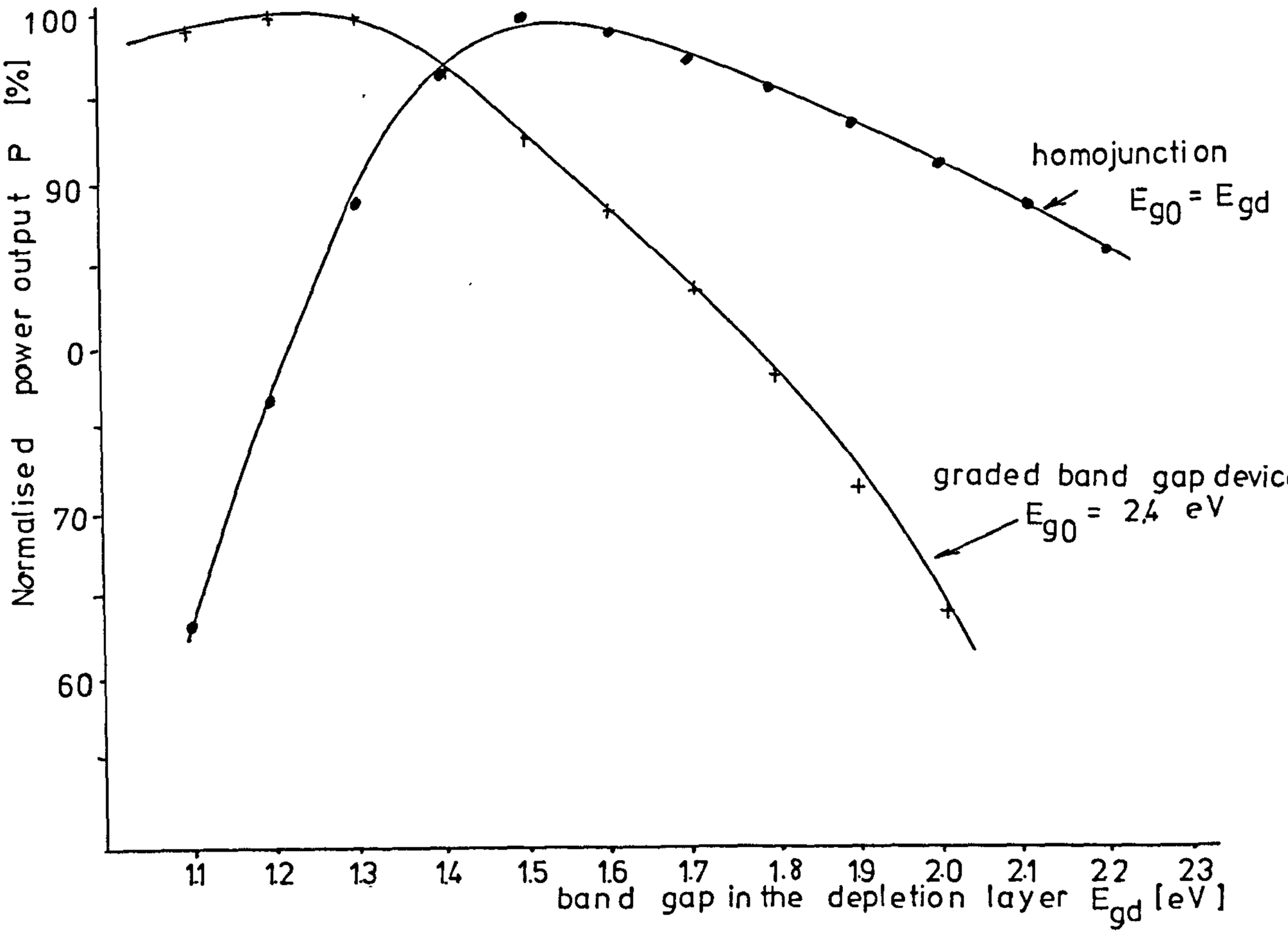

FIGURE 4 19 power output vs the band gap in depletion layer

TABLE I

Spectral irradiance vs wavelength

λ μm	P W $cm^{-2}\mu^{-1}$	λ	P	λ	P
0.30	0.0514	0.50	0.1942	0.950	0.0835
0.305	0.0603	0.505	0.1920	1.000	0.0746
0.310	0.0689	0.510	0.1882	1.1	0.0592
0.315	0.0764	0.515	0.1833	1.2	0.0484
0.320	0.0830	0.520	0.1833	1.3	0.0396
0.325	0.0975	0.525	0.1852	1.4	0.0336
0.330	0.1059	0.530	0.1842	1.5	0.0287
0.335	0.1081	0.535	0.1818	1.6	0.0244
0.340	0.1074	0.540	0.1783	1.7	0.0202
0.345	0.1069	0.545	0.1754	1.8	0.0159
0.350	0.1093	0.550	0.1725	1.9	0.0126
0.355	0.1083	0.555	0.1720	2.0	0.0103
0.360	0.1068	0.560	0.1695	2.1	0.0090
0.365	0.1132	0.565	0.1705	2.2	0.0079
0.370	0.1181	0.570	0.1712	2.3	0.0068
0.375	0.1157	0.575	0.1719	2.4	0.0064
0.380	0.1120	0.580	0.1715	2.5	0.0054
0.385	0.1098	0.585	0.1712	2.6	0.0048
0.390	0.1098	0.590	0.1700	2.7	0.0043
0.395	0.1189	0.595	0.1682	2.8	0.0039
0.40	0.1492	0.60	0.1666	2.9	0.0035
0.405	0.1644	0.605	0.1647	3.0	0.0031
0.410	0.1751	0.610	0.1635	3.1	0.0026
0.415	0.1774	0.620	0.1602		
0.420	0.1747	0.630	0.1570		
0.425	0.1693	0.640	0.1544		
0.430	0.1639	0.650	0.1511		
0.435	0.1663	0.660	0.1486		
0.440	0.1810	0.670	0.1456		
0.445	0.1922	0.680	0.1427		
0.450	0.2006	0.690	0.1402		
0.455	0.2057	0.700	0.1369		
0.460	0.2066	0.710	0.1344		
0.465	0.2048	0.720	0.1314		
0.470	0.2033	0.730	0.1290		
0.475	0.2044	0.740	0.1260		
0.480	0.2074	0.750	0.1235		
0.485	0.1976	0.800	0.1107		
0.490	0.1950	0.850	0.0988		
0.495	0.1960	0.900	0.0889		

TABLE II

Photon flux v.s. photon energy

eV	No s^{-1} cm^{-2}eV	eV	No	eV	No
4.133	5.634 10^{19}	2.480	9.856 10^{21}	1.305	2.907
4.065	6.948	2.455	1.004	1.240	3.028
4.000	8.332	2.431	1.014	1.127	3.200
3.963	9.697 10^{20}	2.408	1.017	1.033	3.396
3.875	1.104	2.384	1.046	0.9538	3.532
3.815	1.359	2.362	1.088	0.8856	3.743
3.757	1.545	2.339	1.113	0.8266	3.933
3.701	1.650	2.318	1.130	0.7749	4.058
3.647	1.714	2.296	1.140	0.7294	4.030
3.594	1.782	2.275	1.153	0.6888	3.765
3.543	1.903	2.254	1.165	0.6526	3.509
3.493	1.967	2.234	1.194	0.6200	3.346
3.444	2.023	2.214	1.209	0.5904	3.384
3.397	2.235	2.195	1.249	0.5636	3.415
3.351	2.429	2.175	1.287	0.5391	3.359
3.306	2.477	2.156	1.327	0.5166	3.592
3.263	2.495	2.138	1.359	0.4960	3.426
3.221	2.544	2.119	1.396	0.4769	3.429
3.179	2.644	2.102	1.418	0.4592	3.436
3.139	2.975	2.084	1.439	0.4428	3.476
3.100	3.713	2.067	1.461	0.4276	3.466
3.061	4.434	2.049	1.481	0.4133	3.398
3.024	4.900	2.033	1.507	0.4000	3.145
2.988	5.148	2.000	1.550		
2.952	5.255	1.968	1.594		
2.977	5.277	1.937	1.643		
2.883	5.291	1.908	1.684		
2.851	5.558	1.879	1.735		
2.818	6.200	1.851	1.778		
2.786	6.877	1.823	1.822		
2.755	7.422	1.797	1.870		
2.725	7.867	1.771	1.906		
2.695	8.165	1.746	1.953		
2.666	8.360	1.722	1.991		
2.638	8.570	1.698	2.037		
2.610	8.894	1.676	2.073		
2.583	9.313	1.653	2.115		
2.556	9.158	1.550	2.301		
2.530	9.314	1.459	2.463		
2.505	9.652	1.378	2.631		

TABLE III

Substitute of the 100 monoenergetic beams

Ev	No $s^{-1}cm^{-2}eV$	eV	No	eV	No
4000	3.000 10^{18}	2.524	3.382	1.084	1.184
3.964	3.591	2.488	3.525	1.048	1.213
3.928	3.683	2.452	3.619	1.012	1.236
3.892	3.881	2.416	3.657	0.976	1.258
3.856	4.265	2.38	3.793	0.94	1.287
3.8	5.066	2.344	3.987	0.904	1.327
3.774	5.366	2.308	4.084	0.868	1.368
3.748	5.623	2.272	4.162	0.832	1.410
3.712	5.866	2.236	4.288	0.796	1.473
3.676	6.042	2.2	4.390	0.76	1.458
3.64	6.200	2.164	4.719	0.724	1.439
3.604	6.369	2.128	4.965	0.688	1.353
3.568	6.637	2.092	4.145	0.652	1.261
3.532	6.901	2.056	5.323	0.616	1.203
3.496	7.067	2.02	5.479	0.58	1.222
3.460	7.217	1.984	5.659	0.544	1.213
3.424	7.688	1.948	5.852	0.508	1.192
3.388	8.183	1.912	6.042	0.472	1.232
3.352	8.729	1.876	6.252	0.436	1.229
3.316	8.879	1.84	6.463	0.400	1.132
3.28	8.956	1.804	6.685		
3.244	9.062	1.768	6.901		
3.208	9.270	1.732	7.111		
3.172	9.727	1.696	7.334		
3.136	1.091 10^{19}	1.66	7.568		
3.1	1.337	1.624	7.803		
3.064	1.576	1.588	8.037		
3.028	1.746	1.552	8.271		
2.992	1.843	1.516	8.501		
2.956	1.888	1.48	8.752		
2.92	1.899	1.444	8.979		
2.884	1.905	1.408	9.248		
2.812	2.295	1.372	9.553		
2.776	2.539	1.336	1.004 10^{20}		
2.74	2.752	1.3	1.05		
2.704	2.907	1.264	1.074		
2.668	3.005	1.228	1.096		
2.632	3.110	1.192	1.113		
2.596	3.286	1.156	1.130		
2.56	3.305	1.12	1.147		

CHAPTER 5

EXPERIMENTAL APPARATUS AND METHODS

In this project the technique used to produce the semiconductor films was resistive vacuum evaporation. This process is well understood and is commonly used even for industrial applications and is thus an attractive way of fabricating solar cells. This chapter describes the equipment used to produce, and the methods used to characterise the semiconductor films.

5.1 Vacuum Evaporator

5.1.1 Introduction

The vacuum evaporator used to deposit the semiconductor films was equipped with eight independent sources and four interchangeable masks so that a complete solar cell could be deposited in a single pumping cycle. It also contained two movable quartz crystals and four shutters, thus making the system very versatile. The whole apparatus was housed inside a pipe glass jar (QVF N^{o} 12/700) with a volume of approximately 0.05 m^{3}. The jar and the 'base plate' containing the sources and the shutters were seated on a stainless steel collar of 33 cm (13") outside diameter which also

containined eight water cooled lead-throughs capable of carrying more than 350A. The interchangeable masks, crystal monitors and a heated substrate block were suspended from a stainless steel "top plate" which covered the top of the glass jar. All the vacuum seals in the system were viton seals. The pumping system consisted of a 6" (15 cm) oil diffusion pump (Balzers DIFF 650) backed by a two stage rotary pump (Balzers DUO 25). The backing and the roughing valves were electromagnetically operated so that the control of the pumping cycle could be carried out by operation of a single four-position lever. The typical background pressure was 2 to 5 10^{-7} torr as measured by an ionisation gauge head mounted inside the glass jar. Figure 5.1 shows the complete evaporation system. The apparatus housed in the glass jar, i.e. the sources, shutters, mask changer and crystal monitors was found very versatile and is further described in the following sections.

5.1.2 The Sources

The eight sources in the system were held by nickel-plated copper clamps which were mounted on the stainless steel disc 'base plate' (outside diameter 11") . Six of these sources were arranged in a circle, around the circumference of the base plate. These sources

were tilted by about 10° relative to the base plate so that the evaporant beam was pointed toward the substrate which was held perpendicularly above the center of this plate. The source-to-substrate distance was 16" (40.5 cm) so that the deviation of the evaporant beam direction from normal incidence at only 10° was considered negligable. The additional two sources were mounted in the center of the base plate.Figure 5.2 shows the arrangement of the sources on the base plate.

The power for the sources was supplied through eight water-cooled lead-throughs consisting of $^{1}/_{4}$" (3.175mm) copper rods soldered into simple glass-to-metal seals. These seals were hard soldered into a 1" BSF screws which fitted into O-ring sealed seatings in the metal collar. The water cooling was provided by circulating water through chrome plated copper tubes wound into spirals and soldered onto the $^{1}/8$" copper rods. The lead troughs and the source clamps were connected by ¼" (6.35 mm) copper rods. The whole assembly was found capable of carrying more than 350A at 6 V without an appreciable rise of the temperature of the lead troughs .

Several types of sources were employed: For the evaporation of the semiconductors, CdS and CdTe, baffled tantalum sources were used. The baffled sources

provide an indirect path for the vapours and thus prevent the ejection of solid particles of the evaporant. The tilting of the evaporator relative to the base plate was especially required by these baffled sources because the evaporant beam emerging from the chimney of the sources was quite directional. Initially baffled sources of approximately 3.4 cm^3 volume (R.D. Mathis N^o ME1) were used but subsequent requirement for a larger capacity source resulted in the use of 7 cm^3 sources (R.D. Mathis N^o SO2O). For the evaporation of metals such as copper and gold, tungsten spiral sources were used. For the evaporation of indium, a metal which melts before it sublimes, a tungsten dimple source was used.

5.1.3 The Substrate

Most of the substrates used in this project were corning 7059 glass slides, i.e. slides made from alumino-borosilicate glass which was stable at relatively high temperatures so that the semiconductor films were not contaminated by migrant components from the substrates. Before deposition, the glass substrates were thoroughly cleaned by a procedure described in appendix IV. A set of clamps were used to hold the substrates in position on a heated copper block. The substrate block was a 4" by 4" copper block screwed into a similar stainless steel block which was suspended

from the top plate by two stainless steel rods. The copper and the stainless steel blocks were separated by $^{1}/16$" ceramic washers resulting in a minimal thermal contact between the two. A resistance heater for the substrate was provided by a tungsten wire woven through a set of eight ceramic tubes fitted into the holes drilled in the copper block. Figure 5.3 shows the substrate block as suspended from the top plate.

5.1.4 The Masks

Four masks were held on a 6½" stainless steel disc which was mounted co-axially on a ½" rod that ran through a Wilson-seal (Edwards ½" rotary shaft seal) screwed to the top plate. Rotation of the shaft allowed the choice of any of the four masks to be made without breaking the vacuum. Transverse motion of the shaft pulled the masks into close contact with the substrate so that the deposited films had well defined, sharp edges. The positioning of the masks relative to the substrate was controlled by a single ball stop fitted onto the substrate block.

The masks were made by a photo-etching process of berillium-copper sheets which were spot-welded onto 2" by 2" stainless steel frames. The photo-etching

process was a standard procedure where the photoresist, spun onto the Berillium Copper sheets, was exposed to U.V. radiation through a master pattern. Subsequently, the exposed photoresist and the metal underneath it were etched away in an acid bath leaving a mask of the desired pattern. Detailed description of the photoetching process is given in appendix V. The position of the cut-out in the mask, relative to the sides of the mask frame, could be controlled with sufficient accuracy and repeatability so that several masks could be used for deposition of thin films with complex geometry. Since the cut out was accurately positioned relative to the sides of the frame, the single ball-stop registration of the masks in the vacuum evaporator was found to be sufficient.

5.1.5 The Crystal Monitors

The use of a quartz crystal oscillator was a very convenient way of monitoring the deposition process. If a specially cut (AT cut) quartz crystal forms a part of a self-resonant circuit then the oscillation frequency is directly proportional to the mass of the crystal. Thus, if the crystal is placed in the evaporant beam and some material is deposited onto the crystal face, the mass of the crystal, and therefore the frequency of oscillations change. Since the mass of deposited film is directly related to its thickness, the change of the crystal oscillator frequency can be calibrated in

terms of the thickness of the deposited films, and the deposition rate may be deduced.

The oscillator circuits were placed outside the vacuum and the output frequency signal was electronically processed resulting in an audio signal, and a d.c. voltage signal proportional to the oscillator frequency. A more detailed description of the crystal monitors is given in appendix VI.

The two quartz crystals were mounted inside stainless steel tube colluminators which were fixed at the extreme ends of an 11" bar. This base was attached to a shaft running through a Wilson-vacuum seal which was fixed to the top plate. The colluminators stopped the vapours from any source, other than the one vertically below, from reaching the crystals so that each crystal monitored a single source. The Wilson-seal arrangement enabled the two crystals to monitor any two diametrically opposed sources at any one time, so that six deposition processes could be monitored in every pumping cycle. The quartz crystal and colluminators, along with the mask changer and the substrate block are shown in figure 5.3.

5.1.5 The Shutters

A set of four shutters were built immediately above four of the six sources. These shutters are crucial to this project because mixed and graded CdS_xTe_{1-x} films were to be made by interleaving a few monolayers of CdS and CdTe, rather than by simultaneous co-evaporation of the two semiconductors. The composition factor 'x' was to be controlled by the adjustment of the thickness of the interleaving layers, rather than by the control of the rates of deposition of CdS and CdTe. (A further discussion of this method of formation of mixed and graded films is given in the following chapter).

Several types of shutters were designed and tested. Initially, a set of solenoid actuated electromagnetic shutters were used. However, it was found that the rise of the temperature of the windings, caused by the current flow, was sufficiently large to result in an unacceptably high outgassing rates from the potting epoxy and from the enamel insulating the wires. An attempt to form similar windings from ceramic coated wires also failed because the ceramic coatings tended to crack, resulting in short circuit paths between the windings.

Subsequently, a set of pneumatically operated shutters was designed and used. In this case the shutters were actuated by the compressions and extentions

of a set of seamless stainless steel bellows the (Drayton Hydroflex N^{o} 121054) transverse motion of which was translated to the rotational motion of the shutters via rack and pinion assemblies. Figure 5.4 shows a bellows assembly mounted on the base plate. The compression and the extention of the bellows was achieved by variation of pressure inside the bellows. When the pressure in the bellows was low, a pre-compressed helical spring mounted above the bellows forced it to compress and the shutter was opened, and conversly, when high pressure was forced into the bellows it expanded and the shutter was closed. The high pressure was provided by a reservoir regulated at 15 psi from a nitrogen cylindar, while the low pressure was provided by another reservoir maintained at 0.1 torr by a small auxillary rotary pump. The switching between the two pressure reservoirs was controlled electronically via an electromagnetic changeover valve (Herion).
Four sets of bellows and spring assemblies were mounted below the base plate and these were controlled by two valves so that one pair of shutters behaved identically and contrary to another pair. A detailed description of the design of the pneumatic shutters is given in appendix VII.

The control of the shutters via the valves was fully electronic and there were three variables that could be pre-selected. Firstly, the periodic time, i.e. the time period in which each pair of shutters

was opened and closed, could be varied from 0.1 to 100 seconds. Secondly, the mark-to-space ratio, i.e. the percentage of the periodic time, during which one pair of shutters was open and the other pair was closed, could be varied between 0% and 99.9% Thirdly, this mark-to-space ratio itself could be smoothly varied between any two limits, and the rate of this variation with respect to time could be controlled so that the mark-to-space ratio could be continuously changed between the two extremes in a time period between 0.5 and 10 minutes. Further details on the operation of the electronic control unit is given in the appendix VIII. It was the choice of these three parameters that determined the composition of graded and mixed CdS_xTe_{1-x} films. The choice of the periodic time determined the thickness of the interleaving layers of CdS and CdTe. The choice of the mark-to-space ratio determined the relative amounts of CdS and CdTe deposited and determined the composition factor 'x'. The choice of the rate of change of mark-to-space ratio determined the rate of change of the band gap with respect to the thickness of the film.

The shutting system and the control unit have been found very versatile and satisfactory.

5.2 Monitoring the Deposition Conditions

Several parameters have been monitored and controlled during the deposition of the semiconductor films because those had an effect on the film properties. The monitored parameters were the vacuum pressure, source and substrate temperatures and the deposition rates.

5.2.1 The vacuum pressure

The pressure was measured at three points in the vacuum evaporator. The backing/roughing pressure was measured by a Pirani type gauge head mounted above the rotary pump. The pressure inside the evaporator was measured by a Hastings thermocouple gauge mounted above the diffusion pump and an ionisation gauge head mounted inside the glass jar. Initially a conventional ionisation gauge head (Edwards 1G5) was used but it was found that Tellurium alloyed with the tungsten filament, causing an early burn-out. Subsequent use of another gauge head (AEI 29D20) with a thoriated irridium filament operating at only about 800^{o}C alleviated the problem. Both types of gauge heads were driven by Edwards ION 7 control unit. Background pressures were typically 2-5$\cdot 10^{-7}$ torr.

5.2.2 The Substrate Temperature

The temperature of the substrate block was measured and controlled by a relay temperature controller (Pye Ether Transitiol) via a NiCr-NiAl thermocouple mounted in a blind hole drilled in the copper block. The temperature of the surface of the substrate was monitored by an electronic thermometer (Cormark 1620) via a small thermocouple stuck to the surface of the glass slides. The surface temperature of the substrate was typically maintained at 180^{o} to 200^{o}C.

5.2.3 The Source Temperature

The rate of evaporation is directly related to the source temperature, and since the rate of evaporation has a marked effect in film properties, monitoring and controlling the source temperature is vital. Initially, the temperature of the sources was monitored by an electronic thermometer and controlled by manual adjustment of the power supplies. Subsequently, however, the power supplied to four of the eight sources was controlled by a phase angle (PID) thyristor temperature controllers (Eurotherm 070) which have been found capable of maintaining the temperature of the sources to within 5^{o}C from the set-point. In all cases the

temperature has been measured by NiCr-NiAl thermocouples wrapped in thin tantalum foil in order to prevent alloying of the thermocouples with the sources. In the case of MEl sources the thermocouples have been placed between inner and outer sheets of the sources, while for the S020 sources the thermocouples were pushed into the caps that cover the loading chamber. The evaporation temperature of In was controlled by placing the thermocouple inside the molten In through a hole drilled in the tungsten source. In all cases, the temperature measured by the thermocouples ought to have been very close to that experienced by the evaporant materials, and certainly was quite reproducable.

5.2.4 The Deposition Rates

In addition to monitoring the source temperatures, the deposition rates were also measured by quartz crystal film thickness monitors. These have been calibrated for given materials and substrate temperatures, by comparison of the thickness of the deposited films, as measured by a Talystep, and the time durations of the evaporations, with the quartz crystal oscillator frequency changes. A two pen y-t chart recorder was connected to the D.C. signal output of the crystal monitor units so that a record of the deposition rates was obtained. In the case of evaporations from the

sources the temperature of which was not controlled by the thyristor controllers, a straight line corresponding to a given pre-calculated rate of deposition was drawn on the chart roll and the power supplied to the sources was manually controlled so that the deposition rates, as displayed by the recorder, followed these pre-determined paths. Since the composition factor 'x' in CdS_xTe_{1-x} films was to be controlled by shutters rather than by the variation of the evaporation rates, the crystal oscillator monitors were found useful in achieving constant deposition rates of CdS and CdTe.

5.3 Deposition Procedures

The work towards the development of a graded band gap solar cell could be subdivided into four sections, which were the preparation and characterisation of pure CdS, and pure CdTe, mixed films of CdS_xTe_{1-x}, and finally diodes with graded band gap surface layers.

Before each deposition the vacuum evaporator was outgassed by heating the jar for about 12 hours at 140°C. The sources and the evaporant materials were also outgassed by heating of the sources for short periods of time at or slightly above the evaporation temperatures.

5.3.1 Deposition of CdS Films

A number of CdS films were deposited in order to establish the growth parameters necessary for deposition of films with desired transport properties. The films deposited had rectangular (12 mm x 3 mm) geometry suitable for Hall Effect measurements. The stoichiometry, and therefore the doping of the CdS films was not controlled by the variation of the deposition rates but rather by co-evaporation of metallic Cd. The rate of deposition of CdS was fixed at about 20 Å/s and the variation of the film properties was achieved by the variation of the deposition rate of Cd, which was initially manually controlled and subsequently controlled

by the controllers. This method of stoichiometry control was more versatile than the conventional one where the source temperature and the temperature of a tube enclosing the evaporant beam is varied in order to maintain the control over the film stoichmetry (135).

The material used in the evaporations consisted of small yellowish-orange crystals of BDH OPTRAN grade CdS rated at 99.999% purity or better. Powdered CdS as supplied by Koch-Light was found to "spit" even when evaporated from baffled sources. The material co-evaporated with CdS from a separate baffled source was Cd shot 99.9999% pure supplied by Koch-Light Labs Ltd.

The control of the rate of deposition of Cd was difficult due to the fact that metallic Cd sublimes so that a large variation in the evaporation rate was caused by small variation of the source temperature. This was overcome by fitting a tantalium cover with a 1mm hole over the baffled source and thereby reducing the evaporation rate, as is predicted by Langmuir's Law (134)
Subsequent to the deposition of the semiconductor films, four metal electrodes were deposited so that two were across the length of the CdS film and two across the width. Two such Hall effect cells could be deposited on every substrate in a single pumping cycle.

5.3.2 Deposition of CdTe Films

A number of CdTe films were deposited in a manner analagous to the one described above for CdS films. The films were also deposited in the geometry suitable for the Hall effect measurements and the film properties were also controlled by the amount of materials co-evaporated with CdTe. However, unlike CdS which was deposited only as an n-type semiconductor, CdTe films were doped both p and n. P-type doping was achieved by co-evaporation of Cu while n-type doping was achieved by co-evaporation of Cd, In or Al.

CdTe used for evaporations was BDH optran grade material rated at at least 99.999% purity. Unlike CdS, CdTe did not show a tendency to "spit" so that the coarse powder form, in which it was supplied, was satisfactory. The copper used for p-type doping was 1 mm wire supplied by Johnson-Mathey Chemicals Ltd.. rated at 99.999% purity. As with all other metals used, copper wire was cleaned in an acid bath and rinsed in de-ionised water before evaporation. Copper was evaporated from a tungsten spiral and with practice an adequate amount of control could be achieved over its deposition rates. Indium, which was found to be the best n-type dopant, was supplied in a form of a 99.999% pure rod by L.P. Electronics Ltd. Little chips were cut from the rod and used in the evaporations from a tungsten dimple source.

5.3.3 Deposition of Mixed CdS_xTe_{1-x} Films

CdS_xTe_{1-x} films with uniform band-gaps, i.e. with constant composition factors 'x' were prepared with the use of the shuttering system described in section 5.1.5. The evaporation rates of CdS and CdTe were fixed and controlled by the temperature controllers, and the resultant deposition rates of about 20 $^{A}/s$ were monitored by the quartz crystal monitors. The evaporation rates of the dopantmaterials were controlled either manually or by temperature controllers and were also monitored by the crystal oscillators. For n-type CdS_xTe_{1-x} mixed films the dopant materials were Cd and or In so that either Cd was co-evaporated in step with CdS and In in step with CdTe, or In was continuously evaporated while CdS and CdTe were shuttered. For p-type mixed films copper was continuously evaporated at a manually controlled constant rate. The composition factor was determined by the setting of the 'ratio' control on the shutter control unit, while the thickness of the interleaving layers, i.e. the times of the evaporation of either CdS or CdTe were determined by the setting of the 'periodic time' control. The mark to space ratio was constant throughout the deposition so that films with uniform band gaps were grown.

Mixed films were prepared in two different geometries. One was suitable for Hall effect measurements, i.e. same geometry was used as for pure CdS and CdTe films. For X-ray diffractometer measurements, however, two large area (12.5 mm x 20 mm) films were grown on

each substrate.

Mixed films of CdS_xTe_{1-x} were prepared throughout the composition range (x=0 to x=1) by variation of the setting of the mark-to-space ratio control.

5.3.4 Deposition of Diodes

Two types of diodes with graded band gap surface layer were made; one having p-CdTe as the base layer, and the other using p-$CdS_{0.5}$-$Te_{0.5}$ as the base layer. However, the procedure of deposition was quite similar for both types of diodes. Firstly, a copper electrode was deposited on the glass substrate. In some cases copper sheets, nickel plated copper sheets, or tin-oxide coated glass slides were used as substrates so that the evaporation of the bottom electrode was unnecessary. Secondly, the p-type base layer was deposited. For the diodes where the base layer consisted of CdTe, the deposition rate of CdTe and its p-type dopant copper, were manually controlled. Alternatively, when p $CdS_{0.5}$ $Te_{0.5}$ served as the base layer, the same rates of deposition of CdS and CdTe were pre-set and controlled by the temperature controllers while the power supplied to the copper source was manually controlled. The composition factor of the base layer (x=0.5) was achieved either by an appropriate setting of the shutter control unit or by maintaining similar deposition rates of CdS

and CdTe and holding both shutters in the open state. The graded band gap surface layer was grown on top of the base layer by allowing the ratio of the shutter opening times to vary smoothly from initial 50% CdS, 50% CdTe to the final 100% CdS. The thickness of the graded layer was determined by the third control on the shutter control unit. The change from p-type to n-type was achieved by stopping the evaporation from the copper source and starting the evaporation from the Cd and/or In sources. In order to be able to form an abrupt junction without interupting the deposition process an additional magnetically operated shutter was built above the In and Cu sources. With this shutter it was possible to maintain both sources at the appropriate evaporation temperatures, and the change from p - to n-type was achieved by operating this shutter with a permenant magnet from the outside of the jar. In some cases, the deposition was interrupted after the deposition of the base layer, in order to anneal the Cu doped films. Finally, when desired, another metal electrode, usually Zinc, was deposited on top of the structure.

Sometimes, when the tin-oxide coated glass slides were used as substrates, the structure was deposited in a reverse order i.e. the graded band gap layer was deposited first, with the wide band gap and facing the substrate. The p-type base layer was then deposited on top of the graded layer.

5.4 Measurement of the Film Properties

Several different measurements were carried out in order to characterise the deposited films. The electronic properties of CdS, CdTe and CdS_xTe_{1-x} films were characterised by the Hall effect measurements. The band gaps of the films were measured by light transmission measurements using a monochromator. The crystal structure was determined by an X-ray diffractometer. The surface properties of the films were investigated in a Scanning Electron Microscope. The composition of some of the films was investigated by an X-ray flourescent analyser. The characteristics of the diodes were measured on a curve-tracer and the solar cell parameters were to be quantified in a Xenon lamp solar simulator.

5.4.1 The Hall Effect Apparatus

The magnetic field necessary for the Hall effect measurements was provided by a permanent magnet with a flux density of 4.2 K Gaus (0.42 T). The magnet was mounted on a trolley so that the field could be applied to the semiconductor films by sliding the magnet to and from the test sample. The current passed through the sample was provided by a 300 V D.C. stabilised power supply. A variable current limiting resistor and a Kithley 616 digital electromer operating in the

ammeter mode were connected in series with the test sample. The Hall voltage was measured by a Kithley 6OOB electromer the output of which was displayed in a servoscribe M: x-t recorder. Any voltage caused by the misalignment of the Hall voltage electrodes was offset by a variable voltage from a battery powered source.

The test sample was held in a specially constructed jig which could fit in the air-gap of the magnet. The jig consisted of a square ($1\frac{1}{8}$" x $1\frac{1}{8}$") stainless steel plate with a machined slot into which the substrate fitted, and a similar square perspex plate $\frac{1}{8}$" thick, which had four 8BA clearance holes in each carrier (coincident with similar tapped holes in the stainless steel plate) and eight lOBA tapped holes arranged to coincide with the eight electrodes of the two test samples on each slide. Small pellets of Indium were placed on each of the film electrodes so that they formed a soft pad with which the lOBA screws formed electric contact when the perspex plate was clamped over the substrate via the four, corner 8BA screws. The electrical connections to the films were then taken through a cover of a blackened perspex box into which the whole structure fitted. This perspex box also had two holes in the sides, into which 1 cm pipe connections were fitted so that nitrogen gas from a liquid nitrogen boiler could be circulated through the box. The

temperature of the samples in the box could then be controlled and varied over a range (-80°C to + 60°C) by varying the rate of boiling of liquid nitrogen and by operating two in-line heaters. Most measurements, however, were done at room temperature, which was constant at 22°C since the whole apparatus was situatedd in a clean air room with controlled atmospheric conditions.

5.4.2 The Band-Gap Measurements

The band gap of CdS, CdTe and mixed and graded CdS_xTe_{1-x} films were measured by a Grub Pearsons model M2 monochromator. A Hilger-Schwartz thermopile (Rank-Hilger model FT4) was used as a light detector the output of which was connected to a phase-sensitive voltmeter (Automatic System Labs. model 110). The phase sensitive voltmeter also received a reference signal from a unit that controlled a light chopper which intercepted the light beam at a rate of 22 times a second. In this way, if correctly adjusted, the phase sensitive voltmeter would measure only the voltage signal that is sinchronous with the reference signal, i.e. the detector output caused by light other than that from the monochromator was ignored by the voltmeter. A servoscribe x-t recorder was connected to the 'in phase' output of the voltmeter so that the desired signal was recorded on the chart-roll. A high power tungsten filament lamp was used as the light source ,

since its spectrum was convenient and continuous in the range of interest (0.7 μm to 1.2μm). The monochromator was calibrated , by determining the wavelength of light which corresponded to given settings of a drum which operated the turntable for a prism. A Mercury lamp was used for calibration because its spectrum contained well defined lines the wavelengths of which are tabulated in "CRC Handbook of Chemistry and Physics" The band gap of the semiconductor films was found by producing two traces on the recorder; one serving as a reference trace and corresponding to uninterrupted light output from the monochromator, and the other representing the light transmitted through the semiconductor film placed in the light path. The difference of these two traces, represented in terms of percentage of reference trace, was then plotted against the drum setting, resulting in a plot of absorption versus the photon energy. The position of the knee in this plot then corresponded to the band gap of the film.

5.4.3 The Crystallographic Measurements

The crystallographic properties of the semiconductor films were measured by an X-ray diffractometer. A set of mixed films with composition factor ranging from 0 to 1 was specially prepared for this purpose because the area of the semiconductor films in the Hall effect cells

was too small. The crystallographic phase of the films was then deduced by comparison of the distribution of the peaks with respect to the angles at which they are detected with the standard X-ray data for CdS and CdTe.

5.4.4 The Surface Analysis

The micro-structure of the thin films was investigated with a Cambridge Steroscope Mk2 Scanning Electron Microscope. The samples to be investigated were cut into small area sections and cemented onto suitable microscope studs using silver 'dag' conducting point. The magnification factor in the microscope was increased to a value sufficiently large (∿ 50000x) to show the grains of the polycrystalline films when the size could then be measured.

5.4.5 The Characteristion of the Diodes

The current - voltage (I-V) characteristics of the (n) CdS_xTe_{1-x}-(p) CdTe and (u)CdS_xTe_{1-x} - (p) $CdS_{0.5}Te_{0.5}$ diodes were plotted by a Telequipment curve tracer. This was a quick and convenient way of assessing the diodes.

5.4.6 The Measurement of Solar Cell Parameters

The parameters of the thin film cells were to be quantified by a specially made solar simulator. This basically consisted of a powerful (∿ 1 KW) Xenon lamp with a spectral output, if suitably filtered, forming a good match with the solar spectrum at AMO. A copper block mounted 15 cm from the lamp served as a substrate table for the solar cells. The temperature of this block could be varied between -20°C and +70°C by varying the power supplied to a heater, built into the block, which worked simultaneously with a small $\frac{1}{8}$" HP refrigerator unit used to cool the block. All electronic measurements on the solar cell were to be carried out by a specially constructed control unit. This unit generated a series of voltage steps, of variable magnitude (1mV-99mV), which were used to bias the cell. The current generated by the cell for each voltage step was measured and thus the I-V characteristic of the cell was generated , and plotted on a X-Y recorder connected to the control unit. In addition, the power output by the cell was to be calculated at each voltage step. From the I-V curve and the power output of the cell it was possible to calculate all the parameters of the solar cell, such as the open circuit

voltage, short circuit current, maximum power, maximum power point (optimum load) and the fill factor.

The efficiency of the cell could have been calculated by comparison of the maximum power output from the cell and the power of the light-source, as measured by a Hilger-Solwartz thermopile (Rank-Hilger FT 31) mounted 15 cm from the light source.

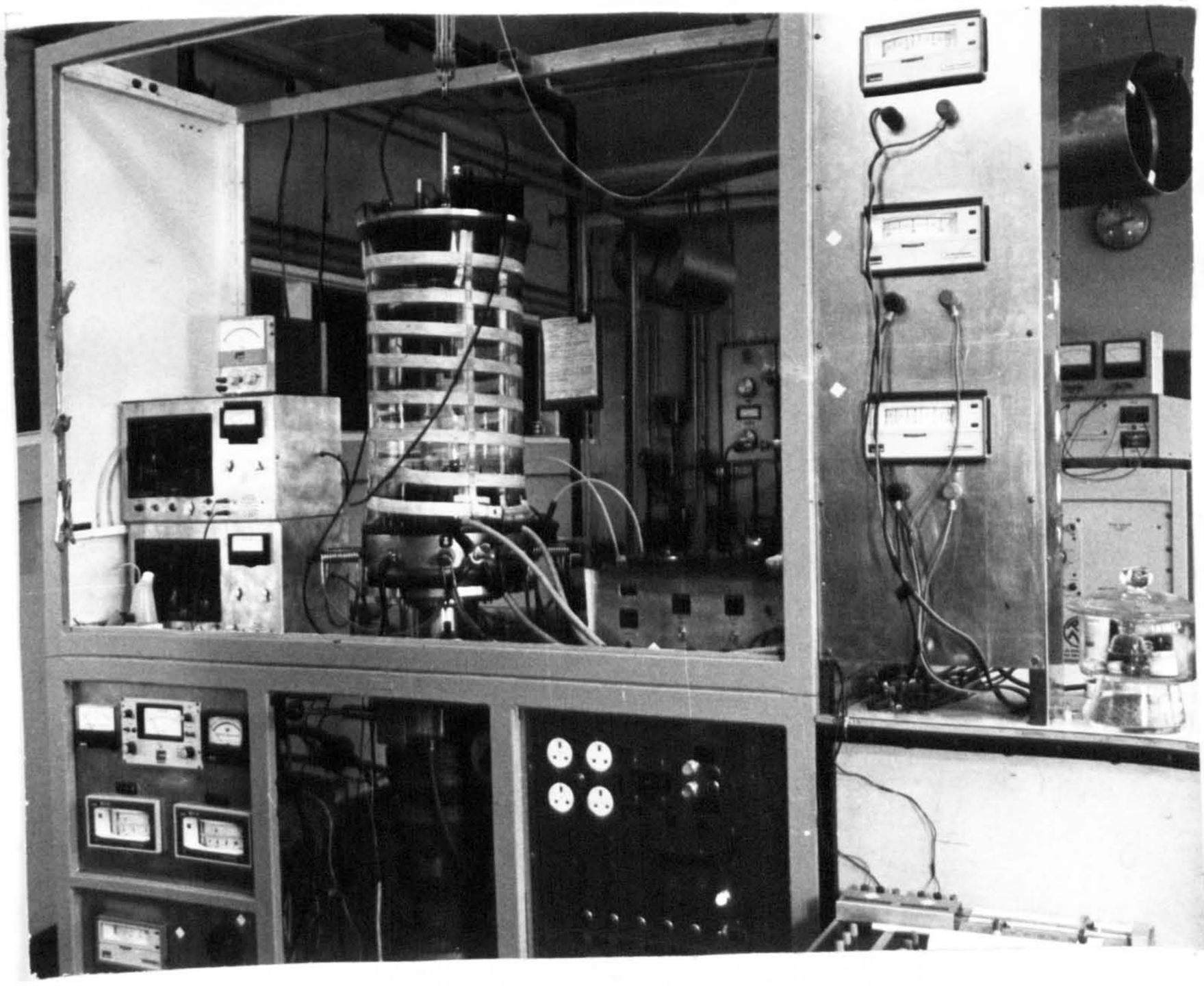

FIGURE 5.1 complete vacuum evaporator

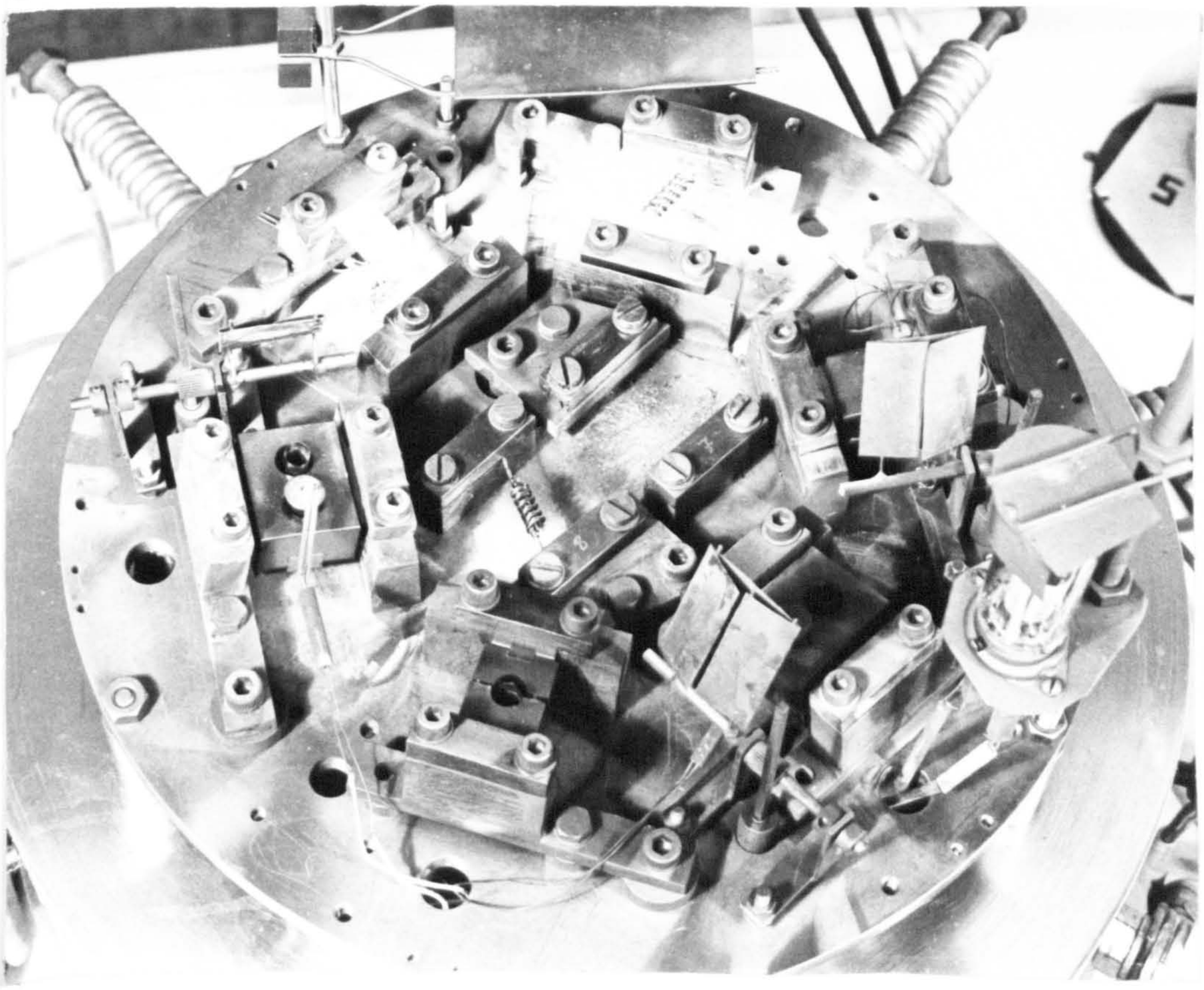

FIGURE 5.2 the base plate

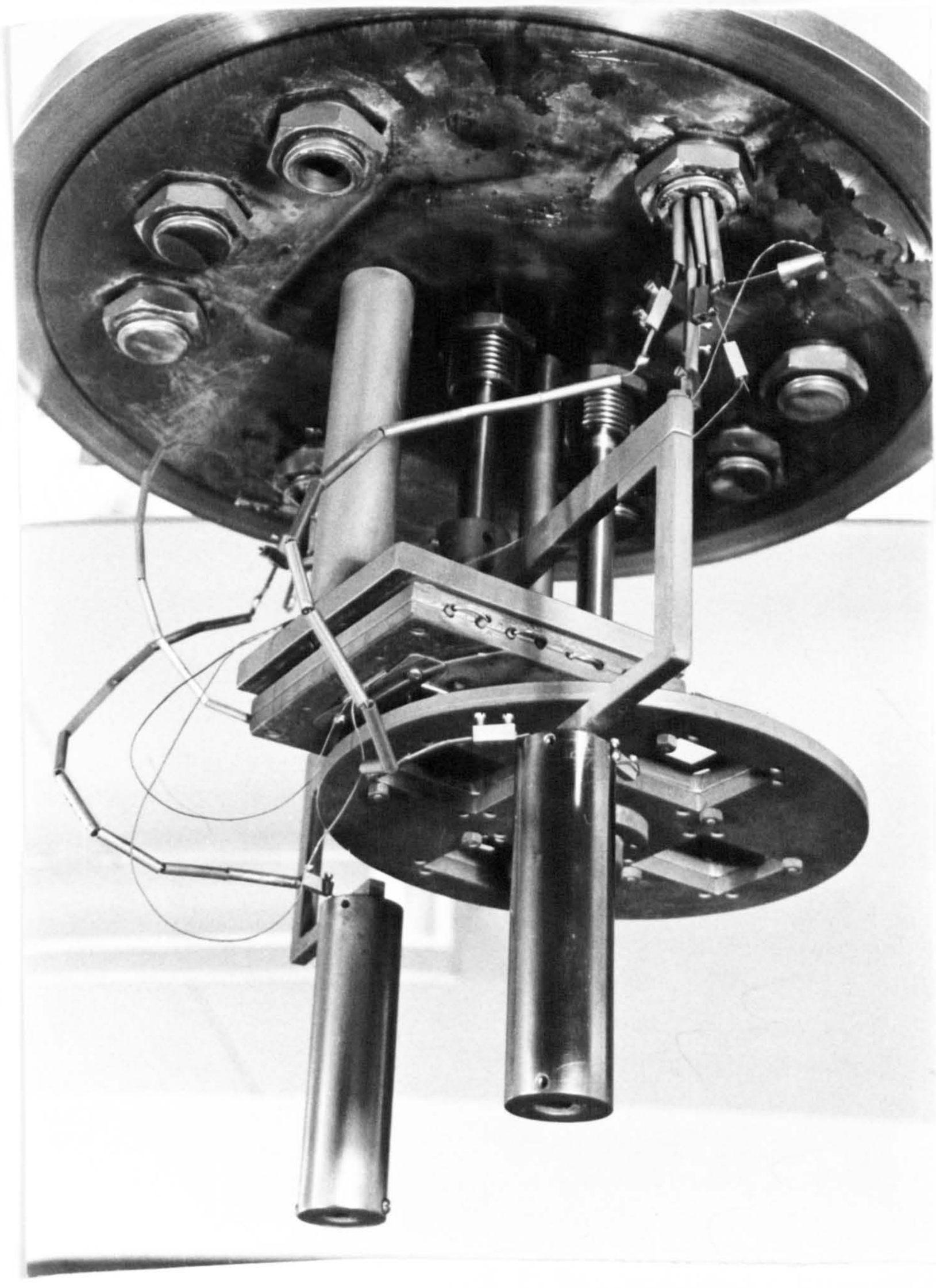

FIGURE 5.3 the "top plate" with the two crystal monitor assemblies, the mask changer and the substrate block

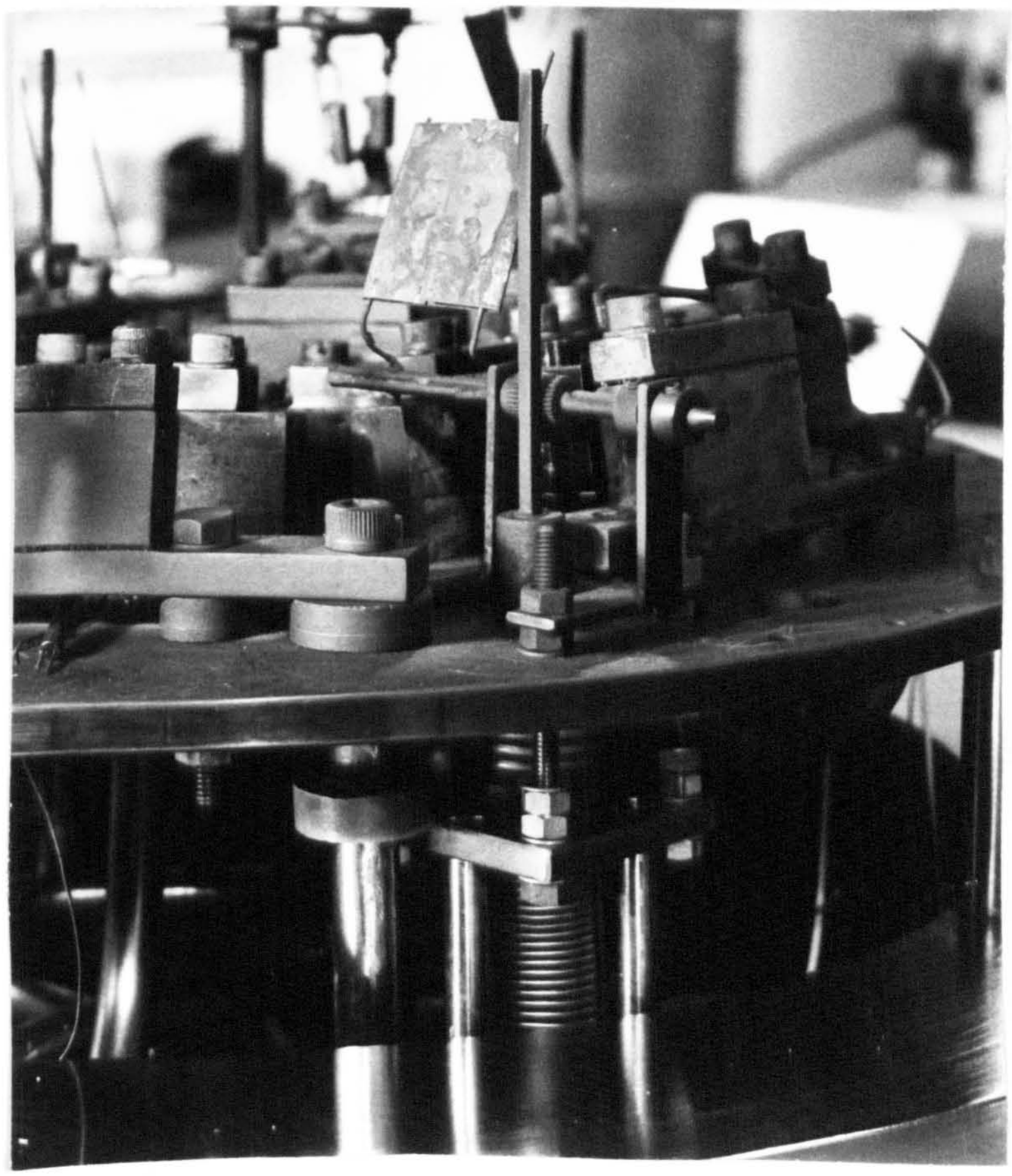

FIGURE 5.4 the bellows shutter mounted on the base plate

CHAPTER 6

Material Properties of CdS, CdTe and Mixed CdS_xTe_{1-x} Films

6.1 Introduction

The experimental work in this chapter is subdivided into three sections. Firstly, pure CdS films were investigated. Secondly, films of CdTe were deposited and investigated, and thirdly CdS_xTe_{1-x} mixed films were made. In spite of the fact that a reasonable amount of work has already been done on vacuum evaporated CdS and CdTe films, the investigation of these films was necessary in order to establish the deposition conditions required to produce films of desired properties and to 'calibrate' the vacuum evaporator. It was assumed that mixed and graded films of CdS_xTe_{1-x} would take on some properties of the constituent semiconductors so that the deposition conditions that resulted in desired properties of CdS and CdTe films were expected to be broadly applicable to the mixed and graded films. Mixed films of CdS_xTe_{1-x} were investigated in order to show that the composition parameter could be controlled by shuttering and that the resultant films were homogenious semiconductor layers. Furthermore, the doping properties of the mixed films had to be investigated in order to determine the deposition conditions that ought to result

in uniformly doped graded band-gap films, and in order to that show if a mixed film base layer for a solar cell could be prepared.

6.2 Cadmium Sulphide Thin Films

6.2.1 Introduction

Due to the fact that CdS thin films could be used for many purposes, a modest amount of work has already been done on thin vacuum evaporated CdS films. When evaporated from a single source, CdS source material dissociates into cadmium and sulphur vapours, which reform CdS upon condensation on the substrate. Having a relatively high degree of ionicity, the CdS condensate can form a good semiconductor layer which can reproduce many properties observed in single crystals of CdS. However, by varying the deposition conditions, such as the source and substrate temperatures, film thicknesses etc., it is possible to produce CdS films with widely differing physical and electronic properties. Thus, the CdS films, deposited on typical amorphous substrate such as glass, may appear in hexagonal, cubic or both phases depending largely on the temperature of the substrate. It is generally accepted that for substrate temperatures greater than about 180^{o}C to 220^{o}C the

CdS films are purely hexagonal [136,137,138]. For substrate temperatures between approximately 70°C and 180°C CdS appears as both phases [136,139,140] while for substrate temperatures less than 70°C the films are purely hexagonal but of poor quality[136,141,142]. In most cases CdS films also appear to condense with a preferred orientation with the c-axis perpendicular to the plane of the substrate [136,139,142,135]. The degree of preferred orientation is found to increase with increasing film thickness [142] and decreasing deposition rates [142,135] provided that the substrate temperature is in excess of approximately 170°C. Similarly the grain size of the CdS films may be controlled to an extent that the larger grains occur in thicker films (>0.5μ) deposited at lower deposition rates on hot substrates (>180°C)[135,136,142,143]. The electrical properties of the vacuum deposited CdS films also vary with the deposition conditions so that, for example, film resistivities between 0.1 Ω cm and 10^7 Ω cm may be obtained in CdS films. The resistivity of the films is found to decrease with higher deposition rates[144,139], lower substrate temperatures [145,146] and larger film thicknesses[142,147]. Most of the variation of the resistivity is due to the variation of the carrier concentration which is caused by the off-stoichiometry of the deposited films. The off-stoichiometry, which in this case is always due to excess cadmium, results

from differing vapour pressures of cadmium and sulphur, and is usually responsible for the doping of the films[146,147,148]. Thus, for example, films deposited on cold substrates (< 100°C), lose the characteristic yellow-orange colour of CdS and are brown due to a great amount of excess cadmium and cadmium oxide present. Furthermore, the carrier concentration and therefore the conductivity of the CdS films may be increased by baking in cadmium vapour or decreased by baking in an inert atmosphere and thus driving the excess cadmium out of the film [146]. Thus, the control of the stoichiometry of the deposited CdS films is crucial in determining their electrical properties. The variation of the resistivity of the films with the film thickness is limited and does not occur in films thicker than about 0.5 μm. The mobility of the carriers in polycrystalline CdS films is found to be limited mainly by scattering at the barriers caused by crystal imperfections [149,150,151]. However, provided that the grain size is larger than about 0.1 μ, the mobility does not depend so much on the size of crystallites as on their orientation. Thus, the use of the various post deposition re-crystallisation techniques which can result in grain sizes of the order of millimeters does not necessarily produce a great improvement of the mobility of the carriers [151,152]. Nevertheless, mobility is influenced by the deposition conditions, and in

particular the substrate temperature which influences the preferred orientation as well as the grain size [143].

Thus it is generally agreed that the optimum conditions for production of solar-cell-grade CdS (low resistivity, high mobility, low density of defects) are the deposition at relatively fast rates (> approximately 50 Å/s) onto substrates maintained at about 200°C. Sometimes a heated tube mounted around the source and the substrate is used to contain a more stoichiometric mixture of vapours in the vicinity of the substrate and thus control the film stoichiometry [135,142,147,148]. In this case, the "hot wall" tube ought to be maintained at around 100 to 150°C for best results. In addition, post deposition treatment, such as annealing at temperatures higher than the substrate temperature , can override some of the effects of the deposition parameters and improve the physical and electronic properties of the as-deposited films[135,146].

6.2.2 Deposition Parameters

A number of CdS films were deposited and characterised using the equipment and techniques described in Chapter 5. The effect of the deposition parameters was not investigated throughout the available range because the aim of this section was to determine a set of deposition conditions that would result in

required film properties rather than to determine the effect of deposition parameters on the CdS films. The parameters that could be varied and that have an effect on the film properties were the control of the doping and the temperatures of the substrate and the sources.

6.2.2.1 The Substrate Temperature

It has been indicated in section 6.2.1 that the optimum substrate temperature for deposition of CdS films of low resistivity and good mobility is around 200^{o}C. Thus, the CdS film were invariably deposited on substrates maintained at temperatures of approximately 190^{o}C $\pm$ 10^{o}C . Higher substrate temperatures were not used because the ultimate aim of the work was to deposit solar cells on plastic substrates which would melt at temperatures in excess of 200^{o}C. Lower substrate temperatures would result in poorer CdS films. Furthermore, the sticking coefficient i.e. the ratio of the amount of material deposited on the substrate and the amount of material actually evaporated is similar for CdS and CdTe for substrate temperature of about 180^{o}C [127].

6.2.2.2 The Rate of Deposition

Initially CdS films deposited at several deposition rates (3 Å/s to 60 Å/s) were investigated and, as expected, the greater that the deposition rate the greater is the film conductivity as is shown in table 6.1. However, a deposition rate of 20 Å/s was subsequently chosen and adhered to. Deposition rates larger than that have meant that in each opening period of the shutters, when the shutters were to be used, thicker interleaving layers would be deposited i.e. larger deposition rates would have required faster shuttering speeds. Thus, for example, at a deposition rate of 20 Å/s, a shuttering frequency of about 3 Hz would be required for deposition of a monolayer in each shutter cycle, assuming a monolayer of CdS is equal to the 'c' lattice parameter i.e. 6.72 Å. It was important to maintain deposition rates low enough , relative to the maximum shutter frequency so that, in an extreme case, a monolayer at a time could be deposited in order to assure that the CdS and CdTe interleaved layers could interdiffuse to form CdS_xTe_{1-x}. Deposition rates much lower than 20 Å/s were incompatable with the chosen method of stoichiometry control and hence resulted in irreproducable results.

6.2.2.3 The Control of Stoichiometry

There are several methods available for doping of CdS films, the most obvious of which is some form of stoichiometry control. Since, due to the other considerations, the evaporation rate of CdS had to be fixed, the conventional control of film stoichiometry via the source temperature was not possible. The "hot wall" technique often used to adjust the film stoichiometry was also not practical because it may not have exerted enough control over the film stoichiometry and because it may not be applicable for the deposition of CdTe films. Thus the most general method of doping the films was chosen, namely that of direct incorporation of a dopant via co-evaporation from a separate source. The obvious dopant for CdS is Cd, so that the control of the amount of evaporated elemental Cd controlled the film stoichiometry and therefore the electronic properties of the CdS films. This technique was seen as very flexible and also adaptable for the deposition of CdTe films. The limitation of the technique was the difficulty of controlling the deposition rates of metallic Cd, especially if very low deposition rates were required , as they would be of low deposition rates if CdS were used. However, as was mentioned in Chapter 5, a cover with a small hole fitted over the Cd source decreased the effective emitting area of the Cd

source and hence decreased the evaporation rate of Cd, as is dictated by Langmuir's law [134]. Figure 6.1 shows the Cd evaporation rates as a function of source temperature for two different hole sizes in the source cover. A cover with a 1 mm hole was found to be adequate and the control of Cd evaporation rate was quite feasable and reproducable. Since the substrate temperature and the deposition rate of CdS were fixed, the properties of the films were adjusted by variation of the deposition rate of Cd.

6.2.3 Experimental Results

6.2.3.1. Electronic Properties

The electronic properties of the CdS films were measured as described in Chapter 5 via four gold electrodes which were found to make an ohmic contact with the semiconductor. The film resistivity was found to be related to the thickness of the deposited layers in accordance with other findings [142,147], as well as the amount of Cd co-evaporated with CdS. Films thinner than about 1500 Å were found to have irreproducable properties and had the tendency of having high resistivities. However, for film thicknesses greater than about 3000 Å the conductivity of CdS was found to be directly related to the amount of excess Cd

co-evaporated with CdS as is shown in figure 6.2. Although the crystal oscillators were calibrated for both CdS and Cd, as was described in Chapter 5, the amount of excess Cd co-evaporated with CdS is expressed in terms of ratio of the frequency changes recorded by the crystal oscillators monitoring Cd and CdS deposition rates (Hz of Cd per 10 KHz of CdS). The calibration factor for deposition of CdS at 20 Å/s on a substrate at 190°C was 25 $^{Hz}/_{Å}$. However, deposition of Cd onto a hot glass substrate at the required low rate resulted in discontinuous films due to a high rate of re-emission of Cd from the substrate (low sticking coefficient). Calibration of the crystal oscillators at higher Cd deposition rate gave a calibration factor of 3.2 $^{Hz}/_{Å}$. However, since this figure does not necessarily apply for low deposition rates and since a totally different sticking coefficient may apply for the case when Cd is co-evaporated with CdS, any further deduction based on this calibration factor may be erroneous. Thus, the evaporation rate of Cd is expressed in terms of "equivalent Hertz" i.e. Hz of Cd per 10 KHz of CdS which ought to be a good measure of the amount of excess Cd incorporated in the CdS films. The deposition rate as measured by the oscillator was found to be more reproducable than the source temperature, but the relation between the two parameters is also shown in figure 6.2. Furthermore , since the aim of this section is to determine a set of deposition parameters

necessary to produce desired film properties, expressing the results in terms of measurable and reproducable quantities was found more useful.

The carrier concentration in the films, as measured by the Hall effect, was found to be similarly related to the amount of the excess Cd, as is shown in figure 6.3. Carrier mobility was calculated from the measured carrier concentration and film resistivity but no obvious relationship between the mobility and the excess Cd was apparent. The carrier mobility was found to be roughly constant and typically between 2 and 4 $cm^2V^{-1}s^{-1}$ although values as large as 6.5 $cm^2V^{-1}s^{-1}$ and as low as 0.5 $cm^2V^{-1}s^{-1}$ were recorded.

Illumination of the CdS films was found to increase both the carrier concentration and the mobility in the films. The effect of illumination was, as expected, larger in films with greater dark resistivities.

The resistivity of the films was also found to vary with the length of time the films were left in the open atmosphere, as is shown for two different films in figure 6.4.

6.2.3.2 Physical Properties

The deposited CdS films were typically yellow and appeared smooth and continuous. Ocassionally, when a great amount of excess Cd was evaporated, the films appeared brownish yellow. The physical micro-properties of the films were investigated by X-ray analysis and scanning electron microscopy.

The X-ray analyses were carried out by a spectrograph operating at the wavelength of 1.5443 Å. The angles at which the diffracted energy peaks were recorded , were then compared with the standard X-ray data for hexagonal and cubic CdS. Three samples were investigated, two of which were prepared at about 190^{o}C substrate temperature while the third was prepared at room temperature. All samples showed the distribution of the peaks that corresponded with the peak distribution of hexagonal CdS. Few peaks could have been ascribed to the cubic phase, but since the rest of the peaks belonging in the cubic series were absent, either the proportion of the cubic phase was very small or these peaks were due to the hexagonal phase and were slightly shifted due to the temperature shift or due to the other minor wavelengths present in the spectrograph. X-ray analyses of the Corning 7059 glass showed no peaks whatsoever so that no error was introduced by the substrates. A rough comparison of the relative intensities

also correlated with the standard data and peaks ascribed to the 100, 002, 101 and 110 phases were found to be the strongest. Energy peaks detected at relatively large angles (>30^{o}) were observed only in the films deposited in a hot substrate, indicating that these films had larger crystallites and a greater degree of preferred orientation.

The surface texture of the films was investigated by an electron microscope. A typical electron micrograph, shown in figure 6.5 indicated that the typical grain size in the CdS films was between 800 Å and 1000 Å.

6.2.4 Discussion

The properties observed in the CdS films are found to be consistant with those observed by other researchers. The dependance of the resistivity in the film thickness has been observed before [142,147]. The 'ageing' of the films, i.e. the increase of the resistivity with the time the films were exposed to the atmosphere has also been observed before [153] and is ascribed to the adsorption and / or absorption of oxygen which, as an acceptor in CdS, compensates the film and increases the resistivity by decreasing the number of free electrons. The increase of the mobility with the illumination is consistent with the barrier scattering mechanism which is assumed to be the dominant mechanism in the polycrystalline CdS films [148,149]. The lack,

or the very small proportion of the cubic present in the CdS films is also a confirmed finding for the films deposited at the substrate temperatures that were used. From the results obtained it was not possible to deduce whether the carrier concentration (resistivity) in the CdS films 'saturates' with increasing amount of excess Cd evaporated, as is shown by the dotted line in figures 6.3 and 6.4, or whether it increases more linearly , as is shown by the solid line. Although, resistivities as low as 0.01 Ω cm were recorded when using very fast deposition rates, there is evidence[146] pointing out that excess Cd may form a deep donor level, 0.09 eV below the conduction band, in which case additional excess Cd incorporated in the CdS films may not necessarily result in a greater number of ionised donors (lower resistivity) which is behaviour not uncommon in wide band gap materials. However, this region of the carrier concentration versus the amount of excess Cd relationship is not of interest in this work.

The significant result in this section is the finding of the deposition conditions (CdS deposition rate 20 Å/s, substrate temperature 190°C, amount of excess Cd deposited about 70 Hz per 10 KHz of CdS (i.e. Cd source temperature of 270°C. (see section 6.2.3.1)) required to deposit films with the desired properties (resistivity 20 to 40 Ω cm, carrier concentration 8 to 10.10^{16} cm^{-3}, mobility 2 to 4 $cm^2V^{-1}s^{-1}$). Furthermore, it was found that the evaporation rate of metallic cadmium can be controlled sufficiently well

in order to reproduce films with properties varying by a factor of approximately two. This variation of the properties of the CdS films can be ascribed to a variety of reasons. Firstly, while the substrate temperature was monitored, the temperature of the quartz crystals was not so that the sticking coefficient and the sensitivity of the thickness monitors could have been different in each deposition. Secondly, in spite of the fact that care was taken, the substrate cleanliness might have been different in each case. Thirdly, the length of time of heating of the sources, including the pre-evaporation degassing, might have had an effect on the film properties via the stoichiometry of the source material [147]. Thus, some variation of the film properties can only be expected . However, the finding of the approximate deposition parameters, especially the rate of deposition of excess cadmium, was successful, and the method used for the control of the film stoichiometry was shown to be valid.

6.3 Cadmium Telluride

6.3.1 Introduction

In spite of the fact that CdTe is a potentially more useful semiconductor than CdS, in the sense that it can be prepared in both p- and n-conductivity types, CdTe thin films have been researched for less than the CdS films. This is due to the fact that the properties of the vacuum deposited CdTe films cannot be controlled as easily as those of CdS films.

Unlike in the single crystals of CdTe, vacuum deposited CdTe films appear in both hexagonal and cubic phases. Several researchers have concentrated on this peculiarity and it was determined that hexagonal CdTe may be prepared under a certain set of deposition conditions [154,155,156,157]. However, the cubic phase is dominant so that the hexagonal CdTe appears only when the films are deposited on substrates hotter than $200^{o}C$ [156,157] in the presence of excess cadmium. It was also determined that, as is the case with CdS, the grain size on the CdTe films increases with increasing substrate temperature [158,159] and that there is a small degree of preferred orientation in the cubic phase, so that the 111 plane lies parallel to the plane of the substrate [154,160]. However, the electrical properties of the films were generally found to be almost

independent of the film composition and the deposition conditions. The material and the temperature of the substrate were found to have a marked effect only on the films subjected to a post-depositional annealing in cadmium vapour [161] but no effect on the as-deposited films. The resistivity of the films, typically about 10^7 cm was found to be independent of the film thickness, and only slightly influenced by the substrate temperature [162]. A thorough investigation of most properties of the vacuum deposited CdTe films, carried out by Glang et al [160] resulted in similar conclusions. Even attempts at doping the films by incorporating some impurities in the source material have failed and the film resistivity could not be decreased. The high resistivity was ascribed to the presence of large potential barriers at the grain boundaries which would limit the carrier mobility, and the inability to incorporate a large enough density of electrically active impurities into CdTe films [160,163]. Subsequently, however, these low resistivity films have been prepared, either by chemical vapour deposition or even by vacuum deposition, by co-evaporation of a dopant and CdTe based solar cells have been made [109,111,127]. Thus the preparation of the CdTe films, and particularly low resistivity CdTe films seemed to be, if at all possible, far more difficult than the preparation of the CdS films.

6.3.2 Deposition Parameters

Most of the variable parameters that could be used in the deposition of CdTe films have been fixed by the considerations described on the previous section. Thus the substrate temperature was obviously to be between 180°C and 200°C, i.e. same as for the deposition of CdS. The deposition rate of CdTe had to be similar to that of CdS so that, when the shutters were to be used, similar thickness of CdS and CdTe were deposited in similar shutter opening periods i.e. when the shutters were to operate at equal opening times for both sources (mark - to - space ratio of 1:1) the composition factor 'x' of the CdS_xTe_{1-x} solid solution was to be equal to about 0.5. Thus the CdTe deposition rate was fixed at about 20 Å/s. The films of CdTe were to be doped by similar technique as was used for CdS, i.e. by co-evaporation of dopant material from a separate source. Thus the only variable deposition parameter was to be the deposition rates of the chosen dopant materials.

6.3.3 Experimental Results

6.3.3.1 Electrical Properties

Both p- and n-type CdTe films were prepared and investigated by the methods described in Chapter 5.

The deposition rate of CdTe was found to be easily controlled and quite reproducable.

P-type doping of CdTe films was achieved by controlled co-evaporation of copper. The resistivity and the Hall coefficient of the films was measured via four vacuum deposited gold electrodes which formed an ohmic contact with CdTe. Several types of sources were used for deposition of copper, but eventually the tungsten spiral was found to be the most convenient and the deposition rate of copper was found to be easily controlled provided that the copper evenly wetted the spiral. The crystal oscillators were calibrated for copper evaporation resulting in a factor of 4.6 Hz/Å relating the frequency change with the film thickness. However, as was described in section 6.2.3.1 the amount of copper incorporated in the films is expressed in terms of equivalent Hertz in order to maintain consistancy.

It was found that the resistivity of the CdTe films was very sensitive to the amount of excess copper evaporated as is shown in figure 6.6. Thus doubling the deposition rate of copper would result in a decrease of film resistivity of several orders of magnitude. It was possible to measure the Hall coefficient only for the low resistivity films and typical carrier concentrations of $1.5.10^{17}$ cm^{-3} were found. The mobility was calculated to be approximately 9 $cm^2V^{-1}s^{-1}$.

It was found that p-type CdTe films age extremely slowly or not at all, and even after two years of exposure to the open atmosphere, the maximum resistivity change was about 100%. The change of resistivity in the highly doped films was only 20% even after 2 years.

N-type CdTe films were prepared by an analagous method as above except that initially cadmium and subsequently indium were used as dopants. With cadmium doped films zinc contacts were used, and again they were found to be ohmic or nearly ohmic. It was found that the CdTe films doped with excess cadmium had invariably very high resistivities; of the order of $10^6 \Omega$ cm as is shown in table 6.2. The resistivity of the films was found to be independent of the amount of excess Cd co-evaporated with CdTe, of the deposition rate of CdTe or of the film thickness and it also did not change with time. Due to the very high film resistivities it was not possible to measure the Hall coefficient of the films.

Consequently, an attempt was made to dope the CdTe with indium, deposition rates of which were found to be relatively easy to control, even at low values by maintaining the source temperature between 700°C and 750°C. For these films indium and subsequently zinc contacts were used. It was found that indium, when evaporated onto glass substrates at room temperature, did not form a conducting metal film in spite of the fact that it appeared continuous. This was

probably caused by some form of coagalation whereby indium would form conducting islands separated by insulating microscopic voids. Hence, zinc contacts were used again and they appeared ohmic. Due to the fact that a number of the doped CdTe films seemed to have high resistivities, an attempt was made to ensure that the contacts were not responsible for this. However, neither baking of the film and contacts at 200^{o}C for several hours in vacuum, nor the use of a four point probe configuration of the contacts made any difference to the measured value of the resistance of the films. Thus the recorded resistivities were assumed to be the property of the films themselves. The resistivity of the indium doped CdTe films appeared to be quite irreproducable , as is shown in table 6.3. The recorded resistivities ranged between the values of 10^{6} cm and 10^{1} cm with no apparent relation to the deposition conditions. For the two low resistivity films that were obtained the Hall coefficients indicated that the carrier concentrations were between approximately $5.10^{16}cm^{-3}$ and $5.10^{17}cm^{-3}$. Consequently, the calculated mobilities had values of between 6 $cm^{2}V^{-1}s^{-1}$ and 0.6 $cm^{2}V^{-1}s^{-1}$ as is also shown in table 6.3. It was noticed, however, that the film resistivity seemed to be increasing from sample to sample i.e. that the number of low resistivity films was higher among the samples deposited immediately after the investigation of cadmium doped films. Thus

the possibility that residual elemental cadmium left from the CdTe and Cd co-evaporation, contaminated the films and reduced their resistivity, was investigated. Several films were then deposited in a system purposely contaminated with pure cadmium, or else CdTe was co-evaporated with both In and Cd. The resistivity of these films appeared to be lower, in some cases substantially so, but also irreproducable, as is shown on table 6.4.

The resistivity of all of the n-type CdTe films was also found to be stable with time. The films were also photosensitive, but the maximum change in the resistivity with illumination was found to be an order of magnitude, even in the high resistivity films.

6.3.3.2 Physical Properties

Films of CdTe were dark brown, and if sufficiently thick, they were non-transparent. They were smooth and continuous and a typical scanning electron micrograph shown in figure 6.7 indicated that the size of the crystallites was between 500 Å and 800 Å. X-ray spectrography of separately prepared CdTe films, yielded a number of reflection peaks distribution of which seemed to form a closer match with the standard data

for hexagonal CdTe than with that of cubic CdTe. The comparison was crude and if there was any preferred orientation of the crystallites the observed relative intensities would be different to those given in standard tables. However, a Laue photograph showed no pattern whatsoever indicating that there is no preferred orientation. The principal X-ray reflection peak occurred at about 19.7^{o} which corresponded to the 100% $^{I}/I_{1}$, reflection from 110 direction of hexagonal CdTe and 60% $^{I}/I_{1}$, reflection from 220 direction of cubic CdTe. However, only a very small peak occurred at 12^{o} which corresponds to the 100% $^{I}/I_{1}$ reflections from both phases. The angles corresponding to the rest of observed relfections (23.3^{o}, 31.1^{o} and 42.2^{o}) appear in the standard data for both phases, but the relative intensities seemed to match hexagonal rather than cubic phase. The experiment was repeated after approximately 2 years and since an identical pattern was obtained, the crystal structure of the film was assumed to be stable. Thus, the hexagonal phase was probably dominant in CdTe films, although a mixture of both phases may have been present.

6.3.4 Discussion

The properties of the CdTe films, though principally in agreement with the results of other researchers (section 6.3.1) were generally found difficult to control. In spite of the fact that low resistivity p-type CdTe was made with surprising ease, n-type films with low resistivity were difficult to prepare. The difficulty of achieving high degrees of doping was assumed to be due to the reasons given by de Nobel [163] and Glag et al [160] i.e. the low solubility in CdTe and the electrical inactivity of the impurities. The apparent decrease of the film resistivity in the presence of cadmium contaminant may have been a true observation. Co-evaporation of Cd with CdTe is a process that is almost analagous to the annealing in Cd vapours, and it is known[163,195] that annealing in Cd vapours "activates" the impurity donors, such as In, in CdTe, and thus reduces the resistivity of the semiconductor.

Nevertheless, since the n-type layer in a graded band gap CdS_xTe_{1-x} solar cell is an alloy of CdS and CdTe, it was assumed that some of the properties, including the doping, of the alloy would probably be more like those of CdS , especially in CdS rich compositions. (see 6.4.1). Thus, the difficulty of

obtaining low resistivity in n-type CdTe films may not be encountered at all in the graded films, especially because the surface layer of the cell is to be graded to the composition of about 50% CdS and 50% CdTe, rather than 100% CdTe. Furthermore, since the CdS rich end of the CdS_xTe_{1-x} layer is to be doped with excess Cd, there may be enough elemental Cd in the system to improve the possibility of doping CdTe rich end of CdS_xTe_{1-x} with In. At worst, the fact that n-type CdTe is difficult to dope implies that CdTe rich graded CdS_xTe_{1-x} may be difficult to dope.

The investigation of p-type CdTe showed that a good quality base layer for a solar cell may be obtained by vacuum co-evaporation of CdTe and Cu (substrate temperature 190, CdTe deposition rate 20 Å/s, amount of copper about 200 equivalent Hz). Furthermore, the fact that copper forms an active acceptor in CdTe implies that CdTe rich solution of CdS_xTe_{1-x} may be doped p-type as well, and thus may also form a good base layer for a solar cell.

6.4 Mixed CdS_xTe_{1-x} Films

6.4.1 Introduction

Most of the known properties of the mixed CdS_xTe_{1-x} films have already been summarised in Chapter 3. The relation between the composition factor and the band gap and crystal phase of the alloys and most of the other material properties of the CdS_xTe_{1-x} films have been confirmed and described. However, aside from some work by Bonnett [127], whereby the resistivity of the mixed as-deposited films was measured as a function of the composition factor, there is no published data on electronic properties of CdS_xTe_{1-x} alloys. Interestingly, Bonnett found that at the composition factor of about 0.5 the resistivity of the mixed films underwent a change of several orders of magnitude, i.e. that the resistivity of CdS rich alloys was quite low (few Ω cm) while that of CdTe rich alloys was very high (10^6 Ωcm), thus confirming that the alloy takes on some of the properties of the principal component.

Most of the thin films of CdS_xTe_{1-x} have been prepared either by flash evaporation of a desired mixture of CdS and CdTe [128,129], or by controlled co-evaporation of CdS and CdTe from two separate sources [127,128]. However, neither of the two techniques

was seen as suitable for preparation of a graded band gap solar cell. The flash evaporation method does not render an obvious way of uniformly doping the films, and, judging from the properties of most of the II-VI semiconductors, it was assumed that the rate of evaporation of the constituent semiconductors would control not only the composition of the alloy, but also the impurity concentration. Thus, the shuttering technique described in Chapter 5, was to be used. This method was not only seen as more conducive to achieving uniform doping, but was also seen as a practical technique because the deposition parameters such as the source and substrate temperatures could be fixed, so that the whole process of growing mixed and/or graded films of CdS_xTe_{1-x} could possibly be automated.

6.4.2 Experimental Results

Two different sets of mixed films were prepared. Firstly, p-type mixed films with a composition of approximately 50% CdTe 50% CdS were prepared and secondly mixed films doped n-type were prepared throughout the composition range. Since the ultimate aim of this work was to prepare a solar cell, the doping characteristics of CdS_xTe_{1-x} mixed films were not investigated thoroughly , but rather, as was the case

with CdS and CdTe, an attempt was made to determine a set of deposition parameters that resulted in desired film properties. The results from sections 6.2 and 6.3 were used as indications for approximate deposition conditions that would probably be required.

6.2.4.1 P-type mixed $CdS_{0.5}Te_{0.5}$ films

For the p-type CdS_xTe_{1-x} films the composition of the deposited mixed films was fixed by the shutter control at 45% $\pm$ 5% CdS and 55% $\pm$ 5% CdTe. Typical resultant band gap of the films, measured by the monochromator as described in Chapter 5, was found to be approximately 1.45 $\pm$ 0.05 eV. The appearance of the films was very similar to that of the pure CdTe films, i.e. smooth and dark brown. These $CdS_{0.45}Te_{0.55}$ films were doped p-type by co-evaporation of metallic Cu in the fashion analagous to the one used in deposition of p-CdTe films. The incorporation of the impurities onto $CdS_{0.45}Te_{0.55}$ films was found to be relatively easy, and films with widely differing resistivities were prepared, as is shown in figure 6.8. Films with resistivities as low as 0.01 cm were obtained by deposition of Cu at a relatively fast deposition rates (700 equivalent Hz). As was the case with p CdTe, the resistivity of $CdS_{0.45}Te_{0.55}$ was found to be very sensitive to the amount of copper evaporated. An attempt

was made to measure the Hall coefficient in these films but the contacts with Cu or Au electrodes were found to be very noisy so that the Hall voltages could not be measured. However, in order to produce low resistivity films (approximately 10 cm) the amount of Cu evaporated was about twice as much as was required for pure CdTe films of similar resistivities. Thus, it was assumed that the carrier concentration in these p $CdS_{0.45}Te_{0.55}$ films was of the order of $10^{17} cm^{-3}$ and that the mobility was several $cm^2 V^{-1} s^{-1}$.

$CdS_{0.45}Te_{0.55}$ films, like p CdTe films, were found to age little or not at all.

6.4.2.2 N-type mixed CdS_xTe_{1-x} films

CdS_xTe_{1-x} films with different compositions were doped n-type by co-evaporation of Cd and In with CdS and CdTe respectively. The composition of the films was determined by the setting of the controls on the shutter control unit and films with compositions varying from 100% CdS to 100% CdTe were prepared. Figure 6.9 shows the relation between the band gap of the mixed films and their composition as determined by the setting of the ratio control in the shutter control unit (see Chapter 5). Comparison with similar curves

obtained by Hill and Richardson[128] indicated that the actual film composition did not deviate appreciably from the intended compositions. In addition , the composition of some of the films was measured by an X-ray energy spectrometer and the measured values corresponded closely (to within approximately 10%) with the compositions pre-set in the shutter control unit. Some films were found to have two distinct separate absorption edges. This was due to some form of poly-phasing where the evaporation of CdS and CdTe resulted in two compositions of CdS_xTe_{1-x} alloys or perhaps in some form of clusters of Te or S atoms and was caused by incomplete inter-diffusion of the interleaved layers of the constituent semiconductors. This phenomena was observed when the shutter periodic time was long (6 seconds or more) and was more common in the CdTe rich samples (50% or more of CdTe) indicating that Te had the smallest diffusion coefficient. However, when shorter shutter periodic times were used polyphasing was not observed, i.e. the deposited films formed homogenious and uniform semiconductor layers. Very short periodic times, however, resulted in p or correlation between the actual and the intended film compositions, particularly when depositing films with compositions close to the extremes of the composition range. This was due to the fact that when high shutter frequencies were used, the time taken for a shutter to swing into open (or shut) state, i.e. the length of time that a shutter is in an undefined state,

represented an appreciable percentage of the total periodic time. It was found that shutter periodic time of 3 to 4 seconds was short enough to prevent polyphasing and long enough to allow good control over the film composition.

Several CdS_xTe_{1-x} films with differing compositions were investigated by X-ray diffractometer. In CdS rich compositions, the distribution of peaks was not the same as in CdS films, but was similar in the sense that the principal peaks occurred at approximately the same positions. For CdTe rich solutions, however, no peaks were detected at or near 19.7^{o} , where the principal reflection occurred in CdTe films. Furthermore, the few reflection peaks that were detected in these films were quite weak indicating that there is no preferred orientation in the CdTe rich films. However, the scanning electron micrographs of a number of films with different compositions, shown in figure 6.10, showed that the grain size in the films is independent of the composition and typically between approximately 700 Å and 1000 Å, as was the case with CdS and CdTe films.

The Hall coefficient and the resistance of the CdS_xTe_{1-x} films was measured via four zinc electrodes which, again, were found to form an ohmic contact with the semiconductor. CdS_xTe_{1-x} films were doped n-type with a relative ease and films with low resistivity values were obtained throughout the composition range by co-evaporation of necessary amounts of Cd and In. However,

films that showed polyphasing i.e. two distinct band-gaps, had invariably very high resistivities (10^5 cm) regardless of the amounts of dopants co-evaporated with the semiconductors. Table 6.5 shows the resistivities of a number of CdS_xTe_{1-x} mixed films of different compositions as a function of the amounts of Cd and In expressed in equivalent Hz incorporated in the films. For similar deposition conditions, the resistivity of the CdTe rich solid solution tended to be higher than that of CdS rich solutions, as is shown in figure 6.11 but could be reduced by increasing the amount of dopants incorporated in the films, as can be deduced from table 6.5.

The Hall coefficient of several films was measured and as is shown in table 6.6, carrier concentration ranging between $1.6 \cdot 10^{16} cm^{-3}$ and $2.5 \cdot 10^{18} cm^{-3}$ were observed. However, no obvious relationship can be seen between the measured carrier concentration and the amount of dopants incorporated in the films, probably due to the fact that the carrier concentration is dependent on three variables namely the amount of In evaporated, the amount of Cd evaporated and the film composition (band gap). However, several facts may be deduced from the table: Firstly, in order to obtain similar carrier concentrations in samples of different compositions (samples 6 and 13.2 or 3.1 and 19.2) a greater amount of dopants is required for films with larger concentrations

of CdTe. Secondly, samples with similar compositions and deposited under similar deposition conditions tend to have similar properties, i.e. the properties of the films appear reproducable (e.g. samples 5 and 16.1) and thirdly, a greater amount of dopants evaporated results in a greater carrier concentration in films of similar composites (e.g. 12.2 and 6 or 4 and 5) The mobility of the carriers calculated from the carrier concentration and resistivity appears to be a function of the carrier concentration alone, and is quite independent of film composition, as is shown by figure 6.12. and table 6.6.

An attempt was made to measure the Hall coefficient of several films with different compositions, as a function of temperature and to deduce the ionisation energy of donors in various alloys. However, noise superimposed in the Hall voltage signal made measurements of the Hall coefficient difficult , particularly at low temperatures, so that no numerical deductions were made based on this data. However, best $\ell n\ \sigma$ vs $^{1}/T$ curve drawn through the measured points did appear to have a knee indicating that there are 2 distinct donor levels present, even in CdTe rich samples.

6.4.3 Discussion

The investigation of mixed CdS_xTe_{1-x} films leads to many valuable conclusions. Primarily it was shown that uniform and homogeneous mixed films may be prepared by the shuttering technique, provided that correct shuttering frequency is used. It was also shown that mixed films may be doped into either conductivity type and that desired impurity concentrations may be achieved throughout the composition range by simultaneous co-evaporation and shuttering of dopant materials. This indicates that the techniques chosen may be applied for the production of a graded band gap cell. Furthermore, a number of assumptions may be now made about the electronic properties of graded band gap films based on measurements on CdS_xTe_{1-x} mixed films. Firstly, uniform impurity concentrations may be achieved in graded CdS_xTe_{1-x} films by a steady increase of deposition rates of Cd and In i.e. of the deposition rates of Cd and In are maintained constant throughout the deposition of graded band gap CdS_xTe_{1-x} layer, the resultant impurity concentration in the graded alloy will not be uniform. This may lead to a slope in a conduction band and an increased slope in the valence band, which should not impede the flow of carriers . However, uneven doping

may result in localised potential barriers and an intrinsic layer whose effect would be to increase the series resistance of the device. However, it ought to be possible to increase the deposition rates of Cd and In and thus maintain uniform doping . Furthermore, Cd and In may prove to be mobile enough in the CdS_xTe_{1-x} structure so that they may diffuse and smooth out any discontinuities in the impurity concentration. Secondly, provided that uniform doping is achieved, the carrier mobility throughout the graded band gap region ought to be uniform i.e. position independent. Thirdly, since the grain size of the CdS_xTe_{1-x} mixed films appears to be composition independant, the crystallite size in graded band gap films, being a strong function of deposition conditions and weak function of the crystal phase, may be expected to be uniform throughout the structure. Fourthly, since there is bowing of the band-gap with the composition factor, grading of the CdS_xTe_{1-x} alloy throughout the composition range is unnecessary. This not only simplifies the achievement of uniform doping throughout the graded layer but also allows the use of band gaps as low as about 1.3 eV in the base layer, which, according to the theory (see Chapter 4) ought to result in better performance. Finally, the investigation of p-type Cu doped $CdS_{0.45}Te_{0.55}$ layers indicates that mixed $CdS_{0.45}Te_{0.55}$ layer, as well as pure CdTe layer

can be used as the base layer of the solar cell i.e. that formation of a true homojunction is feasable. It was assumed that, if lower base layer band gaps are required, the doping of CdS_xTe_{1-x} alloys with decreasing composition factors ought to be achieved with increasing ease.

6.5 Conclusion

The material properties of CdS, CdTe and in particular mixed CdS_xTe_{1-x} indicate that a solar cell with a graded band gap surface layer may be fabricated in alloys of CdS and CdTe by the techniques chosen. Desired doping properties, i.e. the preparation of p-type and n-type semiconductors with uniform density of impurities , may be achieved thereby indicating that a p-n function can be formed. With sufficiently fine control of the deposition process a graded band gap surface layer, as well as a mixed or pure base layer, may be formed with uniform carrier density of approximately 5.10^{16} cm^{-3} and carrier mobility of the order of 5-10 $cm^2V^{-1}s^{-1}$, which are transport properties sufficiently good for a thin film solar cell.

It ought to be mentioned that a separate relatively simple investigation carried out by V.A. Penkithman and B. Brown in a separate vacuum evaporator indicated that the properties of CdS and CdTe films deposited simultaneously in glass and plastic substrates at 200°C do not differ. In these investigations no dopants were co-evaporated with CdS and CdTe, but the electronic and physical properties of the as-deposited CdS and CdTe films indicated that mixed and graded CdS_xTe_{1-x} films deposited in plastic substrates ought to have properties very much like those that they have when deposited on the glass substrates. Furthermore, some of the CdS,CdTe

or CdS_xTe_{1-x} films were subjected to any form of post-deposition beat treatment because of the low melting point of the plastic that was to be eventually used as the substrate material. Nevertheless, it appears that a possible graded band gap solar cell may also be deposited on low cost plastic substrates.

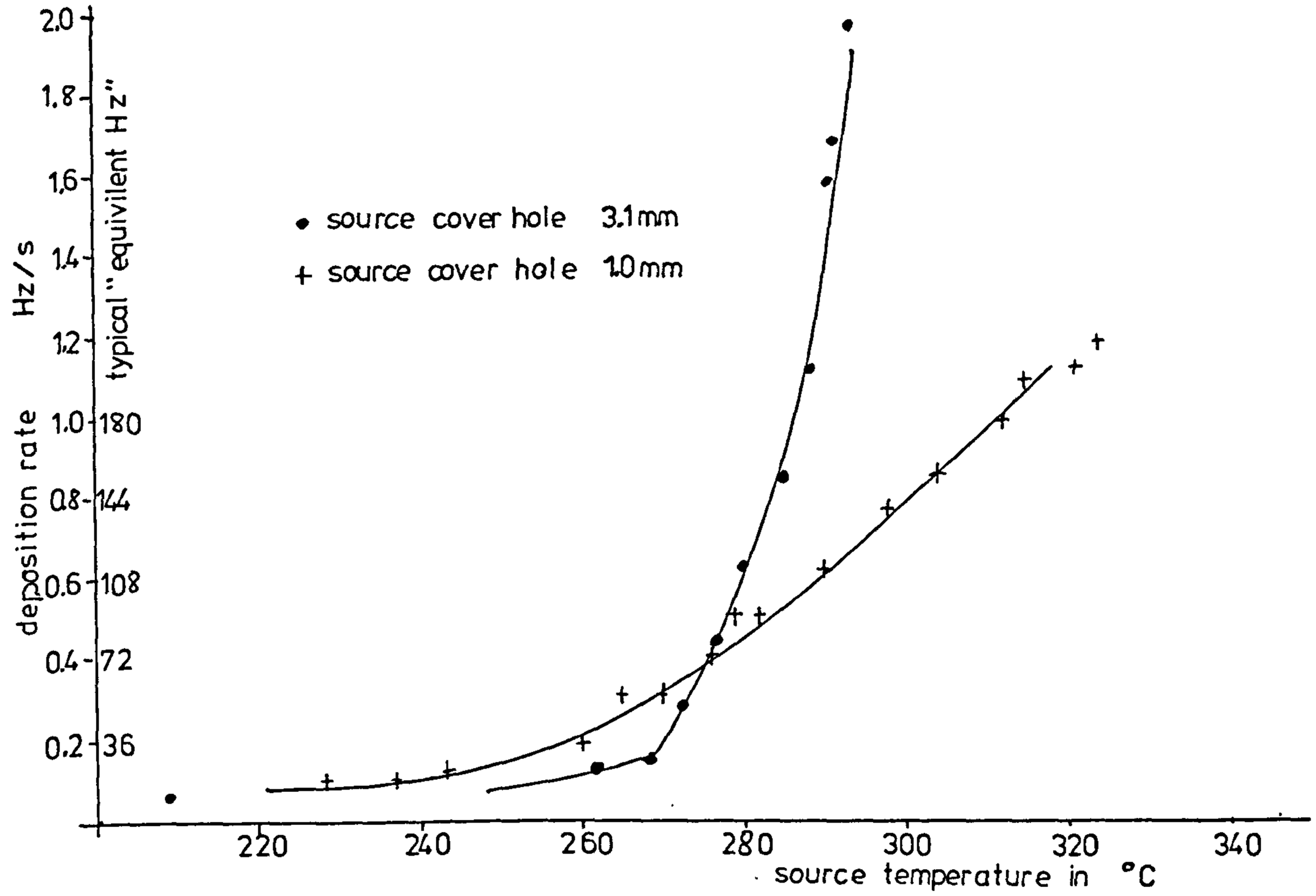

FIGURE 6.1 Cd depcsition rate as a function of source temperature for different source emitting areas

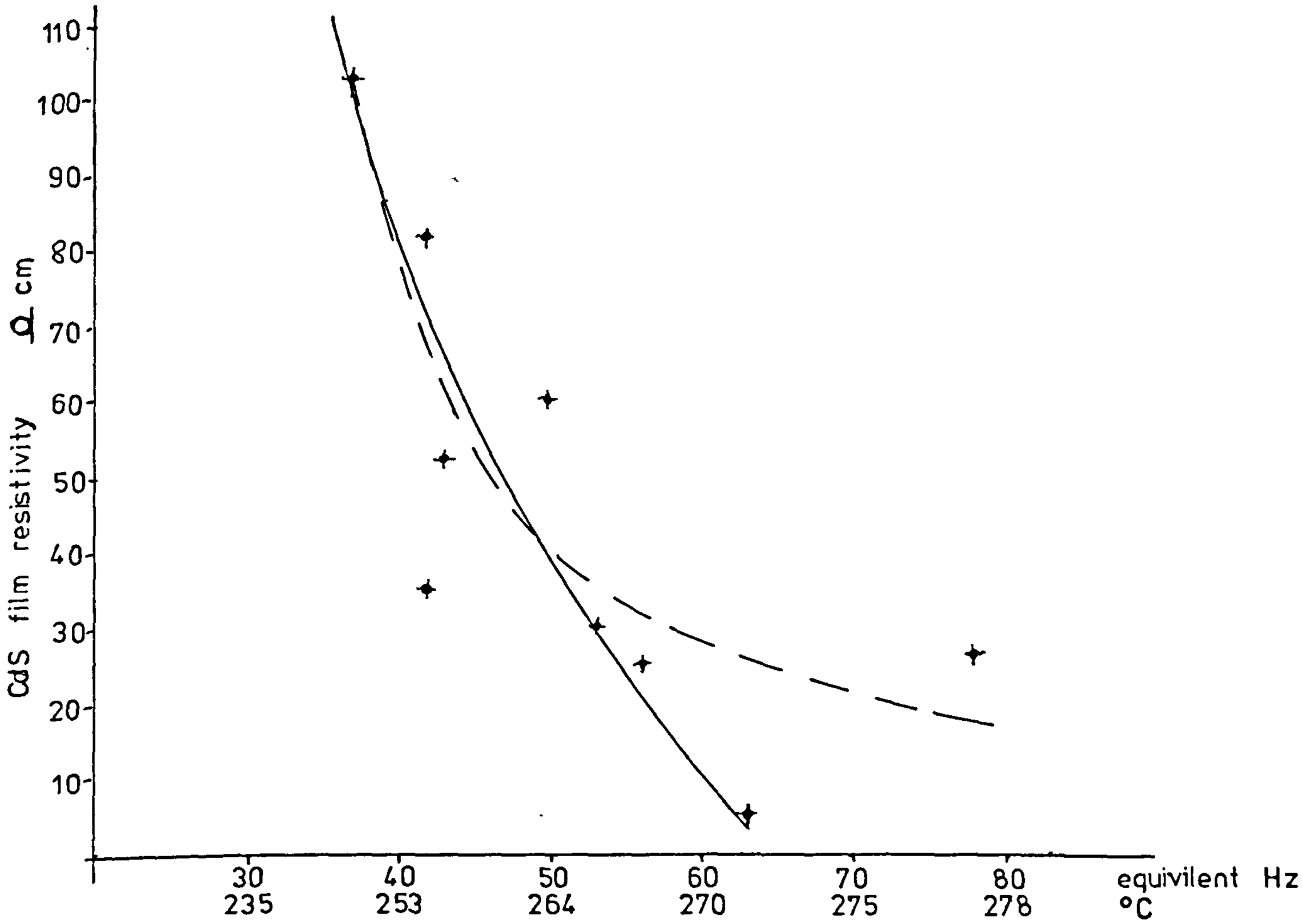

FIGURE 6.2 CdS resistivity as a function of amount of excess Cd expressed in terms of equivilent Hz and °C

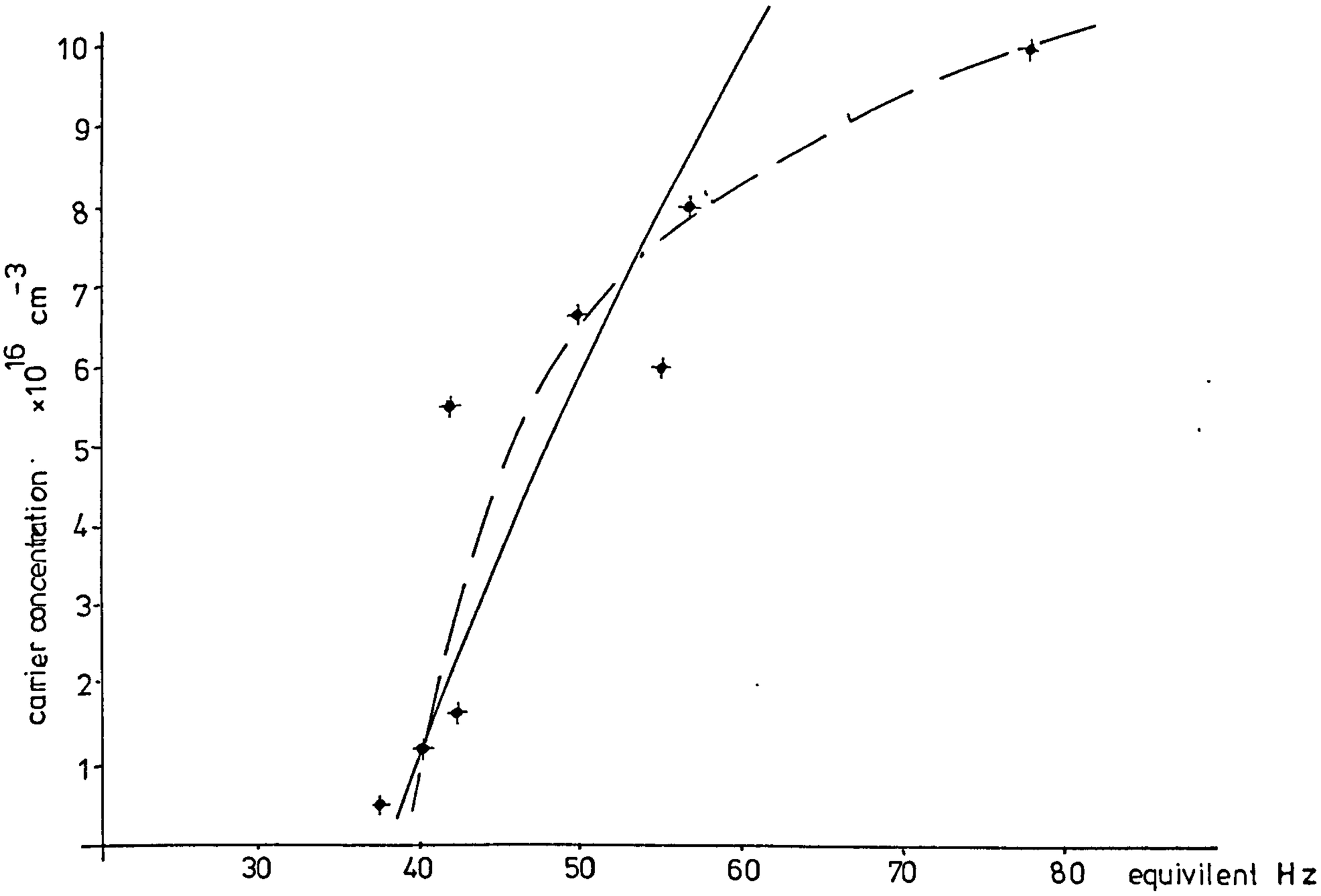

FIGURE 6.3 carrier concetration in CdS films as a function of the amount of excess Cd

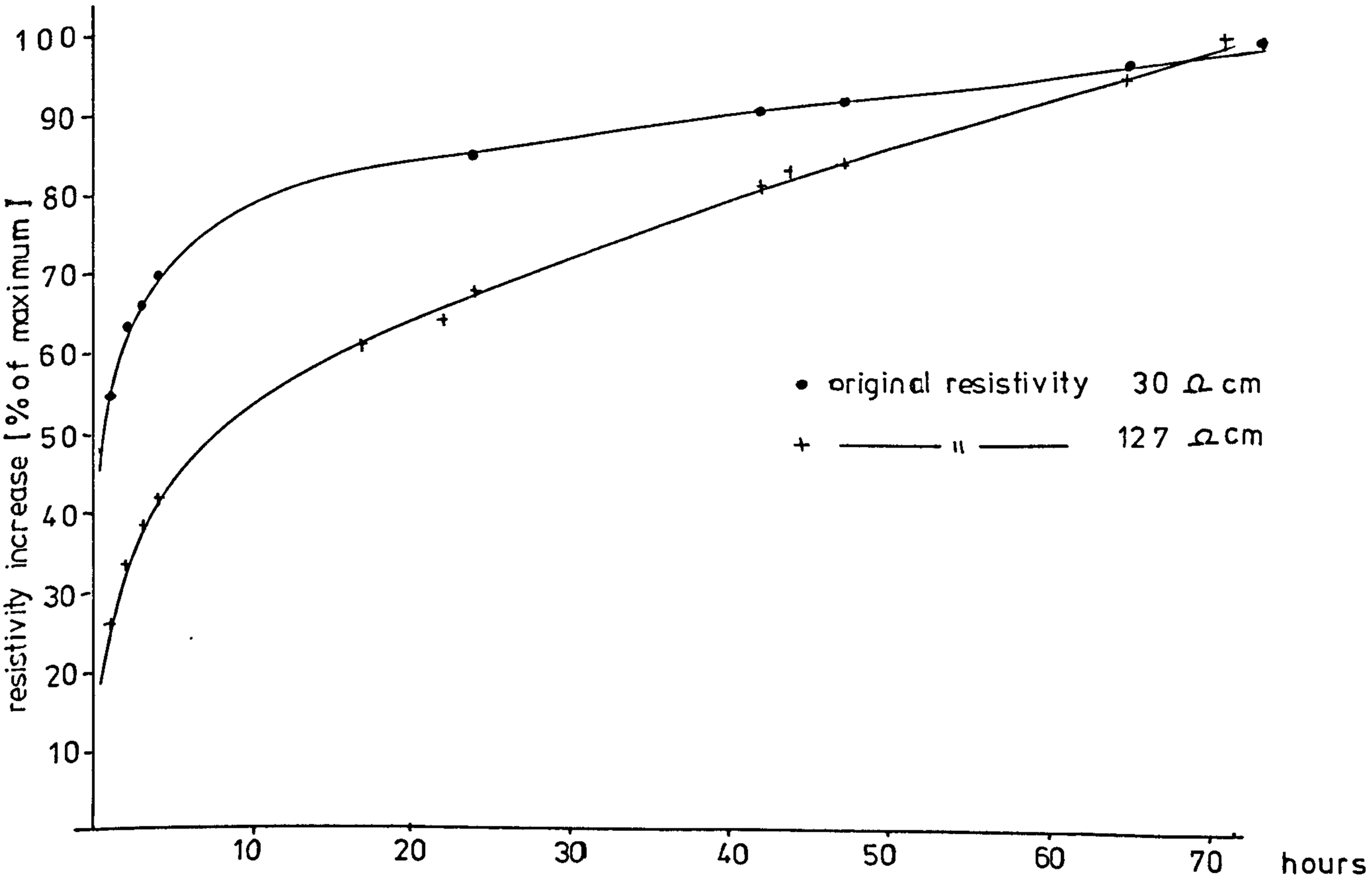

FIGURE 6.4 change in the resistivity of CdS films with time [hours]

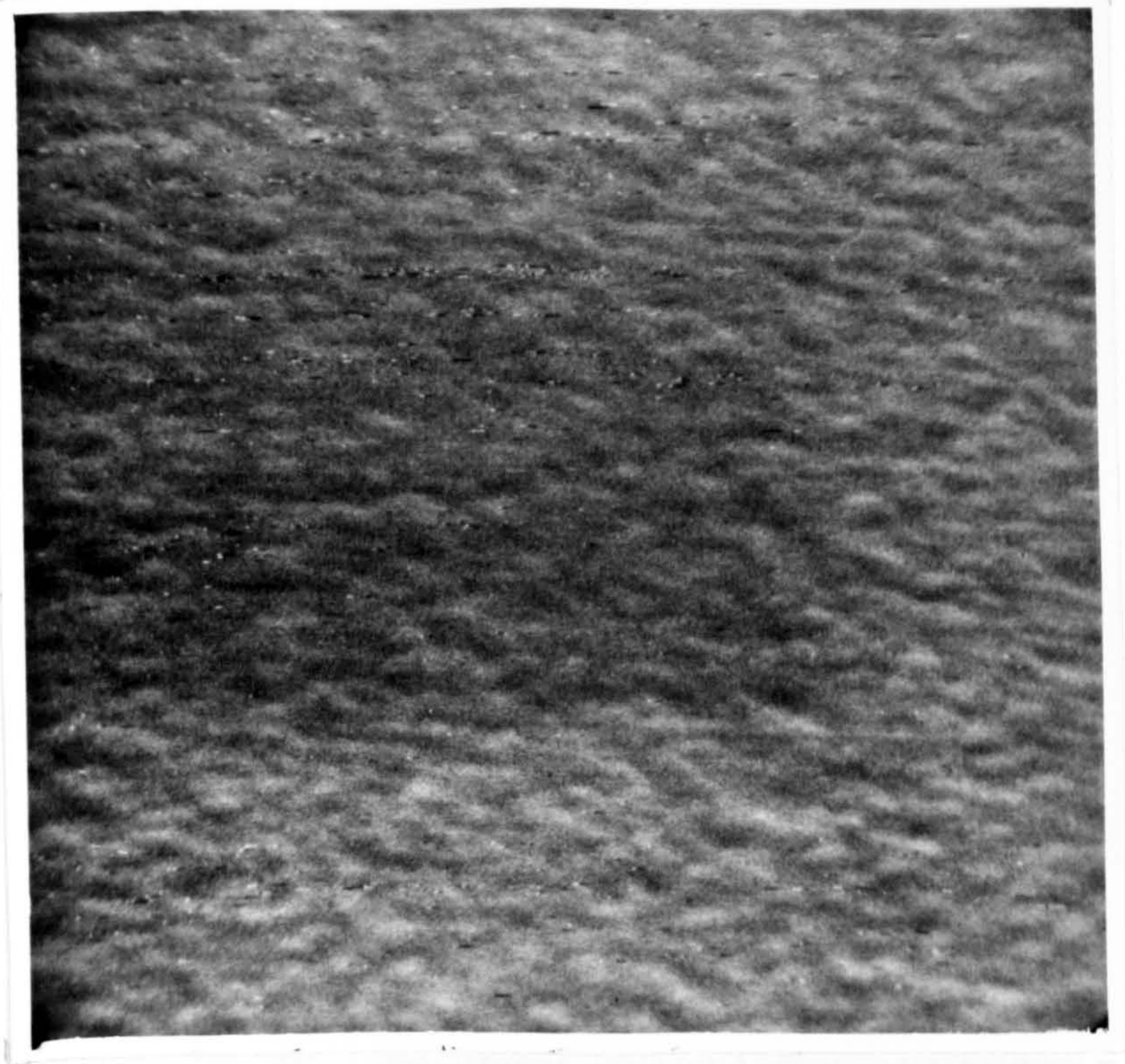

0.1 μm

FIGURE 6.5 scanning electron micrograph of a typical CdS film magnification 43 000 ×

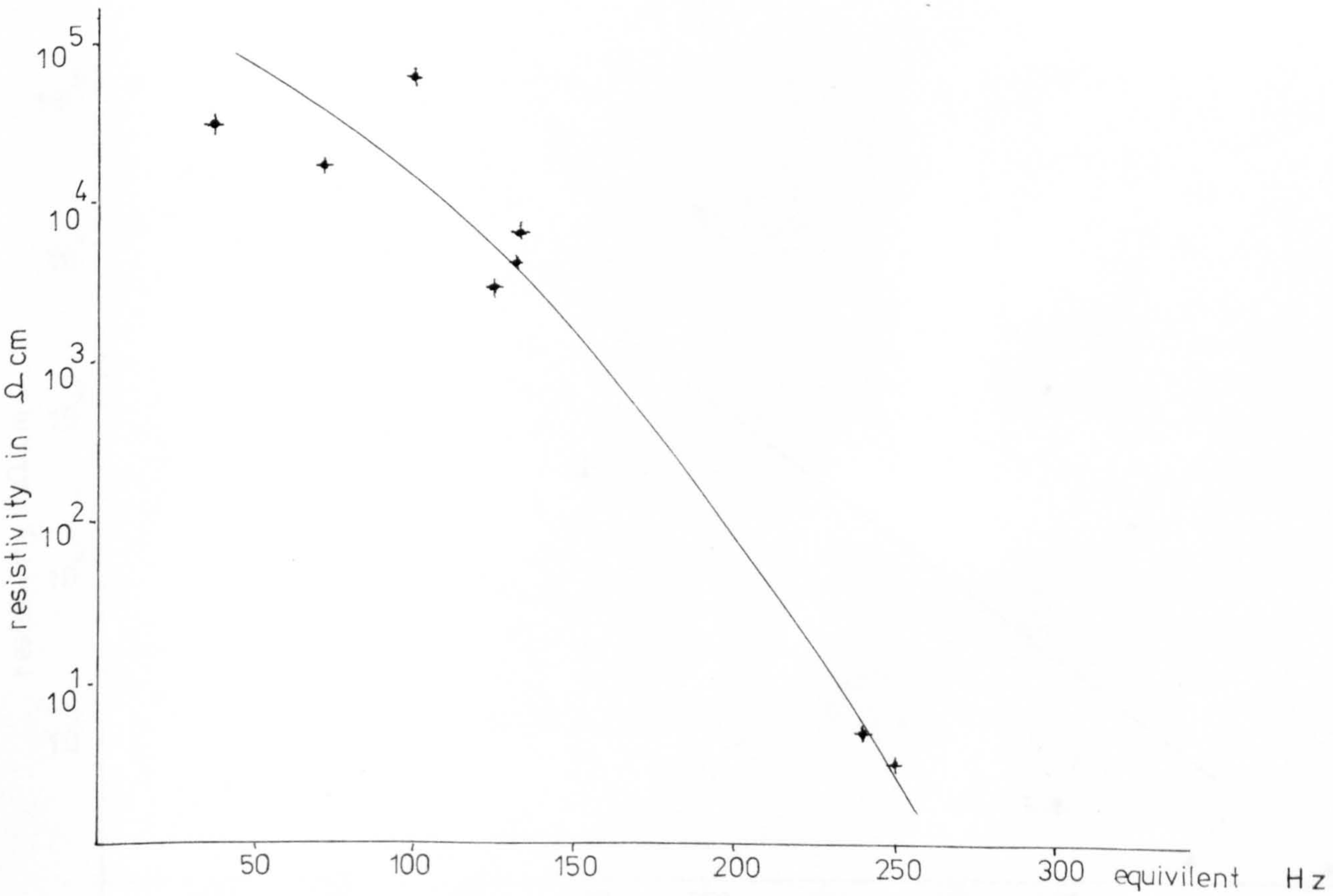

FIGURE 6.6 resistivity of CdTe films as a function of the amount of Cu incorporated in the films

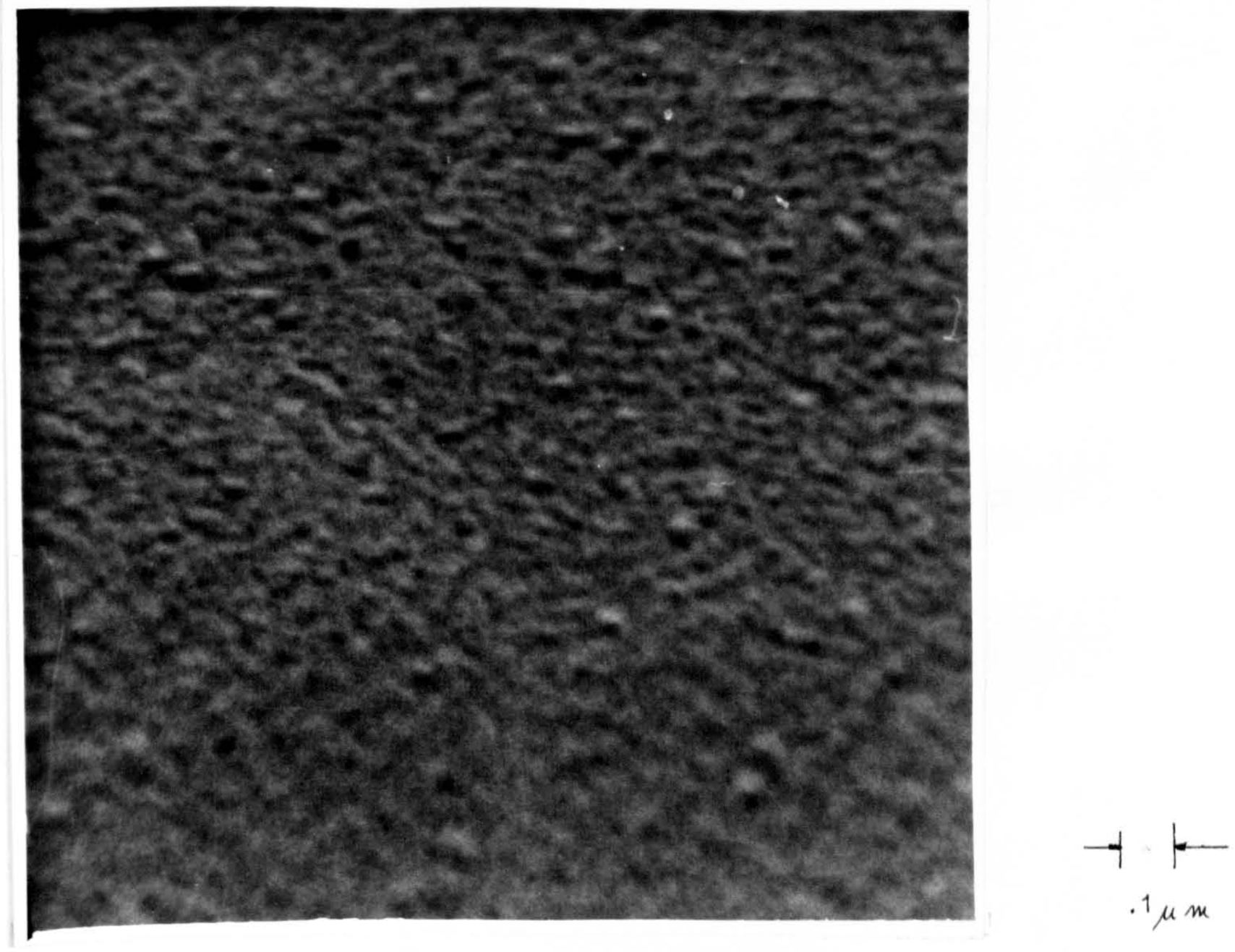

FIGURE 6.7 scanning electron micrograph of a typical CdTe film magnification 60 000 ×

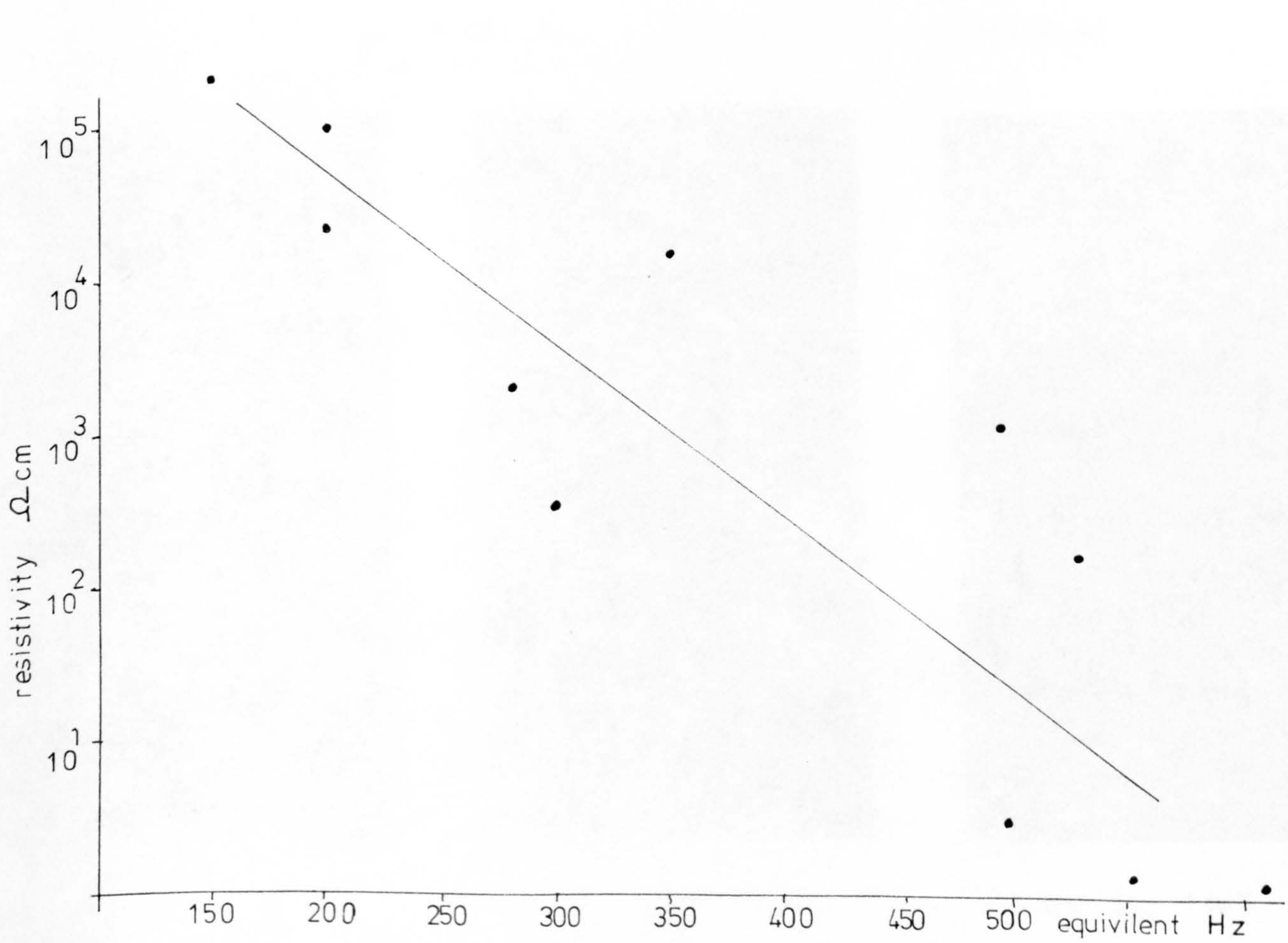

FIGURE 6.8 resistivity of $CdS_{0.45}Te_{0.55}$ mixed films as a function of the amount of evaporated Cu in equivilent Hz

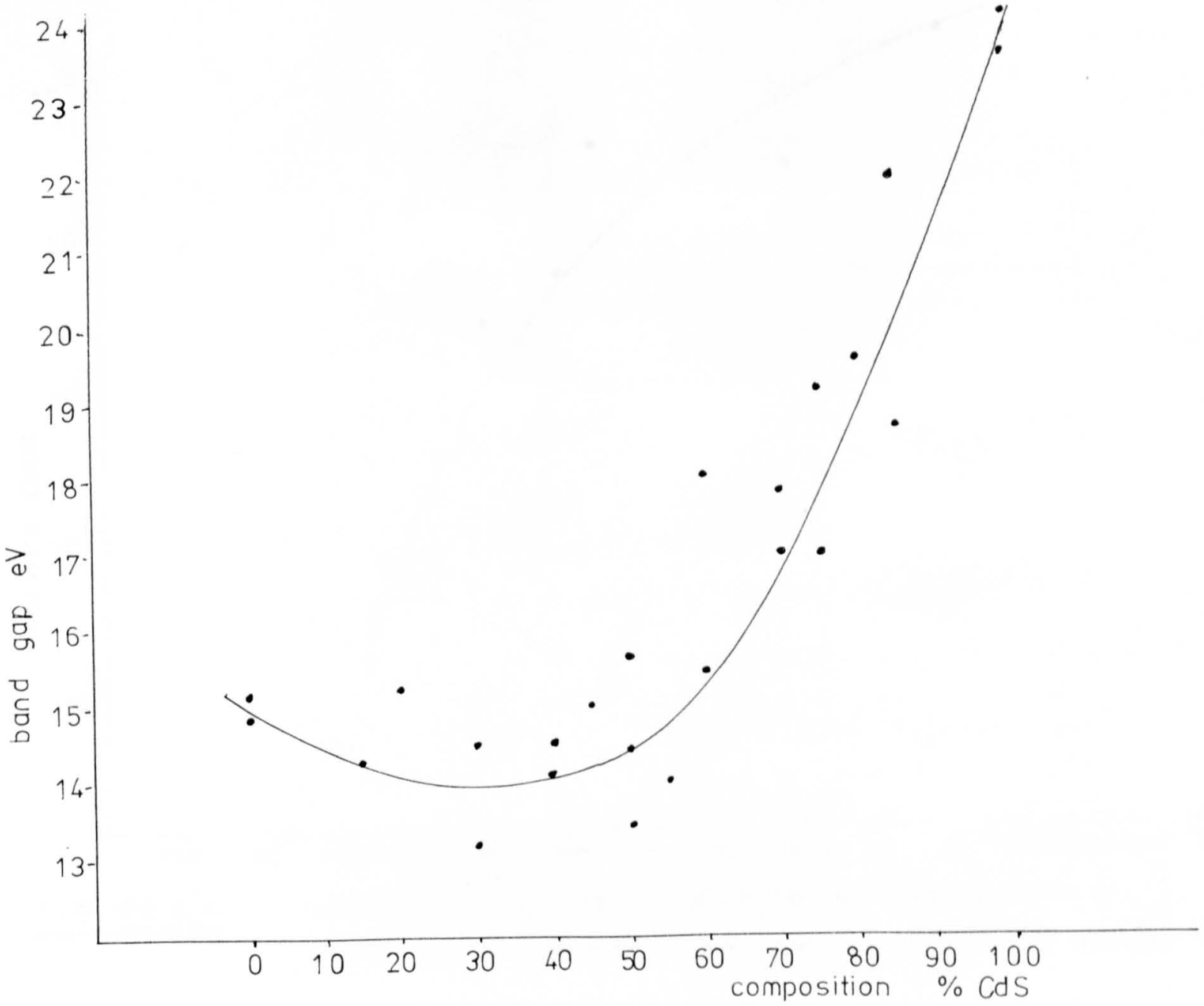

FIGURE 6.9 band gap of CdS_xTe_{1-x} vs film composition as determined by the shutter control unit

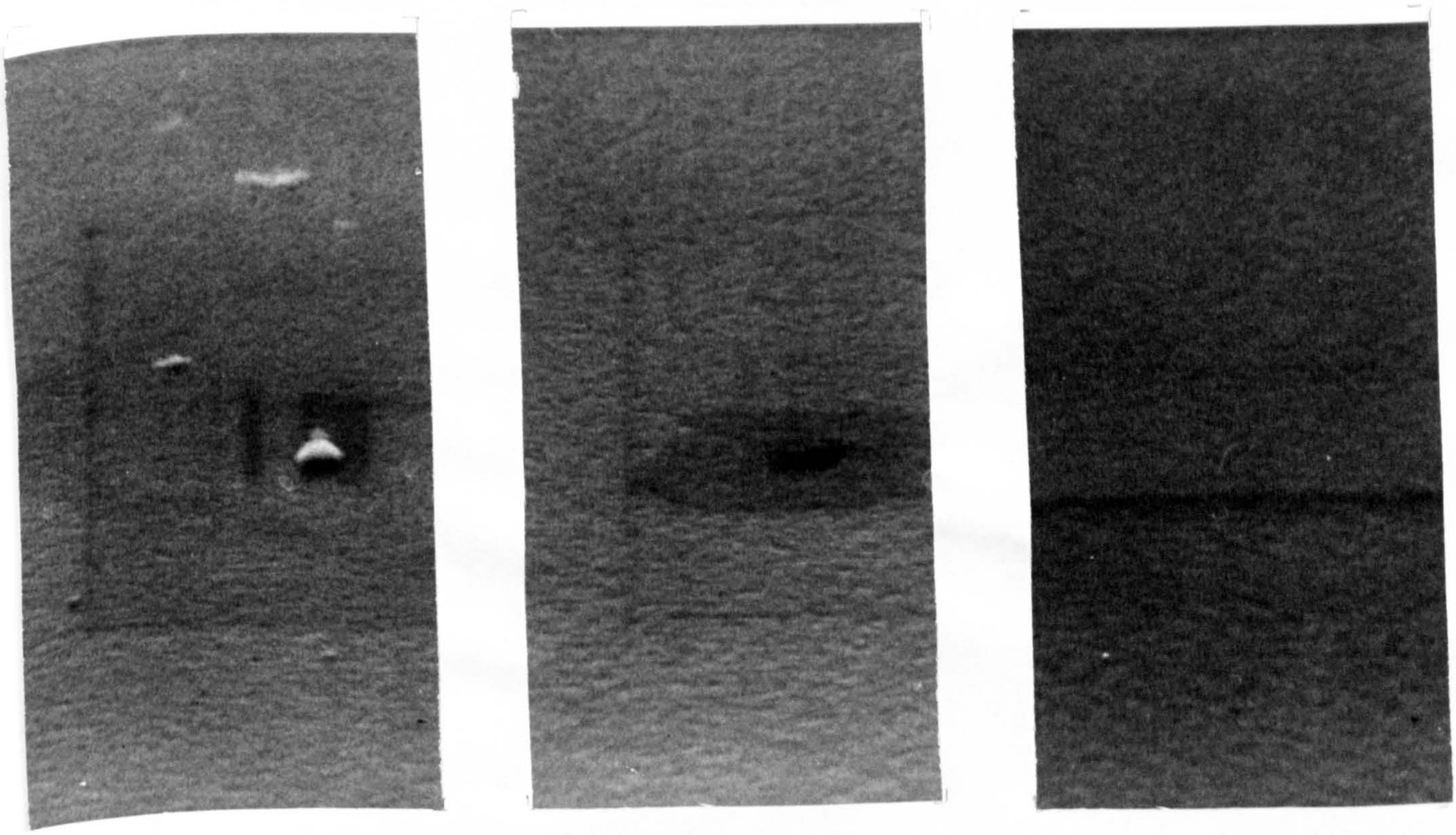

a] band gap 2.0 eV b] band gap 1.7 eV c] band gap 1.4 eV

FIGURE 6.10 SEM micrograph of CdS_xTe_{1-x} films of differing compositions magnification 30 000 ×

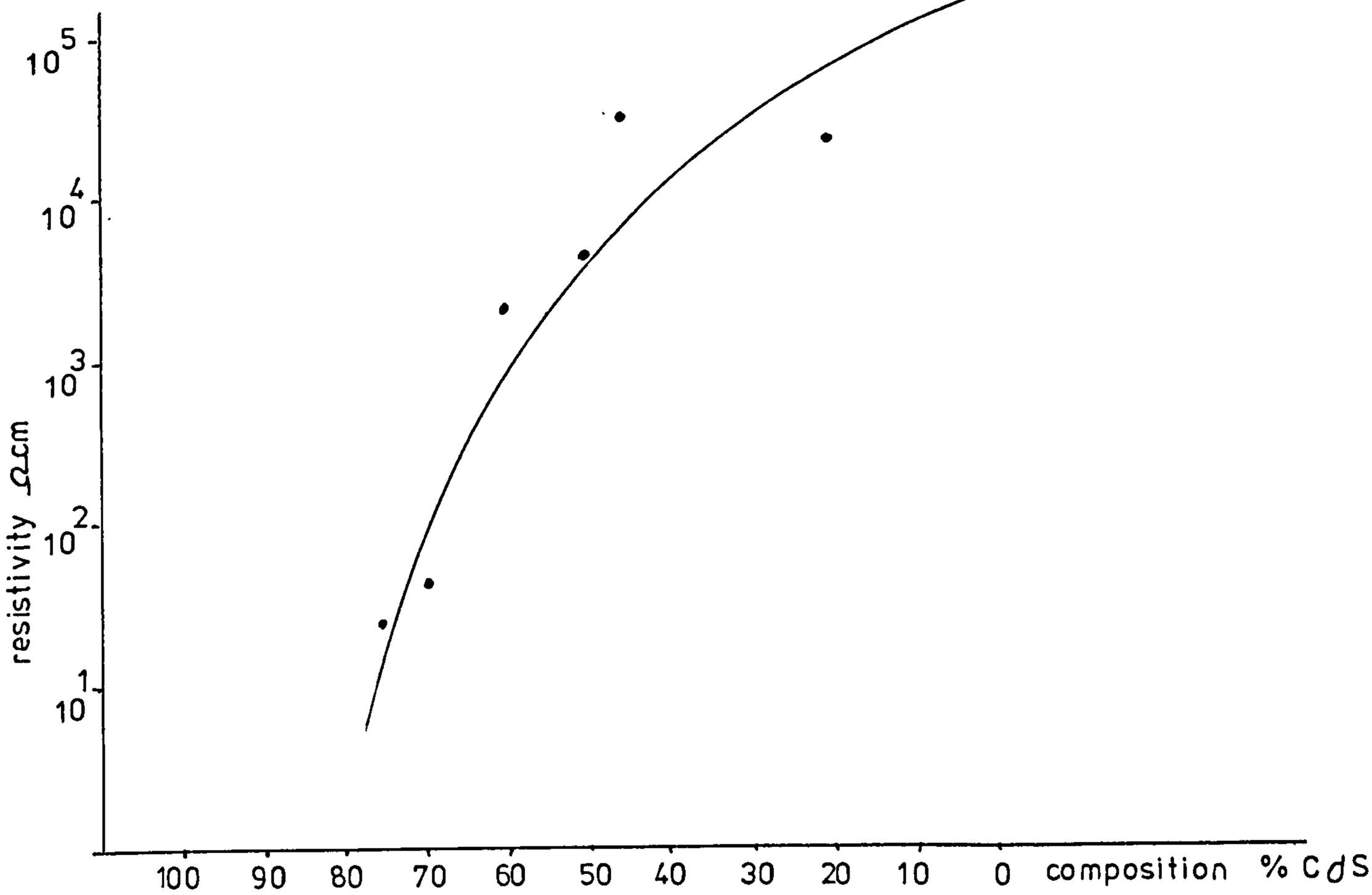

FIGURE 6.11 resistivity of CdS_xTe_{1-x} films of various compositions for a fixed set of deposition parameters [In 250, Cd 40 equivilent Hz]

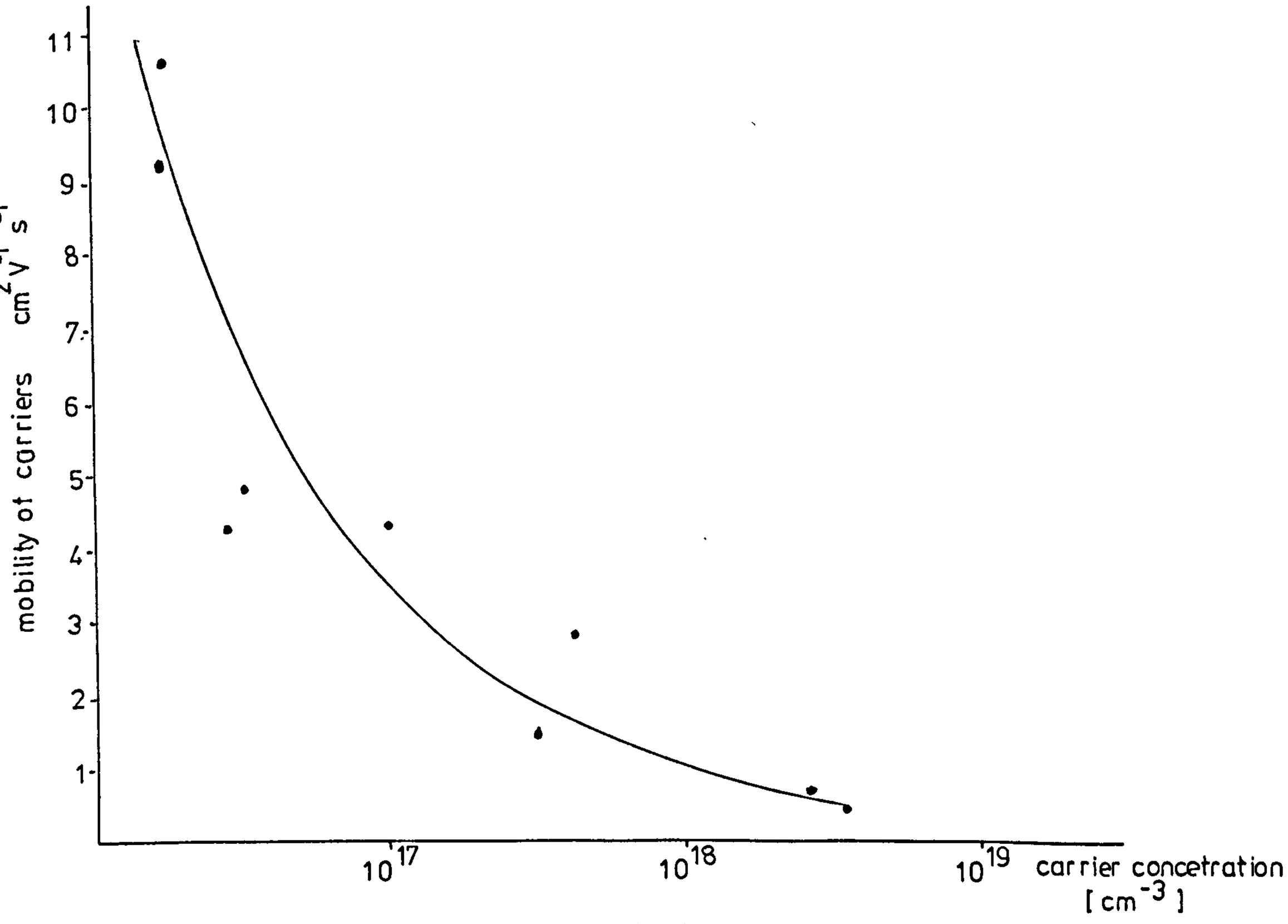

FIGURE 6.12 carrier concetration vs mobility for various compositions of CdS_xTe_{1-x}

DEPOSITION RATE Å/s	THICKNESS Å	RESISTIVITY Ω cm
3	DISCONTINUOUS	FILM
8	2500	$3.2 \cdot 10^4$
26	2800	530
32	3300	61
56	3300	2

TABLE 6.1 CdS resistivity for several deposition rates.

SAMPLE NUMBER	FILM THICKNESS in Å	EXCESS Cd AMOUNT IN EQUIV. Hz	DEPOSITION RATE OF CdTe in Å/s	RESISTIVITY in Ω cm
T 1.1	3300	107	22	$1.7 \cdot 10^6$
T 1.2	3600	107	25	$2.0 \cdot 10^6$
T 2.1	2800	196	19	$1.4 \cdot 10^6$
T 4.1	3350	112	21	$2.2 \cdot 10^6$
T 5.1	3800	128	33	$1.8 \cdot 10^6$
T 5.2	3200	410	21	$3.2 \cdot 10^6$
T 6.2	2500	130	40	$1.2 \cdot 10^6$
T 7.1	2800	195	47	$2.1 \cdot 10^6$
T 7.2	2900	240	14	$1.6 \cdot 10^6$

TABLE 6.2 Resistivity of CdTe coevaporated with excess Cd for various deposition conditions.

SAMPLE NUMBER	FILM THICKNESS in Å	AMOUNT OF In evap. in equiv. Hz	CdTe RATE A/s	RESISTIVITY Ω cm	CARRIER CONC. in cm^{-3}	MOBILITY $cm^2v^{-1}s^{-1}$
10.1	3300	216	19	1.3	7.10^{17}	6.6
10.2	3400	307	19	$1.4 \cdot 10^3$		
11.1	3000	126	20	$1.5 \cdot 10^2$	$6 \cdot 10^{16}$	0.6
11.2	3000	368	20	$9.0 \cdot 10^2$		
12.1	2900	440	23	$5.8 \cdot 10^3$		
12.2	3100	189	21	$4.7 \cdot 10^3$		
13.1	2600	186	17	$6.0 \cdot 10^5$		
13.2	2500	207	17	$2.5 \cdot 10^4$		
14.1	3950	90	26	$5.7 \cdot 10^4$		
14.2	2500	64	19	$1.5 \cdot 10^5$		
15.1	2800	153	19	$6.3 \cdot 10^5$		
16.1	3000	67	20	$1.5 \cdot 10^6$		
17.1	3750	410	21	$1.2 \cdot 10^5$		
17.2	3100	327	22	$7.5 \cdot 10^3$		
19.1	3300	143	22	$2.9 \cdot 10^5$		
19.2	3000	200	22	$3.6 \cdot 10^4$		
20.1	2600	600	20	$1.8 \cdot 10^6$		

TABLE 6.3 Resistivity of CdTe coevaporated with Indium for various deposit conditions.

BAND GAP eV	COMPOSITION % CdS	EXCESS Cd EQUIV Hz	AMOUNT In EQUIV Hz	RESISTIVITY Ω cm
2.2	85	60	200	0.2
1.96	80	30	200	0.1
1.92	75	30	200	6.4
1.85	85	20	200	32.5
1.84	70	20	250	5.3
1.78	70	50	400	1.4
1.75	60	60	400	0.8
1.73	60	50	300	3.3
1.71	60	40	250	56
1.72	73	40	250	18.2
1.7	70	40	250	46
1.62	50	50	200	$8.3.10^4$
1.54	60	40	250	10^5
1.54	60	40	250	$1.6.10^3$
1.5	45	40	250	$5.5.10^4$
1.45	40	50	300	5.8
1.45	50	60	300	$1.3.10^3$
1.41	40	50	350	49.2
1.37	40	150	300	0.02
1.35	30	50	250	$4.6.10^3$
1.32	30	50	300	85
1.43	20	50	250	$1.8.10^4$
1.43	15	50	300	$3.6.10^3$
1.48	10	60	400	68
1.5	0	50	250	10^6

TABLE 6.5 Resistivities of various CdS_xTe films of different composites and for differnet deposition rates

SAMPLE NO	AMOUNT OF In EQUIV Hz	RESISTIVITY Ω cm	TREATMENT
22.1	239	$3.5 \cdot 10^2$	system contaminated with Cd
22.2	212	$7.7 \cdot 10^2$	"
23.1	209	$7.0 \cdot 10^4$	"
23.2	107	$7.0 \cdot 10^4$	"
24.1	200	$1.0 \cdot 10^6$	Cd coevaporated with In & CdTe
24.2	220	$2.0 \cdot 10^6$	"

TABLE 6.4 Resistivity of CdTe coevaporated with In and treated with excess Cd.

BAND GAP eV	COMPOSITION % CdS	In EQUIV Hz	Cd EQUIV Hz	RESISTIVITY Ω cm	CARRIER CONC cm^{-3}	MOBILITY $cm^2V^{-1}s^{-1}$
1.92	75	200	30	6.4	$2.3 \cdot 10^{18}$	0.41
1.45	40	300	50	5.8	$1.9 \cdot 10^{18}$	0.56
1.7	75	250	60	18.2	$2.3 \cdot 10^{17}$	1.4
1.84	70	250	10	5.5	$4.1 \cdot 10^{17}$	2.4
1.32	30	300	50	85	$9.5 \cdot 10^{16}$	4.4
1.7	70	250	40	46	$2.8 \cdot 10^{16}$	4.7
1.7	60	250	40	56	$2.5 \cdot 10^{16}$	4.4
1.85	85	200	20	33	$1.6 \cdot 10^{16}$	10.6
1.41	40	350	50	49	$1.6 \cdot 10^{16}$	9

TABLE 6.6 Carrier concentration and mobility of various CdSTe mixed films for various deposition conditions.

CHAPTER 7

CdS_xTe_{1-x} Solar Cell - Results and Conclusions

It was indicated previously that two types of devices were to be made; one had pure CdTe as the base layer while the other used p $CdS_{0.45}Te_{0.55}$ mixed film base layer. Since the absorption edge of a graded film ought to correspond to the narrow band gap of a graded band gap layer, the band gap of several graded films deposited directly onto glass, was periodically measured over a period of one month. The fact that the position of the absorption edge did not change at all indicated that CdS_xTe_{1-x} films did not homogenise and that the grading of the film composition was stable.

7.1 CdS_xTe_{1-x} Device with CdTe Base Layer

7.1.1 Large Area Devices

Initially, an attempt was made to produce a solar cell of approximately 4 cm^2 area. The geometry of the cell was conventional with a Cu base electrode, a Cu doped p CdTe base layer, 0.5μ to 0.8 μ thick, an n CdS_xTe_{1-x} graded band gap surface layer 0.2μ to 0.5μ thick and a Zn grid electrode with 2 mm bars separated with 4 mm spacings. The deposition procedure used was as described in Chapter 5 and the deposition rates of the source materials

was deduced from results described in Chapter 6. Upon completion of the deposition of CdTe base layer the deposition was interrupted and in some cases the CdTe film was annealed in vacuum at approximately 250^{o}C for several hours in order to improve the uniformity of doping. Copper was chosen for the material for the back electrode not only to insure formation of an ohmic contact with the base layer but also in an attempt to form a p^{+} CdTe layer and thus achieve a back surface field effect. The deposition rates of Cd and In were maintained constant throughout the deposition of the graded band gap layer so that the carrier density in the surface layer might not have been constant, as was discussed in Chapter 6. Most devices thus prepared showed an ohmic current-voltage (I-V) characteristics i.e. either a p-n junction was not formed or a short circuit path between the two electrodes totally obliterated any effect due to a junction. One sample, however, prepared without the Cu back electrode but with heavily doped CdTe layer showed an exponential I-V curve. However, due to the lack of a highly conducting electrode, the series resistance of the cell was of the order of 1 KΩ so that no photocurrent could be measured The photovoltage of the device, when illuminated by the Xenon lamp, was approximately 200 mV. The spectral response of the device indicated that the cell was responsive to a wide range of photon energies as is shown

in figure 7.1. However, the behaviour of this device could not be reproduced in samples subsequently prepared, so that a more rigorous investigation was undertaken.

7.1.2 Small Area Devices

7.1.2.1 Samples with Copper Electrode

A number of samples consisting of circularly shaped n-CdS_xTe_{1-x} graded band gap films with diameters ranging from 4 mm to 1 mm deposited on top of a 4 cm^2 continuous p CdTe films were prepared. Thus, in each deposition several circular "dots" of CdS_xTe_{1-x} with variable diameter were prepared. In addition, separate cut-outs were made in the masks so that layers of p-CdTe and n-CdS_xTe_{1-x} were deposited directly onto glass, rather than onto Cu electrode or onto CdTe base layer respectively. The behaviour of the resultant devices was found to be independent of the area of each "dot" particularly if the dot diameter was less than 2 to 3 mm or of the position of the "dots" in the 4 cm^2 CdTe layer. In most cases each "dot" behaved as a diode especially when the surface contact was not evaporated but was formed by pressing a lump of metal onto the films, i.e. the I-V curve of each area was a diode characteristic typically illustrated by figure 7.2.

Firstly, it was determined that a p-n junction was formed between p CdTe and n CdS_xTe_{1-x} films. A positive voltage applied on the Cu electrode resulted in forward biasing of the diode , as displayed on a curve tracer, thus showing that no Schottkey barrier was formed either between the Cu electrode and a homogeneous p-type semiconductor or between the surface electrode and a homogeneous n-type semiconductor. The conductivity type of each semiconductor layer was then tested by a hot-point-probe method which, though not a rigorous method of characterising a semiconductor, was a good indication of the conductivity type. It was found that the CdS_xTe_{1-x} layer was n-type while the CdTe layer was p-type, thus demonstrating that a Schottkey barrier was not formed either between the Cu electrode and an n-type semiconductor or between the surface electrode and a p-type semiconductor. In addition, almost identical I-V curves were obtained regardless of whether the surface contact was Zn, In or Cd. Thus, the diode characteristic must have been due to a p-n junction between CdTe and CdS_xTe_{1-x}.

The I-V curves of most samples were found to have several similar aspects regardless of the deposition conditions and the relative thickness of the layers. Firstly, it was found that the I-V characteristics were not altered at all by illumination from a

source of light i.e. the diodes had no photoresponse. Secondly, it was found that a current, applied in a forward bias direction, in excess of some value (typically 500 μA) resulted in a linear I-V curve. However, application of a reverse bias current resulted in re-formation of the exponential character of the I-V curve, provided that this current was less than several tens of mA , in which case a permanently linear characteristic was obtained. Thirdly, it was deduced from the slope of the I-V curve that the series resistance of the devices was typically several KΩ.

The high series resistance was ascribed to two factors. It was observed that the area of the exposed Cu electrode immediately adjacent to the CdTe film was thinner than the rest of the exposed electrode, thereby leaving a strip of very thin and therefore high resistance material between the devices and the contacting area of the Cu electrode. Furthermore, the CdS_xTe_{1-x} films deposited onto CdTe tended to have much higher resistivities than the films deposited onto glass, thus contributing to the high series resistance. These two observations and the fact that, if the Cu electrode was thin, the area beneath CdTe layer did not appear metallic but was dark brown, indicated that a large amount of Cu was absorbed by the semiconductor films. This was substantiated by the measurements which showed that CdTe films

deposited onto glass had higher resistivities than those deposited onto the Cu electrode. Thus it was deduced that Cu diffuses through the structure resulting in an increased carrier concentration in the p-CdTe layer (lower resistivity) and in compensation of the n-CdS_xTe_{1-x} graded layer (higher resistivity).

The fact that linear I-V curve was formed by forward biasing and that reverse biasing re-generated exponential characteristic, as is shown in figure 7.3, indicated that by some mechanism a resistive path of several KΩ resistance was formed in parallel with the diodes. This "filament switching" behaviour is not uncommon in thin films and is probably caused by conduction via grain boundaries and pin-holes in the thin films. Production of thicker films tended to reduce but not necessarily eliminate this behaviour.

The lack of the photoresponse of the diodes was ascribed to two possible mechanisms. The life-times of the minority carriers, especially in the heavily p CdTe could have been extremely short. Since even in single crystals of CdTe the carrier lifetimes are as short as 10^{-8}s to 10^{-10}s this was probable. Furthermore, the junction between p CdTe and n CdS_xTe_{1-x} was not a homojunction but rather a heterojunction between two different semiconductors of similar, but not necessarily identical, band-gaps. Thus, a

large recombination current might have existed in the depletion layer thus further reducing any photoresponse of the diodes.

7.1.2.2 Samples without copper electrode

An attempt was made to produce similar "dot" devices without the copper electrode (which was seen as a source of at least some of the problems of the devices) by deposition of the semiconductors onto SnO_2 coated soda-lime glass substrates. Several of these devices were photosensitive, with photovoltages of the order of hundreds of mV. The window effect was also apparent in these samples and the photoresponse was larger when the device was illuminated from the CdS_xTe_{1-x} side than when it was illuminated from CdTe side. Several of these devices were prepared by reverse deposition sequence, i.e. with the n CdS_xTe_{1-x} layer deposited onto glass while p CdTe layer served as the surface layer. However, hot-point-probe measurements showed that both semiconductor layers were of the same conductivity type, indicating that a component from the substrate, probably sodium, diffused through the structure giving rise to an n-n junction. The fact that similar I-V characteristics were obtained in all samples, regardless of the deposition sequence, and that both pure (p) CdTe and (n) CdS_xTe_{1-x} gave

ohmic contact with SnO_2 coated glass, demonstrated that the diode behaviour was not due to a junction between SnO_2 and either of the two semiconductor layers. Furthermore, samples similarly prepared on high resistance ($\sim$ 500 Ω/O) SnO_2 coated Corning 7059 glass showed no photoresponse. However, these samples had very good and sharp I-V characteristics and the critical value of forward bias current required for "filament switching" was found to be increased to typically several mA's.

7.1.3 Discussion

A number of conclusions was drawn from the investigation of the (p) CdTe - (n) CdS_xTe_{1-x} diodes. It was shown that the photoresponse of these devices was very low in spite of the fact that "good" diodes were made. It was determined that the back electrode fabricated from copper acted as a source of very mobile Cu atoms which diffused through the structure lowering the carrier life-time (photoresponse was observed only in samples prepared without the Cu electrode , i.e. either in SnO_2 coated glass or on heavily doped p CdTe films) and probably encouraging some form of conduction in grain boundaries (the critical "switching" forward bias current tended to be higher in samples prepared in SnO_2 coated glass).

Thus material other than copper must be used as a back electrode for these devices. Furthermore, since an n-n type of junction could have been formed between CdTe and graded CdS_xTe_{1-x} , it was deduced that the interface between these two layers behaved more as a heterojunction than a homojunction. This discontinuity at the interface between the two layers may have been worsened by the fact that the deposition was interrupted upon completion of the base layer which could have resulted in a formation of an oxide layer.

Due to the fact that the behaviour of these devices was almost independent of the deposition conditions, it was deduced that the described diode characteristics were dominated by factors common to all devices, such as the Cu electrode , or the interface discontinuities etc.

Thus, it was deduced that a thicker device with a p CdS_xTe_{1-x} base layer deposited on top of an electrode other than copper may have much better performance . Nevertheless, it was also shown that a (p) CdTe-(n)CdS_xTe_{1-x} device may be prepared and even might be quite efficient photovoltaic converter judging from the width of the photoresponse shown in figure 7.1.

7.2 CdS_xTe_{1-x} Devices with $CdS_{0.45}Te_{0.55}$ Base Layer

Initially, several (p) $CdS_{0.45}Te_{0.55}$ - (n)CdS_xTe_{1-x} devices were made by an analagous deposition method as was used for CdTe based devices, i.e. a number of "dots" of CdS_xTe_{1-x} were deposited onto continuous 4 cm^2 film of (p) $CdS_{0.45}Te_{0.55}$. However, this configuration necessitated an interruption of the deposition in order to change the masks and thus perhaps allowed a formation of an oxide layer in the interface and the junction might not have been a homojunction. It was also found that the films showed a tendency to peel around the circumference of the dots. Nevertheless, in some cases the diode characteristics were observed. However these diodes behaved in a similar manner as the ones using pure CdTe as the base layer, particularly when an evaporated Cu or Ag back electrode was used.

Subsequently, cell devices were prepared in a single uninterrupted deposition. A smooth change from deposition of mixed film to deposition of graded film was achieved by operation of the time control on the shutter control unit. The change of the conductivity type was carried out synchronously by operation of an additional manual shutter described in Chapter 5. Since this shutter interrupted only the In and Cu vapours, the (n)CdS_xTe_{1-x} graded layer was

doped with In alone. Thus only CdS and CdTe evaporation was controlled by the pneumatic shutters and either In or Cu were continiously evaporated. A number of 4 cm^2 films were thus deposited consisting typically of approximately 7000 Å thick layer of (p) $CdS_{0.45}Te_{0.55}$ and a 3000 Å thick layer of graded CdS_xTe_{1-x}. The surface contact to these devices was usually not evaporated but the films were probed in a number of places using either an In pad or a contact of In-Hg amalgum [164].

7..2.1 Devices on metal substrates

Several (p) $CdS_{0.45}Te_{0.55}$ - (n)CdS_xTe_{1-x} devices were deposited onto Ni plated copper sheets. Since nickel is a good contacting metal for (p)CdTe [115] it was assumed that it should form a suitable contact with (p)$CdS_{0.45}Te_{0.55}$. Nickel was electroplated on polished copper sheets forming a strong bond and was subsequently washed and dryed in the usual manner.

It was found that devices deposited on these substrates behaved mostly as ohmic layers of resistances of tens of Ω's. In few cases diode characteristics were observed but these were found to deteriorate quite quickly and were not responsive to illumination although the deduced series resistance was low as is shown in figure 7.4. This behaviour was found to be

independent of the deposition parameters and relative thickness of the layers. Thus, it was assumed that this behaviour was related to the substrates themselves and that perhaps due to the microscopic roughness of the substrates a large number of pin-holes and other film faults was formed resulting in short circuit paths between the contacts. Consequently, subsequent devices were deposited onto conducting glass.

7.2.2 Devices on SnO_2 coated glass slides

Several 4 cm^2 devices were deposited onto SnO_2 coated Corning 7059 glass slides by a continuous deposition with either (p) $CdS_{0.45}Te_{0.55}$ or (n)CdS_xTe_{1-x} serving as the surface layer. Using In-Hg analgam as small area surface contacts, diode behaviour was invariably detected in all samples. Typical I-V curves are shown in figure 7.5.

7.2.2.1 Physical Properties of the Films

Since diode behaviour was detected only when the area of the In-Hg contact was small (1-2 mm diameter) it was deduced that the density of pin holes in the films must have been quite large. The fact that larger contacting area resulted in ohmic I-V curves decreased any possibility of measuring the photocurrent

which is directly related to the area of the device. Several attempts made to evaporate a grid surface contact also resulted in ohmic behaviour. In order to decrease the density of pin-holes an attempt was made to deposit a device appreciably thicker than the typical 1μM. However, this was not possible, firstly because after 10-12 minutes of deposition the movement of the pneumatic shutters was impaired by excessive heat expansion of various components on the base plate, and secondly after 10 minutes the power supplies providing 100 to 150 A more than was allowed by the rating of the transformers, were getting quite hot.

The surface texture of several samples was investigated by scanning electron microscopy. Contrary to the case when CdS_xTe_{1-x} was deposited on pure CdTe where the grain size was invariably about 1000 Å, as illustrated in figure 7.6, the grain size of graded films grain on mixed CdS_xTe_{1-x} film was found in few cases to be appreciably larger as is shown in figure 7.7. The large grain size was detected only in samples prepared on SnO_2 coated glass and never in cases where a Cu electrode was used.

7.2.2.2 Series Resistance of the Diodes

The series resistance of the (p)$CdS_{0.45}Te_{0.55}$ (n)CdS_xTe_{1-x} devices, as deduced from the I-V curves , was found to be invariably very high, of the order of 1 KΩ in spite of the fact that film resistivities were typically between 1 and 100 Ω cm. However, since this was not detected in films deposited on Ni, and since the resistance of the SnO_2 coatings themselves was of that order, this behaviour was assumed to be due to the contacts rather than the devices themselves. Due to the fact that it was not possible to find borosilicate glass coated with low resistivity transparent layers, the high series resistance could not be eliminated and thus it was not possible to measure any current photogenerated in any of these devices.

7.2.2.3 Photoresponse of the Diodes

The (p)$CdS_{0.45}Te_{0.55}$ - (n)CdS_xTe_{1-x} devices prepared on SnO_2 coated glass were found to be invariably photosensitive. The window effect was observed in all samples regardless of which of the two semiconductors served as the surface layer, and the photoresponse was larger when (n)CdS_xTe_{1-x} was illuminated as is shown in figure 7.8. Typical photovoltages, which due to the higher series resistance, effectively represented open circuit voltages, were found to be approximately 250 mV when illuminated by a Xenon lamp. The highest photoeffect was observed in the sample with the composition of the base layer corresponding to about 1.4 eV band gap and with a thin (approx 2500 Å) CdS_xTe_{1-x} layer. The spectral response of one of these devices was measured in a monochromator along with a spectral response of a commercially available Si solar cell (R.S. components). As is shown in figure 7.9 the width of the spectral response of the thin film diode is quite impressive, particularly when compared to that of Si solar cell.

An attempt was made to measure the life-times of the minority carriers in these thin film devices, by a method described in ref (165). However aggrevated by large capacitance effects, it was not possible to

obtain a reading of the value of the life-time so that it was assumed that the life-time must be less than 10^{-7}s.

7.2.2.4 The Junction

The p-n junction between mixed CdS_xTe_{1-x} and graded CdS_xTe_{1-x} layers ought to be a homojunction since the deposition was continuous and any change of the band-gap is expected to be gradual. However, since both In and Cu could be quite mobile in the lattice of CdS_xTe_{1-x}, the change of the conductivity type did not necessarily coincide with the change from mixed to graded layers. Furthermore, the junction could possibly also be quite diffused i.e. it was not necessarily an abrupt junction. An attempt to produce a more abrupt junction, assuming that cross-diffusion of In and Cu does take place was made by doping only the extremes of both layers, i.e. by depositing a device with a thin"intrinsic" layer coincident with the change from mixed to graded layer. Although these samples appeared to be stable and slightly more photosensitive the validity of this needs to be investigated further. Although the light and dark characteristic cross, as is shown in figure 7..8, which is normally indicative of a density

of recombination centres in the junction, due to the very high series resistance and thus low photocurrent, this may not be the case.

7.2.2.5 Reproducability and Stability

It was found that the diode characteristics described above could readily be reproduced in suitably prepared samples. In the case when the graded layer was deposited onto glass, the reproducability was found to be improved by deposition of a thin layer (less than 1000 Å) of pure CdS prior to the deposition of the graded layer. These samples, i.e. samples where (p) $CdS_{0.45}Te_{0.55}$ served as the surface layer were found to be more stable than the samples with opposite configuration. This was probably due to the fact that $CdS_{0.45}Te_{0.55}$ absorbed less oxygen than CdS rich end of CdS_xTe_{1-x} and was thus less affected by the atmosphere.

7.2.3 Discussion

Several conclusions and deductions were drawn from the results on the p $CdS_{0.45}Te_{0.55}$ - n CdS_xTe_{1-x} device. Firstly it was shown that it is possible to produce such a device by the method chosen. Although

a working "solar cell" was not produced , the devices made indicated that it may be possible to produce an efficient photovoltaic converter. Secondly, the width of the spectral response demonstrated not only the existance of the device but also, in agreement with findings of Bonnett [125] and with theoretical expectations, the advantage of using a combination of the window effect and the built-in-field effect.

7.3 Conclusions

Since the aim of this project was to demonstrate the possibility and indicate the method of producing a graded band-gap CdS_xTe_{1-x} solar cell, rather than to attempt to optimise the device and produce an efficient photovoltaic converter, the experimental investigation was considered completed.

It was shown that a device with a graded band-gap CdS_xTe_{1-x} surface layer and either CdTe or preferably mixed $CdS_{0.45}Te_{0.55}$ base layer, can be produced by the "shuttering method" used in this project. Although none of the produced devices generated a useful amount of power, and thus none was fully characterised as a solar cell, these devices indicated that, with further development, a thin film solar cell of possibly quite high conversion efficiency, may be produced from alloys of CdS and CdTe. Further research on the subject ought to develop a contact for both p and n types of CdS_xTe_{1-x} produce a thicker device and improve the material quality and stability of the thin film layers. The contacts developed should preferably be transparent to enable the growth of a device where CdS rich CdS_xTe_{1-x} solid solution is not exposed to the atmosphere. Development of low resistance contacts is imperative for any solar cell. Production of devices

thicker than 1μm, by use of bigger power supplies and perhaps a water cooled substrate plate, ought to result not only in a further decrease of the series resistance of the cell, but also in an improvement of the film quality. Thicker films ought to have not only far fewer pin-holes thus making possible the evaporation of large area contact, but also larger and better orientated crystallites. The material quality of the films could be further improved by better control of the deposition parameters. The use of lower deposition rates could also improve the crystallinity of the films and this could result in higher minority carrier life-times. Ability to cool the substrate immediately after the deposition of the device or the use of different dopant materials could lead to prevention of the cross-diffusion of the p and n type impurities and this could improve the control over the formation of the p-n junction.

Nevertheless , in general, CdS and CdTe and most of the II-VI semiconductors, are attractive materials for photovoltaic applications for economic reasons, i.e. these materials , although not as abundant as silicon, can be used to produce large area devices by inexpensive processes such as vacuum evaporation, chemical plating, spraying etc. However these materials , being direct semiconductors, normally

form devices with a narrow spectral response and thus with relatively low conversion efficiences. The demonstration of a possible method of overcoming this and improving the spectral response of CdS-CdTe device to the level where it is higher than that of a Si device, is seen as the most significant finding of this project. Furthermore, in principle, the method used to produce a graded band gap device, could be extended to the production of different II-VI devices for different applications; for example by choice of the value of the band-gap a photodetector with spectral response similar to that of a human eye could be produced.

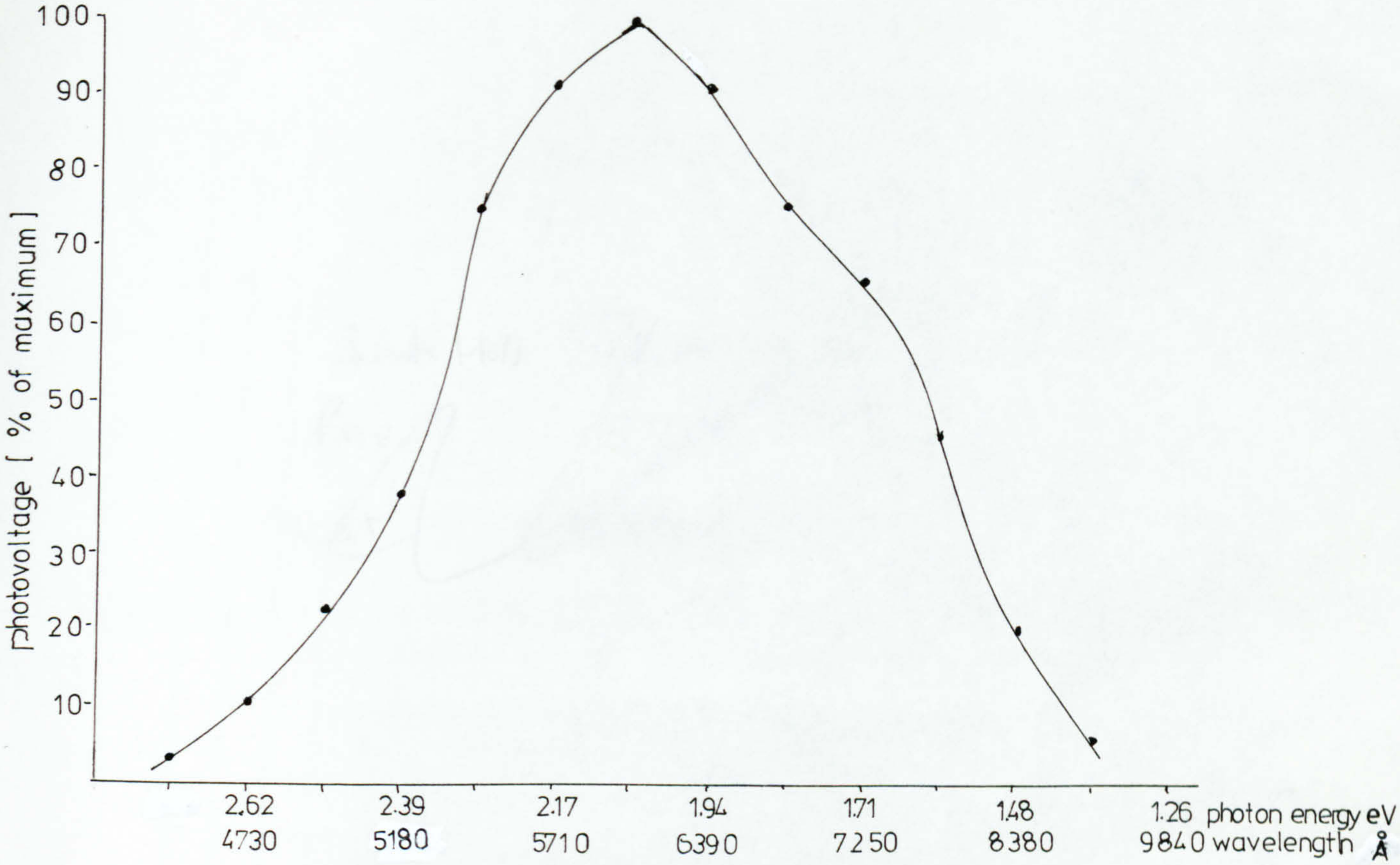

FIGURE 7.1 photoresponse of a device with CdTe base layer

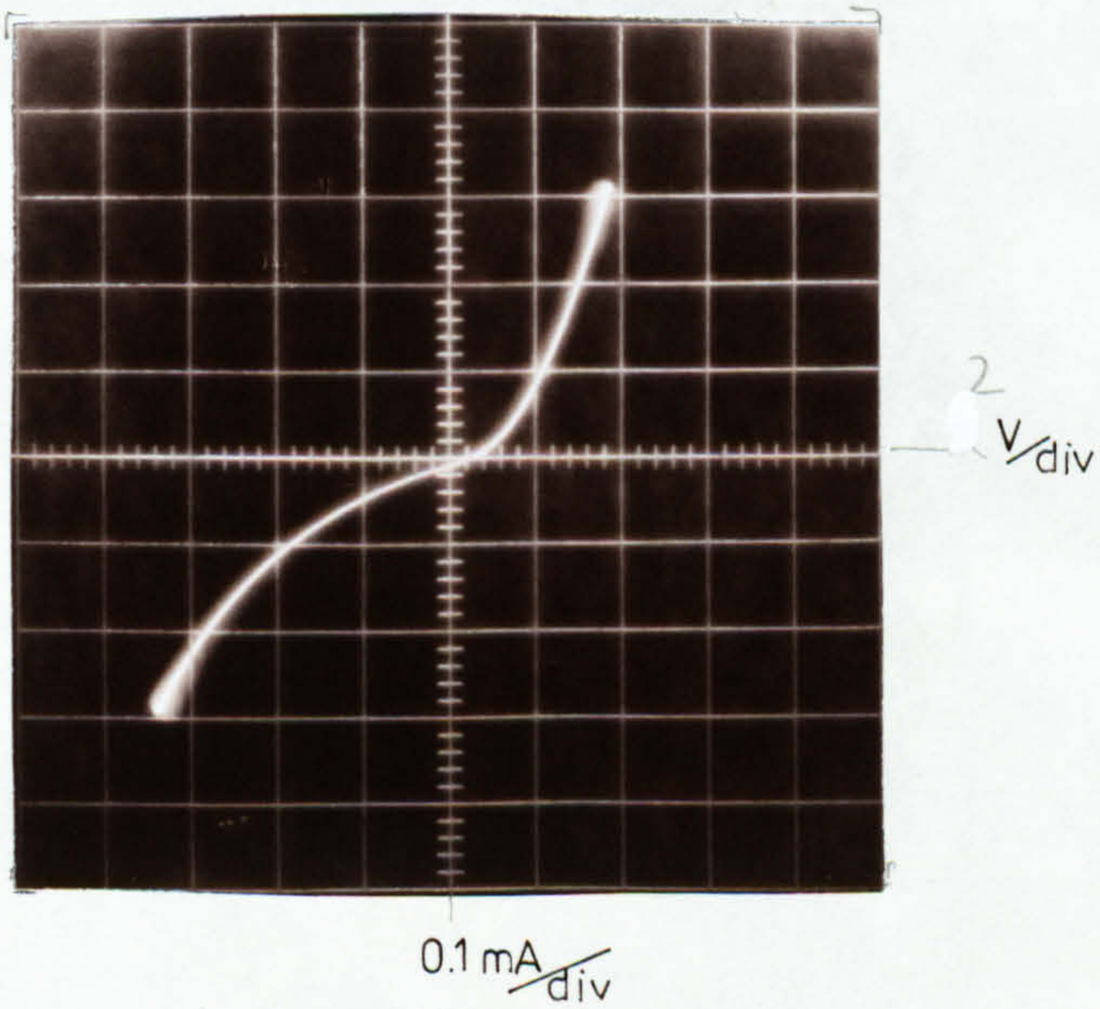

EIGURE 7 2 typical I-V characteristic of a $CdTe—CdS_xTe_{1-x}$ device

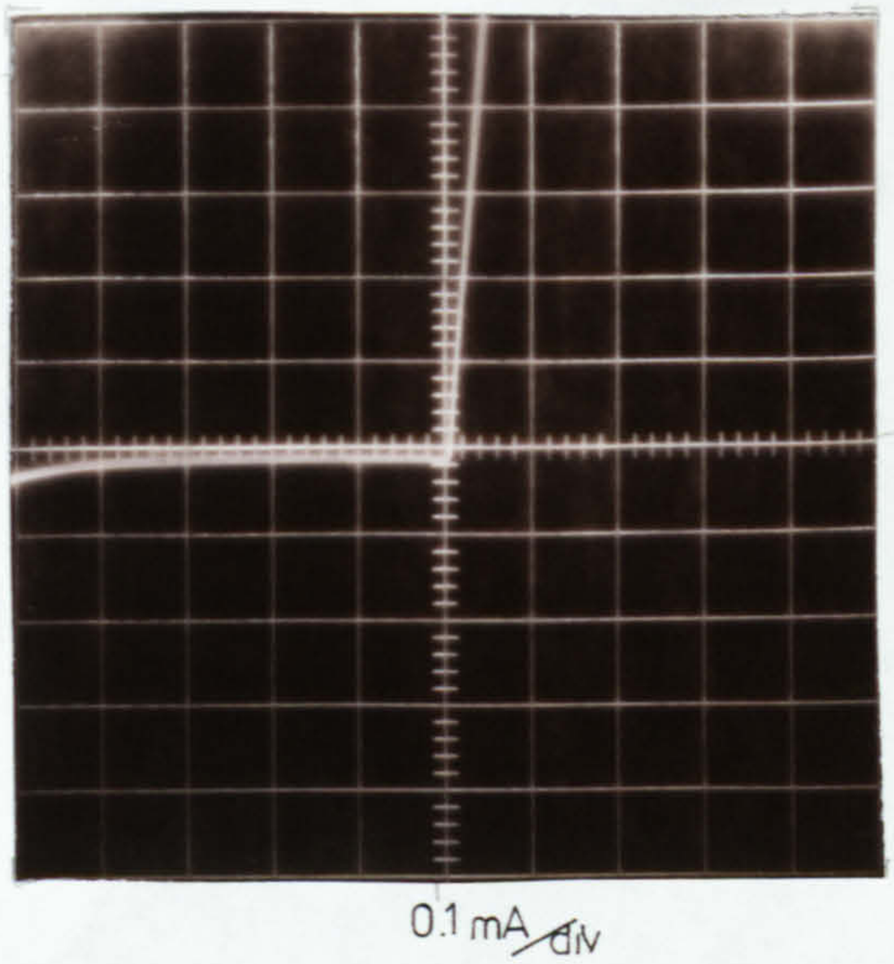

FIGURE 7.3 forward bias breakdown in CdTe base device

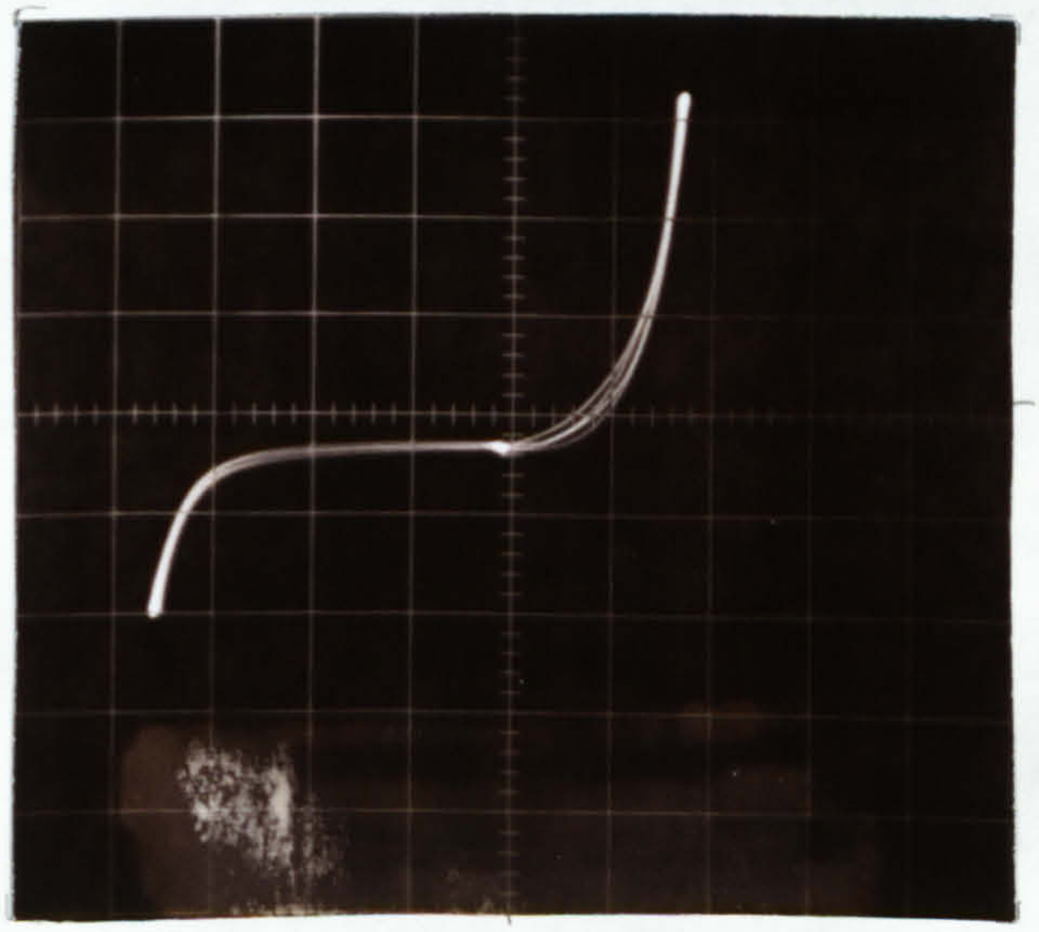

FIGURE 7.4 typical I–V characteristic of a $CdS_{0.45}Te_{0.55}$–CdS_xTe_{1-x} device deposited on Ni plated Cu sheet

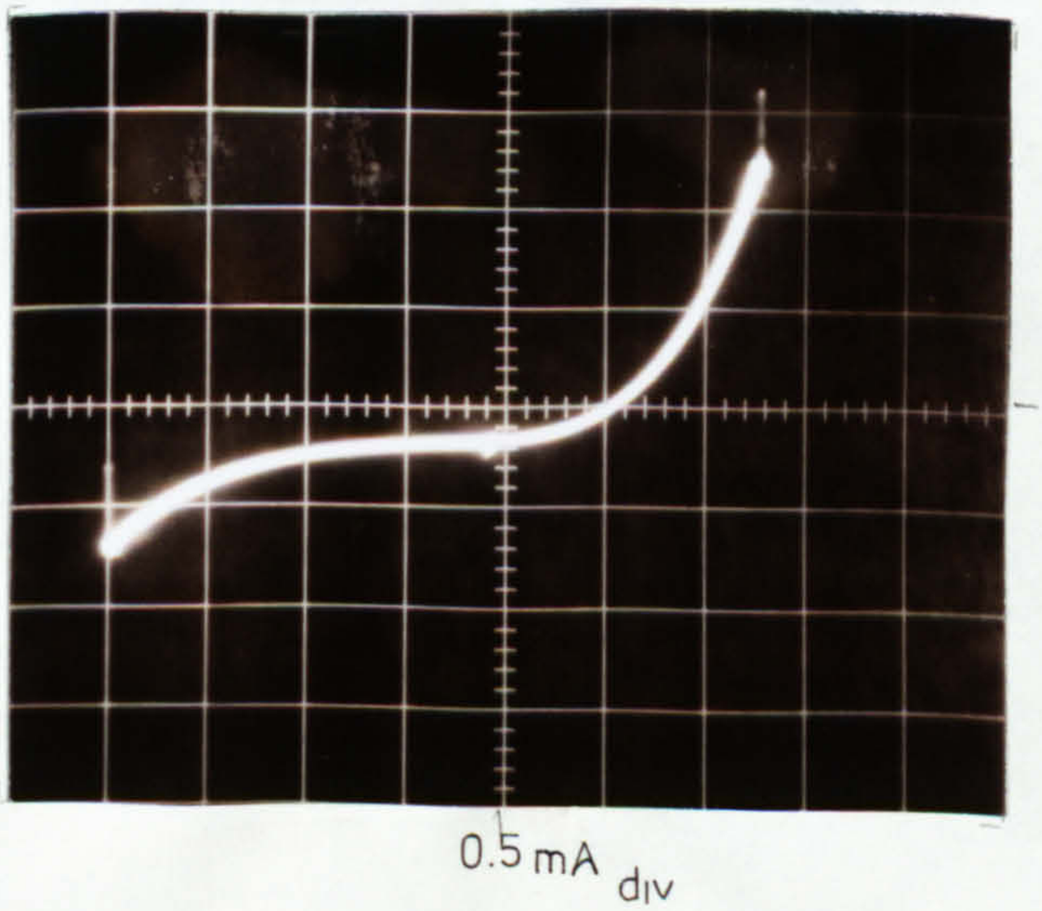

FIGURE 7.5 typical I-V characteristic of a $CdS_{0.45}Te_{0.55}$–CdS_xTe_{1-x} device deposited on SnO_2 coated glass

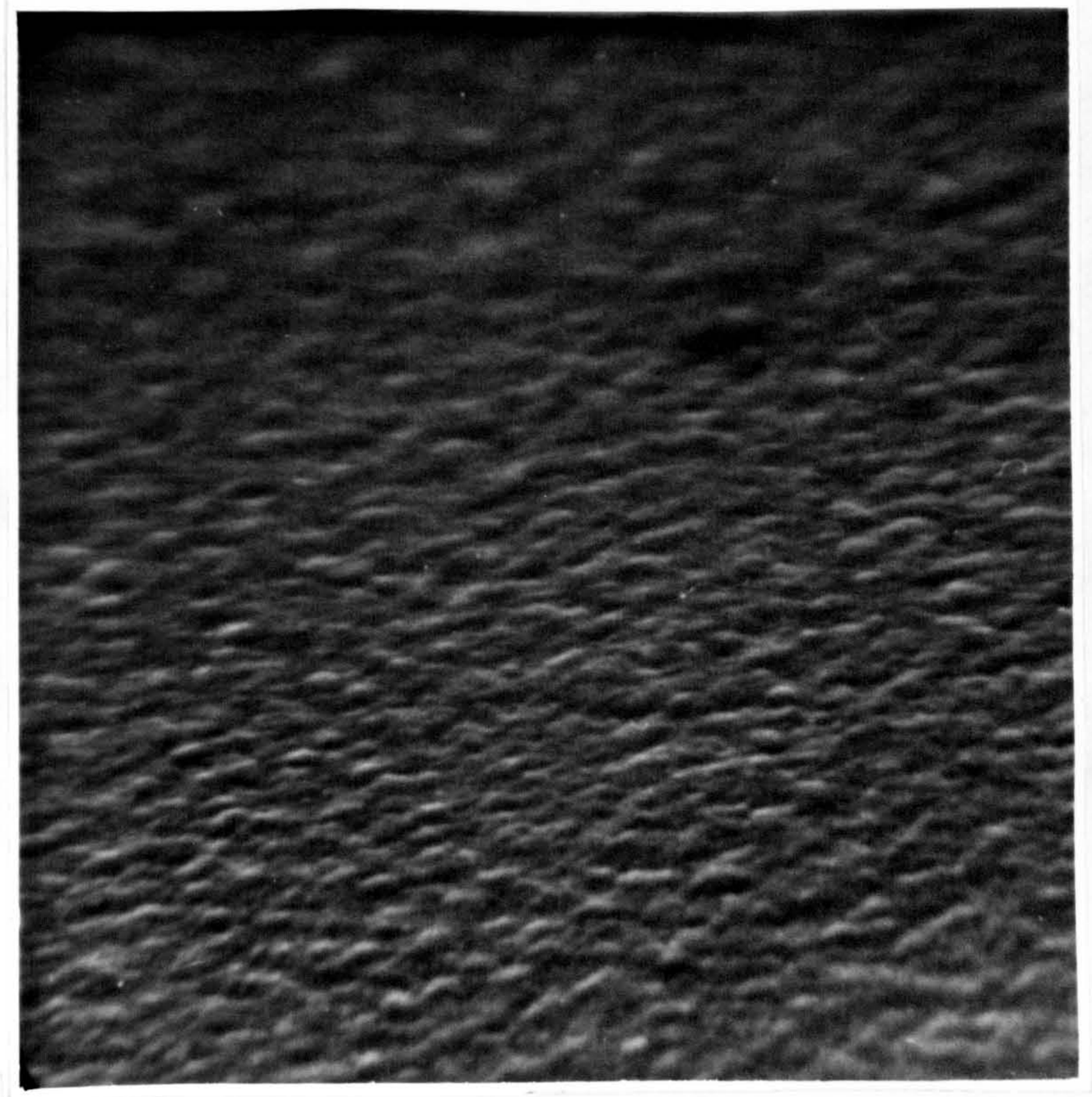

FIGURE 7.6 SEM micrograph of a device with CdTe base layer [typical] magnification 25000 ×

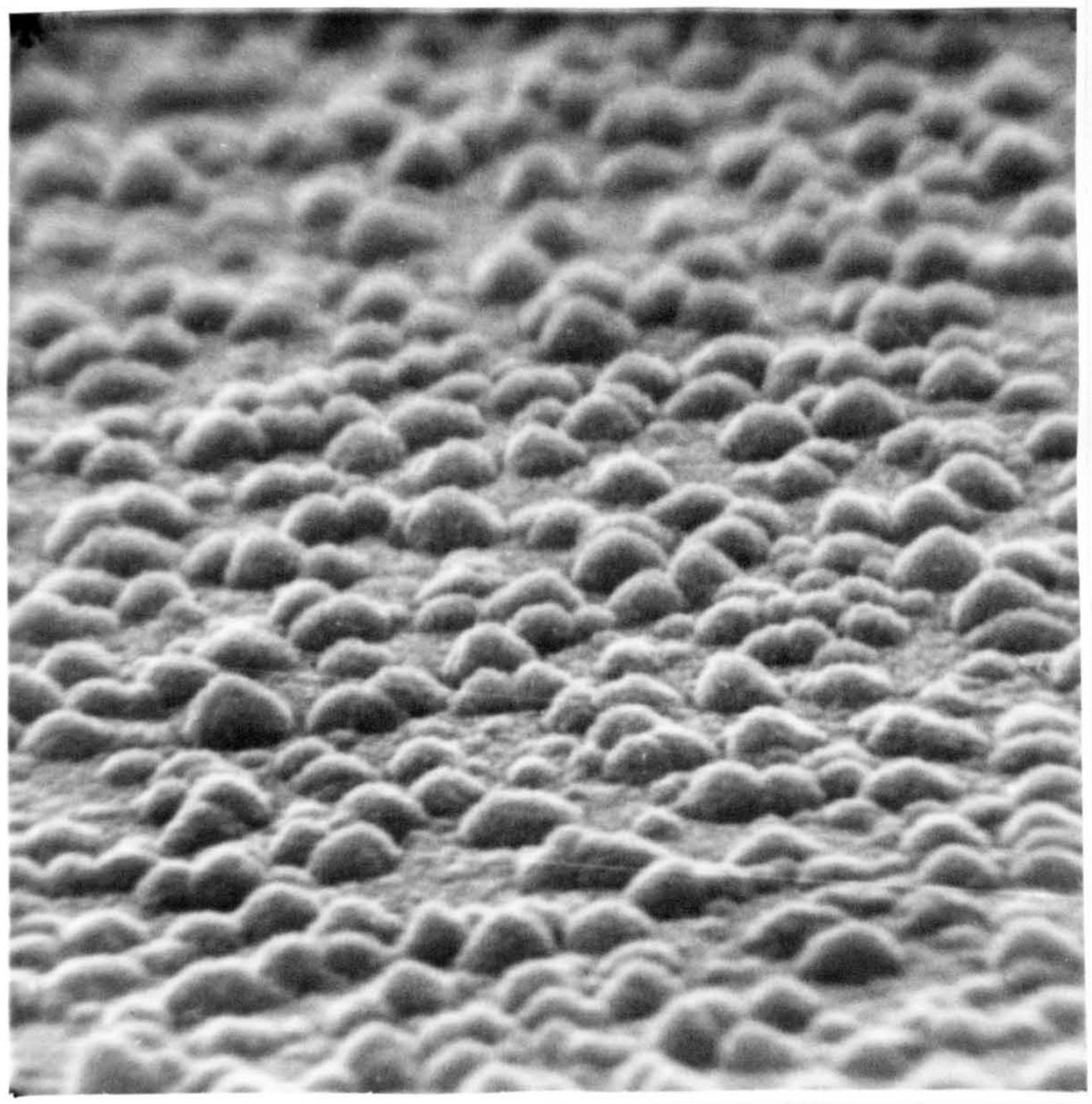

FIGURE 7.7 SEM micrograph of a device with $CdS_{0.45}Te_{.55}$ base layer magnification 25 000.×

TEXT BOUND INTO

THE SPINE

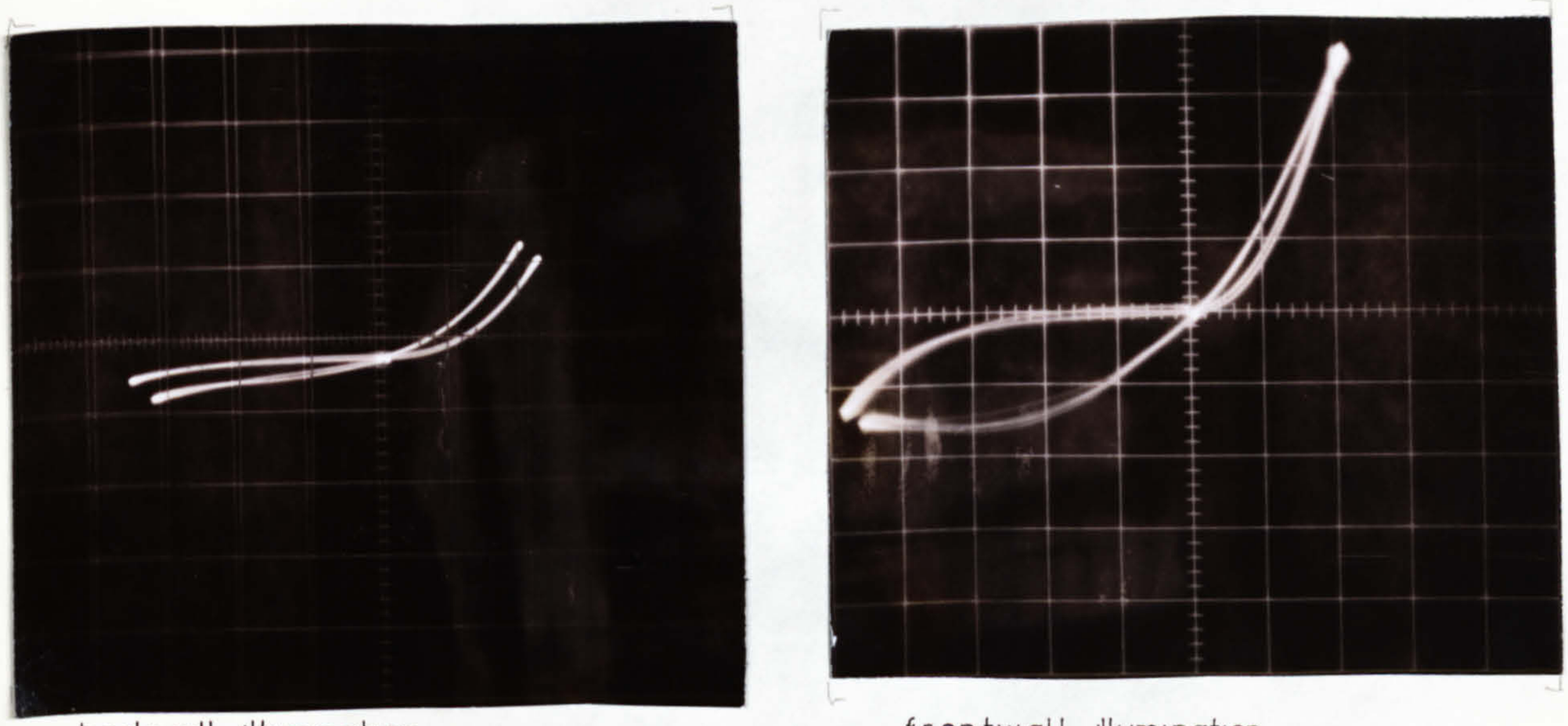

backwall illumination

frontwall illumination

FIGURE 7,8 light and dark I-V characteristics [1V/dv, 01mA/dv] of a device when illuminated from the p-$CdS_{.45}Te_{.55}$ side[a] and from n-CdS_xTe_{1-x} side[b]

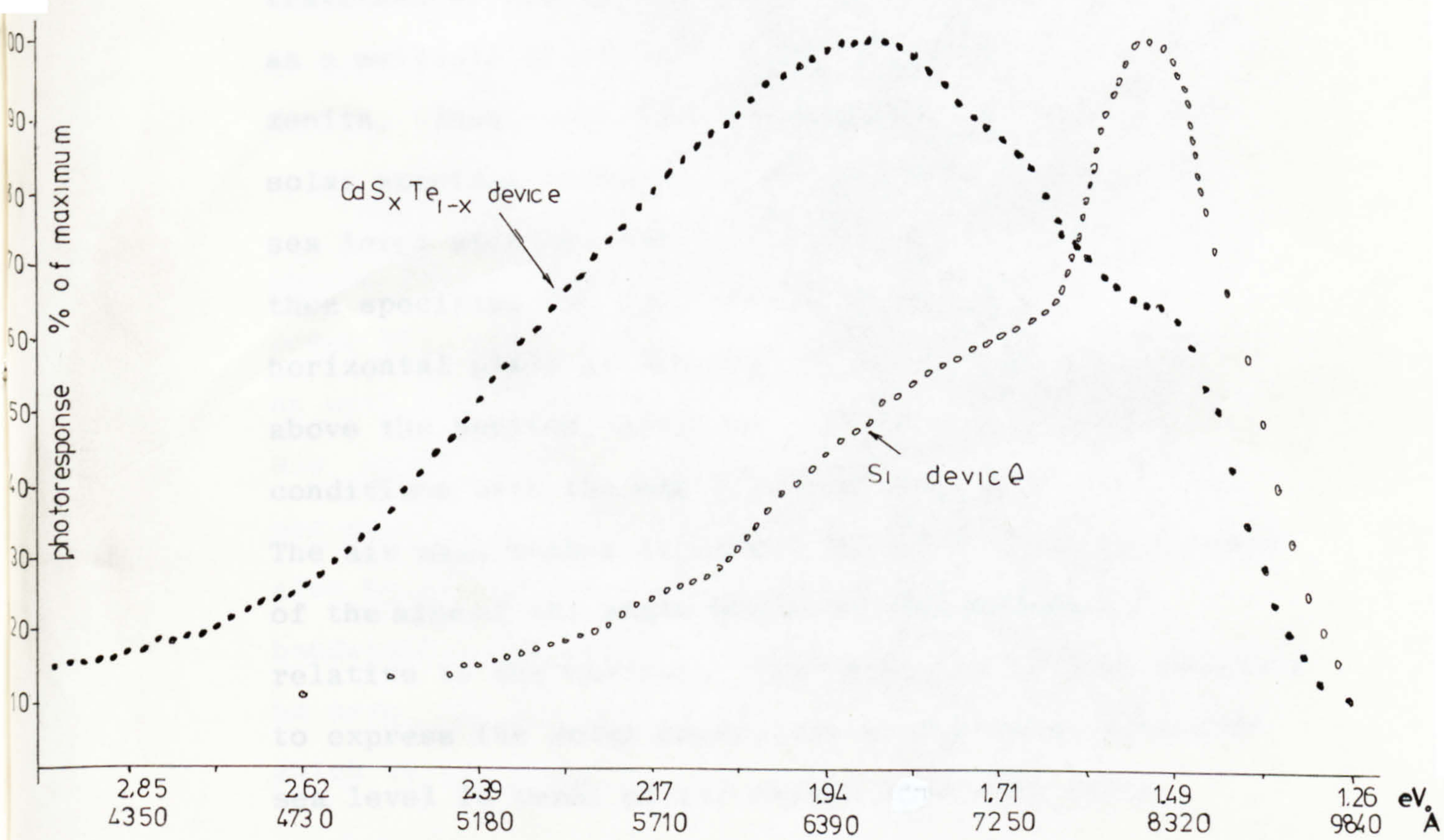

FIGURE 7.9 spectral photoresponse of the CdS_xTe_{1-x} graded band gap device as compared to that of a Si device

Appendix I

Definition of the "Air Mass" Terminology

Since the atmosphere has a marked effect on the solar spectrum the shape of the spectral curve and the value of the solar intensity depend on the length of the path that the light travels through the atmosphere. This length is expressed in terms of "air mass". Thus, air mass zero,abbreviated as AMO specifies the conditions outside the atmosphere. The length of the path through the earths atmosphere traversed by the direct solar radiation is expressed as a multiple of the path length with the sun at the zenith. Thus, air mass one (AM 1) is defined as the solar spectrum incident on a horizontal plane at the sea level with the sun at the zenith. Air mass (AM 2) then specifies the spectral power incident on a horizontal plane at the sea level with the sun 30^{o} above the horizon, air mass 3(AM 3) specifies the conditions with the sun around 20^{o} above horizon etc. The air mass number is simply obtained from the inverse of the sine of the angle which the sun subtends relative to the horizon. Similarly, it is also possible to express the solar conditions at altitudes above the sea level in terms of air masses less than unity.

Appendix II

Transformation of the Solar Curves

As is stated in Chapter 4, the transformation of the solar spectral curve expressed in terms of irradiance (P) in $Wm^{-2}\mu m^{-1}$ versus the wavelength (λ) in μm into a curve expressed in terms of photon flux density (ϕ)in $m^{-2}s^{-1}eV^{-1}$ and photon energy (E) in eV can be carried out by use of two equations. The transformation of the wavelength of the light (λ) onto the photon energy (E) is simply done via the Plank's equation:

$$E = \frac{hc}{\lambda} \quad J = \frac{hc}{q\lambda} \quad eV$$

Transformation of the power irradiance into photon flux density is more complex. By definition, power (P) in $Wm^{-2}\mu m^{-1}$ is the rate of energy arrival on unit area per unit time, i.e. is energy in $Jm^{-2}s^{-1}\mu m^{-1}$. Now, power irradiance is expressed in terms of power per unit bandwidth so that the bandwidth in μm must also be transformed into a bandwidth in eV. The bandwidth , of course, must be finite or the power would be zero, but if the bandwidth is assumed to be small, which it is, then:

$$\frac{\Delta\lambda}{\Delta E} \qquad \frac{d\lambda}{dE} = \frac{hc}{qE^2}$$

where $\Delta\lambda$ is the wavelength bandwidth in μm

ΔE is the energy bandwidth in eV

Thus, power (P) averaged over a small wavelength bandwidth $\Delta\lambda$ may be transformed into energy (T) averaged over a small energy bandwidth ΔE via:

$$T \quad Js^{-1}m^{-2}eV^{-1} = P \quad Wm^{-2}\mu m^{-1} \quad \frac{hc}{qE^2}$$

where T is the total energy carried by all the photons of energy E. Thus, in order to determine the number of photons with energy E, in a bandwidth dE, the total energy present in the bandwidth has to be divided by the energy of the individual photons, i.e.

$$\phi \quad m^{-2}s^{-1}eV^{-1} = \frac{T}{E} = P \quad Wm^{-2}\mu m^{-1} \quad \frac{hc}{qE^2} \quad \frac{1}{qE}$$

which is relation used in Chapter 4.

The division of this curve expressed in terms of photon flux versus photon energy, into 100 monoenergetic beams,was done by simple linear extrapolation. The energy range between 0.4 eV and 4 eV was divided into 100 regions. The total number of photons in each of these regions was found by linear extrapolation between existing points.

In order to test the validity of the transformations, the total energy carried by the 100 photon beams was calculated and compared with the solar constant (1.35 $^{KW}/m^2$). The energy region between 0.4 eV and 4 eV contains 96.83% of the solar constant, and the 100 beams contained 96.16% of the solar constant. Thus, the transformations seems correct and only a slight loss of accuracy is suffered.

APPENDIX III

A) PROGRAM 'SOL' CALCULATING THE PHOTOCURRENT IN A GRADED BAND GAP SOLAR CELL

```
      DIMENSION PHNO (101)
      READ (1,990)EGO,EGW,PERM
      READ(1,991)CN,VN,DN,AN,W,T
      READ(1,992)ALPHA
5     READ(1,993)DIFFN,DIFFP,DLN,DLP
      READ(1,994)TRW
      TOTNO=0.00E00
      TOTENR=0.00E00
10    STEP=0.0360
      ENERGY=4.00
      Q=1.601E-19
      DO 20 I=1,100
      READ(1,993)PHNO(I)
15    TOTNO=TOTNO+PHNO(I)
      TOTENR=TOTENR+PHNO(I)*ENERGY
      ENERGY=ENERGY-STEP
20    CONTINUE
      TOTENR=TOTENR*Q
      PRCTEN=TOTENR*100.00/1.381E3
      WRITE(2,810)TOTNO,TOTENR
      WRITE(2,815)PRCTEN
      EFN=0.0250*ALOG(CN/DN)
      EFP=0.0250*ALOG(VN/AN)
25    V=0.50
      VBI=EGW-(EFN+EFP)-V
      DLW=SQRT((PERM*8.854E-12*VBI)*(AN+DN)/(Q*AN*DN))
      DLWN=AN*DLW/(AN+DN)
      DLWP=DN*DLW/(AN+DN)
30    WRITE(2,800)EFN,EFP,VBI
      WRITE(2,805)DLW,DLWN,DLWP
      FIELD=(EGO-EGW)/W
      BETA=Q/(300.00*1.381E-23)
      SDLP=1.00/(DLP*DLP)
40    WN=W-DLWN
      WP=W+DLWP
      EGDL=EGO-FIELD*WN
      ROOT=SQRT((BETA*FIELD/2.00)**2+SDLP)
      DL1=BETA*FIELD/2.00+ROOT
45    DL2=BETA*FIELD/2.00-ROOT
      SRV=TRW/DIFFP+BETA*FIELD
      C1-SRV-DL2
      C2=DL1-SRV
      C3=EXP(DL2*WN)
      C4=EXP(-ALPHA*WN)
      C5=EXP(-DL*WN)
```

```
50      E1=EXP(DL1*WN)
        CONST1=ALPHA/(DIFFP*(ALPHA*ALPHA*BETA*FIELD-SDLP))
55      PHNOTO=0.00E00
        YPT=0.00E00
        EDLPT=0.00E00
        YDLNA=0.00E00
        YDLNB=0.00E00
        ENERGY=4.00
        DO 100 I=1,100
60      IF(ENERGY.LT.EGO)GOTO 101
        PHNOTO=PHNOTO+PHND(I)
        ENERGY=ENERGY-STEP
100     CONTINUE
101     C9=C2*C3*C5/(C1+C2)
        C11=C2/(C1+C2)
        C15=C11*C1/C2-C9*C1/C2+C4*C5
        C16=C9*C1/C2-C11*C1/C2-C3*C5
        C1=PHNOTO*CONST1
        B1=F1*(DL*C15-DL2*(C9-C11)+ALPHA)/(DL1*C16-DL2*
           (1.0+C9-C11)
        A1=-B1*C3*C5-F1*C4*C5
        YHOLE1=-Q*DIFFP*(DL*A1*E1+DL2*B1*C3-ALPHA*F1*C4)
110     YDLN1=Q*PHNOTO*(EXP(-ALPHA*WN)-EXP(-ALPHA*W)
        YDLP1=Q*PHNOTO*(EXP(-ALPHA*W)-EXP(-ALPHA*WP)
        PHNOTO1=PHNOTO*EXP(-ALPHA*WP)
200     DO 300 J = I, 100
        IF(ENERGY.LT.EGW)GOTO301
        XN=(EGO-ENERGY)/(FIELD)
        C6=EXP(DL1*XN)
        C7=EXP(DL2*XN)
205     C8=EXP(-ALPHA*XN)
        CINT=C1*C6+C2*C7
        C9=C2*C3*C5*C6/CINT
        C10=C2*C4*C5*C6/CINT
        C11=C2*C7/CINT
210     C12=C2*C8/CINT
        C13=DL1*C6
        C14=DL2*C7
        C15=C12*C1/C2-C10*C1/C2+C4*C5
        C16=C9*C1/C2-C11*C1/C2-C3*C5
215     C100=EXP(ALPHA*XN)
        C200=C100*PHNO(J)
        F=CONST1*C200
        B=F*(C13*C15-C14*(C10-C12)+ALPHA*C8)/C13*C16-C14*
          (1.0+C9-C11))
        A=-B*C3*C5-F*C4*C5
        YP=DL1*A*E1*DL2*B*C3-ALPHA*F*C4
        YPT=YPT+YP
        YDLPT=YDLPT+C200
        IF(ENERGY.GT.EGDL)GOTO 223
        YDLNB=(PHNO(J)-C200*EXP(-ALPHA*W))+YDLNB
        GOTO 225
223     YDLNA=YDLNA+C200
225     ENERGY=ENERGY-STEP
300     CONTINUE
```

```
301     WRITE(2,820)I,J
        YHOLE2=-YPT*Q*DIFFP
        YDLN2=YDLNA*Q*(EXP(-ALPHA*WN)-EXP(-ALPHA*W)
        YDLP2=YDLPT*Q*(EXP(-ALPHA*W)-EXP(-ALPHA*WP)
305     YDLN3=Q*YDLNB
        PHNOT2=YDLPT*EXP(-ALPHA*WP)
        TPHNO=PHNOT1+PHNOT2
        F3=-ALPHA*TPHNO/(DIFFN*(ALPHA*ALPHA-1.O(DLN*DLN)))
        B3=F3*(EXP(-ALPHA*T)-EXP(T/DLN))/(EXP(T/DLN)-
           EXP(-T/DLN))
        A3=-B3-F3
310     YELECT=Q*DIFFN*(A3/DLN-B3/DLN-F3*ALPHA)
400     Y P=YHOLE1+YHOLE2
        Y DLN=YDLN1+YDLN2+YDLN3
        Y DLP=YDLP1+YDLP2
        CURRNT=Y P+Y DLN+Y DLP+YELECT
        EFF I=CURRNT*1OO.OO/(TOTNO*Q)
405     EFF P=EFF I*V
        WRITE(2,825)Y P,YHOLE1,YHOLE2
        WRITE(2,83O)Y DLN,YDLN1,YDLN2,YDLN3
        WRITE(2,835)Y DLP,YDLP1,YDLP2
        WRITE(2,84O)YELECT
        WRITE(2,845)CURRNT
410     WRITE(2,85O)EFF I,EFF P
990     FORMAT(F12.3)
991     FORMAT(E15.4)
992     FORMAT(E12.3)
993     FORMAT(E14.3)
994     FORMAT(E15.3)
800     FORMAT(1X,6H EFN= ,F5.3/7H EFP= ,F5.3/7H VBI= , F5.3)
805     FORMAT(1X,6H DLW= ,E12.4/8H DLWN= ,E12.4/8H
                          DLWP= ,E12.4)
810     FORMAT(1X,15H TOTAL NUMBER= ,E12.4/16H TOTAL
                                    ENERGY= ,E12.4)
815     FORMAT(1X,3OH PERCENTAGE OF SOLAR CONSTANT= E12.4)
820     FORMAT(1X,4H I= ,14,1OH   J= ,14)
825     FORMAT(1X,1OH J(HOLE)=E12.4,E15.4,E15.4)
830     FORMAT(1X,1OH J(DLN)=E12.4,E15.4,E15.4,E15.4)
835     FORMAT(1X,1OH J(DLP) = ,E12.4,E15.4,E15.4)
840     FORMAT(1X,11H J(ELECT)= ,E12.4)
845     FORMAT(1X,16H TOTAL CURRENT= ,E12.4)
850     FORMAT(1X,9H EFF(I)= ,E12.3/1OH EFF(P)= ,E12.3)
        STOP
        END
```

(B) PROGRAM 'DELTA' CALCULATING THE DISTRIBUTION OF PHOTOGENERATED CARRIERS IN A GRADED BAND GAP LAYER

```
      DIMENSION PHNO(101),DELTA(51),SLOPE(51),TELTA(51)
      DO 500 I=1,100
      READ (1,999) PHNO(I)
500   CONTINUE
      WRITE(2,643)
      EGO=2.42
      EGW=1.47
      W=5.00E-7
      FIELD=-(EGO-EGW)/W
      BETA=1.601E-19/(300.00*1.381E-23)
      DLP=0.10E-6
      SDLP=1.00/(DLP*DLP)
      DIFFP=5.00E-4
      SRV=1.00E1/DIFFP+BETA*FIELD
      ROOT=SQRT((BETA*FIELD/2.00)**2+SDLP)
      DL1=BETA*FIELD/2.00+ROOT
      DL2=BETA*FIELD/2.00-ROOT
      ALPHA=1.00E7
      CONST4=(ALPHA*ALPHA+BETA*FIELD*ALPHA-SDLP)*DIFFP
      C1=SRV-DL2
      C2=DL1-SRV
      C3=EXP(DL2*W)
      C4=EXP(-ALPHA*W)
      C5=EXP(-DL1*W)
      ENERGY=4.00
      STEP=0.0360
      PHNOT=0.00
      DO 70 L=1,51
      TELTA(L)=0.00E00
70    CONTINUE
      DO 100 I=1,100
      IF (ENERGY .GT. EGO)GOTO 40
      IF(ENERGY.LT.EGW)GOTO 200)
      XN=(EGO-ENERGY)/(-FIELD)
      C6=EXP(DL1*XN)
      C7=EXP(DL2*XN)
      C8=EXP9-ALPHA*XN)
      C9=C2*C3*C5*C6/(C1*C6+C2*C7)
      C10B=C2*C5*C6/(C1*C6+C2*C7)
      C10=C10B*C4
      C11=C2*C7/(C1*C6+C2*C7)
      C12B=C2/(C1*C6+C2*C7)
      C12=C1B*C8
      C13=DL*C6
      C14=DL2*C7
      C15=C12*(C1/C2)-C10*C1/C2+C5*C4
      C15B=C12b*C1/C2-C10B*C1/C2+C5
      C16=C9*C1/C2-C11*C1/C2-C3*C5
      GOTO 60
40    PHNOT=PHNO(I)+PHNOT
      ENERGY=ENERGY-STEP
      FENERG=ENERGY
      GOTO 100
```

```
60      X=0.000
        DO 50 J=1,51
        IF(X.GT.XN) GOTO 80
        ALFA=0.00E00
        E=(-ALPHA*PHNO(I)*EXP(ALPHA*XN))/CONST4
        D=E*(C13*C15-C14*(C10-C12)+ALPHA*C8)/
          C13*C16-C14*(1.0+C9-C11))
        B=D*(C11-C9)+E*(C12-C10)
        A=(B*C1)/C2
        C=0.00E00
        GOTO 90
80      ALFA=ALPHA
        E=ALFA*PHNO(I)*EXP(ALFA*XN)/CONST4
        B=E*(C13*C15-C14*(C10-C12)+ALFA*C8)/(C13*C16-C14*
          (1.0+C9-C11))
        A=-D*C3*C5-E*C4*C5
        C=E
90      E1=EXP(DL*X)
        E2=EXP(DL2*X)
        E3=EXP9-ALPHA*X)
        DELTA(J)=(A*E1+B*E2+C*E3)
        SLOPE(J)=(A*DL1*E1+B*DL2*E2-C*ALPHA*E3)
        WRITE(2,901)DELTA(J),SLOPE(J),X
901     FORMAT(1X,E12.5,E18.5,E16.3)
904     FORMAT(1X,5H XN= ,E15.5)
905     FORMAT(1X,9H ENERGY= ,F7.4)
        TELTA(J)=TELTA(J)+DELTA(J)
        X=X+W/50.0
50      CONTINUE
        WRITE(2,904)XN
        WRITE(2,905)ENERGY
        WRITE(2,888)A,B,E
        ENERGY=ENERGY-STEP
100     CONTINUE
200     XN=0.00E00
        C17=SRV+ALPHA
        C18=EXP(DL1*W)
        F1=-ALPHA*PHNOT/CONST4
        B1=-F1*(C4+C18*C17/C2)/(C3+C18*C1/C2)
        A1=B1*C1/C2+F1*C17/C2
        X=0.00
        DO 600 K=1,11
        E1=EXP(DL1*X)
        E2=EXP(DL2*X)
        E3=EXP(-ALPHA*X)
        DELTA(K)=(A1*E1+B1*E2+F1*E3)
        SLOPE(K)=(A1*D11*E1+B1*D12*E2-F1*ALPHA*E3)
        WRITE(2,901)DELTA(K),SLOPE(K),X
        TELTA(K)=TELTA(K)+DELTA(K)
        X=X+W/50.00
```

```
600     CONTINUE
        WRITE(2,904)XN
        WRITE(2,906)FENERG
        WRITE(2,888)A1,B1,F1
906     FORMAT(1X,9H FENERG= ,F7.4)
902     FORMAT(1X,E15.3)
999     FORMAT(E15.5)
888     FORMAT(1X,4H A= ,E12.3,7H  B=,E12.3,7H  C=E12.3)
643     FORMAT(1X,7H DELTA ,18H      SLOPE , 14H      x)
        WRITE (2,644)
644     FORMAT(1X,7H TELTA)
        DO 680 M=1,51
        WRITE(2,910)TELTA(M)
680     CONTINUE
910     FORMAT91X,E12.5)
        STOP
        END
```

Appendix IV

Substrate Cleaning

The substrates were cleaned in a specially designed glass flask equipped with a holder for size 3" x 1" substrates. Firstly, the flask was filled with a 15% solution of Decon 75 detergent and de-ionised water, and immersed in an ultrasonic bath for 15 to 20 minutes. Secondly, after rinsing in de-ionised water, the flask was re-immersed in an ultrasonic bath and connected to a recirculating water de-ioniser which pumped water through the flask. An automatic timer alternately switched on the ultrasonic bath and the de-ioniser for 6 minute periods. After about 2 hours of such cyclic cleaning, the substrates in the flask were dryed in a stream of warm, dry nitrogen gas from a liquid nitrogen boiler. Prior to any evaporation, the substrates were also outgassed in vacuum for about 12 hours at 250^{o}C.

Substrates other than the glass slides, i.e. the copper and the nickel-plated copper plates, were cleaned in a similar fashion after having been polished with liquid abrasive solution (Brasso).

Appendix V

Production of Masks

The production of masks was a multi-step process which will be described below:

a) Production of master patterns

The patterns which were to be transferred in the masks were first produced at ten times the desired size on Stabiline "cut-n-strip" material, which consisted of a transparent polyester sheets with a thin opaque coating on one side. After scribing the desired pattern of cutting through the combined coating with a blade controlled by a manual coordinatograph (Apollo Scribemaster), islands of the opaque film were peeled off, An x-y axis for alignment purposes was similarly scribed in the plastic sheets.

b) Reduction of the Pattern

The master pattern was reproduced on photographic plate in a 10:1 reduction camera. The x-y axis on the master pattern were aligned with similar axis scribed in the transluscent glass which served as the object plane. A set of 20 fluorescent tubes were mounted below the object plane so that the transluscent glass also served as a light diffuser. The focussing lens (8.5 mm H.R. ANASTINGMAT) and the image plane were held a fixed

distance above the object plane. The photographic plate (AGFA MILIMASK PLATES) was positioned on the image plane by a set of 3 ball stops. After an exposure of 40 seconds, the photographic plates were developed (AGFA G282C), fixed, rinsed and dryed.

c) Preparation of the Mask Material

The masks were made in sheets of Berillium Copper 0.003"(75μ) thick spot welded onto 2" x 2" stainless steel frames. The metal sheets were cleaned by light scrubbing with Shipley Scrub Cleaner 70^{D} and soaking in 8% HCl solution. After rinsing in de-ionised water the metal sheets were dryed by dipping in acetone and blow drying in a stream of warm air.

d) Formation of the Photoresist Layer

The photoresist used for producing of most of the masks was Kodak KPR3 photoresist. A layer of photoresist was formed on top of the Berilliam copper sheet by spin coating process. The spinning of the mask and a layer of liquid photoresist (poured on top of it), at 3000 rpm for a minute in a Headway EC101 spinner resulted in thin, uniform photoresist coating. The coating was dryed in air flow for 15 minutes and hardened by baking at $80^{o}C$ for about 10 minutes.

e) Exposure of Photoresist

The photoresist coating on the mask was exposed through the photographic plate containing the desired pattern, using a high pressure mercury vapour lamp (Repro-125W). The mask was placed on top of the photographic plate and was positioned relative to it by the same 3 ball stop assembly used in the reduction camera. The distance between the lamp and the mask was fixed at 50 cm and the exposure time was 40 second (after the lamp was warmed up for at least 2 minutes). Subsequent to the exposure, the photoresist was developed in KOR developer and the unexposed resist was washed off by spraying with trichloroethylene for 30 seconds. A further bake at 100-120^{o}C for 10 minutes hardened the exposed resist resulting in a sheet of Berillium Copper coated with resist everywhere except for the islands of the desired shape

f) Etching Process

The final step in the production of the masks was to etch away the areas of Berillium Copper not protected by the photoresist. This was done in a hot (60^{o}C) 50% solution of CR20. Continuous, vigorous agitation was found necessary to produce well defined edges in the masks. The back of the mask and other areas not protected by the resist were painted with cellulose paint which was resistant to the etching solution. Upon the completion of the etching process, the paint

was removed in acetone and the resist was stripped off with Shipley Chemicals Penstrip solution.

The masks produced by the above described process were found satisfactory. The edges of the cut out on the masks were well defined and sharp. With sufficient care and experience it was possible to produce a series of slit cut outs as narrow as few tens of microns for masks used in the deposition of the grid electrodes for solar cells.

Appendix VI

Quartz Crystal Monitors

Unlike the modern, commercial units which operate as digital counters, the monitors used were of the analogue type. The signal, from the oscillator whose frequency was controlled by the crystal in vacuum, was compared with the signal from a standard tunable oscillator (Bendix Radio-frequency meter). The beat frequency , i.e. the frequency representing the difference of the two input signals, controlled the D.C. output stage so that the value of the output voltage signal was directly proportional to the beat frequency. The beat frequency signal was also input into a small speaker so that there was an audio output. Since the standard oscillators were tunable, it was possible to retune the beat frequency to any value after every deposition, so that the quartz crystals could be used several times. However, according to the theory, If the quartz crystals are heavily loaded and the resulting resonant frequency change is greater than about 20 KHz then the linear mass to frequency relationship is lost. Therefore fresh quartz crystals were used in every pumping cycle.

The electronic circuit used in the monitors were largely the same as those described in ref A1, with

the exception of the design of the oscillators whose frequency was controlled by the quartz crystals in vacuum. The design of these oscillators was similar to that described by W.H. Lawson (ref A2). The advantage of this design was that the quartz crystals were electrically earthed and this was found to eliminate the interference between the two oscillator systems. The two oscillator circuits were mounted on top of the vacuum jar in order to maintain the crystal to oscillator lead length at a minimum and the power for these circuits was supplied from separate batteries so that the cross-talk via the power supply leads was eliminated.

The large source-to-substrate distance also effectively decoupled the crystals from the sources so that frequency instabilities caused by radiative heating from the sources were kept at a minimum.

A1 - D.S. Chan, Ph.D. Thesis, University of Salford 1975

A2 - W.H. Lawson, J.Sci. Instrum. V44 pp 917 (1967)

Appendix VII

Design of Pneumatic Shutters

Figure 5.4 shows the bellows assembly. The rack and pinion used were Muffet, Ltd RO DP steel rack and a corresponding stainless steel spur gear with an outside diameter of 0.267" (6.78 mm). In order to move the shutter from horizontal to vertical position a rotation of 90^{o} of the spur gear was required. To provide this, the rack needed to move linearly through 0.21" (5.33 mm) which corresponded to a quarter of the spure gear circumference. Therefore, since the seamless bellows must never be extended past its natural length, a spring was used to pre-compress the bellows by 0.21". When the bellows was connected to a high pressure reservoir, sufficient force was exerted to overcome the strength of the spring and to extend the bellows back to its natural length.

The choice of the bellows was governed by three considerations. Firstly, maximum pressure allowed had to be as large as possible because the life-time of the bellows was exponentially related to the pressure it experienced. Secondly, the maximum compression allowed had to be as large as possible, and certainly larger than 0.21" , again due to life-time considerations. Thirdly, the bellows had to be small,

due to the space restrictions in the vacuum evaporator. The bellows chosen were 1¼" stainless steel bellows (Hydroflex No 121054) whose maximum compression and pressure was 0.4" and 380 psi respectively. The spring was then designed to fit the requirements of the bellows . The spring rate of the spring was calculated from two considerations. Firstly, the spring had to be strong enough to overcome the spring rate of the bellows itself (38 lb/m) and to compress it by 0.21". Secondly, the spring had to be such that minimal pressure would be needed to extend the bellows back to its natural length.

In order to compress the bellows, the spring itself would need to be compressed through a distance x, such that

$$R_S x = R_B . 0.21"$$

where R_S and R_B are the spring rates of the spring and bellows respectively. In order to extend the bellows back to the original length the force provided by the pressure of the gas had to be sufficiently high to compress the spring by further 0.21", i.e. the force needed was:

$$F = (0.21 + x)R_S = 0.21R_B + xR_S$$

Since the cross-sectional area of the bellows was 0.3 cm^2, the pressure required to provide this force was:

$$P = 0.7\ R_B + \frac{x}{0.3R_s}$$

Thus, in order to operate at low pressure, a low spring rate was required. However, low R_s meant that the spring itself had to be compressed through a relatively large distance "x" which implied that the overall length of the spring had to be large. Due to the space restrictions a compromise had to be made and a helical spring with a spring rate of 12 lb/m and overall length of 1.28" was chosen (manufactured by F.S. Ratcliffe). This spring rate meant that a pressure as low as 33.3 psi (8.8% of maximum pressure) could be used so that the estimated lifetime of the bellows operating at the compressure of 0.21" (52% of maximum compression) would be around 5000 000 cycles, according to manifacturers estimates. In order to compress the bellows by 0.21" the spring itself was compressed by 0.633" so that the overall working length of the spring was only about 0.64" which was sufficiently small to be accomodated in the vacuum system.

The bellows assembly was connected to the magnetic valves and the pressure reservoirs via ¼" nickle plated

tubes which were estimated to be sufficiently wide not to impede the speed of operation of shutters. All the vacuum seals involved were simple soldered joints. The outgassing rates of the shutter assemblies were negligable even when heated up to temperatures of approximately 70^{o}C.

Appendix VIII

Design of the Control Unit for the Shutters

The pneumatic shutters, i.e. the switching between the high and low pressure reservoirs was controlled by changeover electromagnetic valves capable of switching pressures as high as 60 psi at rates of 90 per minute. The valves themselves were controlled by a specially designed electronic unit. Basically this unit consisted of two voltage step generators and a comparator and the operation of the unit is illustrated shematically in figure A1. The ramp generator generates 1000 steps of fixed size but variable duration so that the time taken to reach the final fixed value of voltage V_{max} can be varied between 0.5 minutes to 10 minutes. The voltage function of this 'slow' ramp generator is schematically represented in fig A1 by the solid line. The other ramp generator sweeps the same voltage range (0 v to V_{max} volts) but at much higher speeds. It also re-starts the sweep every time it reaches the value V_{msx}. Again, the time taken to reach the final voltage value at every sweep can be varied between 0.1 to 100 seconds. The voltage function of this 'fast' generator is represented in figure A1 by dashed lines. The output of the comparator takes one value when the voltage from the fast ramp is between 0v and voltage output

of the slow ramp, and another value when the voltage from the fast ramp is between that of the slow ramp and V_{max}. This comparator output then effectively controls the electromagnetic valves so that at one output value one valve faces high and the other low pressure and conversely at the other output value of the comparator. Thus, the rate at which the fast ramp sweeps the voltage range controls the periodic time of the shutters and therefore the thickness of the interleaving layers of CdS and CdTe . The rate at which the slow ramp sweeps the voltage range controls the rate of the change of the 'mark-to-space' ratio of the shutters and therefore the 'steepness' of grading (overall thickness) of graded band-gap films. In addition it is possible to stopthe slow ramp so that it maintains constantvoltage at any one value between Ov and V_{max} volts. In this case the 'mark-to space' ratio is fixed and it is possible to grow mixed films with uniform band gap. When the fast ramp is stopped, either manually or automatically when the slow ramp reaches V_{max}, both valves are switched to face the high pressure reservoirs so that the shutters are closed. In addition the process may also be started at any point on the slow ramp.

If necessary it would have been also possible to change the characters of the 'slow' ramp so that instead of being linear with time, it could be for example exponential, so that the grading of the band gap would not be linear with respect to its thickness but exponential. This, in essence, simple method of controlling the shutter has been found very versatile and satisfactory.

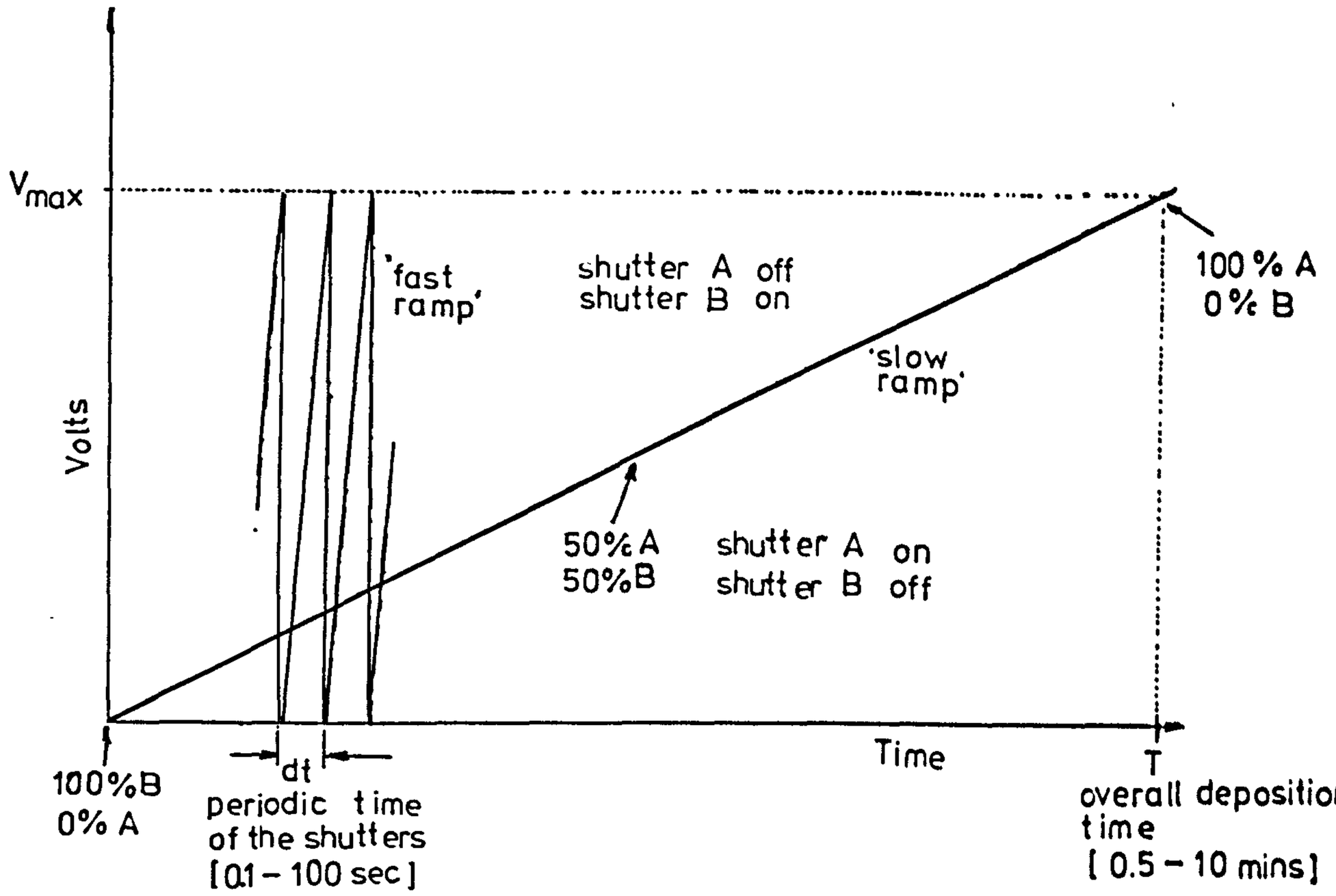

FIGURE A1 Schematic illustration of the shutter control unit

REFERENCES

1. N.A.S.A. Technical Report TR R-351
2. Thekaekara M.P., Applied Optics V.15 pp 915 (1973)
3. De Winter F., Solar energy and the flat plate collector, ASHREA, NY (1975)
4. I.S.E.S., Solar Energy, A UK Assessment (1970)
5. Telkes M., Storage of solar heating and cooling ASHREA, NY (1974)
6. Szokolay S.V., Solar energy and building
7. I.S.E.S. Int. Solar Energy Soc. Conf., U.S.A. LA 1975 pp450
8. Calvert J.G., Introduction to use of solar energy, MgGraw Hill, NY (1964)
9. Wrighton S. et al., Proc. Nat. Acad. Sci. USA pp 1518 (1975)
10. Clark W.D.K., Solar Energy V.17 pp 147 (1975)
11. Cooper J.P., Photosyntheses and Different Environments, Cambridge University Press (1975)
12. Szego P., Proc. 79 Meeting American Inst. of Chem. Eng. (1975)
13. Oswald W.S., Solar Energy V.15 (1974)
14. Chapin D.M., Fuller C.S., Pearson G.L., J. of App. Phys. V. 26 pp 534 (1955)
15. Reynolds D.C., Leies G., Antes L.L., Marburger R.E., Phys. Rev. V 96 pp 533 (1954)
16. Jenny D.A., Loferski J.J., Rappaport P., Phys. Rev V 101 pp 1208 (1956)

17. Wolf M., Proc. Photovoltaic Power Generation, Hamburg Sept. 25 1974, pp 49

18. Shiozawa L.R., Sullivan G.A., Augustine F., 7th IEEE Photovoltaic Spec. Conf. pp 39, IEEE (1968)

19. Morse F.H., Photovoltaic power and its applications, Paris, UNESCO pp 53 (1973)

20. Handy R.S., Solid State Electronics V 10 pp 765 (1967)

21. Wolf M., Rauschenbach H., Advanced Energy Conversion V 3 pp 455 (1963)

22. Loferski S.S., J. App. Phys. V 27 pp 777 (1956)

23. Wolf M., 10th IEEE Photovoltaic Specialist Conference, pp 5, IEEE (1973)

24. KITTL E., 10th IEEE Photovoltaic Specialist Conference, pp 103, IEEE (1973)

25. Wysocki J.J., Rappaport P., J. App. Phys. V 31 pp 571 (1960)

26. Landsberg, P.T., Mallinson J., 11th IEEE Specialist Conference, pp 241, IEEE (1975)

27. Rodot.M., Acta Electronica V 18 pp 4 (1975)

28. De Vos A., Energy Conversion V16 pp 67 (1976)

29. Marfaing Y., Int. Colloq. on Solar Cells, Toulouse, July 6-10, pp 67 (1970)

30. Wolf M., Proc J.R.E. V48 pp 1246 (1960)

31. Shay J.L., Wagner, Sigurd, Bachman, Z. Phys. Chem. V98 pp 365 (1975)

32. Feucht, D.L., J. Vac. Sci. Tech. V14 pp 57 (1977)

33. Rodot M., Cohen-Solal G., Photovoltaic power and its application, Paris July 26, pp 619 (1973)

34. Allison J., Haynos, J., Arndt R., Maulenberg A., Proc Photovoltaic Power Gen., Hamburg (1974) pp 487

35. Wolf M., Energy Conversion Vll pp 63 (1971)

36. Wolf M., Proc. IEEE. V 5l pp 674 (1963)

37. Iles P.A., 9th Photovoltaic Specialist Conf. pp 1 IEEE, (1972)

38. Mandelkorn, J., Lamnek J.H., 9th Photovoltaic Specialist Conference, pp 66, IEEE (1972)

39. Mandelkorn, J., Manneck H., Schudder L.R., lOth Photovoltaic Specialist Conf., pp 207, IEEE (1973)

40. Iles P.A., 8th Photovoltaic Specialist Conf. pp 345, IEEE (197O)

41. Iles P.A., 9th Photovoltaic Specialist Conf. pp 296, IEEE (1972)

42. Spour J.R., Othermer S., Curis D.L., 9th Photovoltaic Specialist Conf., pp 336, IEEE (1972)

43. Iles P.A., Zammrich D.K., lOth Photovoltaic Specialist Conf., pp 2OO, IEEE (1973)

44. Lindmayer, J., Allison J.F., Com.Sat. Tech.Rev. V3 pp 1 (1973)

45. Iles P.A., J. Vac.SchTech. V.14 pp llOO (1977)

46. Smeltzer R.K., Kendall D.L., Kernell G.L., lOth Photovoltaic Specialist Conf. pp 194, IEEE (1973)

47. Sater B.L., Brandhorst H.W., Riley T.S., lOth Photovoltaic Specialist Conf. pp 188, IEEE (1973)

48. Chadda T.B.S., Wolf M., 10th Photovoltaic Specialist Conference, pp 52, IEEE (1973)

49. Loferskii J.J., Rangahtan, N., Cruishan E.G., 9th Photovoltaic Specialist Conf., pp 19, IEEE (1972)

50. Loferski, J.J., Cruisman E.E., Chen L.Y., 10th Photovoltaic Specialist Conf., pp 58, IEEE (1973)

51. Kran A., Photovoltaic Power Generation, pp 77, Hamburg Sept 25 (1974)

52. Anderson W.A., Delahoy, Milano, J. App. Phys. V. 15 pp 3913 (1974)

53. Fonas J.S., Thin solid films, V. 36 pp 387 (1976)

54. Anderson W.A., Vernon, Delahoy, Kim., J. Vac Sci Tech. V 13 pp 1158 (1976)

55. Stephen F., Gordon K., Andersen W.A., J. Electron Materials, V6 pp 107 (1977)

56. Wronski C.R., Carlson, J. Electron Mater V6 pp 95 (1977)

57. Charles H.K., Feldman, Satkiewetz, Int. Elect. Devices, IEEE pp 71 (1976)

58. Chu T.L., Solid State Electronics V19 pp 837 (1976)

59. Martinez J., Alonsio, Criado, Piqeras, Electron Lett, V12 pp 671 (1976)

60. Wronski C.R., App. Phys. Lett V.28 pp 671 (1976)

61. Barret D.L., Myers E.H., Hamilton D.R., Bennet A.I., J. Electrochem Soc. V118 pp 952 (1971)

62. Stepanov A.V., Thermal Technickeshoi Fiziki V. 29 pp 381 (1959)

63. Bates H.E., Jewett D.H., White V.E., 10th Photovoltaic Specialist Conference, pp 197, IEEE (1973)

64. Ciszek T.F., Schwuttke G.H., Photovoltaic Power Generation, pp 159, Hamburg Sept 25 (1974)

65. Ellis B., Moss T.S., Solid State Electronics
V. 15 pp 1 (1971)

66. Hovel H.S., Woodall, J.M., 10th Photovoltaic
Specialist Conference, pp 25, IEEE (1973)

67. Andreey V.M., Kagan, Sov. Phys. Semiconductors,
V 18 pp 8601 (1975)

68. Hovel H.J., Woodhall J.M., J. Electrochem Soc V. 120

69. Moon R.L., James L.W., App.Phys.Lett. V26 pp 467 (1975)

70. Ewan J., Kamath S., Knecthli R.C., 11th Photovoltaic
Specialist Conf. pp 409, IEEE (1975)

71. Dupuis, Yingling, Doudy, App. Phys. Lett. V.31 pp 201
(1977)

72. Huber D., Bogus K., 10th Photovoltaic Specialist
Conf. pp 100, IEEE (1973)

73. Johnston W.D., Callahan, Int. Electron Devices,
pp 461, IEEE (1976)

74. Baliga B.J., Ghandi S.K., Borrego J.M.,
Int.Electron Devices, pp 457, IEEE (1976)

75. Hutchby J.A., Fudrich, J. App. Phys. V. 47 pp. 3152
(1976)

76. Kongai M., Takahashi, Solid State Electronics
V. 19 pp 259 (1976)

77. Larence L.G., Wireless World, Oct 1976

78. Shirland F.A., Advanced Energy Conversion,
V.6 pp 201 (1966)

79. Hill E.R., Karamidas, 6th Photovoltaic Specialist
Conference, pp. 35, IEEE (1967)

80. Potter A.E., Schalla, 6th Photovoltaic Specialist Conference pp 24, IEEE (1967)

81. Fahren Bruch A.L., Bube R.H., 9th Photovoltaic Specialist Conference, pp 118 (1972)

82. Lidquist P.F., Bube R.M., 8th Photovoltaic Specialist Conference, pp 1 (1970)

83. Koek K.W., Int. Electron Devices, pp 465, IEEE (1976)

84. Boer K.W., 11th Photovoltaic Specialist Conf., pp 514, IEEE (1975)

85. Mytton R.J., Moore, Gale, Clark, 9th Photovoltaic Specialist Conf. pp 133, IEEE (1973)

86. Hewig G.H., Pfisterer F., 9th Photovoltaic Specialist Conf., pp 138, IEEE (1973)

87. Vedel J., Castel, Photovoltaic power and its applications, pp 199, Paris July (1973)

88. Coste G.H., Nguyen D., Int. Colloq. in Solar Cells, pp 187, Toulone (1970)

89. Hadley H., Meakin, Phillips, 11th Photovoltaic Specialist Conf., pp 450, IEEE (1975)

90. Besson J., Fremy, Nguyen, Paltz, Photovoltaic power and its applications, pp 117, UNESCO (1973)

91. Vosdani S., Parvezi A., Photovoltaic Power Generation, pp 217, Hamburg, Sept (1974)

92. Pavaslar N.R., Jinha, J. Electrochem Soc. V 124 pp 743 (1973)

93. Akramou K.H., Stash Kov, Yuldashev, Geliotekhnika N4 pp 4 (1976)

94. Jordan J.F., Photovoltaic Power Generation, pp 221, Hamburg Sep (1974)

95. Vedel J., Thin Solid Film, V45 pp 55 (1977)

96. Bube R.H., Yale M.A., J. Electrochem Soc. V.124 pp 1430 (1977)

97. Stanley A.G., App. Solid. State. Electronics, V. 5 pp 251 (1975)

98. Boer K.V., Photovoltaic Power Generation, pp 239, Hamburg Sept (1974)

99. Shay J.L., Wagner, Bachman, Kasper, 11th Photovoltaic Specialist Conf., pp 503, IEEE (1975)

100. Yoshikawa A., Sakai, Solid State Electronics V.20 pp 133 (1977)

101. Wagner J., Shay J.L., J. Electrochem Soc. V. 123 pp 1254 (1976)

102. Beuhler E., Wagner S., Shay J.L., App. Phys. Lett., V 29 pp 121 (1976)

103. Kasper H., Te-1 B., Shay J.L., Schiadone L., Phys. Rev. 137, pp 4485 (1973)

104. Hampshire M.J., Tomlinson R.D., Parke S.I., Elliot E., Thin Solid Film V.20 pp 525 (1974)

105. Kazmerski L.L., J. Vac Sci Tech. V.14 pp 769 (1977)

106. Kazmerski L.L., Sanborn C.A., J. App. Phys. V 48 p 3178 (1977)

107. Vodakov, Naumod, Sov. Phys. Solid State, V 2 pp 1 (1960)

108. Vodakov, Naumod, Sov. Phys. Solid. State, V 3 pp 2718 (1962).

109. Cusano D.A., Solid State Electronics V. 6 pp 217 (1963)

110. Rodot M., Bernard, Lancolu, Rev. Phys. App. V. pp 211 (1967)

111. Lebrun J., Bessonneau, Int. Colloq. in Solar Cells pp 201, Toulouse (1970)

112. Lebrun J., 8th Photovoltaic Specialist Conf.. pp 33, IEEE (1970)

113. Tykvenko, Photovoltaic Power Generation, pp 151, Hamburg, Sep (1974)

114. Fahrenbruch A.L., Mitchell K., Bube R.H., 11th Photovoltaic Specialist Conf., pp 490, IEEE (1975)

115. Bube R.H., NSF/RANN report No. SE/GI 38445Y/PR 175/3

116. Bube R.H., Fahrenbruch A.L., Yale, App. Phys. Lett., V 30 pp 423 (1977)

117. Bube R.H., Yin, Fegelsen, J. App. Phys. V 48 pp 3162 (1977)

118. Olsen L.C., Bohara R., 11th Photovoltaic Specialist Conf., pp 381, IEEE (1975)

119. Page L., IEE Colloq in Electricity from the Sun, London (1975)

120. Yannoni N.F., Int. Colloq in Solar Cells, pp 175, Toulouse (1970)

121. Alvarado F.L., Fltisoiany, IEEE Trans. Industr. App. VIA-12 pp 90 (1976)

122. Emtage P.R., J. App. Phys., V33 pp 1950 (1962)

123. Cohen Solal G., Svob M., Marfaino Y., 9th Photovoltaic Specialist Conf. pp 29, IEEE (1972)

124. Marfaing Y., Bonazzi A., Sev de Phys. App. V 13
pp 145 (1978)

125. Bonnet D., Robenhorst H., Int. Colloq in Solar Cells,
pp 153, Toulouse (1970)

126. Bonnet D., Phys & Chem. of Heterojunctions,
Budapest, V 1 pp 119 (1970)

117. Bonnet D., Physica. Status . Solidi V3 pp 913 (1970)

128. Hill R., Richardson D., Thin Solid Film
V 18 pp 25 (1973)

129. Ohata K., Saraie J., Takaka T., Jap J. of App. Phys.
V 12 pp 25 (1973)

130. Tai H., Makashima S., Hoa S., Physica Status
Solidi V30 pp K115 (1975)

131. Tauc J., Rev. Mod. Phys. V. 29 pp 308 (1957)

132. Marfaing Y., Chevalier J., IEEG Trans. Electron
Devices, VED 18 pp 465 (1971)

133. Konstantinov O., Tsarenkov G.V., Soc. Phys. Semic,
V 10 pp 427 (1976)

134. Langmuir I., Phys. Rev 2 pp 329 (1913)

135. Wilson J.I.B. Woods J., J. Phys. Chem. Sol V 34
pp 171 (1973)

136. Shalmova K.V., Travina, Golic, Sov. Phys. Cryst.
V 8 pp 618 (1964)

137. Deptuch A., Grus, Hordecki, Lepek, Phys. Stat. Sol. A
V 37 pp K 101 (1976)

138. Escoffery C.A., J. App. Phys. V 35 pp 2273 (1964)

139. Bujatti M., Buitt J. App. Phys., Ser 2 V1
pp 983 (1968)

140. Galkin B.D., Troitskaya, Ivanou, Sov. Phys. Cryst. V. 12 pp 760 (1968)

141. Behringer A.J., Corrsin, J. Electrochem. Soc. V 110 pp 1083 (1964)

142. Shallcross F.V., Trans. Metallurgical Soc. AJUW. V 236 pp 309 (1966)

143. Kazmerskii L.L., Berry Allen, J. App. Phys. V 13 pp 3515 (1972)

144. Oliv er W.R., Vacuum V.20 pp 113 (1970)

145. Dresner J., Shalcorss, F.V., Solid State Electronics V.5 pp 205 (1962)

146. Readey D.W., J. Amer. Ceramic Soc., V49 pp 681 (1966)

147. Woods J., Buckley, J. Phys. D. App. Phys. V. 6 pp 1084 (1973)

148. Bleha W.P., Hartman, Kimenz, Peakock, J. Vac. Sci Tech. V 7 pp 135 (1970)

149. Karpovich I.A., Zvonkov, Soc. Phys. Solid. State V 6 pp 2714 (1965)

150. Mankarious R.G., Solid State Electronics V 7 pp 702 (1964)

151. Muller R.S., Watkins, Proc IEEE V 52 pp 425 (1964)

152. Dresner J., Shalcross , J. App. Phys. V 34 pp 2390 (1963)

153. South G., Hughes D.M., Thin Solid Film V20 pp 135 (1974)

154. Shalimova K.V., Bulateu, Voronkou, Dmitrieu, Soc. Phys. Crgst. VII pp 431 (1967)

155. Paparoditis C., Syruanarayanon , Compte Redn. Acad. Sci B V265 pp 498 (1968)

156. Palatnik L.S., Marincheva, Sorokin, Inorg. Mater. V 10 pp 357 (1974)

157. Spinolesku I., Phys. Stat. Sol V 15 pp 761 (1966)

158. Shiojiri M., Suito, Jap of App. Phys. V3 pp 314 (1964)

159. Tolutis V.B., Litov Fiz. Sbornik V5 pp 495 (1965)

160. Glang R., Kren, Patrick, J. Electrochem Soc. V 110 pp 407 (1963)

161. Shimulite E., Bagochinuaite, Litov Fiz. Sbornik V. 5 pp 965 (1964)

162. Konorov P.P., Shevechenko, Sov. Phys. Solid State. pp 1027 (1961)

163. De Nobel D., Phillips Res. Rep V14 pp 361 (1959)

164. Hill R, Richardson D, Wilson S, J. Phys D; App. Phys. V5 pp 185 (1972)

165. Hampshire M.S. Int. J. Elect. Eng. Educ. V 9 pp 110 (1971)